

**THE ROLE OF NICOTINIC RECEPTOR FUNCTION IN THE DEVELOPMENT  
OF SYNAPSES AND IN DIABETES-INDUCED DYSAUTONOMIAS**

By

Arjun Sriram Krishnaswamy

Department of Physiology

McGill University

Montréal, Québec, Canada

August 2009

A thesis submitted to the Faculty of Graduate Studies and Research in partial  
fulfillment of the requirements for the degree of Doctor of Philosophy

For Kate and my Family

## ABSTRACT

Autonomic circuits depend critically on cholinergic synaptic transmission to develop and function normally, and severe dysautonomias emerge if cholinergic transmission is disrupted. Yet, we do not fully understand how synaptic activity helps cholinergic synapses develop on autonomic neurons nor do we understand whether or not disrupted postsynaptic nAChRs render cholinergic synapses non-functional, resulting in dysautonomias. To study these two issues, I investigated sympathetic neurons from mice with a disruption in the  $\alpha 3$  nAChR subunit gene ( $\alpha 3$  KO). I hypothesized that (1) the loss of  $\alpha 3$  subunits would remove functional nAChRs from cholinergic synapses and abolish synaptic transmission; (2) the loss of postsynaptic activity would prevent cholinergic nerve terminals from developing normally; and (3) functional  $\alpha 3$  nAChRs are inactivated by diabetes-induced reactive oxygen species (ROS) to render cholinergic synapses non-functional and cause dysautonomias. To test these hypotheses I combined electrophysiological, molecular biology and imaging techniques to examine cholinergic synapses on sympathetic neurons in  $\alpha 3$  KO mice.

I found that the loss of  $\alpha 3$  prevents the appearance of functional nAChRs on sympathetic neurons and abolishes synaptic transmission through sympathetic ganglia. In spite of this, morphologically normal cholinergic synapses form and persist for months on sympathetic neurons from  $\alpha 3$  KO mice. Surprisingly, in the absence of postsynaptic activity the presynaptic terminals are immature and lack high-affinity choline transporters (CHTs). As a result, they cannot sustain ACh release and become quickly depleted. Moreover, using *in vivo* gene transfer strategies I demonstrate that CHT expression in nerve

terminals is induced and maintained by signals downstream of postsynaptic activity; converting these immature terminals that deplete rapidly to mature terminals capable of sustaining ACh release.

Since the loss of  $\alpha 3$  subunits in  $\alpha 3$  KO mice inactivates the sympathetic nervous system and produces severe dysautonomias, I wondered whether dysautonomias that progress during diabetes are produced by disrupted  $\alpha 3$  nAChRs. To investigate this, I elevated extracellular glucose levels to those seen during diabetes in sympathetic neuron cultures and then simultaneously measured changes in cytosolic ROS levels and whole-cell ACh-evoked currents. I discovered that increased extracellular glucose elevates intracellular ROS and induces a use-dependent, long-lasting rundown of ACh-evoked currents. Using adenoviruses to express mutated  $\alpha 3$  subunits in  $\alpha 3$  KO sympathetic neurons, I identified a highly conserved ring of cysteines in the receptor pore that are attacked by ROS to trap nAChRs into a long lasting inactivated state. Finally, using  $\alpha 3$  KO mice and *in vivo* gene transfer strategies, I demonstrate that these cysteines are attacked on sympathetic neurons to inactivate nAChRs, depress synaptic transmission and produce cardiovascular and thermoregulatory dysautonomias in diabetic mice.

My results (1) establish that  $\alpha 3$ -containing nAChRs are required for cholinergic synaptic transmission on sympathetic neurons; (2) demonstrate that activity-dependent signals induce and maintain CHT in developing cholinergic nerve terminals; and (3) reveal that diabetes-induced ROS traps nAChRs in an inactivate state, depresses cholinergic transmission and results in dysautonomias. Taken together, my results suggest that diseases that elevate cytosolic ROS would disrupt postsynaptic nAChRs and disrupt activity-dependent

retrograde signals that induce and maintain CHT to produce could severe, long lasting dysautonomias.

## RÉSUMÉ

Les circuits autonomes nécessitent la transmission synaptique cholinergique pour un développement et une fonction normale. Le résultat d'une perturbation de cette transmission cholinergique est l'apparition de dysautonomies sévères. Hors, nous ne comprenons pas complètement comment l'activité synaptique aide au développement des synapses cholinergiques sur les neurones autonomes, ni si les dysautonomies sont la conséquence d'une perturbation des nAChRs post-synaptiques ayant comme résultat des synapses cholinergiques non-fonctionnelles. Pour en savoir plus sur ces deux sujets, j'ai étudié des neurones sympathiques provenant de souris qui possèdent une perturbation du gène sous-unité  $\alpha 3$  nAChR ( $\alpha 3$  KO). J'ai formulé l'hypothèse que (1) la perte des sous-unités  $\alpha 3$  éliminerait les nAChRs fonctionnels des synapses cholinergiques et supprimerait la transmission synaptique ; (2) l'absence d'activité post-synaptique empêcherait le développement normal des terminaisons nerveuses cholinergiques ; et (3) les dérivés réactifs de l'oxygène (DRO) provoqués par le diabète causent l'inactivation des nAChRs fonctionnels produisant des synapses cholinergiques non-fonctionnelles et les dysautonomies qui les accompagnent. J'ai combiné plusieurs méthodes notamment l'électrophysiologie, la biologie moléculaire, et des techniques d'imagerie pour tester ces hypothèses en examinant les synapses cholinergiques sur des neurones sympathiques dans des souris  $\alpha 3$  KO.

J'ai trouvé que la perte de  $\alpha 3$  empêche l'apparition de nAChRs fonctionnels dans les neurones sympathiques et supprime la transmission synaptique à travers les ganglions sympathiques. Malgré cela, des synapses cholinergiques morphologiquement normales se forment et persistent pendant

plusieurs mois dans les neurones de souris  $\alpha 3$  KO. Étonnement, en l'absence d'activité post-synaptique, les terminaisons pre-synaptiques sont immatures et ne possèdent pas de transporteurs à haute affinité de choline (CHTs). L'absence de CHTs à comme résultat l'incapacité de soutenir le relâchement d'ACh causant son épuisement rapide. De plus, en utilisant des techniques de transferts de gènes *in vivo*, je démontre que l'expression de CHT dans les terminaisons nerveuses est provoquée et maintenue par des signaux en aval de l'activité synaptique, ce qui transforme les terminaisons immatures qui s'épuisent rapidement en ACh, en terminaisons matures capables de soutenir le relâchement d'ACh.

Puisque la perte des sous-unités  $\alpha 3$  dans les souris  $\alpha 3$  KO cause l'inactivation du système nerveux sympathique et engendre des dysautonomies sévères, je me suis questionné à savoir si les dysautonomies qui se produisent durant le diabète ont pour cause des nAChRs  $\alpha 3$  perturbés. Pour tester cette question, j'ai élevé les niveaux de glucose extracellulaire dans les cultures de neurones sympathiques à des niveaux équivalents pendant le diabète. Après ceci, j'ai mesuré simultanément les changements de DRO cytosoliques et les changements dans les courants associés à l'ACh dans toute la cellule. J'ai découvert que l'augmentation extracellulaire de glucose augmente les niveaux de DRO intracellulaire et produit une réduction de longue durée des courants causés par l'ACh associée à l'utilisation des synapses. En utilisant des adénovirus pour causer l'expression de sous-unités  $\alpha 3$  mutées dans les neurones sympathiques  $\alpha 3$  KO, j'ai identifié un anneau de cystéines très conservé à travers les espèces dans le pore du récepteur qui est attaqué par DRO. Cette attaque maintient les nAChRs dans un état d'inactivation de longue durée. Finalement, en utilisant des souris  $\alpha 3$  KO et des techniques de transfert de

gènes *in vivo*, je démontre que ces cystéines sont attaquées dans les neurones sympathiques ayant comme résultat l'inactivation des nAChRs et la réduction de la transmission synaptique. Ce qui cause des dysautonomies cardiovasculaires et thermorégulatrices dans des souris diabétiques.

Mes résultats (1) établissent que des nAChRs incluant  $\alpha 3$  sont nécessaires pour la transmission synaptique cholinergique dans les neurones sympathiques; (2) démontrent que des signaux qui dépendent de l'activité synaptique provoquent et maintiennent l'expression de CHT dans les terminaisons nerveuses cholinergiques en développement ; et (3) dévoilent que les DRO produits par le diabète maintiennent les nAChRs dans un état d'inactivation, réduisent la transmission cholinergique et causent des dysautonomies. Ensemble, mes résultats suggèrent que des maladies qui augmentent les niveaux de DRO cytosoliques perturberaient les nAChRs post-synaptiques et perturberaient les signaux causés par l'activité synaptique qui provoquent et maintiennent l'expression de CHT ayant comme conséquences des dysautonomies sévères et de longue durée.

## ACKNOWLEDGEMENTS

I couldn't have done this degree without the help of several people. I am pretty bad at writing these things so please forgive me if I forget any names. First, Ellis – I joined the lab not really knowing whether science was for me or whether I would really be any good at it. I am glad to say that working with you over the last 6 years I've learned a lot (I should say everything) about being a good and careful scientist, but more than this I've realized I really love doing science – thank you. I've learned a lot in your lab and I hope we stay good friends for years to come. I'd have to say a lot of the hands-on skills, troubleshooting techniques and lab-time management skills I've learned in the past 6 years or so have come from my good friend and colleague Brigitte. Thanks for everything Brigitte, your lively personality and warm heart made the last 6 years a real joy. I should say that I learned many things alongside Nancy – you became a lot better at many of these things than I did, but luckily you were around to help me do them when the time came. Thank you Linda for teaching me how to think and write clearly – Just don't read the thesis too carefully! ☺. Thanks to other members of the Cooper lab past and present for your friendship: Veronica, Celine, Alona, Dave V and Dimitar. People say that the best way to become better at what you do (probably said it a lot more eloquently than this) is to make smart friends, or better still ones who are smarter – I've got the latter kind in spades. Thank you Chamel, Mario, Scott, Maclean, Rob, Nick, Thanos, Steve and Dave for the science talks, the regular talks, the beers and the laughs. Move down to Boston or I won't have any friends. Special thanks to Mario for doing some last minute abstract translation! Thanks to so many on the 11<sup>th</sup> and 12<sup>th</sup> - Eric, Armin, Soroush, Marion, Jess, Matthieu, Ana, Roy, Val I know I am forgetting people. Thanks to many members of the physiology department for their advice and support throughout my PhD.: Charles, Monroe, Pejmun, Kathy, John (W and O). Thank you family for putting up with me, Mamaji, Ammama, and Paati for reminding me what was important. Mom, Dad, Vijai, Pooja you've done more than I can write about here and this is your accomplishment too. Thank you to my new family, the Logues especially for putting up with my tendency to stay and work rather than come and visit. Last but not least, thank you Kate. I couldn't have pushed myself as hard nor could I have kept my spirits up as high without your love and support. This accomplishment is yours too (especially after the last few days!). Well I think I should wrap up here, science has been a blast so far, looking forward to more.

## CONTRIBUTION TO PUBLICATIONS

Chapters 2, 3, 4, and 5 of my thesis are duplicates of the following four

manuscripts:

1. Rassadi S\*, **Krishnaswamy A\***, Pie B, McConnell R, Jacob MH, Cooper E. (2005) A null mutation for the alpha3 nicotinic acetylcholine (ACh) receptor gene abolishes fast synaptic activity in sympathetic ganglia and reveals that ACh output from developing preganglionic terminals is regulated in an activity-dependent retrograde manner. *J Neurosci* 25:8555–8566. [S.R. and A.K. contributed equally to this work.]
2. **Krishnaswamy A**, Cooper E. (2009) An activity-dependent retrograde signal induces the expression of the high-affinity choline transporter in cholinergic neurons. *Neuron* 61(2):272-86.
3. Campanucci VA, **Krishnaswamy A**, Cooper E. (2008) Mitochondrial reactive oxygen species inactivate neuronal nicotinic acetylcholine receptors and induce long-term depression of fast nicotinic synaptic transmission. *J Neurosci.* 28(7):1733-44.
4. Campanucci VA\*, **Krishnaswamy A\***, Cooper E. (2009) Hyperglycemia produces dysautonomias by inactivating neuronal nicotinic acetylcholine receptors. Manuscript submitted for publication. [V.C. and A.K. contributed equally to this work.]

I have not included the following manuscript in the body of my thesis because it does not directly relate to the main focus of my thesis. A copy of each this document appears in the appendix:

5. Caffery PM\*, **Krishnaswamy A\***, Sanders T, Hartlaub H, Klysik J, Cooper E, Hawrot E. Knock-in a bungarotoxin sensitivity enables visualization and pharmacological characterization of postsynaptic  $\alpha 3$ -containing nicotinic acetylcholine receptors in a novel mouse model. *Manuscript under review Eur. J. Neurosci.* [P.C. and A.K. contributed equally to this work.]

## CONTRIBUTION TO ORIGINAL SCIENCE

My findings reveal novel use-dependent mechanisms that underlie the functional properties of cholinergic synapses. In chapter 2, I demonstrate that postsynaptic nAChRs expressed at cholinergic synapses on sympathetic ganglia contain  $\alpha 3$  nAChR subunits. Moreover, I show that in the absence of  $\alpha 3$ , morphologically normal synapses form on these neurons but nerve terminals cannot output normal levels of ACh. In this chapter I developed preliminary results that were initiated by my colleague S. Rassadi. All of the experiments in this study, analysis and figures were performed by me except for images of cholinergic synapses acquired on an electron microscope that were provided by our collaborator Dr. M. Jacob and synaptic transmission data in figures 2 and 4 that I generated with S. Rassadi.

In chapter 3, I follow up on our observation that ACh output from nerve terminals is impaired in the absence of postsynaptic activity and demonstrate that this deficiency results from a loss of high-affinity choline transporters (CHT) expression in presynaptic neurons. Furthermore using *in vivo* gene transfer methods I demonstrate that retrograde signals that depend on postsynaptic activity induce and maintain the levels of CHT in nerve terminals and allow these nerve terminals to sustain synaptic transmission. Moreover, using immunofluorescence techniques, confocal microscopy and electron microscopy, I make the surprising discovery that synaptic activity is not required for cholinergic synapses to persist on autonomic neurons. All of the experiments, analysis and figures in this study were performed by me except for the electron microscopy and the generation of adenoviruses, performed by B. Pie and N. Grenier.

In chapter 4, V. Campanucci and I discover a novel form of nAChR modulation that results from elevated cytosolic reactive oxygen species (ROS). Together we show that mild elevations of cytosolic ROS induce a use-dependent, long lasting inactivation of nicotinic acetylcholine receptor currents on sympathetic neurons. Furthermore, we show that ROS inactivates nAChRs *in vivo* and depresses synaptic transmission through autonomic ganglia. In this study, I deprived neurons of NGF and studied the consequences on receptor function *in vitro* and *in vivo*; and examined the direct role of ROS on synaptic transmission by recording from sympathetic neurons in intact ganglia with electrodes containing antimycin-A. I also performed the analysis and figures for this paper

In chapter 5, V. Campanucci and I generalize our findings from chapter 4 to hyperglycemia-induced cytosolic ROS and dysautonomias that appear during the progression of diabetes. In this study we show that elevated extracellular glucose in culture increases ROS in sympathetic neurons and inactivates nAChRs. Furthermore, I identify a highly conserved ring of cysteine residues located in the receptor pore that gets attacked by ROS to trap nAChRs in an inactive state. Moreover, I demonstrate that ROS attacks these cysteines in mouse models of type 1 and type 2 diabetes to inactivate nAChRs, depress synaptic transmission and produce dysautonomias. In this paper I developed V. Campanucci's preliminary results on hyperglycemia-induced ROS and inactivation of nAChRs and extend the study to mouse models of diabetes. All of the experiments, analyses, and figures were performed by me and the generation of adenoviruses were performed by B. Pie and N.Grenier.

In the appendix, I have included a manuscript currently under review entitled "Knock-in  $\alpha$ -bungarotoxin sensitivity enables visualization and

pharmacological characterization of postsynaptic  $\alpha 3$ -containing nicotinic acetylcholine receptors in a novel mouse model (Cafferty et al., 2009; see the appendix). In this paper I collaborate with Dr. E. Hawrot's lab at Brown University to characterize cholinergic synapses in mice that express chimeric  $\alpha 3$  subunits that bind  $\alpha$ -bungarotoxin. The antibodies directed against nAChRs that are currently available are not specific enough to study receptor localization; the goal of this study was to develop a mouse model where we could visualize postsynaptic nAChR puncta on sympathetic neurons. In this study I correlated synaptic transmission from  $\alpha 3$  knock-in mice with morphological counts of  $\alpha$ -bungarotoxin positive receptor puncta using immunofluorescence techniques and confocal microscopy. We show that  $\alpha 3$  knock in strategy combined with  $\alpha$ bgtx is a useful way to probe the function and distribution of nAChRs on sympathetic neurons. Moreover, I use these mice to examine the stability of postsynaptic receptor clusters following denervation.

## TABLE OF CONTENTS

ABSTRACT	I
RESUME	IV
ACKNOWLEDGEMENTS	VII
CONTRIBUTION TO PUBLICATIONS	VIII
CONTRIBUTION TO ORIGINAL SCIENCE	IX
<b><u>CHAPTER 1:</u></b>	<b>1</b>
<b>Introduction</b>	
<b>1.1 General Introduction and Rationale</b>	<b>1</b>
<b>1.2 The Sympathetic Nervous System</b>	<b>5</b>
1.2.1 Superior Cervical Ganglion	6
1.2.1.1 Location and Target Innervation of the SCG	6
1.2.1.2 Innervation of SCG Neurons and Topography	6
<b>1.3 Development of Cholinergic Synapses on Sympathetic Neurons</b>	<b>7</b>
1.3.1 Axon Guidance and Dendrite Outgrowth	7
1.3.1.1 Axon Guidance	8
1.3.1.2 Dendrite Outgrowth	8
Nerve Growth Factor	8
Activity-Dependent Signals	10
1.3.2 Initial Contact and Synaptic Differentiation	11
1.3.2.1 Agrin	11
1.3.2.2 Cell Adhesion Molecules	12
1.3.2.3 Receptor Scaffolds	14
1.3.3 Synapse Maturation and Refinement	15
<b>1.4 Cholinergic Synaptic Transmission</b>	<b>16</b>
1.4.1 Presynaptic Nerve Terminals	16
1.4.1.1 Choline Acetyltransferase	16
1.4.1.2 Vesicular Acetylcholine Transporter	17
1.4.1.3 The Cholinergic Gene Locus	18
1.4.1.4 The High-Affinity Choline Transporter	19
1.4.1.5 Regulation of High-Affinity Choline Transporters	20
1.4.2 Postsynaptic Domain	22
1.4.2.1 Nicotinic Acetylcholine Receptors on Sympathetic Neurons	22
Structural Features	22
A Cluster of nAChR Subunit Genes	23
Composition of Postsynaptic Receptors	24
1.4.2.2 Muscarinic Receptors	25
1.4.2.3 Acetylcholinesterase	26
1.4.2.4 Nicotinic Receptors and Dysautonomias	27

<b>1.5 Summary of the Problem and Approach</b>	29
1.5.1 The Role of Activity in Cholinergic Synapse Formation on Neurons	29
1.5.2 The Role of ROS Produced by Diabetic Hyperglycemia and nAChR Function on Sympathetic Neurons	30
1.5.3 Experimental Approach	30
<b>CHAPTER 2:</b>	<b>32</b>
<b>A null mutation for the alpha3 nicotinic acetylcholine (ACh) receptor gene abolishes fast synaptic activity in sympathetic ganglia and reveals that ACh output from developing preganglionic terminals is regulated in an activity-dependent retrograde manner</b>	
<b>Foreword</b>	32
Background and Rationale	
Hypothesis	
Experimental Outline	
<b>Abstract</b>	34
<b>Introduction</b>	35
<b>Methods and Materials</b>	37
Mice	
Neuron Cultures	
Extracellular Recordings	
Intracellular Recording	
Whole-Cell Recording	
Calcium Imaging	
Adenovirus	
Ultrastructural Studies	
Immunocytochemistry	
<b>Results</b>	44
ACh-Evoked Currents Are Absent on $\alpha 3^{-/-}$ Neurons and Restored by Overexpressing $\alpha 3$ cDNA	
SCG From $\alpha 3^{-/-}$ Mice Lack Synaptic Transmission	
Sympathetic Neurons in $\alpha 3^{-/-}$ SCG Lack Fast EPSPs	
Muscarinic Responses on $\alpha 3^{-/-}$ and WT Neurons Are Similar	
Morphological Synapses Form on Neurons without Synaptic Activity	
ACh Release from Preganglionic Varicosities Requires Fast Synaptic Activity	
Preganglionic Terminals in $\alpha 3^{-/-}$ Ganglia Lack Functional High-Affinity Choline Transporters	
<b>Discussion</b>	53
Functional nAChRs on Postsynaptic SCG Neurons Require $\alpha 3$ Subunits	
Fast Synaptic Transmission is not Required for the Development of Morphological Synapses	
Presynaptic Output in $\alpha 3^{-/-}$ SCG is Impaired	

High-Affinity Choline Transporter Function  
Retrograde Control of Transmitter Output at Developing Synapses

<b>CHAPTER 3:</b>	<b>60</b>
<b>An activity-dependent retrograde signal induces the expression of the high-affinity choline transporter in cholinergic neurons</b>	
<b>Foreword</b>	<b>60</b>
Background and Rationale	
Hypothesis	
Experimental Outline	
<b>Abstract</b>	<b>62</b>
<b>Introduction</b>	<b>63</b>
<b>Methods and Materials</b>	<b>66</b>
Mice	
Extracellular and Intracellular Recordings	
Adenoviruses	
Immunohistochemistry	
In Situ Hybridization	
Ultrastructural Studies	
Statistics	
<b>Results</b>	<b>74</b>
Survival of $\alpha 3$ KO Mice Raised as an Outbred Strain	
Synapses Persist in the Absence of Fast Synaptic Activity in SCG of $\alpha 3$ KO Mice	
CHT Is Absent in Preganglionic Neurons of $\alpha 3$ KO Mice	
Postnatal Appearance of CHT in WT and $\alpha 3$ KO Sympathetic Ganglia	
Viral Expression of $\alpha 3$ in $\alpha 3$ KO Mice Establishes Fast Synaptic Transmission in Sympathetic Ganglia	
Establishing Postsynaptic Activity in $\alpha 3$ KO Ganglia Induces the Appearance of CHT Presynaptically	
Postsynaptic Activity Is Required for the Continual Appearance of CHT in Presynaptic Terminals	
<b>Discussion</b>	<b>87</b>
Electrophysiologically Silent Synapses Persist without Postsynaptic Activity	
Expression of the High-Affinity Choline Transporter Requires a Retrograde Signal(s) Downstream of Postsynaptic Activity	
<b>CHAPTER 4:</b>	<b>94</b>
<b>Mitochondrial reactive oxygen species inactivate neuronal nicotinic acetylcholine receptors and induce long-term depression of fast nicotinic synaptic transmission</b>	
<b>Foreword</b>	<b>94</b>

Background and Rationale	
Hypothesis	
Experimental Outline	
<b>Abstract</b>	96
<b>Introduction</b>	97
<b>Methods and Materials</b>	99
Primary Cultures	
Whole-Cell Recording	
Intracellular ROS Measurement	
Antioxidant Treatment	
Statistics	
<b>Results</b>	107
Rundown of ACh-Evoked Currents on Sympathetic Neurons in Short-Term Cultures	
Increasing the Antioxidant Content of the Cytosol Prevents Rundown of ACh-Evoked Currents on Neurons in Short-Term Cultures	
Elevations in Cytosolic ROS Induce Long-Lasting, Use-Dependent Inactivation of Neuronal nAChRs	
Mitochondrial ROS Induces Long-Lasting, Use-Dependent Rundown of Neuronal nAChRs	
Mitochondrial ROS Induce Long-Lasting, Use-Dependent Rundown of $\alpha 4\beta 2$ nAChRs	
Muscle nAChRs are not Inactivated by Cytosolic ROS	
Elevation of Mitochondrial ROS Leads to Long-Term Depression of Fast Nicotinic Synaptic Transmission in Intact Ganglia	
Transient Disruption in NGF Signaling Leads to Long-Term Depression of Fast Nicotinic Synaptic Transmission in Intact Ganglia	
<b>Discussion</b>	119
<b>CHAPTER 5:</b>	<b>124</b>
<b>Hyperglycemia produces dysautonomias by inactivating neuronal nicotinic acetylcholine receptors. Manuscript submitted for publication</b>	
<b>Foreword</b>	124
Background and Rationale	
Hypothesis	
Experimental Outline	
<b>Abstract</b>	126
<b>Introduction</b>	127
<b>Methods and Materials</b>	129
Animals	
Primary Cultures	

Whole Cell Recording  
 Intracellular ROS Measurements  
 Extracellular and Intracellular Recording  
 Heart Rate and Temperature Measurements  
 Adenoviruses  
 Statistics

<b>Results</b>	135
Hyperglycemia Inactivates Nicotinic Acetylcholine Receptors on Autonomic Neurons	
Hyperglycemia Depresses Synaptic Transmission in Sympathetic Ganglia	
Sympathetic Hypofunction in Hyperglycemic Mice	
Depressed Synaptic Transmission in Leptin (ob/ob) and Leptin Receptor(db/db) Mutant Mice	
Hyperglycemia –Induced ROS Inactivates nAChRs Through Cys Residues at the Inner Mouth of the Channel Pore	
<b>Discussion</b>	143
 <b>CHAPTER 6:</b>	<b>147</b>
<b>General Discussion and Conclusion</b>	
<b>Discussion</b>	147
Expression of the High-Affinity Choline Transporter Requires a Retrograde Signal(s) Downstream of Postsynaptic Activity	
Electrophysiologically Silent Synapses Persist without Postsynaptic Activity	
Cytosolic ROS attack a highly conserved ring of cysteine residues in the channel pore and inactivate nAChRs	
Diabetes-induced ROS inactivates nAChRs, depresses synaptic transmission and results in dynautonomias	
<b>Conclusion</b>	157
 REFERENCES	159
 APPENDIX 1	A1

## CHAPTER 1: INTRODUCTION

### 1.1 GENERAL INTRODUCTION AND RATIONALE

A complex exchange and processing of information within neural circuits produces a wide range of behaviours from homeostasis and movement to emotions and memory. These coordinated circuit properties require a precise combination of functional synapses formed among neurons, and serious diseases emerge if synapses are non-functional or if synapses are formed inappropriately. Yet, we do not fully understand how functional synaptic connections form so precisely between neurons. For my PhD, my main interest was to learn more about how functional synapses form.

Synapses develop over a long period that begins in the embryo and extends well into adolescence (Waites et al., 2005). The early events of synapse formation are largely complete by birth and involve a complex interplay of guidance molecules, trophic signals, and cell–cell adhesion interactions that guide growing axons to find target neurons and form synapses with them (Waites et al., 2005). These initial synapses produce neural circuits that give animals behaviours they require at birth. However, more mature circuits are required to produce behaviours that they will need throughout life. Several important properties of neural circuits mature in response to synaptic activity, including increases in strength and precision of synaptic connections. However, the specific effects of synaptic activity on the postnatal development of synapses are not well understood.

To understand this issue better, several groups have disrupted synaptic transmission in mice to study the development of synapses without activity. In these experiments, researchers studied mice that lack proteins crucial for neurotransmitter release from presynaptic nerve terminals. One such study examined the development of synapses in mice that lack the critical vesicle release protein Munc18. Munc18 is expressed ubiquitously at nerve terminals and is a soluble protein that stabilizes the levels of syntaxin1a on synaptic vesicle membranes (Sudhof, 2004). Syntaxin1a normally interacts with its partner synaptobrevin at presynaptic membranes to form SNARE complexes that are crucial for synaptic vesicle fusion. Given this important role in vesicle fusion, Verhage and colleagues (2000) reasoned that if they were to disrupt the Munc18 gene then they would abolish synaptic transmission.

Indeed, these knockout mice cannot compensate for the loss of Munc18 and as a result the levels of syntaxin1a are reduced by approximately 70% (Toonen et al., 2005). Using electrophysiological recordings from neocortical slices and from intact neuromuscular junction (NMJ), the authors demonstrate that spontaneous and evoked neurotransmitter release onto cortical neurons and skeletal muscle is completely absent in Munc18 knockout mice. These results indicate that the reduced syntaxin1a levels that result from the loss of Munc18 causes a complete and widespread loss of synaptic transmission.

Remarkably, the complete and permanent loss of synaptic transmission had little effect on the assembly of the brain at birth. Brain areas that form late in embryogenesis, such as the neocortex appeared identical in null mutants and control littermates at birth (Verhage et al., 2000). Immunolabeling patterns for growth cone markers such as GAP43, and presynaptic markers such as synapsin 1 were similar to those observed in control mice, indicating that targeting of fiber

pathways and synthesis of synaptic components proceeds normally in the absence of synaptic transmission. These results strongly indicate that activity-dependent mechanisms are not required for the initial assembly of synapses and the basic plan of the central nervous system (CNS).

Following this initial assembly of neural networks, these mice develop massive neurodegeneration. Brain areas that form early in embryogenesis, such as the lower brain stem were almost completely lost by embryonic day 18 (E18) and showed large numbers of degenerating synapses as well as extensive cell death of mature neurons. The midbrain and basal forebrain degenerated later but it was equally severe; apoptotic bodies were readily observable with hemotoxylin and eosin staining. Many neurons stained positive with the apoptotic marker TUNEL and large numbers of activated macrophages were detected in degenerating areas (Verhage et al., 2000). Taken together, these results suggest that while activity-dependent mechanisms are not required for synapses to form, they are required for synapses to persist on neurons.

On the one hand, this interpretation makes sense because during normal development weak synaptic connections are well known to be eliminated from neural circuits (Katz and Shatz, 1996). On the other hand, the perinatal lethality produced by the widespread loss of synaptic transmission complicates this interpretation, making it hard to decipher whether these synapses regress as a result of inactivity or as a result of anoxia or necrosis. Moreover, this lethality makes it difficult to look at the long-term effects of activity on synapse development, particularly its role in synapse maturation. In order to clarify these issues, the goal would be to avoid lethality. One way to do this would be to eliminate activity at a specific group of developing synapses and study the consequences.

One approach would be to silence synapses by removing postsynaptic neurotransmitter receptors. Unlike vesicle release proteins that are shared among all synapses, neurotransmitter receptors differ considerably among synapses. The loss of a particular type of neurotransmitter receptor should only silence a particular class of synapse while leaving synaptic transmission at other classes intact. However, the results from such an experiment on CNS neurons would be complicated to interpret because many neurons in the CNS receive multiple kinds of synapses; a silent class of synapses on these neurons could still receive signals produced by the synaptic activity of other classes. A simpler approach would be to silence synapses on neurons that express only one main form of postsynaptic receptor.

A potentially suitable group of neurons for this approach are peripheral sympathetic neurons. These neurons are excited almost exclusively by cholinergic nicotinic synapses, suggesting that removal of postsynaptic nicotinic receptors should abolish both local and global synaptic activity. Moreover, the sympathetic nervous system can be completely destroyed in mice without reducing postnatal survival (Smeyne et al., 1994). Given these features, we inferred that removing nicotinic acetylcholine receptors (nAChRs) from sympathetic neurons of mice should silence developing cholinergic synapses without affecting postnatal mouse survival, making these mice an ideal model to study the relationship between synaptic activity and the precise formation of functional cholinergic synapses.

## 1.2 THE SYMPATHETIC NERVOUS SYSTEM

The sympathetic nervous system is part of the autonomic nervous system (ANS) and helps regulate homeostasis by adjusting the function of various body organs and glands in response to an external or internal environmental change, such as stress or a change in body posture. The sympathetic nervous system regulates many physiological processes, including body temperature, blood pressure, respiration, cardiac output, blood glucose levels, gastrointestinal peristalsis and ejaculation (Glebova and Ginty, 2005). In most cases, the sympathetic nervous system is activated in response to homeostatic imbalances detected by a distributed network of nuclei in the CNS that include the hypothalamus and the brainstem (Iverson et al., 2000). In other cases, the sympathetic nervous system is activated by homeostatic imbalances detected by local sensory organs such as arterial baroreceptors. In all cases, signals that activate the sympathetic nervous system are relayed by preganglionic neurons contained within in the intermediolateral horn of the thoracic spinal cord (Gibbins and Morris, 2006; Iverson et al., 2000).

Working with the sympathetic nervous system offers a number of advantages because the anatomy and physiology of sympathetic ganglia are well understood. All sympathetic neurons are motor neurons that are contained within superficial, pre- and paravertebral ganglia that make them easy to access and manipulate. Sympathetic axons grow through discrete, easily accessible fiber bundles to form excitatory noradrenergic synapses with endocrine glands, exocrine glands, cardiac muscle and smooth muscle throughout the body. Sympathetic neurons are innervated by the axons of preganglionic neurons that enter sympathetic ganglia through a discrete, easily accessible sympathetic trunk

fiber bundle. Like synapses on CNS neurons, preganglionic cholinergic synapses form almost entirely (90%) on the dendrites of sympathetic neurons (Forehand, 1985). Unlike synapses on CNS neurons, these cholinergic synapses are the major, if not the only, type of synapse formed on sympathetic neurons, simplifying the study of synapse development (Gibbins and Morris, 2006). The best characterized sympathetic ganglion and the model preparation for my PhD work is the superior cervical ganglion (SCG).

### **1.2.1 Superior Cervical Ganglion**

#### ***1.2.1.1 Location and target innervation of the SCG***

The SCG is the most rostral of the paravertebral chain of sympathetic ganglia and regulates a number of glands, arteries and muscles in the head. The SCG is located at the bifurcation of the common carotid artery and receives afferent innervation from the axons of preganglionic neurons in the intermediate horn of the spinal cord. Ganglionic responses are sent through the external carotid nerve to superficial targets in the face or through the internal carotid nerve to deep targets in the skull. These include superficial targets such as arterial smooth muscles and sweat glands in the face and deep targets such as the iris muscle and pineal gland in the skull (Glebova and Ginty, 2005; Møller and Baeres, 2002). Compared to the immense structural complexity of synaptic connections in the CNS, circuitry in the SCG that control sympathetic responses in the head is remarkably simple.

#### ***1.2.1.2 Innervation of SCG neurons and topography***

Each neuron in mature rodent SCG typically receives synaptic contacts from about 1-5 different preganglionic neurons located in an average of four of eight spinal segments (C8-T7) (Purves and Lichtman, 1978). Preganglionic

neurons in each spinal segment regulate specific end-organ responses. Stimulating the ventral roots of T1 dilates the pupil whereas stimulating the ventral roots of T4 causes vasoconstriction in the ear; T2 and T3 affect both eye and ear but T2 has stronger eye effects than ear and T3 has stronger ear effects than eye (Purves and Lichtman, 1978). This topography of end-organ responses is produced by a precise pattern of preganglionic synapses on individual SCG neurons. A feature of innervation to rodent SCG neurons is that they almost always receive synapses from preganglionic neurons in contiguous spinal segments (Purves and Wigston, 1983). Commonly, one of these spinal segments provides the dominant innervation to the cell, while adjacent segments contribute innervation that diminishes as a function of distance from the dominant segment (Nja and Purves, 1977a, 1977b). In this way, synapses from T1 inputs would dominate an SCG neuron that innervates iris muscle, followed by slightly less involvement of synapses from T2 inputs, then even less from T3 inputs and finally no synapses from T4 inputs.

### **1.3 DEVELOPMENT OF CHOLINERGIC SYNAPSES ON SYMPATHETIC NEURONS**

The sequence of cholinergic synapse formation on autonomic neurons is similar to synapse formation elsewhere in the nervous system and can be roughly separated into three phases: (1) Axon guidance and dendrite outgrowth; (2) Initial contact and synaptic differentiation; and (3) Synapse maturation and refinement.

### **1.3.1 Axon Guidance and Dendrite Outgrowth**

#### ***1.3.1.1 Axon guidance***

At embryonic day 11 (E11), preganglionic neurons extend axons through the ventral roots of the spinal cord into the sympathetic trunk (Rubin, 1985a) and arrive at the SCG at E12-E13 (Rubin, 1985b). Preganglionic axons from rostral spinal segments are the first to arrive in the SCG, followed by axons from more caudal segments (Rubin, 1985a). In the developing chick, these axons can even target and grow towards the location of surgically removed ganglia (Yip, 1987). Moreover, lumbar chick preganglionic neurons that normally innervate pelvic sympathetic ganglia will innervate cervical sympathetic ganglia if these neurons are transplanted to rostral segments of the spinal cord (Yip, 1987). These observations suggest that axons make growth decisions in response to local factors and not in response to long-range guidance cues or cell-autonomous mechanisms. Membrane-bound local factors, such as the ephrin ligands and ephA receptors and longer-range secreted factors, such as the netrins and semaphorins, are critical for axons of CNS neurons to find postsynaptic targets (Garner et al., 2006). Whether these factors also guide preganglionic axons and help them target sympathetic neurons is unknown.

#### ***1.3.1.2 Dendrite outgrowth***

SCG neurons are geometrically complex and have dendritic arbors that are formed from 4-5 primary dendrites and numerous higher order branches (Voyvodic, 1987). A body of work indicates that dendrite growth in SCG is controlled by target-derived nerve growth factor (NGF) and by signals that depend on synaptic activity.

***Nerve growth factor.*** Dendrite growth on SCG neurons is strongly influenced by the size of the target they innervate (Purves and Lichtman, 1978).

Varying the target size has direct effects on the size of sympathetic neuron dendrites. For example, dendrite growth on sympathetic neurons in the SCG is markedly decreased when they innervate surgically reduced submandibular glands. On the other hand, dendrite growth on sympathetic neurons in the SCG is increased when they innervate surgically-ligated, large submandibular glands (Voyvodic, 1989). The reason for this behaviour is that large targets secrete large amounts of NGF that cause sympathetic neurons to grow dendrites (Glebova and Ginty, 2005; Purves and Lichtman, 1978).

NGF binds TrkA receptors at sympathetic nerve terminals and is then thought to be internalized as a receptor-ligand complex and transported back to the cell bodies as a signaling endosome (Glebova and Ginty, 2005). NGF is a required survival factor for sympathetic neurons but also affects a number of processes as these neurons differentiate, including the growth of dendrites. NGF injected into neonatal (Snider, 1988) or adult mice (Ruit et al., 1990) causes dendrites to grow and increases arbor complexity on SCG neurons. Conversely, perturbations that reduce NGF signaling in these neurons, such as sympathetic axotomy or injections of NGF antisera, reduce dendrite growth on sympathetic neurons (Ruit et al., 1990). Presumably, this NGF signaling mechanism serves to match the cholinergic excitation that sympathetic neurons receive with the noradrenergic excitation needed by smooth muscle targets. The larger the target a sympathetic neuron innervates the more preganglionic synapses it needs to drive that target.

The molecular mechanisms that connect NGF-TrkA signaling with dendrite growth are unclear. NGF does not appear to initiate dendrite outgrowth since sympathetic neurons grow dendrites before they innervate targets and receive NGF (Rubin 1985c). However, dendrite growth appears shortly after

preganglionic neurons enter the SCG and form cholinergic synapses, suggesting that activity-dependent signals initiate dendrite growth.

**Activity-dependent signals.** Dendrite growth in the SCG begins at E14 shortly after the first preganglionic axons arrive at the SCG (E12-E13), suggesting that signals that depend on synaptic transmission cause sympathetic neurons to grow dendrites. Support for this idea comes from a study by Valliant and colleagues (2002) where they quantified dendrite growth on cultured sympathetic neurons depolarized by high- $K^+$ . The authors found that levels of phosphorylated microtubule associated protein 2 (MAP2) increase sharply in sympathetic neurons depolarized by high- $K^+$  and correlate strongly with the rate of dendrite growth. The authors go on to show that depolarization causes  $Ca^{2+}$  influx through voltage gated  $Ca^{2+}$  channels, activates  $Ca^{2+}$ /calmodulin activated kinase 2 (CaMKII) and phosphorylates MAP2. They also show that NGF-TrkA signaling can phosphorylate MAP2 via the mitogen-activated protein kinase ERK. Since phospho-MAP2 is well known to bind microtubules tightly and increase their stability, these observations suggest that dendrite growth on sympathetic neurons begins when dendritic microtubules become more stable. Dendrite growth on cultured sympathetic neurons was stalled if either  $Ca^{2+}$ -activated or NGF-activated pathways were inhibited, indicating that a synergy of NGF and activity-dependent signals influence dendrite growth. However, more work will be needed to verify that NGF and activity-dependent signaling work together to grow dendrites on sympathetic neurons *in vivo*. One way to examine the relative contribution of synaptic activity on sympathetic dendrite growth would be to study cholinergic synapses that develop without synaptic activity.

### **1.3.2 Initial Contact and Synaptic Differentiation**

Electrophysiological techniques detect synaptic contacts in developing SCG as early as E13 (Rubin, 1985c), indicating that preganglionic axons form synapses rapidly after they arrive (E12). By E14, synapses can be observed using an electron microscope and are located predominantly on the cell bodies of developing SCG neurons, since many of these neurons have poorly developed dendrites (Forehand, 1985; Rubin, 1985c). The signals that help preganglionic axons contact and form cholinergic synapses on developing sympathetic neurons are not well characterized.

In the CNS, axonal growth cones form transient contacts with target neurons that stabilize if pre and postsynaptic neurons express matching adhesion molecules. Signals that depend on these adhesion interactions then attract vesicles that contain presynaptic release machinery, postsynaptic scaffolds and postsynaptic receptors to the sites of contact to form synapses (Ziv and Garner, 2004). Neuromuscular synapses are formed differently. The postsynaptic apparatus is differentiated by a proteoglycan called agrin that is secreted by motor nerve terminals. In response to agrin, several features of the postsynaptic domain develop, including the appearance of muscle nAChRs (Sanes and Lichtman, 2001). Sympathetic neurons share features of both CNS synapses and neuromuscular synapses: recent evidence points to roles for both agrin (Gingras et al., 2002, 2007) and cell-adhesion molecules in cholinergic synapse assembly (Triana-Baltzer et al., 2006, 2008).

#### **1.3.2.1 Agrin**

At NMJs, agrin is secreted by cholinergic nerve terminals to organize end plates and accumulate nAChRs at postsynaptic domains (Sanes and Lichtman, 2001). For this reason, mice that lack agrin have severely disrupted NMJs that

lack muscle nAChRs and as a result these mice do not survive (Gautam et al., 1996). In contrast, cholinergic synapses on sympathetic neurons still form and function in agrin-null mice, but form in lower numbers, indicating that agrin plays a more subtle role at neuronal cholinergic synapses. In these experiments, Gingras and colleagues (2002) immunostained SCG neuron cultures for a presynaptic marker, synaptophysin, and a postsynaptic marker,  $\beta 2$  nAChR subunit, and counted the colocalization between these two markers to measure synapse numbers. They found 50% fewer colocalized synaptophysin/ $\beta 2$  nAChR puncta in SCG cultures from agrin-null mice compared to cultures from control mice. Moreover, in a follow-up study the authors repeated the same experiment and found 30% fewer colocalized puncta on SCG tissue sections from embryonic agrin-null mice (Gingras et al., 2007). The reduced number of synapses correlated with a ~40% decrease in the peak-size of excitatory postsynaptic potentials (EPSPs) recorded from individual SCG neurons (Gingras et al., 2007). Synapse formation is reduced in these mice, but not eliminated like one would predict given the role for agrin at neuromuscular synapses. Moreover, rapsyn proteins that scaffold muscle nAChRs in response to agrin signaling are undetectable at ganglionic synapses (Feng et al., 1998), again indicating that agrin plays a more subtle role in neuronal cholinergic synapse assembly. One reason for this might be that agrin shares the responsibility of cholinergic synapse assembly on sympathetic neurons with cell-cell adhesion signals.

#### **1.3.2.2 Cell adhesion molecules**

The cell adhesion molecules that induce and align cholinergic synapses in mouse sympathetic ganglia are not well characterized. These molecules are better characterized on chick parasympathetic neurons and recent work identifies

neuroligins, synaptic cell adhesion molecules (SynCAMs) and L1-cell adhesion molecules (L1-CAMs) as important players in this process (Neff et al., 2009). In these studies, the authors overexpressed neuroligins, SynCAMs and L1-CAMs in cultured ciliary neurons and quantified the colocalization of presynaptic synaptophysin with postsynaptic nAChR subunits  $\alpha 3$  or  $\alpha 7$  to measure the ability of these molecules to induce and align cholinergic synapses. They found that synaptophysin clusters were induced among neighbouring neurons in culture that overexpress any of these three molecules (Triana-Baltzer et al., 2006, 2008), indicating that all three are individually sufficient to induce presynaptic specializations. Moreover, when the authors electroporated ciliary neurons *in ovo* with dominant negative constructs against neuroligin, SynCAM or L1-CAM they reduced the number and size of synaptophysin puncta as well as the number of colocalized synaptophysin/ $\alpha 3$  puncta (Triana-Baltzer et al., 2008), further confirming the role for these molecules in organizing presynaptic nerve terminals.

Of these three cell adhesion molecules, the role for neuroligins is best understood. Typically neuroligins reach across the synaptic cleft, interact with presynaptic neurexins (either  $\alpha$  or  $\beta$ -types) and interact with intracellular scaffold proteins to align vesicle release sites with postsynaptic receptors (Ziv and Garner, 2004). Consistent with this, when Conroy and colleagues (2007) overexpressed neuroligins in cultured ciliary neurons they observed an increase in the frequency of spontaneous synaptic events, indicating an increase in the number of functional release sites. Conversely, when they overexpressed dominant-negative constructs to disrupt  $\beta$ -neurexins they reduced the frequency of spontaneous events, indicating that neuroligin-neurexin interactions align

vesicle release sites with postsynaptic nicotinic receptors (Conroy et al., 2007). However, disrupted neuroligin-neurexin interactions do not affect nAChR clusters like they affect presynaptic release sites (Triana-Baltzer et al., 2008) because nAChRs are attached securely to a complex of postsynaptic scaffold proteins.

### **1.3.2.3 Postsynaptic receptor scaffolds**

Sympathetic neurons express several common scaffold molecules at postsynaptic domains to anchor nAChRs and signaling proteins at cholinergic synapses, but the molecular links between nAChRs and scaffolds are not well characterized. Neuronal nAChRs colocalize with the scaffold proteins postsynaptic density 93 (PSD93), SH3 and ankyrin-containing protein (Shank/ProSAP) and guanylate kinase-associated protein (GKAP/SAPAP) (Parker et al., 2004). Of these proteins PSD93 appears to be the most important since synaptic nAChRs are unstable on denervated SCG neurons in mice that lack PSD93 (Parker et al., 2004). How these receptors are targeted to postsynaptic domains and how nAChRs attach to scaffolds is unknown. Experiments with cholinergic synapses on chick ciliary neurons indicates that the large intracellular loop that links transmembrane domains 3 and 4 on nAChR subunits might interact with scaffolds and help target nAChRs to specific domains (Temburni et al., 2000). For example,  $\alpha 3$ -containing nAChRs are directed to the postsynaptic domains underneath nerve terminals, whereas  $\alpha 7$ -containing nAChRs are directed to the extrasynaptic regions. However, chimeric  $\alpha 7$  nAChRs that contain the cytoplasmic loop of  $\alpha 3$  are targeted to domains underneath nerve terminals, suggesting that residues in the loop region direct nAChRs to specific postsynaptic domains. More work will be needed to identify what these residues

are, and how they connect  $\alpha 3$ -containing receptors to the main scaffold molecules PSD93 and PSD95.

### **1.3.3 Synapse Maturation and Refinement**

Synapse maturation and refinement elsewhere in the nervous system are typically under the control of activity dependent mechanisms (Katz and Shatz, 1996). Refinement is well documented in the SCG: At birth, several (~7-8) preganglionic axons innervate individual SCG neurons but during early postnatal development these axons are gradually eliminated until only a few (1-3) persist (Purves and Lichtman, 1978). This refinement occurs without any preganglionic cell death and is instead produced by a coordinated rearrangement of connections in the SCG. Furthermore, refinement does not begin until birth (Purves and Lichtman, 1980) when the sympathetic nerves are strongly driven; the sympathetic nervous system is not strongly driven *in utero* since homeostatic processes such as thermoregulation are controlled by the mother's body. This strongly suggests that activity-dependent mechanisms play a role in the maturation and refinement of cholinergic synaptic connections in the SCG. This role has not been examined directly.

However, one activity-dependent factor that is known to influence cholinergic synapses in SCG is brain derived neurotrophic factor (BDNF) (Causing et al., 1997). In this study, Causing and colleagues (1997) immunostained SCG for synapsin1a, a protein involved in vesicle release, and compare the number of synapsin1a-positive puncta between the SCG of mice that overexpress BDNF and the SCG of BDNF-null mice. The authors report that synapsin1a-positive puncta increase dramatically on sympathetic neurons that

overexpress BDNF, but are decreased on sympathetic neurons that lack BDNF. These results suggest that BDNF released by sympathetic neurons causes preganglionic neurons to form nerve terminals, and possibly synapses, but more work will be needed to verify this idea.

## **1.4 CHOLINERGIC SYNAPTIC TRANSMISSION**

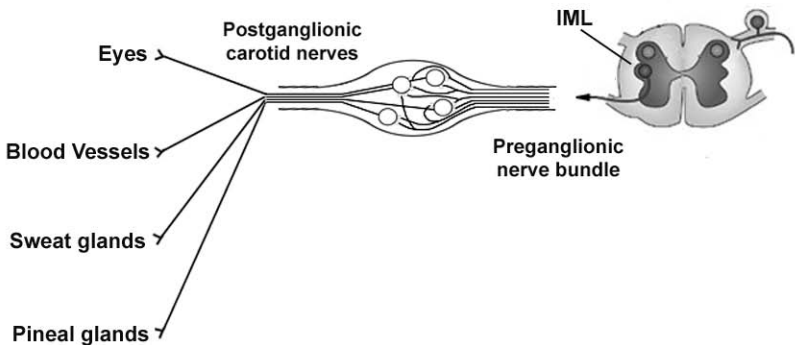
Cholinergic synapses are well understood in terms of structure and function. We have identified many of the proteins involved in acetylcholine synthesis and nAChR function. Briefly, nerve terminals become excited when depolarized by action potentials and release vesicles filled with acetylcholine (ACh) to fuse with specialized active zones on the terminal membrane. Once they fuse, ACh is then released into the synaptic cleft where it binds to nAChRs that are anchored at postsynaptic density, opens these receptors and depolarizes sympathetic neurons (Figure 1.1).

### **1.4.1 Presynaptic Nerve Terminals**

#### ***1.4.1.1 Choline acetyltransferase***

In nerve terminals, ACh is synthesized from choline and acetyl-coenzymeA (acetyl-CoA) by choline acetyltransferase (ChAT). ChAT is a highly-conserved 70kDa protein that is present in two forms at cholinergic nerve terminals (Oda, 1999; Wu and Hersh, 1994). Site-directed mutagenesis experiments have revealed that Histidine 426 of ChAT is an essential residue that catalyzes the acid/base reaction that produces ACh from choline and acetyl-CoA (Carbini and Hersh, 1993). A similar study showed that Arginine 452 of rat ChAT binds the 3' phosphate of coenzyme A (Wu and Hersh, 1995), but the site

# A Superior Cervical Ganglion



# B

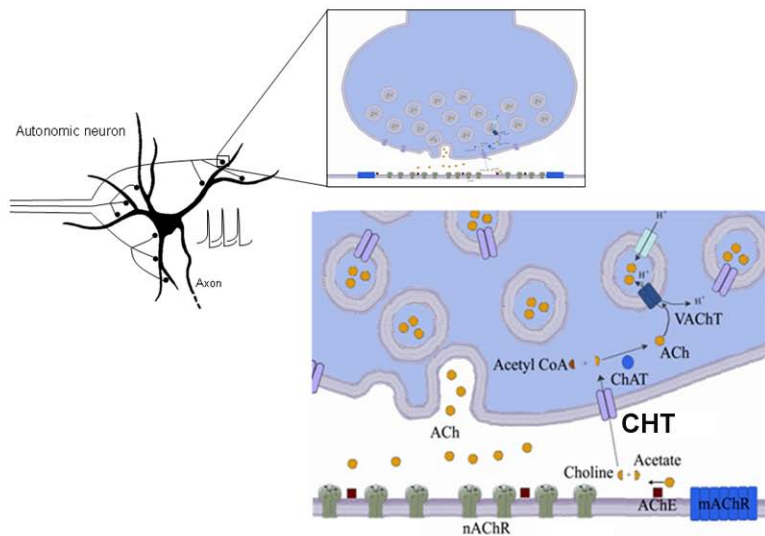


Figure 1.1

**FIGURE 1.1** The superior cervical ganglion and cholinergic synaptic transmission. **A** A schematic drawing of the superior cervical ganglion (SCG) and its innervation. The SCG is innervated by cholinergic preganglionic neurons located in the intermediate lateral horn of the spinal cord. SCG neurons are noradrenergic motor neurons that regulate a variety of targets in the head including the iris muscle, blood vessels in the ear, sweat glands on the face and pineal glands. Preganglionic axons enter the SCG through a discrete, easily accessible preganglionic fiber bundle and postganglionic neurons exit the SCG through an easily accessible postganglionic carotid nerve. **B** Adult SCG neurons receive cholinergic synapses predominantly on their dendrites. Nerve terminals become excited when depolarized by action potentials and release vesicles filled with acetylcholine (ACh) to fuse with specialized active zones on the terminal membrane. Once they fuse, ACh is then released into the synaptic cleft where it binds to nAChRs that are anchored at postsynaptic density, opens these receptors and depolarizes sympathetic neurons (Figure 1.1 B).

that binds choline on ChAT has not been identified. The general consensus is that the majority of ChAT (~80% of enzyme activity) exists as a soluble protein but a portion (~20% of enzyme activity) is bound to the membrane (Oda, 1999; Wu and Hersh, 1994). ChAT is thought to be attached to membrane phospholipids via a glycosylphosphatidylinositol (GPI) linkage (Carroll, 1994; Smith and Carroll, 1993). Both cytoplasmic and membrane associated versions of ChAT can synthesize ACh *in vitro*, but the functional significance of these two versions *in vivo* is unclear (Oda, 1999). An attractive idea is that soluble ChAT is bound to membranes so that it synthesizes ACh locally at synaptic vesicle membranes to be easily pumped into vesicles by the vesicular acetylcholine transporter. This idea is supported by immuno-electron microscopy (immuno-EM) experiments that show ChAT immunoreactivity to be localized predominantly to synaptic vesicles (Martinez-Murillo et al., 1989). Although a more recent study disputes this claim and instead shows broad ChAT immunoreactivity that fills the entire nerve terminal (Lan et al. 1995). Clearly more work is necessary to identify why ChAT is segregated into these two cellular compartments.

#### **1.4.1.2 Vesicular acetylcholine transporter**

Newly synthesized ACh is concentrated in synaptic vesicles by the vesicular ACh transporter (VAChT). VAChT is synthesized as a 500-600 aa protein that has 12 putative transmembrane domains based on its amino acid sequence (Eiden, 1998). Immuno-EM experiments using antibodies directed against the c-terminus of VAChT indicate that the c-terminus faces the cytosol and the n-terminus faces the vesicle lumen (Eiden, 1998; Weihe et al., 1998). VAChT couples the energy of transporting protons from the vesicle lumen, down their concentration gradient to the cytosol, with the transport of ACh out of the cytosol into the vesicle lumen. VAChT has a surprisingly low  $K_m$  for ACh,

approximately 5mM, suggesting a high concentration of ACh in nerve terminals (Eiden, 1998). The gene that encodes VACht was identified some 15 years ago in *torpedo californica* (Varoqui et al., 1994) and was then quickly identified in rat (Usdin et al., 1995) and human (Erickson et al., 1994). Surprisingly, the entire VACht coding region is contained within the first intron of the ChAT gene (Eiden, 1998). The 80kb region of the genome that codes for VACht and ChAT genes, called the cholinergic gene locus, also contains regulatory sequences that express both enzymes simultaneously in cholinergic neurons (Eiden, 1998; Weihe et al., 1998).

#### **1.4.1.3 The cholinergic gene locus**

ChAT and VACht proteins are nearly always produced together and produced early in the differentiation of cholinergic neurons by local or target derived factors (Lecomte et al., 2005; Weihe et al., 1998). Yet the way these two transcripts are produced in mammals is complicated. The structure of the nematode cholinergic gene locus is similar to mammals and in these animals the two genes are transcribed together and then separated by mRNA splicing events (Eiden, 1998). A similar mechanism may generate VACht and ChAT mRNA transcripts in rodents since VACht and ChAT mRNAs that contain a common first exon have been isolated from rodent cholinergic neurons (Bejanin et al., 1994; Eiden, 1998). However, VACht and ChAT mRNAs that contain this common exon are the least abundant of five different ChAT mRNAs and four different VACht mRNAs (Hahm et al., 1997), suggesting that rodent cholinergic neurons favour other methods of producing ChAT and VACht mRNA. This idea is supported by the observation that ChAT transcription can start from 4 different start sites and VACht transcription from at least 3 of these sites (Eiden, 1998). It is not known which of these sites is used most frequently by cholinergic neurons.

All ChAT mRNAs produce the same ChAT protein and all VAcHT mRNAs produce the same VAcHT protein. Given this, it is likely that splicing-induced differences among ChAT mRNAs and splicing-induced differences among VAcHT mRNAs affect their translation or specify their subcellular location. Although these enzymes are important for proper signaling by cholinergic signaling, the rate limiting step for ACh synthesis in nerve terminals is the uptake of choline from the synaptic cleft.

#### **1.4.1.4 The high-affinity choline transporter**

Historically, much of what is known about ACh synthesis and release from cholinergic nerve terminals was first worked out in sympathetic preganglionic nerve terminals (Birks and McIntosh, 1961; Tuček, 1978). Choline is produced in the synaptic cleft by a membrane-bound acetylcholinesterase that rapidly cleaves ACh into choline and acetate. In order to resynthesize acetylcholine and sustain transmission, nerve terminals must recover choline from the synaptic cleft. The transport of choline from the synaptic cleft into the terminal lumen is the rate limiting step for ACh synthesis and is mediated by the high affinity choline transporter (Ferguson and Blakely, 2004; Tuček, 1978). High affinity choline uptake was first described in 1961 by Birks and McIntosh but it took another 40 years for the gene encoding the high-affinity choline transporter (CHT) to be cloned (Apparsundaram et al., 2000, 2001; Okuda et al., 2000; Okuda and Haga, 2003). The CHT gene in mice is ~25kb in length and contains nine exons. The gene codes for a transmembrane protein made up of 13 transmembrane domains with an n-terminus that faces the synaptic cleft and a cytoplasmic c-terminus (Ferguson and Blakely, 2004). Choline transport into the terminal lumen by CHT depends on extracellular Na<sup>+</sup> and Cl<sup>-</sup>, a feature that initially put CHT in the family of Na<sup>+</sup>/Cl<sup>-</sup> neurotransmitter-transporters that include the transporters

for  $\gamma$ -amino butyric acid (GABA), serotonin and dopamine. However, CHT does not share any appreciable homology with any neurotransmitter transporters, nor is it similar to the low-affinity choline transporter that transports choline for biosynthesis pathways (Ferguson and Blakely, 2004). Instead, CHT belongs to the SLC5 family of mammalian  $\text{Na}^+$ -dependent transporters such as glucose transporters that help intestinal and renal cells reabsorb water and glucose (Ferguson and Blakely, 2004).

Recently, researchers showed that CHT  $V_{\text{max}}$  on cholinergic synaptosomes increases in response to depolarization, is sensitive to botulinum neurotoxin C and to extracellular calcium (Ferguson et al., 2003). These results indicate that CHT is located on a reserve pool of synaptic vesicles that are recruited to the plasma membrane under conditions of high-frequency or sustained firing (Ferguson and Blakely, 2004). CHT would normally be internalized in clathrin-coated vesicles but active mechanisms keep the rate of CHT externalization high in order to keep CHT at the membrane (Ribeiro et al., 2005, 2006). The use-dependent delivery of CHT to membranes is an attractive mechanism because it increases choline transport when nerve terminals need to replenish their stores of ACh. Without CHT, nerve terminals would become rapidly depleted of ACh and synaptic transmission would fail. For this reason, mice that lack CHT die shortly after birth because the nerve terminals at their NMJs cannot re-synthesize ACh (Ferguson et al., 2004).

#### ***1.4.1.5 Regulation of high-affinity choline transporters***

Given its vital role in cholinergic synaptic transmission, it is surprising how little we know about the signals that regulate CHT in cholinergic neurons. The CHT gene is not part of the cholinergic gene locus, suggesting that CHT levels are regulated by signals that are different from those that regulate ChAT and

VACHT levels. In the mouse striatum, only half of VACHT-positive vesicles contain CHT (Ferguson and Blakely, 2004). Since both proteins are targeted to synaptic vesicles this observation suggests that the levels of CHT are regulated later in cholinergic synapse development than VACHT levels. The mechanisms that express CHT at nerve terminals are unknown. However, several studies indicate that CHT levels are sensitive to perturbations of cholinergic synaptic transmission (Bazalakova and Blakely, 2006).

Mice that are heterozygous for a deletion in the gene that encodes ChAT have half as much ChAT protein and would therefore be predicted to have lower levels of ACh at synapses. In fact, ChAT heterozygote mice have normal ACh levels because they increase the levels of CHT at nerve terminals (Brandon et al., 2004). Mice that lack acetylcholinesterase are forced to use the less-efficient butyrylcholinesterase to breakdown ACh and would also be predicted to have lower levels of ACh due to lower synaptic choline concentrations. Yet again, these mice have normal ACh levels because they increase the levels of CHT at nerve terminals (Volpicelli-Daley et al., 2003). Mice that overexpress human acetylcholinesterase have 4x the normal levels of this enzyme at cholinergic synapses and would be predicted to have reduced cholinergic transmission since ACh would be cleaved too quickly in the synaptic cleft. Yet again, these mice compensate and have normal cholinergic signaling, in part, from an increase in CHT levels at nerve terminals (Beeri et al. 1997). In all of these cases, neurons compensate for reduced cholinergic signaling by increasing CHT levels in nerve terminals to accelerate choline transport and sustain ACh synthesis. But what mechanisms signal to increase the levels of CHT?

One clue is that cholinergic synapses require a long maturation period in order to develop the ability to sustain ACh output (Letinsky, 1974; Pilar et al.,

1981; Polo-Parada et al., 2001, 2004, 2005; Rafuse et al., 2000). Given that high-affinity choline uptake is the rate limiting step for ACh synthesis and given that CHT is particularly important for sustaining ACh output, it is likely that the nerve terminals at these synapses are increasing the levels of CHT. Since CHT appears to be regulated late in cholinergic synapse maturation, separate from VAChT and ChAT, and since CHT levels compensate for perturbed cholinergic signaling, is it possible that CHTs are expressed at nerve terminals in response to signals that depend on synaptic activity? If true, this would mean that cholinergic synapses on inactive neurons, such as those that lack postsynaptic nAChRs, would be unable to signal presynaptic terminals to express CHT and would result in nerve terminals that cannot sustain ACh synthesis.

## **1.4.2 Postsynaptic Domain**

### ***1.4.2.1 Nicotinic acetylcholine receptors***

**Structural features.** Of the 11 neuronal nAChR subunit genes identified, five are expressed by rodent SCG neurons:  $\alpha 3$ ,  $\alpha 5$ ,  $\alpha 7$ ,  $\beta 2$ , and  $\beta 4$  (De Koninck and Cooper, 1995; Mandelzys et al., 1994). All subunits share structural features and all encode polypeptides with a conserved extracellular large n-terminal domain, three conserved transmembrane domains, a cytoplasmic loop that varies in size and is thought to connect subunits to scaffolds and a fourth transmembrane domain with a relatively short and variable extracellular c-terminal sequence (Albuquerque et al., 2009) (Figure 1.2A). The two main classes of subunits, termed alpha and beta are distinguished by a pair of cysteines in the n-terminus of alpha subunits. The paired cysteine residues are a critical feature of these receptors since they connect two parts of the extracellular

domain to form the ACh-binding pocket (Albuquerque et al., 2009; Leonard and Bertrand, 2001). This paired cysteine motif also forms the binding pocket for ionotropic GABA receptors, glycine receptors and serotonergic receptors. Together with nAChRs, these receptors form a superfamily of cys-loop receptors.

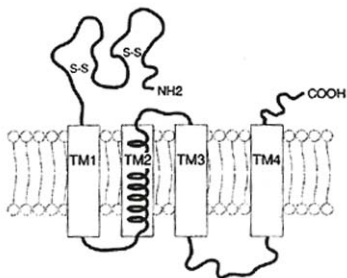
Neuronal nAChRs are cation-selective, exhibit considerable calcium permeability and display strong inward rectification. Earlier work from our lab demonstrated that inward rectification is produced by an interaction between intracellular polyamines and negatively charged residues at an intermediate position on the second transmembrane domain of each nAChR subunit (Haghighi and Cooper, 1998, 2000). At positive membrane potentials, polyamines are attracted to the receptor pore and become immobilized by negatively charged residues on each subunit that together form a ring at the narrowest region of the pore (Figure 1.2C). However, at negative membrane potentials the pore is unplugged because polyamines are electrostatically repulsed from the membrane. Interestingly, when Haghighi and Cooper (2000) mutated these critical negative residues to neutralize their charge, they observed significant reductions in the single channel conductance and calcium permeability of these receptors. This observation predicts that natural mutations in this region of the channel or perhaps post-translational mechanisms that modify this region of the channel would both reduce receptor function. Whether such mutations exist or whether post-translational mechanisms can affect this region of nAChRs on sympathetic neurons unknown. If nAChRs are altered and inactivated by such mechanisms it would depress synaptic transmission through sympathetic ganglia.

***A cluster of nAChR subunit genes.*** In mice, the  $\alpha 3$  subunit gene is located on chromosome 9 and is part of a gene cluster that includes the  $\beta 4$  and

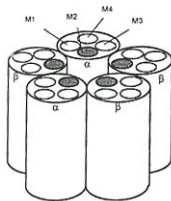
$\alpha 5$  subunit genes (Boulter et al., 1990). The tight spatial organization of this gene cluster suggests that regulatory elements are shared by the three genes. Indeed, elements in the 3' region of  $\beta 4$  and elements in the region between  $\alpha 3$  and  $\beta 4$  coordinate the expression of the  $\alpha 3$  and  $\beta 4$  genes (Gotti and Clementi, 2004). For example, an enhancer that co-ordinately activates  $\alpha 3$  and  $\beta 4$ , called  $\beta 4 3'$ , is located in the terminal portion of the  $\beta 4$  gene (McDonough and Deneris, 1997; Xu et al., 2006). The  $\alpha 5$  subunit is transcribed in the opposite direction to  $\alpha 3$  and  $\beta 4$  and is thought to have its own unique promoter and enhancer elements (Gotti and Clementi, 2004; Leonard and Bertrand, 2001). It is likely that  $\beta 4$  subunits are the main  $\beta$  subunits used by sympathetic neurons to form nAChRs because sympathetic neurons from mice with a disruption in the  $\beta 4$  gene have significantly reduced ACh-evoked currents (Xu et al., 1999b). That currents are present at all indicates that either  $\beta 2$  is upregulated to compensate for the loss of  $\beta 4$  or sympathetic neurons normally express low levels of  $\beta 2$ .

***Composition of postsynaptic receptors.*** For most neuronal nAChRs, 2  $\alpha$  subunits must be combined with 3  $\beta$  subunits to form a functional receptor (Cooper, 1991) (Figure 1.2B). The exceptions to this stoichiometry are the  $\alpha 7$  and  $\alpha 9$  subunits that form homomeric pentamers without incorporating any  $\beta$  subunits. Homomeric  $\alpha 7$ -containing nAChRs bind the muscle nAChR blocker,  $\alpha$ -bungarotoxin ( $\alpha$ bgt) (Couturier et al., 1990; Drisdell and Green, 2000), and in rat hippocampus are located on nerve terminals where they can increase intraterminal  $\text{Ca}^{2+}$  and increase glutamate release (Sharma et al., 2003, 2008). The precise composition of the postsynaptic nAChRs on sympathetic neurons is unknown; work from our lab indicates that the  $\alpha 3$  subunit is the main ligand-binding subunit expressed by these neurons.

A



B



C

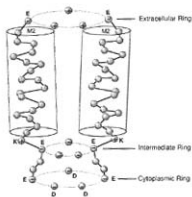


Figure 1.2

**FIGURE 1.2** nAChR subunit structure, stoichiometry and features of the pore region. **A** All subunits share structural features: a conserved extracellular large n-terminal domain, three conserved transmembrane domains (TMs), a cytoplasmic loop that varies in size and is thought to connect subunits to scaffolds and a fourth transmembrane domain with a relatively short and variable extracellular c-terminal sequence. **B** Most neuronal nAChRs are heteropentamers formed from 2  $\alpha$  subunits and 3  $\beta$  subunits. The second transmembrane domain of each subunit (M2) lines the pore region. **C** A schematic drawing of the negatively charged ring of glutamic acid residues that produce rectification. Negatively charged residues at an intermediate position on nAChR subunit form a ring at the narrowest region of the pore to immobilize polyamines and produce rectification. (Adapted from Changeux JP. Sci Am. 1993 Nov;269(5):58-62.)

Using RNase protection assays to measure RNA levels from cultured sympathetic neurons at different times following dissociation, DeKoninck and Cooper (1995) showed that the most abundant transcripts after a week in culture were  $\alpha 3$  and  $\beta 4$ . Furthermore, they showed that the levels of  $\alpha 3$  mRNA increase as a function of days in culture, whereas the levels of  $\beta 4$  mRNA remained constant, indicating that  $\beta$  subunits are in excess and suggesting that neurons regulate the number of nAChRs at the membrane by regulating  $\alpha 3$ . In a separate study, our lab measured the levels of mRNA in developing sympathetic neurons *in vivo* (Mandelzys et al., 1994). RNase protection assays on lysates of rodent SCG taken at birth, at postnatal day 7 (P7) and at P14 revealed that the levels of  $\alpha 3$  and  $\alpha 7$  transcripts increase dramatically over the first two postnatal weeks, whereas the levels of  $\beta 2$ ,  $\beta 4$  and  $\alpha 5$  remain relatively constant (Mandelzys et al., 1994). Moreover, the increases in the amount of  $\alpha 3$  and  $\alpha 7$  transcripts correlate well with increases in ACh-evoked current densities on sympathetic neurons isolated acutely from the same time points. The role of  $\alpha 7$  receptors on mouse sympathetic neurons is poorly understood. Clearly these receptors are expressed by mouse sympathetic neurons but given that  $\alpha$ bgt cannot block rodent ganglionic transmission (Brown and Fumagalli, 1977; Chiappinelli and Dryer, 1984) they are unlikely to mediate fast synaptic transmission. Given these results and given that  $\alpha 3$  and  $\beta 4$  are regulated together, a more likely scenario is that postsynaptic nAChRs on sympathetic neurons are composed predominantly of  $\alpha 3\beta 4$  receptors.

#### **1.4.2.2 Muscarinic receptors**

In contrast to nAChRs that are focally concentrated at synapses, muscarinic receptors on rodent sympathetic neurons are widely distributed over

their somatic and dendritic surfaces, with higher densities on the soma (Ramcharan and Matthews, 1996). Muscarinic receptors activate when large amounts of ACh released from nerve terminals spills over into extrasynaptic regions (Brown and Selyanko, 1985). Five muscarinic genes have been identified in mammals, M1 – M5, and are divided into two functional classes: the even numbered muscarinic receptors are coupled preferentially to  $G_{i/o}$  pathways and the odd numbered muscarinic receptors are coupled preferentially to  $G_q$  (Brown et al., 1997). The class of muscarinic receptors expressed by sympathetic neurons is not clear (Brown et al., 1997). Stimulation of M1 receptors on cultured sympathetic neurons produces a small but sustained inward current called the M-current (Brown et al., 1997). It is thought that signals downstream of M1 close a class of KCNQ2/3  $K^+$  channels (Wang et al., 1998)

#### **1.4.2.3 Acetylcholinesterase**

Acetylcholinesterase is critical to terminate cholinergic signaling, and it does so by rapidly cleaving ACh into choline and acetate. Acetylcholinesterase is anchored to the membrane through a GPI-linkage. Individual molecules can multimerize and form catalytically active dimers, tetramers or dodecamers (Soreq and Seidman, 2001). Rodent SCG neurons express acetylcholinesterase predominantly on their extracellular membranes but also express some cholinesterase on intracellular membranes (Goudou et al., 1985). Extracellularly expressed acetylcholinesterase is distributed widely over the cell bodies of sympathetic neurons *in vitro* and *in vivo* and is found predominantly as a tetramer (Fernandez et al., 1996).

#### **1.4.2.4 Nicotinic receptors and dysautonomias**

The normal development and function of cholinergic synapses on sympathetic neurons is important because cholinergic synaptic transmission links the activity of CNS homeostatic command centers with sympathetic homeostatic control of the body. Consistent with this, people who develop antibodies against  $\alpha 3$ -type nAChRs develop autoimmune autonomic ganglionopathies (AAG) (Vernino et al., 2008). These patients present with severe, widespread autonomic failure that reaches peak severity within a few days or weeks. Recovery is slow and incomplete with many symptoms that persist throughout life. Sympathetic failure is commonly manifested as cardiovascular abnormalities such as orthostatic hypotension, and thermoregulatory abnormalities such as an inability to sweat (Vernino et al., 2008).

Experimental AAG can be induced in rabbits by immunization with ganglionic nAChRs (Vernino et al., 2003) and can be induced in mice by injections of IgG from an affected individual (Vernino et al., 2004). Both species develop the features of autonomic failure similar to those seen in AAG patients, including gastrointestinal dysmotility, dilated and poorly responsive pupils, decreased lacrimation, reduced heart rate variability, dilated bladder, reduced levels of plasma catecholamines, and hypotension. Moreover, rabbits immunized with ganglionic nAChRs develop chronic AAG. Remarkably, neurons in autonomic ganglia are largely spared, and post-ganglionic nerve fibers remain anatomically intact (Vernino et al., 2009). Dysautonomias in AAG result from a loss of functional  $\alpha 3$ -containing nAChRs rather than widespread degenerative damage to autonomic ganglia (Vernino et al., 2004).

For this reason, antibodies isolated from the serum of patients with AAG have direct effects on the ganglionic  $\alpha 3$  nAChRs *in vitro* and *in vivo* (Vernino et

al., 2004, 2009; Wang et al., 2007). Preliminary experiments reveal that the antibodies produced by these patients specifically target  $\alpha 3$  subunits and are able to reduce ACh-evoked currents on cell lines that express  $\alpha 3\beta 4$  nAChRs (Wang et al., 2007). Furthermore, a recent study reveals that synaptic transmission on acutely isolated mouse sympathetic ganglia is significantly depressed when exposed to autoantibodies (Vernino et al., 2004, 2009). Taken together, these results indicate that  $\alpha 3$ -containing nAChRs are critical for normal autonomic function and homeostasis.

The progression of many diseases and syndromes involves the development of dysautonomias like those found in patients with AAG. One increasingly common example is diabetes. Dysautonomias are common in diabetes and are often overlooked but have serious consequences on the quality of life experienced by patients (Vinik et al., 2003). Common symptoms include resting tachycardia, orthostasis, exercise intolerance, intraoperative cardiovascular liability and silent myocardial infarction (Vinik and Zeigler, 2007). Diabetics do not develop dysautonomias as a result of autoantibodies against  $\alpha 3$ -containing nAChRs (Winston and Vernino, 2009), but are instead thought to develop dysautonomias as a result of free radical damage to the autonomic nerves, produced by elevated serum glucose (Brownlee, 2001; Tomlinson and Gardiner, 2008).

Given that targeted disruption of  $\alpha 3$  subunits in humans produces AAG and given that nAChRs on sympathetic neurons are targeted to the mitochondria rich soma-dendritic domain (De Biasi, 2002), it is possible that  $\alpha 3$ -containing nAChRs are inactivated by elevated reactive oxygen species (ROS) during

diabetes (Brownlee, 2005), depressing synaptic transmission and contributing to the progression of dysautonomias.

## **1.5 SUMMARY OF THE PROBLEM AND APPROACH**

There are several unresolved issues about how cholinergic synapses form and how these synapses function. For my PhD, I have worked on two issues: (1) The role of activity in cholinergic synapse formation on neurons; and (2) The role of ROS produced by diabetic hyperglycemia and their impact on nAChR function on sympathetic neurons.

### **1.5.1 The Role of Activity in Cholinergic Synapse Formation on Neurons**

For my PhD, I focused on several questions about the role of synaptic activity in cholinergic synapse formation and maturation:

1. Do cholinergic synapses require synaptic activity to form? If not, do they require synaptic activity to persist?
2. Given that cholinergic synapses require a relatively long maturational period, do activity-dependent signals play a role in this process? If so, what are the mechanisms that are responsible for this process?
3. Do postsynaptic scaffold proteins that anchor nAChRs require synaptic activity to assemble?
4. Do dendrites require synaptic activity to grow and develop normally?
5. Do nerve terminals require signals that depend on synaptic activity to express choline transporters and sustain ACh output?
6. What is the composition of postsynaptic nAChRs that mediate synaptic transmission on autonomic neurons?

During my PhD, I have worked on all of these issues and have answered questions 1-3 and 5-6 in two studies that are presented in this thesis as chapters 2 and 3. I am in the process of completing a study based on question 4 and have not included it in this thesis.

### **1.5.2 The Role of ROS Produced by Diabetic Hyperglycemia and nAChR**

#### **Function on Sympathetic Neurons**

We had several questions about this process:

1. Can reactive oxygen species inactivate nAChRs?
2. If question 1 is true, do they inactivate nAChRs *in vivo* and depress synaptic transmission?
3. How do ROS inactivate nAChRs?
4. If questions 1 and 2 are true, can ROS produced by diabetic hyperglycemia also inactivate nAChRs, depress synaptic transmission and produce dysautonomias?

During my PhD, I have worked on all four of these issues and have answered questions 1-4 in two studies that are included in this thesis as chapters 4 and 5. Chapter 4 is published and Chapter 5 is a submitted manuscript.

### **1.5.3 Experimental Approach**

The ideal model to study both of these problems would be to examine sympathetic neurons that do not express nAChRs. With such a model, I could (1) study the postnatal development of silent cholinergic synapses to learn more about the role of activity-dependent signals in cholinergic synapse formation; and (2) use the nAChR-null sympathetic neurons to investigate structural features of nAChRs that might be disrupted by ROS.

Several lines of evidence, presented above, indicate that the postsynaptic nAChRs must contain an  $\alpha 3$  subunit in order to be expressed. Therefore, one potentially feasible way to remove nAChRs from sympathetic neurons would be to study sympathetic neurons from mice with a disruption in the  $\alpha 3$  nAChR subunit gene.

These mice have been generated by Xu and colleagues (1999a) and survive birth with severe dysautonomias. Mice that lack  $\alpha 3$  have several dysautonomias that include extreme bladder enlargement, dribbling urination, urinary stones and widely dilated pupils that are unresponsive to light (Xu et al., 1999a). These phenotypes strongly suggest that the  $\alpha 3$  subunit is an essential component of postsynaptic nAChRs on autonomic ganglia and suggest that without  $\alpha 3$  cholinergic synaptic transmission on sympathetic neurons is abolished.

## CHAPTER 2:

# A NULL MUTATION FOR THE $\alpha 3$ NICOTINIC ACETYLCHOLINE (ACh) RECEPTOR GENE ABOLISHES FAST SYNAPTIC ACTIVITY IN SYMPATHETIC GANGLIA AND REVEALS THAT ACh OUTPUT FROM DEVELOPING PREGANGLIONIC TERMINALS IS REGULATED IN AN ACTIVITY-DEPENDENT RETROGRADE MANNER

## FOREWORD

### Background and Rationale

Several lines of evidence indicate that synaptic activity is important for synapses to mature and for synapses to persist. These issues have been difficult to test directly because mice that lack synaptic activity die embryonically or die shortly after birth. In this chapter I investigate cholinergic synapses on autonomic ganglia from  $\alpha 3$  KO mice.

### Hypothesis

I hypothesize that (1)  $\alpha 3$  subunits are essential for sympathetic neurons to express functional nAChRs and for fast-synaptic transmission; (2) that morphologically normal, electrophysiologically silent cholinergic synapses will form on sympathetic neurons from  $\alpha 3$  KO mice but will be unable to persist; (3) That cholinergic nerve terminals at these electrophysiologically silent synapses will be functionally immature.

### **Experimental Outline**

To test the first hypothesis I will dissociate sympathetic neurons from neonatal SCG and use whole-cell patch clamp techniques to see whether the loss of  $\alpha 3$  subunits disrupts functional nAChRs. If cultured neurons lack functional nAChRs, I will record intracellularly from sympathetic neurons using sharp microelectrodes while stimulating preganglionic nerves to see whether the loss of functional nAChRs abolishes cholinergic synaptic transmission. These experiments should establish the model of electrophysiologically silent cholinergic synapses. To test the second hypothesis, I will use observe the ultrastructure of cholinergic synapses in  $\alpha 3$ -null mice. To test the third hypothesis, I will immunostain  $\alpha 3$  KO SCG tissue sections for presynaptic release proteins and ACh synthesis enzymes. Finally I will measure functional maturity of the cholinergic nerve terminals by comparing extrasynaptic muscarinic responses recorded intracellularly from sympathetic neurons in  $\alpha 3$  KO SCG with those on sympathetic neurons from WT SCG.

## ABSTRACT

In vertebrates, synaptic activity exerts an important influence on the formation of neural circuits, yet our understanding of its role in directing presynaptic and postsynaptic differentiation during synaptogenesis is incomplete. This study investigates how activity influences synaptic differentiation as synapses mature during early postnatal life. Specifically, we ask what happens to presynaptic terminals when synapses develop without functional postsynaptic receptors and without fast synaptic transmission.

To address this issue, we investigated cholinergic nicotinic synapses in sympathetic ganglia of mice with a null mutation for the  $\alpha 3$  nicotinic ACh receptor gene. Disrupting the  $\alpha 3$  gene completely eliminates fast excitatory synaptic potentials on postganglionic sympathetic neurons, establishing a crucial role for  $\alpha 3$ -containing postsynaptic receptors in synaptic transmission. Interestingly, the preganglionic nerve terminals form morphologically normal synapses with sympathetic neurons, and these synapses persist without activity in postnatal animals. Surprisingly, when stimulating the preganglionic nerve at physiological rates, we discovered a significant decrease in ACh output from the presynaptic terminals in these  $\alpha 3^{-/-}$  sympathetic ganglia. We show that this decrease in ACh output from the presynaptic terminals results, in part, from a lack of functional high-affinity choline transporters. We conclude the following: (1) fast synaptic transmission in mammalian SCG requires  $\alpha 3$  expression; (2) in the absence of activity, the preganglionic nerve forms synapses that appear morphologically normal and persist for several weeks; and (3) to sustain transmitter release, developing presynaptic terminals require an activity-dependent retrograde signal.

## INTRODUCTION

Synaptogenesis is directed by both activity-independent and activity-dependent mechanisms (Sanes and Lichtman, 1999; Tao and Poo, 2001; Cohen-Cory, 2002). Strong support for this view comes from recent studies on embryonic mice that lack proteins essential for transmitter release (Verhage et al., 2000; Misgeld et al., 2002; Washbourne et al., 2002). However, because such embryos die at birth, it has been difficult to determine the longer term consequences of the absence of activity during synapse formation and differentiation in postnatal animals.

To address this issue, we investigate the development of synapses in sympathetic ganglia of mice because sympathetic activity is not essential for embryonic development (Crowley et al., 1994; Smeyne et al., 1994; Fagan et al., 1996). One can, therefore, investigate postnatal animals carrying mutations that disrupt ganglionic synaptic transmission and determine how synapses differentiate and mature in these ganglia without synaptic activity. Specifically, we ask the following: (1) whether the presynaptic terminals establish morphological synapses when postsynaptic receptor function is disrupted; and (2) as synapses form, whether the absence of postsynaptic activity in sympathetic neurons affects the functional properties of the presynaptic terminals.

In vertebrates, neuronal nicotinic ACh receptors (nAChRs) mediate fast excitatory synaptic transmission between cholinergic preganglionic axons and postsynaptic sympathetic neurons (Role, 1992; Sargent, 1993; McGehee and Role, 1995). Five nAChR genes are expressed by rodent sympathetic neurons:  $\alpha 3$ ,  $\alpha 5$ ,  $\alpha 7$ ,  $\beta 2$ , and  $\beta 4$  (Mandelzys et al., 1994; De Koninck and Cooper, 1995); however, the precise subunit composition of the postsynaptic receptors is

unknown. In avian autonomic ganglia, both  $\alpha 3$ -containing and  $\alpha 7$ -containing receptors contribute to fast synaptic transmission (Zhang et al., 1996; Ullian et al., 1997; Chang and Berg, 1999); however, the role for  $\alpha 7$ -containing receptors in synaptic transmission in mammalian sympathetic ganglia is less well understood. We have shown previously that the developmental increase in ACh-evoked current densities on sympathetic neurons correlates well with the increase in  $\alpha 3$  mRNA expression (Mandelzys et al., 1994; De Koninck and Cooper, 1995). Moreover, in ganglia,  $\alpha 3$ -containing receptors are located postsynaptically (Loring et al., 1988), and preganglionic neurons to the superior cervical ganglia (SCG) do not express  $\alpha 3$  (Wada et al., 1989). Based on these observations, we reasoned that deleting the  $\alpha 3$  gene (Xu et al., 1999) would seriously disrupt postsynaptic activity in the SCG without altering presynaptic function.

Here we show that, without  $\alpha 3$  expression, fast synaptic transmission in sympathetic ganglia is completely absent. Remarkably, the preganglionic nerve does not require fast nicotinic transmission to establish synapses with postganglionic sympathetic neurons, and these electrophysiologically disrupted synapses persist well into postnatal life. However, we show that the output of transmitter from the preganglionic terminals is significantly impaired, in part, because these preganglionic terminals lack functional high-affinity choline transporters. Our results indicate that fast synaptic transmission in SCG requires  $\alpha 3$  expression and that the functional maturation of presynaptic terminals in SCG requires an activity-dependent retrograde signal.

## METHODS AND MATERIALS

### Mice

A colony of  $\alpha 3$  neuronal nAChR-deficient mice was maintained by breeding heterozygous animals and genotyping pups by PCR (Xu et al., 1999). The survival rate of homozygote  $\alpha 3^{-/-}$  pups in our colony was similar to that reported by Xu et al. (1999): ~20% died within the first few postnatal days, and >60% survived until postnatal day 10 (P10) to P12, with many surviving at least 3 weeks. Most experiments were done with SCG from neonatal (P7–P10)  $\alpha 3^{-/-}$  pups and wild-type (WT) littermates. In a few experiments, we used ganglia from P21  $\alpha 3^{-/-}$  and WT animals.

### Neuron Cultures

We cultured SCG neurons from P4–P8 mice as described previously for SCG from neonatal rats (McFarlane and Cooper, 1992). Briefly, ganglia were dissociated for 30 min at 37°C in trypsin (180–200 U/ml; Worthington, Freehold, NJ) dissolved in HBSS buffered with HEPES and adjusted to pH 7.4 with NaOH, washed with HBSS, and plated on laminin-coated coverslips in growth media. The growth media consists of L-15 media supplemented with vitamins, cofactors, penicillin–streptomycin, 5% rat serum, and NGF (25–50 ng/ml). Cultures were fed every 3 d and treated with cytosine arabinoside (10  $\mu$ M; Sigma, St. Louis, MO) from days 2 to 4 to eliminate non-neuronal cells.

### **Extracellular Recordings**

Ganglia were dissected rapidly from neonatal pups, pinned down in a recording chamber (7 ml volume), and perfused continuously at 10 ml/min with oxygenated Ringer's solution at 22°C. The preganglionic nerve in the cervical sympathetic trunk was connected to an S88 stimulator and SIU5 stimulus isolation unit (Grass Instruments, Quincy, MA) with a suction electrode. The postganglionic trunk was connected to an alternating current differential amplifier (DP-301; Warner Instruments, Hamden, CT) with a suction electrode; the postganglionic compound action potentials were amplified, filtered at 100 Hz (low-pass cutoff) and 1 kHz (high-pass cutoff), digitized at 44 kHz by a pulse code modulation unit (PCM701; Sony, Tokyo, Japan), and stored on a videocassette recorder (Sony). The data were transferred to a Pentium II-based personal computer with Patchkit (Alembic Software, Montreal, Quebec, Canada) and analyzed off-line with Igor (WaveMetrics, Lake Oswego, OR). All drugs were added directly to the oxygenated Ringer's solution.

### **Intracellular Recording**

For intracellular recordings, neonatal ganglia were placed in a small recording chamber (1.5 ml volume) perfused continuously at 3–4 ml/min with oxygenated Ringer's solution at 36–37°C; the chamber was mounted on a fixed stage of dissecting microscope (SMZ-10; Nikon, Tokyo, Japan), and the ganglia were held down with minutia pins. The cervical sympathetic trunk was connected to a stimulator (4710 ORTEC dual channel; EG&G, Gaithersburg, MD) with a suction electrode, and the preparation was left undisturbed for 2–3 h while being continuously perfused with oxygenated Ringer's solution at 36–37°C. To record from ganglion cells, we used 70–120 M $\Omega$  glass microelectrodes (G150F-4;

Warner Instruments) made with a DMZ universal puller (Zeitz Instruments, Munich, Germany). Stable intracellular recordings were achieved with a high inertial precision microdrive (Inchworm 8200; EXFO, Vanier, Quebec, Canada) attached to a micromanipulator (SM11; Narshige, Tokyo, Japan) that drove the electrode through the ganglion. The recording electrode was filled with 2 M KAc and connected by a thin silver chlorided wire to the head stage of an Axoclamp 2A amplifier (Axon Instruments, Union City, CA) used in current-clamp mode; depolarizing or hyperpolarizing constant current pulses were applied through the recording electrode. Membrane potentials were sampled, displayed, and stored on a Pentium II-based personal computer. Stimulation and acquisition was done with Patchkit software (Alembic Software), and the data were analyzed off-line with IGOR. The preganglionic nerve was stimulated with brief (0.1–0.3 ms) voltage pulses applied to the cervical sympathetic trunk through the suction electrode. All drugs were dissolved in oxygenated Ringer's solution: for long-term (>1 h) applications, drugs were added directly to the perfusion; for shorter (seconds to minutes) applications, drugs were added directly to the bath through a separate perfusion line. Only neurons with membrane potentials greater than –40 mV were included in this study.

For the experiments with hemicholinium (HC-3), first we stimulated the preganglionic nerve at 20 Hz for 2 s in the presence of neostigmine (10  $\mu$ M) and hexamethonium (100  $\mu$ M) and recorded the muscarinic response from SCG neurons intracellularly. Next, we added HC-3 (10  $\mu$ M), waited  $\sim$ 15 min, and then stimulated the preganglionic nerve at 20 Hz for 2 s at 1 min intervals. The first response after 15 min in HC-3 was comparable to the responses before adding HC-3; the subsequent responses in HC-3 decayed rapidly (see Results). For

experiments with low- $\text{Ca}^{2+}$ , high- $\text{Mg}^{2+}$  Ringer's solution, we lowered  $\text{Ca}^{2+}$  to 0.5 mM and increased  $\text{Mg}^{2+}$  to 5 mM.

### **Whole-Cell Recording**

Whole-cell patch-clamp recordings were made with VE-2 amplifier (Alembic Software) at room temperature. The patch electrodes had resistances of 2–5 M $\Omega$ . Membrane currents were filtered at 1.5 kHz with a four-pole Bessel filter, sampled at 2.5–5 kHz, displayed, and stored on-line. Patchkit software was used for stimulation and data acquisition. The patch electrodes were filled with the following (in mM): 65 KF, 55 KAc, 5 NaCl, 0.2  $\text{CaCl}_2$ , 1  $\text{MgCl}_2$ , 10 EGTA, and 10 HEPES, pH adjusted to 7.3 with KOH. The neurons were perfused continuously throughout the recording at 1 ml/min with perfusion media consisting of the following: 140 mM NaCl, 5.4 mM KCl, 0.33 mM  $\text{NaH}_2\text{PO}_4$ , 0.44 mM  $\text{KH}_2\text{PO}_4$ , 2.8 mM  $\text{CaCl}_2$ , 0.18 mM  $\text{MgCl}_2$ , 10 mM HEPES, 5.6 mM glucose, 2 mM glutamine, 5  $\mu\text{g/ml}$  phenol red, 2  $\mu\text{M}$  tetrodotoxin, and 1–2  $\mu\text{M}$  atropine, pH adjusted to 7.4 with NaOH. ACh was dissolved in perfusion media and applied by pressure ejection from pipettes with tip diameters of 5–10  $\mu\text{m}$  positioned 20–30  $\mu\text{m}$  from the soma (Mandelzys et al., 1994).

### **Calcium Imaging**

Ratiometric fluorescence imaging with fura-2 AM (Molecular Probes, Eugene, OR) was used to measure ACh-induced changes in intracellular free  $\text{Ca}^{2+}$  concentration. Neurons were incubated at 37°C for 30 min to 1 h with L-15  $\text{CO}_2$  (Sigma) containing fura-2 AM (10  $\mu\text{M}$ ), washed once with perfusion medium (see above, Whole-cell recording), and left for 20–30 min at room temperature. The cultures were then placed on the stage of an inverted microscope (Axiovert

200 M; Zeiss, Oberkochen, Germany) and viewed through a 40x, 1.3 numerical aperture Plan Neofluor oil-immersion objective (Zeiss). The cells were continuously perfused throughout the recording at 1 ml/min with perfusion media at 37°C. ACh (100  $\mu$ M) was dissolved in perfusion media and applied to neurons by pressure ejection from pipettes with tip diameters of 5–10  $\mu$ m positioned 20–30  $\mu$ m from the soma. As a control, we applied 40 mM  $K^+$ , which produced a clear increase in intracellular  $Ca^{2+}$  from both WT and  $\alpha 3^{-/-}$  neurons. Fluorescent images were obtained by exciting the cultures with either 340 or 380 nm wavelength for 100–200 ms from a 150 W xenon arc lamp (LAMBDA DG-4; Sutter Instruments, Novato, CA) and collecting 510 nm emissions with a cooled CCD camera (CoolSnap HQ; PhotoMetrics, Tucson, AZ), all controlled by Metafluor software (Universal Imaging Corporation, West Chester, PA). Images were acquired with Metafluor at 1/s during the ACh application and 0.2/s between applications and analyzed off-line with Metafluor and Igor. The 340/380 ratios were converted to calcium concentration using a fura-2 calcium calibration kit (Molecular Probes).

### **Adenovirus**

Full-length  $\alpha 3$  neuronal nAChR subunit cDNA was ligated into pAdTrack-cytomegalovirus (CMV), and replication-deficient viral vectors were made according to He et al. (1998). All viruses were titered in duplicate with the cytopathic effect method (Nyberg-Hoffman et al., 1997). SCG cultures were infected at day 2 with 50 infectious particles/ $\mu$ l overnight, rinsed twice with virus-free medium, and stimulated with 40 mM  $K^+$  for 12–24 h to obtain high expression from the CMV promoter (Wheeler and Cooper, 2001).

### **Ultrastructural Studies**

Ganglia were placed directly into 2% paraformaldehyde–2% glutaraldehyde in phosphate buffer (PB) 0.1 M at room temperature on a shaker for 30 min and then cut in half and fixed for an additional 60–90 min. Next, the tissue was rinsed three times, 10 min each, in 0.1 M PB at room temperature and postfixed in 1% OsO<sub>4</sub> plus 1.5% potassium ferricyanide in H<sub>2</sub>O on a shaker for 1 h at room temperature. The tissue was rinsed briefly with distilled H<sub>2</sub>O, dehydrated in graded series of ethanol concentrations up to 100%, placed in 100% propylene oxide for 10–15 min for two times, and then in a 1:1 mixture of propylene oxide and Embed812 on a shaker for 1 h, in a 1:2 mixture on a shaker for 2 h, and then 100% Embed812 on a shaker overnight at room temperature. The next day, the tissue was embedded in Embed812 and polymerized (24 h in an oven at 60°C). Thin sections of ganglia were cut on an ultramicrotome (UltracutE; Reichert-Jung, Nussloch, Germany), stained with 2% aqueous uranyl acetate and 3% lead citrate, and viewed with a Philips (Aachen, Germany) CM10 electron microscope.

### **Immunocytochemistry**

Freshly dissected ganglia were placed in 0.5% paraformaldehyde in 0.1 M PB for 1 h, overnight in 40% sucrose in 0.1 M PB, and then embedded in OCT compound and frozen immediately by immersion in 2-methylbutane cooled in liquid nitrogen. Frozen sections (30 µm) from these ganglia were cut with a cryostat and placed onto Probe-on Plus slides (Fisher Scientific, Houston, TX); the sections were rinsed with PBS for 30 min, blocked for 1 h in 10% normal donkey serum in PBS and 0.5% Triton X-100 at room temperature for 1 h, and then overnight in primary antibodies (polyclonal goat anti-VACHT (1:750; Chemicon, Temecula, CA), polyclonal goat anti-choline acetyltransferase (ChAT)

(1:50; Chemicon), monoclonal mouse anti-neurofilament (1:800; Sternberger Monoclonals, Lutherville, MD), polyclonal goat anti-vesicular ACh transporter (VAChT) and rabbit anti-synaptobrevin (1:400; Synaptic Systems, Göttingen, Germany), rabbit anti-synaptotagmin (1:200; Synaptic Systems), or anti-syntaxin 1a (1: 400; Synaptic Systems) in PBS-containing 10% normal donkey serum at 4°C. The sections were rinsed three times with PBS and then placed in secondary antibodies [donkey anti-goat FITC and/or donkey anti-mouse rhodamine (Jackson ImmunoResearch, West Grove, PA)] in PBS-containing 10% normal donkey serum for 1 h at room temperature, then rinsed three times with PBS, and mounted with Vectashield (Vector Laboratories, Burlingame, CA). Nonspecific staining, judged by processing sections without the primary antibody, was very low.

A series of z-stacks (0.3  $\mu\text{m}/\text{plane}$ ) were obtained with a confocal microscope (LSM 510; Zeiss) and a 63x, 1.4 numerical aperture Plan Neofluor oil-immersion objective. Images were quantified off-line with MetaMorph (Universal Imaging Corporation). All z-stacks were thresholded at twice the background pixel intensity obtained from a line scan of the image. For quantification of VAChT-positive terminals and for colocalization, we took running averages of three consecutive planes through the entire z-stack, and only images present on three consecutive planes and 1–3  $\mu\text{m}$  in diameter were counted.

## RESULTS

### **ACh-Evoked Currents Are Absent on $\alpha 3^{-/-}$ Neurons and Restored by Overexpressing $\alpha 3$ cDNA**

Peripheral autonomic neurons express two different subtypes of nAChRs:  $\alpha 3$ -containing receptors and  $\alpha 7$ -containing receptors (McGehee and Role, 1995; Rosenberg et al., 2002). We have shown previously that  $\alpha 3$  is highly expressed in rodent sympathetic neurons and that the developmental increase in ACh-evoked current densities correlates well with the increase in  $\alpha 3$  mRNA expression (Mandelzys et al., 1994; De Koninck and Cooper, 1995). To determine whether deleting the  $\alpha 3$  gene would abolish ACh-evoked currents, we recorded from freshly isolated sympathetic neurons with whole-cell patch-clamp techniques while applying ACh exogenously. Brief ACh (100  $\mu$ M) application onto freshly dissociated neurons from a WT neonatal SCG evoked a large inward current (Fig. 1A); the average ACh-evoked current density on neurons from WT SCG was 62.3 pA/pF ( $n = 25$ ) (Fig. 1B). Conversely, ACh (100  $\mu$ M) applied to dissociated neurons from  $\alpha 3^{-/-}$  ganglia evoked no change in membrane current (Fig. 1A,B). These results suggest that sympathetic neurons require the expression of  $\alpha 3$  subunit for the appearance of ACh-evoked inward currents.

To test this idea directly, we infected dissociated neurons from  $\alpha 3^{-/-}$  ganglia with adenoviruses constructed to express  $\alpha 3$  cDNA (Ad  $\alpha 3$ ) and the reporter gene green fluorescent protein (GFP) (Wheeler and Cooper, 2001) and then recorded from infected neurons 48–72 h later.  $\alpha 3^{-/-}$  neurons infected with Ad  $\alpha 3$  had ACh-evoked inward currents that were similar in magnitude and time course to those on WT neurons (Fig. 1A); ACh-evoked current densities on  $\alpha 3^{-/-}$

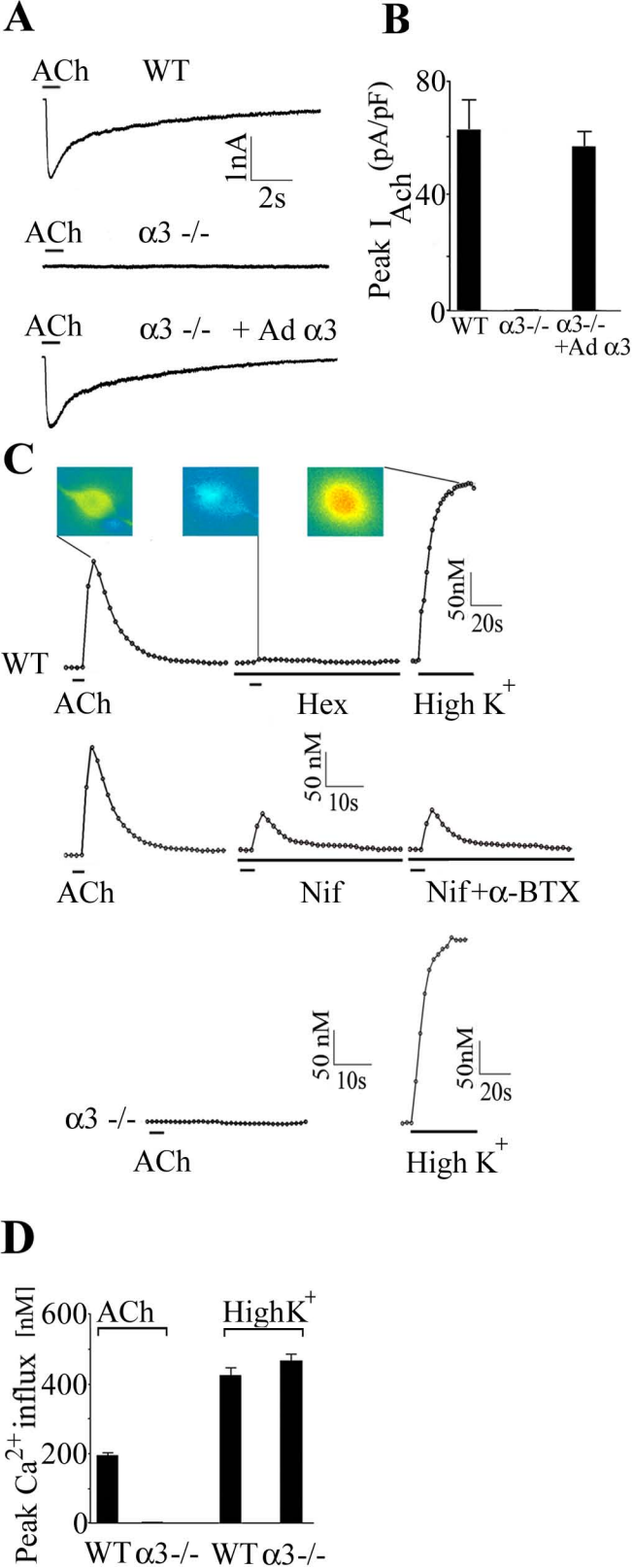


**Figure 2.1**

**FIGURE 2.1** Sympathetic neurons in  $\alpha 3^{-/-}$  SCG lack ACh-evoked currents and nAChR-induced changes in intracellular calcium. *A*, Whole-cell recordings from P7 WT SCG neuron in culture for 2 d (top), P8  $\alpha 3^{-/-}$  SCG neuron in culture for 2 d (middle), and P8  $\alpha 3^{-/-}$  neuron in culture for 5 d and infected with Ad  $\alpha 3$  at day 2 in culture (bottom). A brief application of ACh (100  $\mu$ M) produced a large, rapid inward current on the WT SCG neuron and on the  $\alpha 3^{-/-}$  neuron infected with Ad  $\alpha 3$  but produced no detectable inward current from the  $\alpha 3^{-/-}$  SCG neuron. *B*, Mean ACh-evoked current densities on the three types of neurons shown in *A*. Each column represents the mean  $\pm$  SEM;  $n = 25$ –27. None of the 25 neurons from  $\alpha 3^{-/-}$  ganglia had detectable ACh-evoked inward currents; however, infecting  $\alpha 3^{-/-}$  neurons with  $\alpha 3$  cDNA restores ACh-evoked current densities to WT levels. *C*, P6 WT and  $\alpha 3^{-/-}$  neurons in culture for 1 d were loaded with fura-2 AM and imaged with 340 and 380 nm excitation. The 340/380 ratios were converted to intracellular  $\text{Ca}^{2+}$  concentrations and plotted over time. A brief application of ACh (100  $\mu$ M) produced a large, rapid increase in intracellular  $\text{Ca}^{2+}$  concentration in the WT SCG neuron, which was reversibly blocked by hexamethonium (100  $\mu$ M). The middle three traces in *C* show that a large fraction of the ACh-induced increase in intracellular  $\text{Ca}^{2+}$  was blocked by nifedipine (Nif) (5  $\mu$ M) and unaffected by  $\alpha$ Bgt (0.5–1  $\mu$ M). The bottom two traces in *C* show that ACh (100  $\mu$ M) produced no detectable change in intracellular  $\text{Ca}^{2+}$  concentration in the  $\alpha 3^{-/-}$  SCG neuron. Depolarizing neurons with 40 mM  $\text{K}^{+}$  produced large increases in intracellular  $\text{Ca}^{2+}$  in WT and  $\alpha 3^{-/-}$  neurons. The 340 and 380 images were obtained at 1 s intervals during ACh applications and 5 s intervals during high  $\text{K}^{+}$  at 37°C. The inset shows the actual 340/380 images from a WT neuron at the peak of the ACh response, in the presence of hexamethonium (Hex), and at the peak of the high  $\text{K}^{+}$  response. *D*, Mean change in calcium influx induced by ACh (100  $\mu$ M) and high  $\text{K}^{+}$  (40 mM) for WT and  $\alpha 3^{-/-}$  neurons. ACh did not induce detectable changes in intracellular  $\text{Ca}^{2+}$  in  $\alpha 3^{-/-}$  neurons; however, all  $\alpha 3^{-/-}$  neurons responded to high  $\text{K}^{+}$ . The values are the mean  $\pm$  SEM;  $n = 32$ –47.

neurons infected with Ad  $\alpha 3$  were not significantly different from those on WT neurons (Fig. 1B), whereas  $\alpha 3^{-/-}$  neurons infected with control viruses expressing GFP alone had no detectable ACh-evoked currents ( $n = 27$ ) (data not shown). The results in Figure 1, A and B, indicate that expressing  $\alpha 3$  cDNAs in neurons from  $\alpha 3^{-/-}$  SCG is sufficient to restore ACh-evoked currents to wild-type levels on these neurons.

We did not observe  $\alpha 7$ -type currents on freshly dissociated neurons from  $\alpha 3^{-/-}$  ganglia. One possibility is that such  $\alpha 7$ -containing receptors produce their effects by mobilizing  $\text{Ca}^{2+}$  from internal stores (Sharma and Vijayaraghavan, 2003). To test this, we blocked muscarinic receptors with atropine (2  $\mu\text{M}$ ) and monitored changes in cytoplasmic  $\text{Ca}^{2+}$  with the calcium indicator fura 2 in response to brief ACh (100  $\mu\text{M}$ ) applications. In neurons dissociated from P7 WT SCG, ACh (100  $\mu\text{M}$ ) applications produced a large increase in cytoplasmic  $\text{Ca}^{2+}$  that was reversibly blocked by hexamethonium (100  $\mu\text{M}$ ), an nAChR antagonist (Fig. 1C,D). Most of the ACh-induced increase in  $\text{Ca}^{2+}$  was attributable to depolarization-induced  $\text{Ca}^{2+}$  influx through L-type  $\text{Ca}^{2+}$  channels, and a fraction was attributable to an  $\alpha$ -bungarotoxin ( $\alpha\text{Bgt}$ )-insensitive  $\text{Ca}^{2+}$  influx through nAChRs ( $n = 31$ ) (Fig. 1C). Conversely, ACh (100  $\mu\text{M}$ ) produced no change in cytoplasmic  $\text{Ca}^{2+}$  in dissociated neurons from  $\alpha 3^{-/-}$  SCG, although all  $\alpha 3^{-/-}$  SCG neurons responded to depolarization with a large increase in cytoplasmic  $\text{Ca}^{2+}$  when exposed to high  $\text{K}^+$  (40 mM) (Fig. 1C,D).

### **SCG From $\alpha 3^{-/-}$ Mice Lack Synaptic Transmission**

Because isolated  $\alpha 3^{-/-}$  SCG neurons do not have functional nAChRs (Fig. 1), we anticipated that synaptic transmission in  $\alpha 3^{-/-}$  ganglia would be severely

disrupted. To test this, we stimulated the preganglionic nerve and recorded from the postganglionic trunk of the SCG from neonatal  $\alpha 3^{-/-}$  mice and their WT littermates.

Suprathreshold stimuli applied to the preganglionic nerve of SCG from neonatal WT mice produced large compound action potentials (Fig. 2A); these compound action potentials were reversibly blocked by hexamethonium (100  $\mu$ M). In addition, because we recorded close to the ganglion, we could also detect the preganglionic afferent volley preceding the postganglionic compound action potential. Results similar to those in Figure 2A were obtained from all (18 of 18) WT SCG.

In contrast, suprathreshold stimuli applied to the preganglionic nerve of SCG from  $\alpha 3^{-/-}$  littermates failed to evoke detectable compound action potentials in all (25 of 25) ganglia examined, although the preganglionic afferent volleys were clearly present (Fig. 2A). These results in Figure 2A indicate that the preganglionic nerve does not evoke suprathreshold EPSPs on sympathetic neurons in  $\alpha 3^{-/-}$  ganglia.

### **Sympathetic Neurons in $\alpha 3^{-/-}$ SCG Lack Fast EPSPs**

To test whether the preganglionic nerve evoked subthreshold EPSPs, we recorded intracellularly from neurons in neonatal SCG. Stimulating the preganglionic nerve in a P8 WT ganglia produced large, fast suprathreshold EPSPs on SCG neurons lasting tens of milliseconds (Fig. 2B). These EPSPs were reversibly blocked by hexamethonium (100  $\mu$ M), indicating that the synapses were cholinergic and mediated by nAChRs (Fig. 2B). We observed

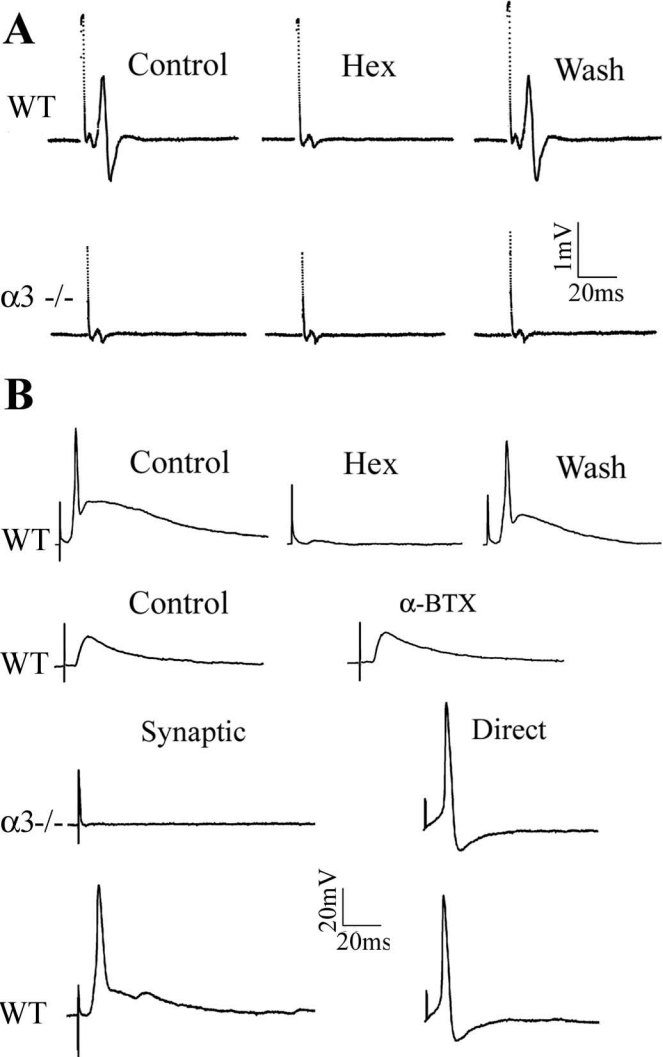


**Figure 2.2**

**FIGURE 2.2** No postganglionic compound action potential or fast EPSPs on sympathetic neurons in  $\alpha 3^{-/-}$  superior cervical ganglion. *A* shows postganglionic compound action potentials and preganglionic potentials recorded from the sympathetic trunk of a P7 WT SCG (top traces) in response to suprathreshold stimuli to the preganglionic nerve. In WT ganglia, hexamethonium (Hex) (100  $\mu$ M) reversibly blocked the compound action potential but had no effect on the preganglionic potential. In P7  $\alpha 3^{-/-}$  ganglia (bottom trace), suprathreshold stimuli to the preganglionic nerve failed to evoke postganglionic compound action potentials, whereas the preganglionic potentials were unchanged. *B*, Stimulating the preganglionic nerve evoked large suprathreshold EPSPs from a P8 WT sympathetic neuron recorded intracellularly; the EPSPs were reversibly blocked by hexamethonium (100 $\mu$ M) but unaffected by  $\alpha$ Bgt (0.5 $\mu$ M). Stimulating the preganglionic nerve failed to produce any change in membrane potential on a P8  $\alpha 3^{-/-}$  sympathetic neuron, demonstrating that fast synaptic EPSPs are absent in  $\alpha 3^{-/-}$  ganglia. Direct intracellular current injection, conversely, evoked fast, overshooting action potentials (right) on both WT and  $\alpha 3^{-/-}$  neurons, indicating that  $\alpha 3^{-/-}$  neurons do not require fast synaptic transmission to express voltage-gated currents that underlie the action potential.

similar results from all neurons (27 of 27) in neonatal WT SCG.  $\alpha$ -Bgt (0.5  $\mu$ M) had no effect on these EPSPs ( $n = 5$ ) (Fig. 2B).

Conversely, stimulating the preganglionic nerve in P8  $\alpha 3^{-/-}$  ganglia failed to produce any detectable change in membrane potential (Fig. 2B). Similar results were obtained from all neurons (53 of 53) in neonatal  $\alpha 3^{-/-}$  ganglia. These results demonstrate that fast synaptic transmission requires  $\alpha 3$ -containing nAChRs. Moreover, our results indicate that, in  $\alpha 3^{-/-}$  ganglia, (1) no other nAChR  $\alpha$  subunit substitutes for the missing  $\alpha 3$  to restore fast synaptic transmission, and (2) no other transmitter system compensates for the absence of cholinergic-nicotinic transmission at these synapses.

Although fast excitatory synaptic transmission is absent from sympathetic neurons in  $\alpha 3^{-/-}$  neonatal SCG, direct electrical stimulation of these neurons evoked overshooting action potentials that were similar in magnitude and time course to those on neurons in WT SCG (Fig. 2B). This indicates that  $\alpha 3^{-/-}$  neurons continue to differentiate electrically and do not require fast synaptic activity to express voltage-gated currents that underlie the action potential.

### **Muscarinic Responses on $\alpha 3^{-/-}$ and WT Neurons Are Similar**

Stimulating the preganglionic nerve in P7 WT ganglia at 20 Hz for 2 s while blocking the nAChRs with hexamethonium (100  $\mu$ M) produced a 5–7 mV slow EPSP that was blocked by atropine (Fig. 3A). Deleting the  $\alpha 3$  nAChR subunit gene abolishes fast nicotinic EPSPs, but we expected that these slow muscarinic EPSPs in  $\alpha 3^{-/-}$  ganglia would be unaffected; however, this was not the case. In P7  $\alpha 3^{-/-}$  ganglia, we observed no detectable slow EPSPs when we applied similar stimulations to the preganglionic nerve (Fig. 3A). This

unanticipated absence of slow EPSPs in  $\alpha 3^{-/-}$  ganglia raised several questions. Are the postsynaptic muscarinic responses normal? Do the preganglionic nerves innervate sympathetic neurons in  $\alpha 3^{-/-}$  ganglia? If they innervate the SCG neurons and form synapses, can they release normal amounts of ACh?

To address whether the muscarinic responses are normal, we directly applied ACh to the ganglia. Muscarinic receptors on rat sympathetic neurons are not focally concentrated at synapses but are widely distributed over their somatic and dendritic surfaces, with higher densities on the soma (Ramcharan and Matthews, 1996). For acetylcholine to reach muscarinic receptors during synaptic transmission, it must diffuse from the synapses (Brown and Selyanko, 1985). We applied increasing concentrations of ACh to the ganglia while recording from SCG neurons intracellularly to measure the muscarinic response. We adjusted the concentration of ACh (typically  $\sim 100 \mu\text{M}$ ) to give us responses that mimicked the nerve-evoked response in WT ganglia without acetylcholinesterase (see below). We refer to this concentration as 1x and measured the response of neonatal WT and  $\alpha 3^{-/-}$  SCG neurons to four ACh concentrations: 0.01x, 0.1x, 1x, and 5x (Fig. 3B,C). We observed no significant difference in muscarinic responses among WT and  $\alpha 3^{-/-}$  neurons (Fig. 3B,C); moreover, the responses were unaltered by acetylcholinesterase inhibitors. These results show that the appearance of functional muscarinic receptors on SCG neurons does not require fast synaptic activity and that the muscarinic response on WT and  $\alpha 3^{-/-}$  neurons is not different.

### **Morphological Synapses Form on Neurons without Synaptic Activity**

The absence of nerve-evoked slow EPSPs in  $\alpha 3^{-/-}$  SCG is not attributable

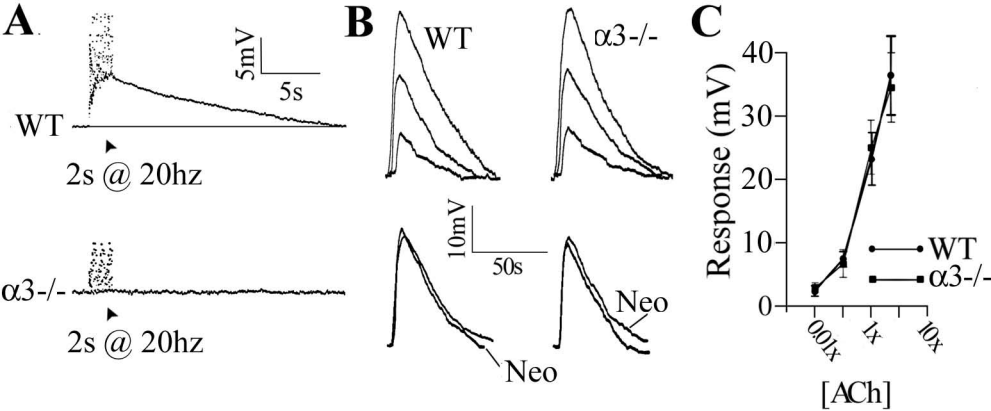


**Figure 2.3**

**FIGURE 2.3** The absence of slow EPSPs but normal muscarinic responses in  $\alpha 3^{-/-}$  ganglia. *A*, Stimulating the preganglionic nerve with a 20 Hz train for 2 s in the presence of hexamethonium (100  $\mu$ M) produced a slow depolarization in a P7 WT neuron (top). A similar 20 Hz train stimulation produced no detectable change in membrane potential in a P7  $\alpha 3^{-/-}$  neuron (bottom). The stimulus artifacts were removed for clarity. Experiments were done at 37°C. *B*, Depolarization of a P7 WT SCG neuron (left) and a P8 $\alpha 3^{-/-}$  SCG neuron (right) induced by three ACh concentrations (0.1x, 1x, and 5x) applied directly to each ganglia. [1x represents the concentration of ACh that produced a similar depolarization to that after preganglionic nerve stimulation (2 s at 20 Hz in neostigmine) and was usually 100 $\mu$ M added to the perfusion solution.] Below shows response to 1x ACh with and without neostigmine (Neo). *C*, ACh dose–response relationship for 11 WT (●) and 9  $\alpha 3^{-/-}$  (■) neurons. The values are the means  $\pm$  SEM;  $n = 11$  for WT and 9 for  $\alpha 3^{-/-}$ . There is no significant difference in the muscarinic response between neurons in WT and  $\alpha 3^{-/-}$  ganglia. All experiments were done in the presence of hexamethonium (100  $\mu$ M) and at 37°C.

to the lack of postsynaptic muscarinic responsiveness but is more likely attributable to the low amount of ACh released from the presynaptic terminals. Therefore, we determined whether the density of cholinergic varicosities in P7  $\alpha 3^{-/-}$  ganglia was altered. As a marker for cholinergic varicosities, we immunostained for VACht (Fig. 4A). We found no significant differences in either the number of cholinergic varicosities (Fig. 4B) or the mean VACht fluorescence (data not shown) in  $\alpha 3^{-/-}$  compared with WT ganglia.

The density of cholinergic varicosities in P21 ganglia was approximately twofold greater than in P7 for both  $\alpha 3^{-/-}$  and WT ganglia (Fig. 4C,D). At P21, there was no significant difference in the density of cholinergic varicosities between  $\alpha 3^{-/-}$  and WT ganglia.

In addition, we immunostained for vesicle-associated membrane protein (VAMP), synaptotagmin, syntaxin 1a, or ChAT in >670 varicosities from 25 ganglia (Fig. 5). More than 90% of these proteins colocalized with VACht in presynaptic varicosities; ChAT also localized to preganglionic axons. We found no significant differences in immunostaining for these proteins between WT and  $\alpha 3^{-/-}$  ganglia.

Next, we used electron microscopic analysis to determine whether these preganglionic terminals formed morphological synapses on sympathetic neurons in the absence of activity. We quantified 29 synapses from nine different ganglia in neonatal  $\alpha 3^{-/-}$  mice and 36 synapses from six different WT littermates and found no significant difference in morphology of synapses in SCG from WT and  $\alpha 3^{-/-}$  mice (Fig. 6A–F). The synapses have the characteristic features of accumulations of synaptic vesicles adjacent to the presynaptic surface membrane, enhanced postsynaptic density, a parallel arrangement and

thickening of the presynaptic and postsynaptic membranes, and a widened synaptic cleft. We measured the number of docked vesicles at the active zone, synaptic cleft width, length of specialized presynaptic and postsynaptic membrane, number of multivesicular bodies, and diameter of small clear synaptic vesicles and of large densecore vesicles. We found no significant differences in any of these parameters in WT versus  $\alpha 3^{-/-}$  SCG (Table 1). These results indicate that morphologically normal synapses are established in ganglia in the absence of fast synaptic activity.

### **ACh Release from Preganglionic Varicosities Requires Fast Synaptic**

#### **Activity**

Our results indicate that the postsynaptic muscarinic responsiveness in  $\alpha 3^{-/-}$  neurons is normal, that the density of cholinergic varicosities in  $\alpha 3^{-/-}$  ganglia is similar to those in WT ganglia, and that the preganglionic nerve in  $\alpha 3^{-/-}$  ganglia forms morphologically normal synapses. This suggests that the absence of slow EPSPs in  $\alpha 3^{-/-}$  ganglia results from a presynaptic malfunction in transmitter output.

If ACh released from cholinergic varicosities in  $\alpha 3^{-/-}$  ganglia was lower than that released from varicosities in WT ganglia, most of the ACh might be hydrolyzed by acetylcholinesterase before it could diffuse to the muscarinic receptors and is therefore incapable of producing slow EPSPs. To test this, we inhibited the acetylcholinesterase with neostigmine. In control solution, a brief (2 s) 20 Hz train in a P6 WT ganglion produced a small 5–7 mV slow depolarization, whereas in the presence of neostigmine (10  $\mu$ M), a similar stimulation produced a large (~25 mV) slow EPSP lasting 1–2 min that was reversibly blocked by

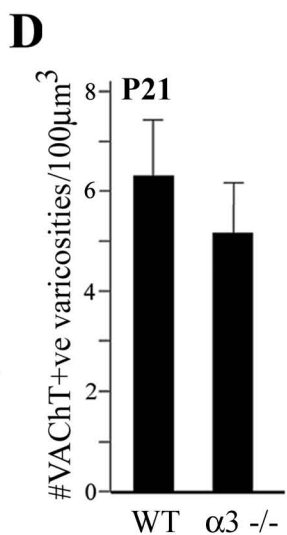
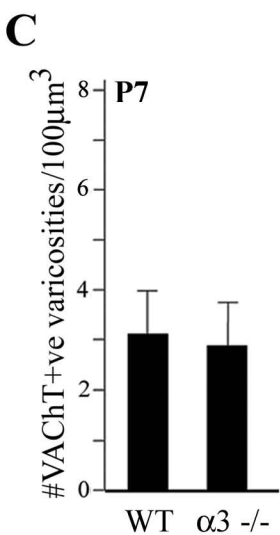
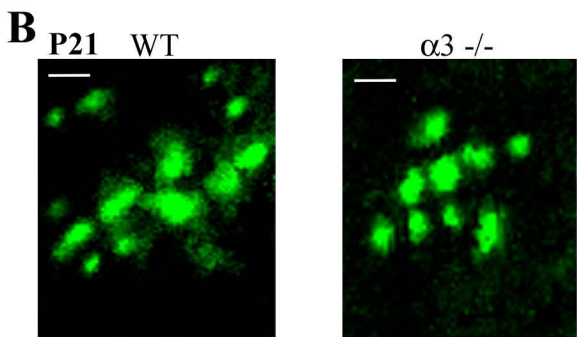
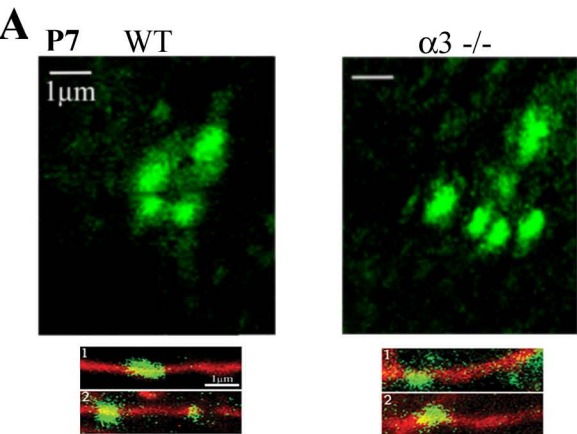


**Figure 2.4**

**FIGURE 2.4** The densities of preganglionic varicosities in  $\alpha 3^{-/-}$  ganglia are similar to those in WT ganglia. *A*, Confocal images of VAcHt-positive varicosities in P7 WT and  $\alpha 3^{-/-}$  ganglia. The bottom panels show higher magnification images of VAcHt-positive varicosities (green) located on neurofilament-positive preganglionic axons (red). Scale bars, 1  $\mu\text{m}$ . *B*, Average number of VAcHt-positive varicosities in P7 WT and  $\alpha 3^{-/-}$  ganglia. More than 450 varicosities were counted from confocal images in WT and  $\alpha 3^{-/-}$  ganglia. The number of varicosities in each ganglion was normalized to a constant volume, and the values are the mean  $\pm$  SEM;  $n = 5$ . *C*, Confocal images of VAcHt-positive varicosities in P21 WT and  $\alpha 3^{-/-}$  ganglia. *D*, Average number of VAcHt-positive varicosities in P21 WT and  $\alpha 3^{-/-}$  ganglia. More than 270 varicosities were counted from confocal images in WT and  $\alpha 3^{-/-}$  ganglia. The number of varicosities in each ganglion was normalized to a constant volume, and the values are the mean  $\pm$  SEM;  $n = 3$ .

atropine (10  $\mu$ M) (Fig. 7A). In neonatal  $\alpha 3^{-/-}$  SCG in control solution, a 2 s, 20 Hz train applied to the preganglionic nerve produced no detectable response; however, after adding neostigmine (10  $\mu$ M), the 20 Hz train produced a small (5–7 mV) atropine-sensitive depolarization that lasted only 10–20 s (Fig. 7A). These nerve-evoked depolarizations in neostigmine were reversibly blocked by perfusing the ganglia with low- $\text{Ca}^{2+}$ , high- $\text{Mg}^{2+}$  Ringer's solution ( $n = 3$ ) (data not shown). We obtained similar results from P21 ganglia (Fig. 7B). These results suggest that cholinergic varicosities in  $\alpha 3^{-/-}$  ganglia can release ACh but in significantly smaller amounts than varicosities in WT ganglia.

The muscarinic responses recorded from WT sympathetic neurons varied directly with the number of stimuli applied to the preganglionic nerve (Fig. 7C) (Brown and Selyanko, 1985). The integrated muscarinic responses on WT sympathetic neurons increased dramatically with increasing number of stimuli to the preganglionic nerve (Fig. 7C,D). In sharp contrast, the muscarinic responses from sympathetic neurons in  $\alpha 3^{-/-}$  ganglia were difficult to detect unless the preganglionic nerve was stimulated for at least 1 s at 20 Hz (Fig. 7C, inset). Moreover, increasing numbers of stimuli to the preganglionic nerve in  $\alpha 3^{-/-}$  ganglia had little effect on the magnitude of the response (Fig. 7C). These results indicate that ACh output from preganglionic varicosities is dramatically reduced in  $\alpha 3^{-/-}$  ganglia.

In WT ganglia, the muscarinic responses to successive stimuli (2 s at 20 Hz) decreased slowly (Fig. 8A,B); the second application delivered after a 60 s rest was  $\sim 80\%$  of the initial response and eventually leveled off to  $\sim 70\%$  of initial response after five to six intervals (Fig. 8B). In contrast, the muscarinic responses in  $\alpha 3^{-/-}$  ganglia decreased sharply as if the stores of ACh became rapidly

depleted (Fig. 8A,B); the second response was ~25% of the initial response (Fig. 8B) and became undetectable after the third or fourth application (Fig. 8B). This rapid depletion suggests that, when cholinergic nicotinic synapses develop without functional postsynaptic nAChRs and fast synaptic activity, the preganglionic varicosities are abnormal in their ability to synthesize and/or store ACh.

### **Preganglionic Terminals in $\alpha 3^{-/-}$ Ganglia Lack Functional High-Affinity**

#### **Choline Transporters**

Synthesis of ACh in preganglionic terminals depends predominantly on the acute uptake of extracellular choline by the Na<sup>+</sup>-dependent, HC-3-sensitive, high-affinity choline transporter, particularly during high-frequency firing (Birks and MacIntosh, 1961; Okuda et al., 2000; Ferguson et al., 2004). If the deficit in ACh output from preganglionic varicosities in  $\alpha 3^{-/-}$  ganglia results from impaired high-affinity choline transporters then (1) HC-3 should have little effect on ACh output from  $\alpha 3^{-/-}$  varicosities, and (2) blocking the high-affinity choline transporter in WT ganglia should lead to ACh depletion whose kinetics mimic those of terminals in  $\alpha 3^{-/-}$  ganglia.

To test the first prediction, we inhibited the high-affinity choline transporter with HC-3 (10  $\mu$ M) in  $\alpha 3^{-/-}$  ganglia and stimulated the preganglionic nerve at 20 Hz for 2 s in neostigmine-containing solution. Inhibiting the high-affinity choline transporter had no effect on the muscarinic response in  $\alpha 3^{-/-}$  ganglia, indicating that  $\alpha 3^{-/-}$  terminals lack functional high-affinity choline transporters (Fig. 8C).

To test the second prediction, we stimulated the preganglionic nerve at 20 Hz for 2 s at 1 min intervals while perfusing with HC-3 (10  $\mu$ M) (see Materials and

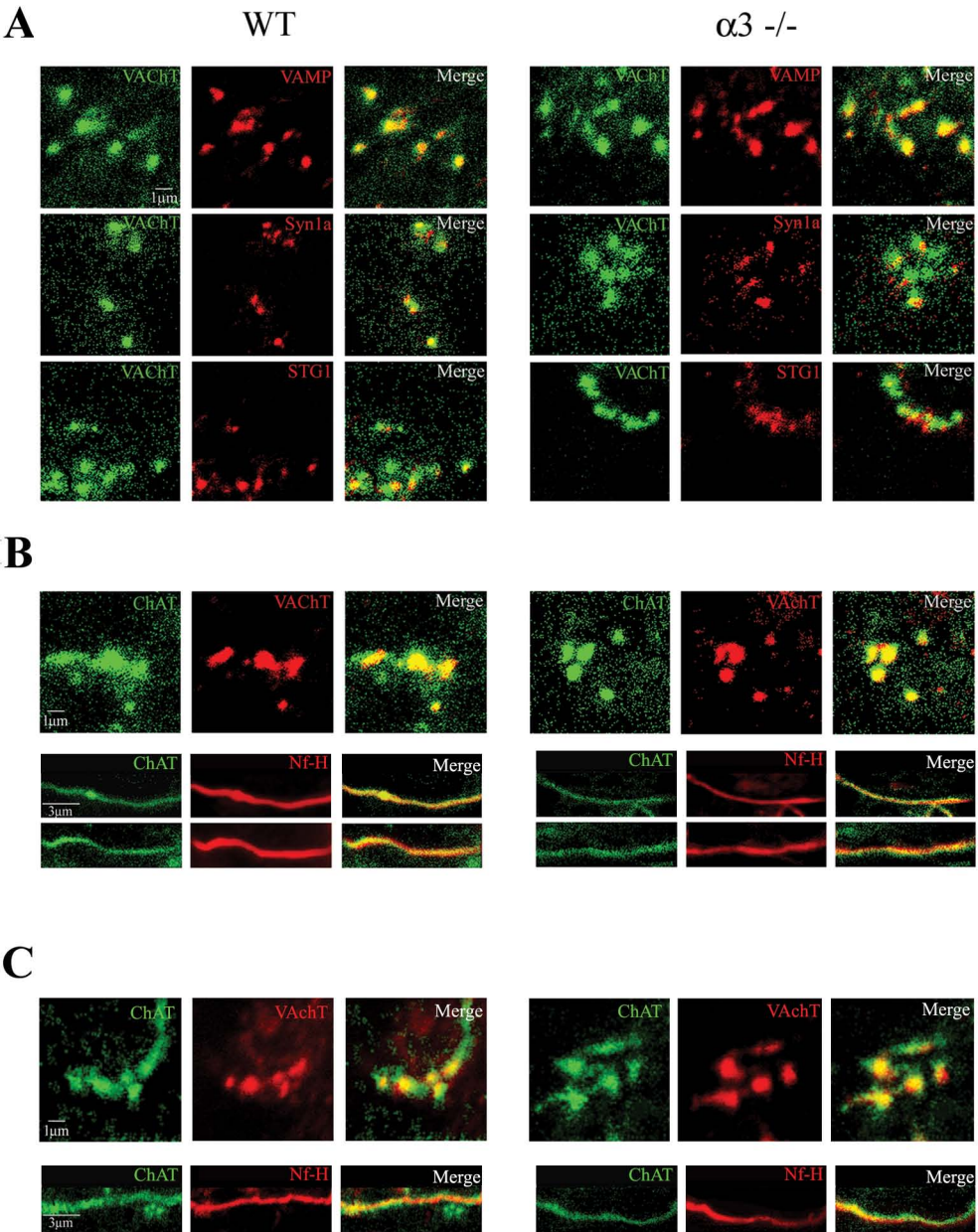


**Figure 2.5**

**FIGURE 2.5** The preganglionic varicosities in  $\alpha 3^{-/-}$  ganglia contain ChAT, VACHT, and SNARE (soluble *N*-ethylmaleimide-sensitive factor attachment protein receptor) proteins and are similar to those in WT ganglia. Immunostaining of varicosities in WT ganglia (left set) and  $\alpha 3^{-/-}$  ganglia (right set) for VACHT, synaptobrevin (VAMP), syntaxin 1a (Syn1a), synaptotagmin (STG1), and ChAT. In *A*, the left columns show immunostaining for VACHT (green), the middle columns show immunostaining for VAMP (synaptobrevin) (top, red), syntaxin 1a (middle, red), and synaptotagmin (bottom, red), and the right columns are the merged images of the left and middle columns. The top three sets of panels show that VAMP, syntaxin 1a, and synaptotagmin colocalize with VACHT in presynaptic varicosities in P7WT and  $\alpha 3^{-/-}$  ganglia. Scale bar, 1  $\mu\text{m}$ . In *B*, the left columns show immunostaining for ChAT (green), the middle columns show immunostaining for VACHT (red) in presynaptic varicosities (top panels) and neurofilament (Nf-H, red) along preganglionic axons (bottom 2 panels). The right columns are the merged images of the left and middle columns and show that ChAT is present in preganglionic axons and in presynaptic varicosities in P7 WT and  $\alpha 3^{-/-}$  ganglia. *C*, Similar to *B* but from P21 WT and  $\alpha 3^{-/-}$  ganglia. Scale bars (in *B*, *C*): 1  $\mu\text{m}$  for the varicosities; 3  $\mu\text{m}$  for axons.

Methods). After blocking the high-affinity choline transporter, the response decayed rapidly and was no longer detectable after the fourth interval, similar to what we observed from terminals in  $\alpha 3^{-/-}$  ganglia (Fig. 8B).

In addition, when we rested the terminals in  $\alpha 3^{-/-}$  ganglia for 5 min, the response to 20 Hz, 2 s stimulation recovered (Fig. 8D). Similarly, in WT ganglia treated with HC-3, after a 5 min rest, the muscarinic response recovered to approximately one-third of control, likely using the low-affinity choline transporter to resynthesize ACh (Fig. 8C). This ACh output from WT terminals in HC-3, however, decayed quickly and was undetectable after the third or fourth interval, mimicking the kinetics for depletion and recovery observed in  $\alpha 3^{-/-}$  terminals (Fig. 8D).

The lack of effect of HC-3 on terminals in  $\alpha 3^{-/-}$  ganglia and the rapid depletion of ACh from WT terminals treated with HC-3 together indicate that preganglionic terminals in  $\alpha 3^{-/-}$  ganglia lack functional high-affinity choline transporters.

## DISCUSSION

Our main findings in this study are as follows: (1) sympathetic neurons must express the  $\alpha 3$  nAChR gene to acquire fast nicotinic-type ACh-evoked inward currents; (2) morphologically normal synapses are established on neurons that lack functional postsynaptic receptors; (3) when synapses in SCG develop without fast synaptic activity, the output of transmitter from the presynaptic terminals is impaired; and (4) the decrease in transmitter output results from a

lack of functional high-affinity choline transporters on presynaptic terminals. We discuss each of these findings in more detail below.

### **Functional nAChRs on Postsynaptic SCG Neurons Require $\alpha 3$ Subunits**

Deleting the  $\alpha 3$  gene completely disrupts fast synaptic transmission between presynaptic and postsynaptic neurons. Interestingly, we observed no compensatory upregulation of other nAChR subunit genes in the SCG of  $\alpha 3$  nAChR null mice, nor did we observe the upregulation of any other transmitter system to restore fast synaptic transmission in SCG in the absence of  $\alpha 3$ -containing receptors.

This lack of compensatory upregulation to restore synaptic transmission was unexpected. Recent work has demonstrated that, when activity is perturbed, synapses dynamically adjust their strengths to ensure that firing rates are maintained within some functional range (Turrigiano and Nelson, 2004). These important homeostatic mechanisms have a clear role in the activity-dependent refinement of connectivity. Our observation of the lack of compensatory mechanisms does not necessarily contradict this principle of synaptic homeostasis but indicates that, if synaptic transmission in sympathetic ganglia is drastically perturbed during embryogenesis, then homeostatic mechanisms cannot restore synaptic transmission. It may become impossible to trigger such homeostatic mechanisms when the average level of postsynaptic depolarization at developing synapses is absent for long periods of time.

From work done in avian ciliary ganglia (Zhang et al., 1996; Ullian et al., 1997; Chang and Berg, 1999; Rosenberg et al., 2002), we had anticipated that SCG neurons in mice would have  $\alpha 7$  responses. However, we did not detect any

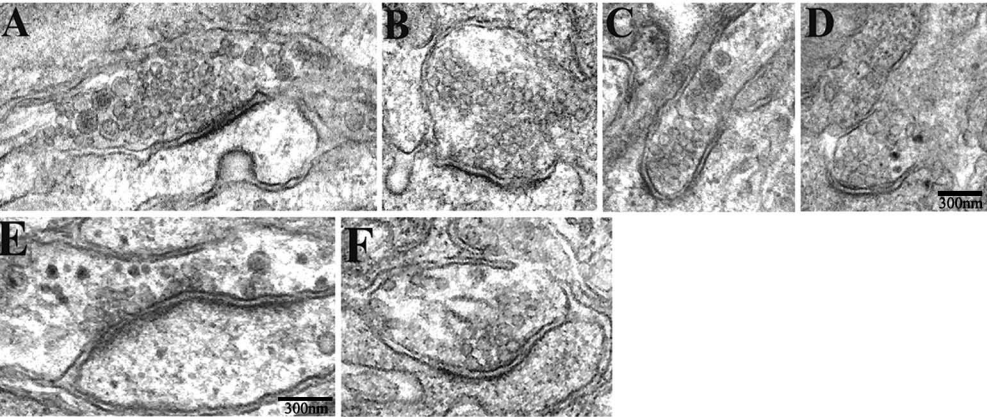


**Figure 2.6**

**FIGURE 2.6** The ultrastructure of synapses in  $\alpha 3^{-/-}$  ganglia are similar to those in WT ganglia. *A–F*, Electron micrographs of synapses in P7 in  $\alpha 3^{-/-}$  (*A, C, E*) and WT (*B, D, F*) SCG. The synapses have the characteristic morphological features: accumulations of synaptic vesicles adjacent to the presynaptic membrane, enhanced postsynaptic density, a parallel arrangement and thickening of the presynaptic and postsynaptic membranes, and a widened synaptic cleft. Scale bars, 300 nm.

**TABLE 2.1 Quantification of synaptic parameters in the SCG of  $\alpha 3$  null-mutant and control littermates at neonatal P6-P7**

	$\alpha 3^{-/-}$	Control
Small clear synaptic vesicles (nm, diameter)	30 $\pm$ 1.5	33 $\pm$ 1.2
Large dense core vesicles (nm, diameter)	71 $\pm$ 3.3	71 $\pm$ 5.6
Docked vesicles (# per synapse)	0.9 $\pm$ 0.3	1.1 $\pm$ 0.2
Multivesicular bodies (# per synapse)	0.7 $\pm$ 0.2	0.5 $\pm$ 0.3
Synaptic cleft width (nm, diameter)	25 $\pm$ 1.2	24 $\pm$ 0.7
Active zone length (nm, diameter)	261 $\pm$ 30	263 $\pm$ 22
PSD length (nm, diameter)	265 $\pm$ 19	273 $\pm$ 29

Data represent means  $\pm$  SEMs;  $n = 29$   $\alpha 3^{-/-}$  synapses and 36 control synapses from 9  $\alpha 3^{-/-}$  and 6 control animals, respectively. Docked vesicles per synapse are defined as those that are located less than one vesicle diameter from the presynaptic plasma membrane. PSD, Postsynaptic density.

$\alpha 7$  depolarizations in neurons in intact  $\alpha 3^{-/-}$  ganglia; in fact, we did not detect any ACh-induced whole-cell currents in isolated  $\alpha 3^{-/-}$  neurons, nor did we detect any changes in intracellular calcium. Because  $\alpha 7$  mRNA levels are regulated by activity (De Koninck and Cooper, 1995; Brumwell et al., 2002), the absence of synaptic activity on  $\alpha 3^{-/-}$  sympathetic neurons may have caused a downregulation of  $\alpha 7$ -containing receptors. Alternatively, rodent sympathetic neurons may not express conventional  $\alpha 7$  receptors on their cell bodies (Helekar et al., 1994; Cuevas and Berg, 1998). Importantly, by overexpressing  $\alpha 3$  in  $\alpha 3^{-/-}$  neurons with adenoviruses, we restored the ACh-evoked current densities to levels found on WT neurons. Therefore,  $\alpha 3$  expression is critical for the appearance of functional nAChRs on sympathetic neurons.

### **Fast Synaptic Transmission is not Required for the Development of Morphological Synapses**

Previous observations indicate that morphological synapses can form on neurons *in vivo* in the absence of presynaptic function. Our results demonstrate that electrophysiologically silent synapses are established on  $\alpha 3^{-/-}$  SCG neurons and are consistent with observations that the initial events in synapse formation proceed without activity (Verhage et al., 2000; Misgeld et al., 2002; Washbourne et al., 2002). In rodent SCG, synaptogenesis starts at embryonic day 13–14 (Rubin, 1985), although most synapses form during the early postnatal period. If neurons in embryonic  $\alpha 3^{-/-}$  ganglia lack synaptic activity like those in postnatal  $\alpha 3^{-/-}$  ganglia, then it is likely that some of the synapses that we observed in P7  $\alpha 3^{-/-}$  ganglia have been maintained without activity for  $\sim 2$  weeks.

Morphologically, the presynaptic terminals at these electrophysiologically silent synapses appear normal; we observed no significant difference in the vesicle population in the terminals of  $\alpha 3^{-/-}$  ganglia compared with those of WTs, nor was there any significant difference in the number of docked vesicles at the active zones. In addition, we did not detect any differences in the presence of choline acetyltransferase, VACHT, VAMP, syntaxin 1a, or synaptotagmin between terminals in  $\alpha 3^{-/-}$  ganglia and those of WTs. Unexpectedly, however, we discovered that these morphologically normal terminals release significantly less ACh than those in WT ganglia.

### **Presynaptic Output in $\alpha 3^{-/-}$ SCG is Impaired**

We used the muscarinic response to quantify differences in ACh release from the preganglionic nerve in WT versus  $\alpha 3^{-/-}$  ganglia. Muscarinic receptors on rat sympathetic neurons are widely distributed over their somatic and dendritic surfaces and are not focally concentrated at synapses, as demonstrated in a definitive study by Ramcharan and Matthews (1996) using light and electron microscopic autoradiography.

In WT ganglia, when we stimulated the preganglionic nerve at 20 Hz in control solutions, we recorded slow, small (~5 mV) muscarinic depolarizations on sympathetic neurons that became significantly larger and more prolonged when we inhibited cholinesterase activity. Conversely, stimulating the preganglionic nerve under identical conditions in  $\alpha 3^{-/-}$  ganglia produced markedly smaller muscarinic responses. In fact, unlike WT ganglia, we could not detect a muscarinic response in  $\alpha 3^{-/-}$  ganglia unless we inhibited the esterase.

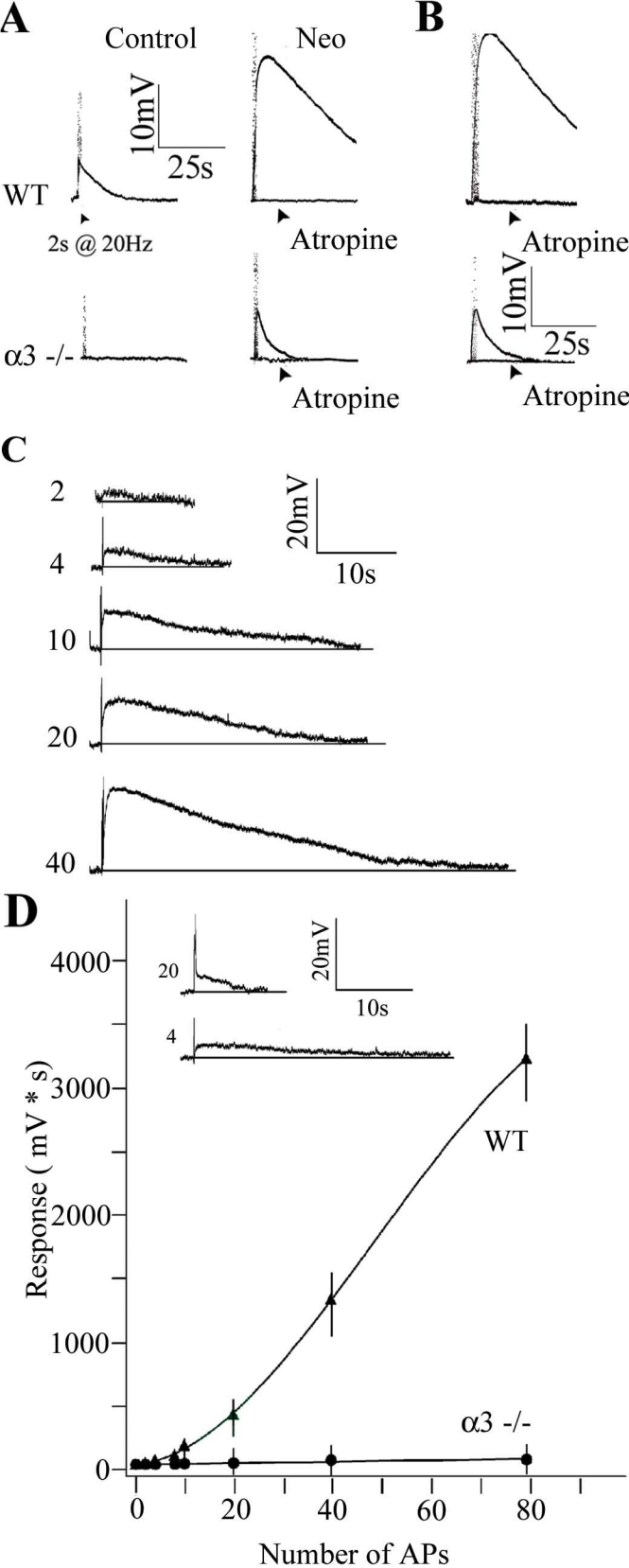


**Figure 2.7**

**FIGURE 2.7** Reduced ACh output from preganglionic varicosities in  $\alpha 3^{-/-}$  SCG. *A*, Top traces, Stimulating the preganglionic nerve at 20 Hz for 2 s produced a small, slow muscarinic depolarization on a P6 WT SCG neuron in control solution with hexamethonium (100  $\mu$ M) (left); the response increased  $\sim$ 4.5-fold after adding neostigmine (10  $\mu$ M) (Neo) to inhibit acetylcholinesterase (right) and was blocked by adding atropine (3  $\mu$ M). Bottom traces, Stimulating the preganglionic nerve at 20 Hz for 2 s produced no detectable response from a P8  $\alpha 3^{-/-}$  SCG neuron (left); however, after inhibiting cholinesterase with neostigmine (10  $\mu$ M) (right), preganglionic nerve stimulation produced a small muscarinic response that was blocked by atropine (3  $\mu$ M). *B*, Response from a P21 WT (top) and  $\alpha 3^{-/-}$  (bottom) SCG neuron after inhibiting cholinesterase with neostigmine (10  $\mu$ M). *C*, Muscarinic responses on a P8WT neuron increased with the number of stimuli applied to the preganglionic nerve. The preganglionic nerve was stimulated at 20 Hz; the number of stimuli delivered to the preganglionic nerve is indicated at the left of each trace. *D*, Integrated muscarinic responses from neurons in WT ( $\blacktriangle$ ) and  $\alpha 3^{-/-}$  ( $\bullet$ ) ganglia were plotted against the number of applied stimuli to the preganglionic nerve. The solid line represents a fourth-order polynomial fit to the data. The inset compares the response of a P7 WT neuron after four stimuli to the response of a P7  $\alpha 3^{-/-}$  neuron to 20 stimuli. The values are the means  $\pm$  SEM ( $n = 8$  for WT and  $n = 7$  for  $\alpha 3^{-/-}$  neurons). All experiments were done with neostigmine (10  $\mu$ M) and hexamethonium (100  $\mu$ M) added to the perfusion fluid at 37°C. AP, Action potential.

We observed no significant difference in postsynaptic muscarinic responsiveness in WT versus  $\alpha 3^{-/-}$  SCG neurons. Moreover, we observed no difference in the density of preganglionic cholinergic varicosities between WT and  $\alpha 3^{-/-}$  ganglia. Therefore, the difference in response to preganglionic stimulation in WT and  $\alpha 3^{-/-}$  ganglia must result from differences in presynaptic release of ACh. Because preganglionic neurons in rodents do not appear to express the  $\alpha 3$  gene (Wada et al., 1989), it seems unlikely that the absence of  $\alpha 3$  can account for the low ACh output from terminals in  $\alpha 3^{-/-}$  ganglia. Moreover, our experiments on ACh output were done in blocking concentrations of hexamethonium, thereby eliminating any possible contribution of presynaptic nAChRs to the difference in transmitter output between varicosities in  $\alpha 3^{-/-}$  and WT ganglia (Liang and Vizi, 1997; Rogers and Sargent, 2003).

### **High-Affinity Choline Transporter Function**

Instead, our results suggest that the low ACh output from varicosities in  $\alpha 3^{-/-}$  ganglia result from malfunction, dysregulation, and/or low expression of the high-affinity HC-3-sensitive, choline transporter CHT (Okuda et al., 2000; Ferguson et al., 2004). Choline uptake through CHT is thought to be the rate-limiting determinant of ACh synthesis, particularly during activity-induced increases in release (Birks and MacIntosh, 1961). We show that repetitive stimulation depletes transmitter rapidly from terminals in  $\alpha 3^{-/-}$  ganglia, unlike those in WT, and that  $\alpha 3^{-/-}$  terminals recover slowly from depletion with a 5–10 min rest; these results are consistent with a malfunction/misexpression of the high-affinity choline transporter. Relevantly, we show that HC-3 significantly reduced ACh output from WT preganglionic terminals when stimulated with a 20

Hz train but had no effect on ACh output from terminals in  $\alpha 3^{-/-}$  ganglia; these results indicate that functional high-affinity choline transporters are absent from terminals in  $\alpha 3^{-/-}$  ganglia.

### **Retrograde Control of Transmitter Output at Developing Synapses**

Our results suggest that the absence of functional CHT and the low ACh output from presynaptic terminals in  $\alpha 3^{-/-}$  ganglia result from a lack of an activity-dependent retrograde signal. Recently, it has been demonstrated that CHT resides on a subset of vesicles in cholinergic terminals (Ferguson et al., 2003); moreover, it has been proposed that this subpopulation of CHT-containing vesicles are specifically recruited for release during prolonged periods of activity, delivering CHT to the membrane of the terminal, enabling high-affinity choline uptake for continued ACh synthesis (Ferguson et al., 2003). Therefore, if this recruitment depends on an activity-dependent retrograde signal, then the absence of such a signal could account for the reduced amount of ACh released from terminals in  $\alpha 3^{-/-}$  ganglia and fewer functional CHT on the membrane. Alternatively, it has been shown that the expression of CHT in motor neurons is downregulated when the axon is axotomized and subsequently upregulated during reinnervation of muscle (Oshima et al., 2004). This suggests that motor axons receive an activity-dependent retrograde signal from muscle that regulates the expression of CHT.

In two paralytic zebrafish mutants, *Sofa potato* and *Nic*, the postsynaptic muscle is not sensitive to ACh, and, although the NMJs in these mutants are morphologically normal, the junctions have no spontaneous or evoked endplate potentials (Westerfield et al., 1990; Li et al., 2003). Nonetheless, vesicle recycling

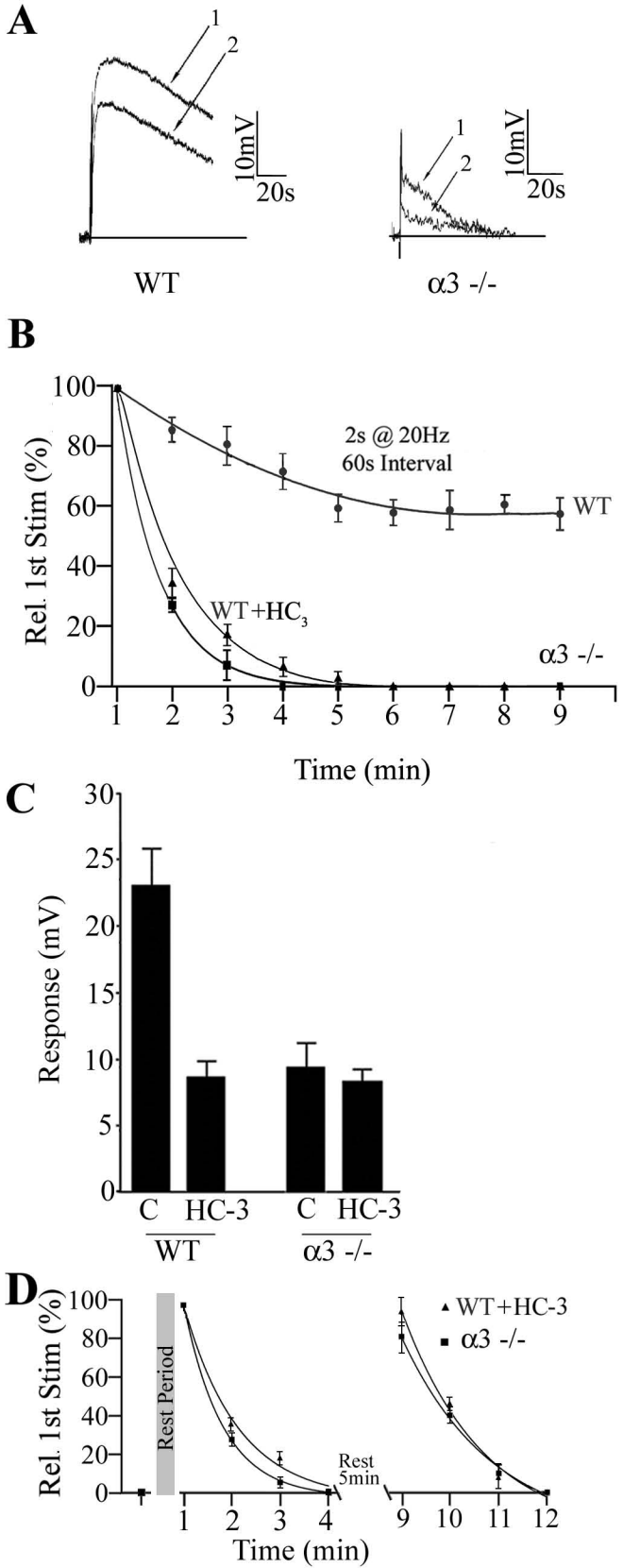


Figure 2.8

**FIGURE 2.8** ACh output from  $\alpha 3^{-/-}$  varicosities after burst stimulation depletes rapidly, recovers slowly, and is independent of the high-affinity choline transporter. *A*, Muscarinic depolarizations on a P7 neuron in a WT ganglion (left) and P7 neuron in an  $\alpha 3^{-/-}$  ganglion (right) in response to paired stimuli to the preganglionic nerve (2 s at 20 Hz) delivered 40 s apart. *B*, The response to a series of stimuli (2 s at 20 Hz) delivered at 60 s intervals and normalized to the first response in the series. In WT ganglia, the response declined gradually to  $\sim 70\%$  of the initial response and leveled off after five to six trials. In  $\alpha 3^{-/-}$  ganglia, conversely, the response declined rapidly and was not detectable after the third stimulus. In WT ganglia treated with HC-3 (10  $\mu\text{M}$ ), the response declined similarly and was not detectable after the fourth interval. The solid lines are single-exponential fits to the data. *C*, The bar graph shows that blocking the high-affinity choline transporter in WT ganglia with HC-3 (20  $\mu\text{M}$ ) decreased transmitter output to  $\sim 30\%$  of the control level, whereas HC-3 (20  $\mu\text{M}$ ) had little effect on responses in  $\alpha 3^{-/-}$  ganglia. *D* shows the peak muscarinic responses from P7 WT neurons treated with HC-3 ( $\blacktriangle$ ) and from P7  $\alpha 3^{-/-}$  neurons ( $\blacksquare$ ) when stimulated with two consecutive series of four stimuli (2 s at 20 Hz every 60 s) with 5 min rest intervals between each series; the response recovered almost completely after each rest interval and then rapidly became depleted. All experiments were done with neostigmine (10  $\mu\text{M}$ ) and hexamethonium (100  $\mu\text{M}$ ) added to the perfusion fluid at 37°C. The values are the means  $\pm$  SEM;  $n = 5$  for neurons in WT ganglia and  $n = 6$  for neurons in  $\alpha 3^{-/-}$  ganglia.

in the presynaptic terminals at these inactive neuromuscular junctions (NMJs) proceeds normally, as revealed by optical measures of exocytosis with FM1-43 [*N*-(3-triethylammoniumpropyl)-4-(4-(dibutylamino)styryl) pyridinium dibromide] (Li et al., 2003). If autonomic synapses in mice develop similarly to NMJs in zebrafish, then it is unlikely that the difference in ACh output that we observed between varicosities in  $\alpha 3^{-/-}$  and WT ganglia is attributable to a difference in vesicular release or recycling; instead, it suggests that an activity-dependent retrograde signal influences the output of transmitter by regulating some other process.

Two good examples of activity-dependent retrograde signaling that affect presynaptic transmitter output at developing synapses are the studies on NMJ in *Drosophila* (Petersen et al., 1997; Davis et al., 1998; DiAntonio et al., 1999; Haghghi et al., 2003) and the studies on *Xenopus* nerve–muscle junctions in culture (Tao and Poo, 2001). Extrapolating from the studies in *Drosophila*, we anticipate that depolarization, calcium influx, and the subsequent activation of CaM kinase II in the postsynaptic cell are crucial steps in regulating retrograde signals that influence transmitter output from presynaptic terminals (Haghghi et al., 2003). The studies on *Xenopus* nerve–muscle cocultures suggest that neurotrophins act as an activity-dependent retrograde signal to boost transmitter release (Tao and Poo, 2001). Because BDNF plays an important role in the developmental innervation of sympathetic ganglia (Causing et al., 1997), it will be interesting to discover whether BDNF is involved in activity-dependent retrograde signaling that regulates transmitter output from preganglionic terminals.

**CHAPTER 3:**  
**AN ACTIVITY-DEPENDENT RETROGRADE SIGNAL INDUCES THE**  
**EXPRESSION OF THE HIGH-AFFINITY CHOLINE TRANSPORTER IN**  
**CHOLINERGIC NEURONS**

**FOREWORD**

**Background and Rationale**

In Chapter 2, I demonstrate that morphologically normal cholinergic synapses form on sympathetic neurons that lack postsynaptic activity but ACh output from presynaptic nerve terminals is impaired. In chapter 3, I follow up on two observations from chapter 2: (1) I found that we could phenocopy the deficit in ACh output from nerve terminals in  $\alpha 3$ -null ganglia in WT ganglia by blocking CHT with hemicholinium-3 on WT nerve terminals, suggesting that nerve terminals in  $\alpha 3$  KO ganglia have low ACh output because they lack high affinity choline transporters (2) I found that morphologically normal synapses form on sympathetic neurons in  $\alpha 3$ -null ganglia but, I was unsure whether or not these synapses were stable and could persist without synaptic activity.

**Hypothesis**

I hypothesize that (1) signals downstream of postsynaptic activity regulate the expression of presynaptic choline transporters and that (2) signals downstream of postsynaptic activity are not required for synapses to persist on sympathetic neurons.

### **Experimental Outline**

To test these hypotheses, I will first need to extend the postnatal survival of  $\alpha 3$ -null mice. To do this I will take advantage of the hybrid vigor that mice experience when put on mixed genetic background. I believe that the loss of synaptic transmission on autonomic neurons combined with the inbred background severely reduces the fitness of  $\alpha 3$  null mice on a C57 Bl/6 background. To improve their survival, I will breed  $\alpha 3$  heterozygote mice onto a C57 Bl/6 X CD1<sup>+</sup> mixed genetic background to generate outcrossed  $\alpha 3$  heterozygotes and then mate these outcrossed mice together to produce  $\alpha 3$  KOs with hybrid vigor. To test whether presynaptic CHT is regulated by signals that depend on postsynaptic activity I will measure the presence of CHT functionally using electrophysiology and directly using immunofluorescence techniques in rescued  $\alpha 3$ -null mice. To determine whether synapses persist without synaptic activity I will quantify the number of synapses in  $\alpha 3$ -null ganglia over the first month using immunofluorescence techniques, electron microscopy and confocal microscopy.

**ABSTRACT**

A well-accepted view of developing circuits is that synapses must be active to mature and persist, whereas inactive synapses remain immature and are eventually eliminated. We question this long-standing view by investigating nonfunctional cholinergic nicotinic synapses in the superior cervical ganglia (SCG) of mice with a disruption in the  $\alpha 3$  nicotinic receptor (nAChR) subunit gene, a gene essential for fast synaptic transmission in sympathetic ganglia. Using imaging and electrophysiology, we show that synapses persist for at least 2–3 months without postsynaptic activity; however, the presynaptic terminals lack high-affinity choline transporters (CHTs), and as a result, they are quickly depleted of transmitter. Moreover, we demonstrate with rescue experiments that CHT is induced by signals downstream of postsynaptic activity, converting immature terminals to mature terminals capable of sustaining transmitter release in response to high-frequency or continuous firing. Importantly, postsynaptic neurons must be continually active to maintain CHT in presynaptic terminals.

## INTRODUCTION

The neurotransmitter acetylcholine (ACh) is involved in several physiological and cognitive processes, such as sleep, attention, memory, autonomic function, and movement, and debilitating diseases emerge when presynaptic terminals release insufficient amounts of acetylcholine. For proper signaling by cholinergic neurons, the presynaptic terminals must be able to release ACh continuously in response to high-frequency or sustained firing. To keep up with high demand, ACh is constantly resynthesized from choline and acetyl-CoA by choline acetyltransferase (ChAT) and concentrated in synaptic vesicles by the vesicular ACh transporter (VAChT) (Eiden, 1998; Deutsch, 1971; Wu and Hersh, 1994). The rate-limiting step for ACh synthesis is choline reuptake from the extracellular fluid through the high-affinity choline transporter (CHT).

The existence of a high-affinity choline uptake system has been known for over 50 years (Birks and MacIntosh, 1961; Bazalakova and Blakely, 2006; Ribeiro et al., 2006); however, the gene encoding CHT has been identified only recently (Apparsundaram et al., 2000; Apparsundaram et al., 2001; Okuda et al., 2000; Okuda and Haga, 2003). CHT is located on a reserve pool of vesicles; as these vesicles are recycled during high-frequency or sustained firing, CHT becomes localized in the presynaptic membrane, enabling choline to be transported from the synaptic cleft to the terminal for new ACh synthesis (Ferguson et al., 2003). Consequently, the ability of cholinergic neurons to maintain ACh release continuously in response to high-frequency firing depends critically on the expression and targeting of CHT. For example, in mice that lack

the CHT gene, the neuromuscular junctions cannot sustain ACh release, and these mice die shortly after birth (Ferguson et al., 2004).

In view of the important role for CHT in cholinergic signaling, it is surprising how little we know about what regulates the appearance of CHT as cholinergic neurons develop. Conceivably, CHT might be expressed early during cholinergic differentiation by the same or similar signals that induce the expression of the cholinergic gene locus, an 80 kb region in mammals that contain ChAT and VAcHT genes and the regulatory sequences responsible for ChAT and VAcHT in cholinergic neurons (Eiden, 1998; Weihe et al., 1998). On the other hand, cholinergic synapses require a relatively long maturation process before they can maintain high-frequency or sustain firing (Letinsky, 1974; Pilar et al., 1981; Polo-Parada et al., 2001; Polo-Parada et al., 2004; Polo-Parada et al., 2005; Rafuse et al., 2000). Therefore, an alternative possibility is that CHT is induced much later during development, possibly by extrinsic signals related to functional synapse formation, such as those downstream of postsynaptic activity. By distinguishing between these two alternatives, we will learn more about what regulates the appearance of CHT, and the conversion of immature terminals to mature terminals capable of sustaining transmitter release in response to high-frequency or repetitive firing.

A conclusive way to decide whether the induction of CHT requires signals mediated by synaptic activity is to investigate the appearance of CHT in cholinergic terminals at nonfunctional, silent synapses: if CHT is present in the presynaptic terminals at these silent synapses, one could exclude the possibility that its appearance is induced by synaptic activity. Carrying out these experiments in mammals is complicated because animals without functional cholinergic synapses die at birth, limiting observations to relatively immature

synapses in newborn animals (Misgeld et al., 2002; Schoch et al., 2001; Verhage et al., 2000; Varoqueaux et al., 2002; Varoqueaux et al., 2005; Washbourne et al., 2002). Ideally, to address these issues *in vivo*, one would like to investigate cholinergic synapses that are not crucial for the survival of the animal. One system that satisfies these requirements is cholinergic nicotinic synapses in the superior cervical ganglia (SCG) of mice with a disruption in the  $\alpha 3$  nicotinic receptor (nAChR) subunit gene.

Expression of the  $\alpha 3$  nAChR subunit gene is essential for ACh-evoked inward currents on sympathetic neurons (Rassadi et al., 2005) and normal autonomic function (Xu et al., 1999), and deletion of  $\alpha 3$  abolishes fast synaptic activity in sympathetic ganglia. These mice live during the early postnatal period, but unfortunately, when  $\alpha 3$  KO mice are raised as inbred strains, they die during the first week after birth, insufficient time to investigate fully the development and maturation of these silent synapses. However, we discovered to our surprise that the autonomic abnormalities and the high neonatal mortality are not linked: when  $\alpha 3$  KO mice are raised as an outbred strain, they live in good health for several months in the complete absence of fast synaptic transmission in sympathetic ganglia.

Using sympathetic ganglia from outbred  $\alpha 3$  KO mice, we show that synapses persist for at least 1–2 months without postsynaptic activity; however, CHT is absent from the presynaptic terminals. By combining immunocytochemistry, confocal microscopy, and electrophysiological and *in vivo* gene transfer experiments, we show that CHT appears late during development and is induced by signals downstream of postsynaptic activity. Moreover, we show that postsynaptic neurons must be continually active to maintain CHT in presynaptic terminals.

## **METHODS AND MATERIALS**

### **Mice**

A colony of C57BL/6/J  $\alpha 3$  KO mice (gift from Dr. A. Beaudet) was maintained by breeding heterozygous animals. To produce  $\alpha 3$  KO mice as an outbred strain, we mated C57BL/6/J  $\alpha 3^{+/-}$  males to CD<sup>+</sup> females (Charles River, St. Constant, Quebec) and then mated the F1 heterozygotes to produce  $\alpha 3$  KO mice on a mixed C57BL/6/J - CD<sup>+</sup> background. All genotyping of pups was done by PCR (Xu et al., 1999). Most experiments were done with superior cervical ganglia (SCG) from neonatal pups (P0–P14) and young adults (P21–P60)  $\alpha 3$  KO mice and WT littermates.

### **Extracellular and Intracellular Recordings**

Ganglia were pinned down in a small recording chamber (1.5 ml volume) with minutia pins, perfused continuously at 3–4 ml/min with oxygenated modified Tyrode's solution supplemented with glucose (5.6 mM) and choline (0.01 mM) (pH = 7.3–7.4) at 36°C–37°C, and viewed through a dissecting microscope (SMZ-10; Nikon, Tokyo, Japan). The preganglionic nerve in the cervical sympathetic trunk was connected to a stimulator (Warner instruments) with a suction electrode and the postganglionic trunk was connected to an alternating current differential amplifier (DP-301; Warner Instruments, Hamden, CT) with a suction electrode. The postganglionic compound action potentials were amplified (1000 $\times$ ), filtered at 10 Hz (low-pass cutoff) and 3 kHz (high-pass cutoff), digitized, displayed, and stored on a Pentium II-based personal computer with Patchkit (Alembic Software, Montreal, Quebec, Canada). The data were analyzed off-line

with Igor (WaveMetrics, Lake Oswego, OR). All drugs were added directly to the oxygenated Ringer's solution.

To record from ganglion cells intracellularly, we used 40–80 M $\Omega$  glass microelectrodes (G150F-4; Warner Instruments) made with a DMZ universal puller (Zeitz Instruments, Munich, Germany) and filled with 1 M KAc. Stable intracellular recordings were achieved with a high inertial precision microdrive (Inchworm 8200; EXFO, Vanier, Quebec, Canada) attached to a micromanipulator (SM11; Narshige, Tokyo, Japan) that drove the electrode through the ganglion. The recording electrode was connected by a thin silver chlorided wire to the head stage of an Axoclamp 2A amplifier (Axon Instruments, Union City, CA) used in current-clamp mode; depolarizing or hyperpolarizing constant current pulses were applied through the recording electrode, and membrane potentials were filtered at 10 kHz, sampled, displayed, and stored on a Pentium II-based personal computer. Stimulation and acquisition was done with Patchkit software (Alembic Software), and the data were analyzed off-line with IGOR. The preganglionic nerve was stimulated with brief (0.1–0.2 ms) voltage pulses applied to the cervical sympathetic trunk through the suction electrode. For experiments with the conductance mutant,  $\alpha 3^{E240A}$ , we averaged  $\sim 30$ –50 trials to resolve the EPSPs. All drugs were dissolved in oxygenated Tyrode's solution modified as above. Only neurons with membrane potentials greater than  $-40$  mV were included in this study.

To determine whether synapses could sustain transmission, we stimulated the preganglionic nerve for 1 min with a 10 Hz train and measured the changes in EPSPs over 60 s by averaging ten EPSPs at 10 s intervals following the start of the 60 s train, normalized to the average of first ten EPSPs in the train. For these experiments, usually curare (5–10  $\mu$ M) was added to make the

EPSPs were subthreshold; omitting curare had no significant effect on these results with 10 Hz trains. Only neurons with stable membrane potentials during the train were included in these experiments.

### **Adenoviruses**

Full-length  $\alpha 3$  neuronal nAChR subunit cDNA was ligated into pAdTrack-cytomegalovirus (Ad $\alpha 3$ /CMV) or pAdTrack-synapsin 1 (Ad $\alpha 3$ /Syn), and replication-deficient viral vectors were made according to He et al. (1998). All viruses were titered in duplicate with the cytopathic effect method (Nyberg-Hoffman et al., 1997). Neonatal animals (P0–P21) and young adult (P28–P60)  $\alpha 3$  KO animals were infected with Ad $\alpha 3$ /CMV or Ad $\alpha 3$ /Syn adenovirus by injecting the vectors intraperitoneal (50–100  $\mu$ l at  $10^7$  pfu dissolved in L15) for pups younger than P10; for older mice, we injected virus i.v. through the tail vein. As controls, we infected mice with AdGFP/CMV and AdGFP/Syn, adenoviral vectors that express GFP from either the hCMV or synapsin 1 promoter. For Ad $\alpha 3^{E240A}$ /Syn, we mutated  $\alpha 3$  at position 240 using Quick-Change Site-Directed Mutagenesis kit (Stratagene, La Jolla, CA) and verified the change by sequencing (Haghighi and Cooper, 2000).

We obtained weak expression in sympathetic neurons when we infected P1  $\alpha 3$  KO mice with Ad $\alpha 3$ /hCMV: 7 days post infection, only about 10% of ganglia had detectable compound action potentials (CAPs) and these CAPs were considerably smaller than those from WT ganglia; in addition, we found that only about one in ten neurons had detectable EPSPs and their amplitudes were only 1–3 mV. Moreover, we observed only weak GFP fluorescence in SCG; however, stimulating ganglia from infected mice overnight with high  $K^+$  resulted in abundant GFP-positive SCG neurons, demonstrating that adenoviral vectors infect SCG

neurons well but that the hCMV promoter functions poorly, presumably because the postganglionic sympathetic neurons in  $\alpha 3$  KO mice are not active (Wheeler and Cooper, 2001; and Wheeler and Cooper, 2004).

### **Immunohistochemistry**

Freshly dissected ganglia were placed in 0.5% paraformaldehyde (PFA) in 0.1 M phosphate buffer (PB) for 1 hr, overnight in 40% sucrose in 0.1 M PB, and then embedded in OCT compound and frozen immediately by immersion in 2-methylbutane cooled in liquid nitrogen. Frozen sections (30  $\mu$ m) were cut from these ganglia with a cryostat and placed onto Probe-on Plus slides (Fisher Scientific, Houston, TX); the sections were rinsed with PBS for 30 min, blocked for 1 hr in 10% normal donkey serum (DS) in PBS and 0.5% triton X-100 (TX) at room temperature for 1 hr, and then overnight in primary antibodies (polyclonal goat anti-VACht (1:750; Chemicon, Temecula, CA), rabbit anti-CHT (1/1000) (a gift of Dr. R. Blakely), or anti-postsynaptic density 93 (rabbit anti-PSD93; 1/100, Synaptic Systems) and anti-postsynaptic density 95 (goat anti-PSD95; 1/100, Synaptic Systems) or rabbit anti-PSD93 and anti-Sh3 ankyrin repeat contain protein (goat anti-Shank; 1/400, Chemicon) or rabbit anti-PSD93 and anti-guanylate kinase associated protein (goat anti-GKAP; 1/400, Synaptic Systems) in PBS containing 10% normal donkey serum at 4°C. The sections were rinsed three times with PBS and then placed in secondary antibodies (Alexa 488 donkey anti-goat antibodies [1/1000, Molecular Probes] and rhodamine donkey anti-mouse antibodies [Jackson ImmunoResearch, West Grove, PA]) in PBS containing 10% normal donkey serum for 1 hr at room temperature; the sections were then rinsed three times with PBS and mounted with Vectashield (Vector Laboratories, Burlingame, CA). For diaphragm experiments, freshly dissected

P28 diaphragms were placed in 4% PFA for 1 hr, then blocked and permeabilized in 10% DS in PBS and 3% TX at room temperature for 3 hr. Diaphragms were then placed in primary antibodies polyclonal goat anti-VACHT (1/750) and rabbit anti-CHAT (1/1000) in PBS containing 10% normal donkey serum at 4°C. For spinal cord experiments, we took P28 WT and  $\alpha 3$  KO mice and perfused them with PBS for 2–4 min followed by 2% PFA for 2 min. Then we rapidly dissected the thoracic segment of the spinal cord, placed them in a solution of 2% PFA for 1 hr, and froze them immediately by immersion in 2-methylbutane cooled in liquid nitrogen. Cross-sections of spinal cord were always cut the following day and stained as above with goat-anti choline acetyltransferase (1/100 ChAT, Chemicon) and rabbit anti-CHAT (1/1000) primary antibodies. Nonspecific staining, judged by processing sections without the primary antibody, was very low.

For imaging, a series of z stacks (0.3  $\mu\text{m}/\text{plane}$ ) was obtained with a confocal microscope (LSM 510; Zeiss) and a 63 $\times$ , 1.4 numerical aperture Plan Neofluor oil-immersion objective. We set values for detector gain, detector offset, and amplifier offset by imaging ten different WT P28 SCG stained for VACHT and CHAT and found values that captured the distribution of intensities within an image depth of 8 bits. We used these acquisition parameters for all subsequent VACHT and CHAT images. For images acquired from SCG stained for synaptic proteins, where the intensity of staining was less important, we adjusted the acquisition settings to optimize the staining for these proteins in WT sections and applied these settings to image  $\alpha 3$  KO sections. These images were acquired as a z stack, where the xy dimensions of each plane were 66.5  $\mu\text{m} \times 66.5 \mu\text{m}$  (at 1024  $\times$  1024 pixels) and the plane thickness was 0.33  $\mu\text{m}$ .

Images were quantified off-line with MetaMorph (Universal Imaging Corporation). First, we measured the mean minimal intensity (MI) for green and for red (usually 30–50 AU for all conditions) on each plane of the stack by taking a line scan through the center of the image and used twice MI to set the threshold for each plane. Next, we made running averages of three consecutive planes through the entire z stack; these stacks of three averaged planes were then split up into red (CHT) and green (VACHT) components. We used MetaMorph analysis software to define VACHT-positive varicosities using three criteria:  $0.7 \mu\text{m}^2 \leq \text{area} \leq 7.0 \mu\text{m}^2$ ;  $0.5 \leq \text{shape factor } (p) \leq 1$ ;  $2\text{MI} \leq \text{intensity} \leq 256$ . To quantify the proportion of CHT-positive terminals, we transferred the VACHT-positive regions from the VACHT stack onto the CHT stack and measured the number of colocalized CHT-VACHT terminals as a fraction of the total number of VACHT-positive terminals. To quantify CHT levels, we measured average pixel intensities from colocalized CHT-VACHT terminals; terminals without CHT were excluded from this average.

The representative images in figures of CHT- and VACHT-stained SCG were created by averaging three consecutive image planes from a z stack, cropping the averaged image, splitting the color components of the cropped image, thresholding each color channel individually to  $2\times$  the value of background intensity, and adding the two component images back together. VACHT-positive spots present in only the first or the last plane of three consecutive planes were removed for clarity from the final cropped image. We processed the representative images of synaptic protein staining in a similar way, except that after thresholding the individual components, we maximized intensity values in the component images to highlight the overlapped staining on the

merged image. Occasionally, we used the low pass filter tool, with a  $2 \times 2$  convolution kernel, in Metamorph to remove single pixel noise from our images.

### **In Situ Hybridization**

Our procedures for in situ hybridization were similar to those that we used previously (Rosenberg et al., 1997). Briefly we carried out experiments with fresh-frozen and prefixed, cryoprotected cryostat sections of P21–P28 thoracic spinal cord. For fresh-frozen sections, spinal cords were rapidly dissected, embedded in O.C.T. mounting compound, and then frozen in isopentane cooled in liquid nitrogen. For prefixed sections, mice were perfused transcardially using PBS followed by 4% PFA, spinal cords removed, and left in 40% sucrose overnight and then frozen in isopentane cooled in liquid nitrogen. Frozen tissue samples were cut at 60  $\mu\text{m}$  thickness with a  $-20^\circ\text{C}$  cryostat and placed onto Probe On Plus slides (Fisher Scientific, Pittsburgh, PA). Fresh-frozen spinal sections were rinsed in PBS for 30 min to remove O.C.T., fixed for 5 min with 3% paraformaldehyde in 0.1 M Na phosphate buffer (0.1 M  $\text{NaH}_2\text{PO}_4/0.1$  M  $\text{Na}_2\text{HPO}_4$ , pH 7.4), rinsed with PBS, rinsed with DEPC water, dehydrated with alcohol, air-dried at room temperature, and then prehybridized for 3 hr at  $43^\circ\text{C}$  in a solution containing salmon sperm DNA (250  $\mu\text{g}/\text{ml}$ , Pharmacia), ribonucleoside vanadyl complex (20 mM, New England Biolabs, Beverly, MA),  $4 \times$  SSC (0.3 M NaCl, 0.03 M Na citrate in DEPC water), 50% formamide, and 0.1% tween-20. Then the prehybridization solution was replaced with the hybridization solution, prepared as above but without tween-20 and with 5–10  $\text{ng}/\mu\text{l}$  of labeled RNA probes (see below). Prefixed spinal cord sections were rinsed in PBS for 30 min to remove O.C.T., rinsed with DEPC water, dehydrated with alcohol, and then followed the same processing as fresh-frozen section. For imaging, a series of z

stacks (1.4  $\mu\text{m}/\text{plane}$ ) were obtained with a confocal microscope (LSM 510; Zeiss) and a 20 $\times$ , 0.5 numerical aperture Plan Neofluor water-immersion objective. To reconstruct spinal cords, individual averaged planes were stitched together using Adobe Photoshop CS2. Adjacent sections were immunostained for ChAT to identify the intermediate lateral nucleus and ventral horn.

The labeled RNA probes were made from the last 518 bp of the 3' end of the CHT cDNA (obtained from Adgene). Briefly, Alexa 594-labeled sense and antisense CHT probes were synthesized by in vitro transcription with T7 and SP6 RNA polymerase, respectively, using an RNA FISH tag red kit (Invitrogen, Carlsbad, CA, USA).

### **Ultrastructural Studies**

Ganglia were rapidly dissected from P28 WT and P28  $\alpha 3$  KO mice, placed directly into 2% paraformaldehyde/2% glutaraldehyde in phosphate buffer (PB) 0.1 M at room temperature on a shaker for 30 min, and then cut in half and fixed for an additional 60–90 min. The tissue was then rinsed three times in 0.1 M PB at room temperature (10 min each), postfixed in 1%  $\text{OsO}_4$  plus 1.5% potassium ferricyanide in  $\text{H}_2\text{O}$  on a shaker for 1 hr at room temperature, rinsed briefly with distilled  $\text{H}_2\text{O}$ , dehydrated in graded series of ethanol concentrations up to 100%, placed in 100% propylene oxide for 10–15 min (twice), and embedded in Embed812 and polymerized (24 hr in an oven at 60°C). Thin sections of ganglia were cut on an ultramicrotome, stained with 2% aqueous uranyl acetate and 3% lead citrate, viewed with a Philips (Holland) EM410 electron microscope, and digital images were captured by Megaview 2 cooled-CCD camera at 10°C and a GraBIT digital input board with analySIS analysis software (Olympus, Munster, Germany) and stored as 1280  $\times$  1024 pixel images

at 8 bits and analyzed off-line. To quantify synaptic morphology, we analyzed our images with Metamorph. For some images of large synapses in  $\alpha 3$  KO SCG, the sections were tilted at different angles before acquisition and then summed into a single image that encompassed the whole synapse.

### **Statistics**

To test for differences in the proportion of terminals with CHT, we used the binomial test. We defined  $p$  and  $q$  empirically as percent of VAcHT-positive terminals with or without CHT, respectively. For analyses where we compared VAcHT-positive terminals from  $\alpha 3$  KO and WT, we set the expected ratio of  $p:q$  as that in age-matched WT SCG. In  $\alpha 3$  KO mice infected with virus, we set the expected ratio of  $p:q$  as that in age-matched  $\alpha 3$  KO SCG. For each condition, we calculated the standard deviation using the normal approximation to the binomial distribution and used the  $z$  score to test for significant differences. All values for binomial distributions and probabilities were calculated using SISA online statistical software. For all other statistical testing, we used an unpaired two-sample  $t$  test assuming equal variance. All values reported in the Results are the means  $\pm$  SEM.

All procedures for animal handling were carried out according to the guidelines of the Canadian Council on Animal Care (CCAC).

## **RESULTS**

### **Survival of $\alpha 3$ KO Mice Raised as an Outbred Strain**

Homozygous  $\alpha 3$  KO mice raised as an inbred strain on a C57BL/6/J background are smaller and weaker than WT littermates and generally die within

the first two postnatal weeks (Xu et al., 1999) ([Figure 1A](#)). This phenotype might be expected for mice with an autonomic nervous system that functions poorly (Xu et al., 1999). However, because inbred strains have a generalized decrease in a number of fitness characteristics, including body weight, lifespan, fecundity, litter size, and resistance to disease (Silver, 1995), it raised the possibility that the inbred background was, in part, responsible for the poor fitness and premature death of these homozygous  $\alpha 3$  KO C57BL/6/J mice. To test this, we generated homozygous  $\alpha 3$  KO animals on an outbred background by crossing heterozygote  $\alpha 3$  KO C57BL/6/J mice with CD-1<sup>+</sup> mice, an outbred strain. Although genetically undefined, these homozygous  $\alpha 3$  KO outcrossed mice exhibited hybrid vigor in many of their fitness characteristics (Silver, 1995), including low neonatal mortality and rapid growth. Most relevant for our study, these animals live for several months in good health ([Figure 1A](#)), and many of the homozygote female  $\alpha 3$  KO outbred mice reproduce.

### **Synapses Persist in the Absence of Fast Synaptic Activity in SCG of $\alpha 3$ KO**

#### **Mice**

We showed previously that a deletion in the  $\alpha 3$  neuronal nAChR subunit gene abolishes fast synaptic transmission in SCG from neonatal homozygote  $\alpha 3$  KO C57BL/6/J mice and that isolated SCG neurons lack ACh-evoked inward currents (Rassadi et al., 2005). Given the dramatic improvement in overall phenotype when  $\alpha 3$  KO mice are put on a mixed genetic background, we wondered whether these mice had inadvertently developed some degree of synaptic transmission in autonomic ganglia. To test this, we measured synaptic transmission in the SCG from  $\alpha 3$  KO outcrossed mice ( $n = 150$ ) ranging in ages from postnatal day 1 (P1) to P60. Preganglionic nerve stimulation failed to evoke

compound action potentials from any  $\alpha 3$  KO ganglia (Figure 1B); moreover, when recording directly from sympathetic neurons with intracellular electrodes, we failed to detect any nerve-evoked changes in membrane potentials from neurons ( $n = 200$ ) in intact SCG from over 75  $\alpha 3$  KO outbred mice (Figure 1B). In contrast, all WT ganglia ( $n = 50$ ) tested had large compound action potentials, and all sympathetic neurons ( $n = 80$ ) examined in intact WT ganglia had suprathreshold nerve-evoked EPSPs (Figure 1B). These results indicate that fast synaptic transmission is completely absent in sympathetic ganglia of  $\alpha 3$  KO outbred mice.

Although synaptic transmission was absent, when we examined ganglia from 4- to 5-week-old  $\alpha 3$  KO mice at the ultrastructural level, morphological synapses were readily apparent and appeared normal (Figure 1C). Both WT and  $\alpha 3$  KO synapses had the characteristic features of accumulations of synaptic vesicles adjacent to the presynaptic surface membrane, enhanced postsynaptic density, parallel arrangement of pre- and postsynaptic membranes, and a widened synaptic cleft. We quantified 45 synapses from 11 different ganglia in 1-month-old  $\alpha 3$  KO mice and 33 synapses from five ganglia in WT littermates and found no significant difference ( $p > 0.2$ ) in length of the PSD ( $293.07 \pm 25.7$  nm for WT and  $325.5 \pm 19.9$  for  $\alpha 3$  KO). These results indicate that electrophysiologically silent synapses exist in sympathetic ganglia of 1-month-old  $\alpha 3$  KO mice.

Interestingly, the presynaptic terminals at synapses in 1-month-old  $\alpha 3$  KO ganglia had cross-sectional areas that were  $\sim 40\%$  larger than those in WT ganglia ( $1.17 \pm 0.004 \mu\text{m}^2$  for  $\alpha 3$  KO [ $n = 39$ ] versus  $0.675 \pm 0.002 \mu\text{m}^2$  for WT [ $n = 33$ ;  $p < 0.001$ ]). Moreover, a subset of presynaptic terminals in  $\alpha 3$  KO ganglia (roughly 5%–10%) were  $\sim 3.5$ -fold ( $3.96 \pm 0.07 \mu\text{m}^2$ ) larger and formed a cluster

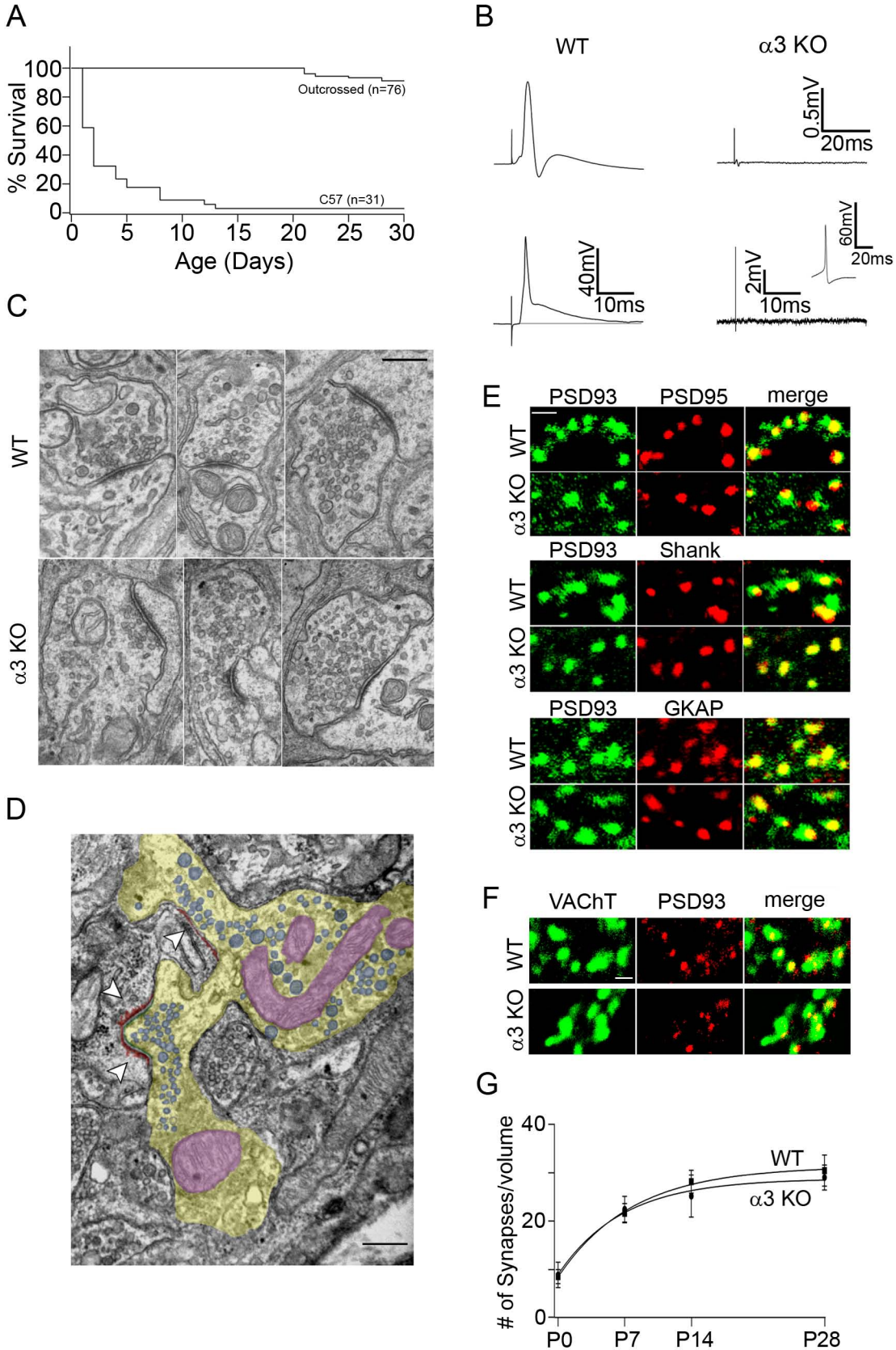


**Figure 3.1**

**FIGURE 3.1** Morphology and Postnatal Development of Electrophysiologically Silent Synapses in SCG of  $\alpha 3$  KO Mice **A** Survival curve for 31  $\alpha 3$  KO C57BL/6/J mice from ten litters and 76  $\alpha 3$  KO outcrossed mice from 25 litters over the first postnatal month. Roughly 80% of inbred  $\alpha 3$  KO C57BL/6/J mice died within the first 5 days after birth, whereas  $\sim 90\%$  of the  $\alpha 3$  KO outcrossed mice survived for at least 28 days. **B** Sympathetic neurons from  $\alpha 3$  KO mice lack fast synaptic transmission. The top traces show extracellular compound action potentials recorded from the sympathetic trunk in P28 WT and P28  $\alpha 3$  KO SCG; the lower traces show nerve-evoked EPSPs recorded intracellularly from sympathetic neurons in P28 WT and P28  $\alpha 3$  KO SCG. Suprathreshold stimulation of the preganglionic nerve could not evoke compound action potentials or EPSPs from P28  $\alpha 3$  KO SCG; the inset on the lower right shows that direct stimulation evokes action potentials on  $\alpha 3$  KO neurons. **C** Ultrastructure of synapses in P28 WT ganglia (top row) and P28  $\alpha 3$  KO ganglia (bottom row). Scale bar, 200 nm. **D** Electron micrograph of a large presynaptic terminal from a P28  $\alpha 3$  KO SCG. This image was pseudocolored for clarity: presynaptic terminal (yellow), presynaptic vesicles (blue), mitochondria (violet), and postsynaptic densities (red); the arrowheads mark synapses. These large terminals were observed in roughly 5%–10% of synapses in SCG from  $\alpha 3$  KO ganglia at 1 month. **E** Proteins present in the postsynaptic complex on sympathetic neurons in P28 WT and P28  $\alpha 3$  KO ganglia: PSD93 (left column, green), PSD95 (middle column, top), Shank (middle column, middle), and GKAP (middle column, bottom). Colocalization (right column) of PSD93 with PSD95 (top), Shank (middle), GKAP (bottom). The proportion of PSD93 spots that colocalized with the core scaffolding proteins in  $\alpha 3$  KO SCG ( $92\% \pm 2\%$  for PSD95;  $88\% \pm 3.6\%$  for GKAP;  $89\% \pm 2.7\%$  for Shank;  $n = \sim 1800$  in five ganglia) was not significantly different from those in WT ganglia ( $93\% \pm 2.3\%$  for PSD 95;  $87\% \pm 4.2\%$  for GKAP;  $90\% \pm 3.2\%$  for Shank;  $n = \sim 1500$  in five ganglia;  $p > 0.2$ ). These data indicate that scaffolding proteins of the postsynaptic densities coassemble without postsynaptic activity or depolarizations mediated by postsynaptic nAChRs. Scale bar, 0.5  $\mu\text{m}$ . **F** Immunostaining for VAcHT (left; green) and PSD93 (middle; red) in WT SCG (top row) and  $\alpha 3$  KO ganglia (bottom row). Over 95% of PSD93 puncta colocalize with VAcHT-positive terminals (right column). Scale bar, 1.0  $\mu\text{m}$ . **G** Shows that the relative number of synapses in WT (■) and  $\alpha 3$  KO SCG (●) increases to the same extent over postnatal development. Synapses were taken as colocalized PSD93/VAcHT puncta and normalized to volumes encompassed by four adjacent neuronal nuclei. Over 60 Volumes were counted per ganglia from five different WT and  $\alpha 3$  KO mice per time point. There is no significant difference ( $p > 0.2$ ) between the relative number of synapses in WT and  $\alpha 3$  KO ganglia at any time point. Error bars represent  $\pm$  SEM.

of two to three synapses spaced within 1–3  $\mu\text{m}$  of each other ([Figure 1D](#)); such large terminals and synaptic clusters were not detected in WT ganglia. These observations suggest that presynaptic terminals grow larger in the absence of postsynaptic activity, perhaps in response to a growth signal emitted by the postsynaptic neuron to compensate for the lack of synaptic transmission. Qualitatively, the frequency of observing synapses in 1-month-old  $\alpha 3$  KO ganglia at the ultrastructural level was similar to that in WT ganglia. However, it is difficult to obtain a quantitative measure of the number of synapses with EM, as the density of synapses in sympathetic ganglia is relatively low (Forehand, 1985). Therefore, to estimate the relative density of synapses in  $\alpha 3$  KO and WT ganglia, we used immunocytochemistry and confocal microscopy.

Previous work has shown that at least four scaffolding proteins colocalize at cholinergic synapses in mice autonomic ganglia (Brenman et al., 1996; Parker et al., 2004): the postsynaptic density proteins, PSD93 and PSD95, guanylate kinase-associated protein (GKAP/SAPAP), and SH3 and ankyrin-containing protein (Shank/ProSAP). We immunostained 1-month-old  $\alpha 3$  KO and WT ganglia for PSD93 together with PSD95, GKAP, or Shank and observed abundant discrete PSD93-positive spots in the neuropil between adjacent neuronal cell bodies; a high proportion of these PSD93 spots (>90%) colocalized with the other three core scaffolding proteins ([Figure 1E](#)). Moreover, the proportion PSD93 spots that colocalized with the core scaffolding proteins in  $\alpha 3$  KO ( $92\% \pm 2\%$  for PSD95;  $88\% \pm 3.6\%$  for GKAP;  $89\% \pm 2.7\%$  for Shank;  $n = \sim 1800$  in five ganglia) was not significantly different from those in WT ganglia ( $93\% \pm 2.3\%$  for PSD 95;  $87\% \pm 4.2\%$  for GKAP;  $90\% \pm 3.2\%$  for Shank;  $n = \sim 1500$  in five ganglia;  $p > 0.2$ ); this demonstrates that neither postsynaptic activity nor  $\alpha 3$ -

containing nAChRs is required for the assembly of this complex in sympathetic ganglia.

To identify synapses, we immunostained for PSD93 to mark postsynaptic sites and the vesicular ACh transporter (VAChT) to mark cholinergic presynaptic terminals ([Figure 1F](#)). Over 95% (n = 300) of the discrete PSD93 spots colocalized with VAChT-positive spots in both WT and  $\alpha 3$  KO ganglia: these discrete spots likely represent synaptic contacts. To estimate synapse number over postnatal development we counted the number of colocalized PSD93/VAChT spots in WT and  $\alpha 3$  KO ganglia of different ages.

In both WT and  $\alpha 3$  KO ganglia, synapses are already present at birth (Rassadi et al., 2005), and we show that the relative number of synapses increases ~3-fold over the first two postnatal weeks; thereafter, the relative number of synapses remains stable for at least 1 month ([Figure 1G](#)). There is no significant difference ( $p > 0.2$ ; n = 1500) between the number of synapses in WT and  $\alpha 3$  KO ganglia over the first postnatal month. These results indicate that (1) synapse formation in mice SCG does not require signals downstream of postsynaptic activity and that (2) electrophysiologically silent synapses in SCG can persist for at least 1 month.

### **CHT Is Absent in Preganglionic Neurons of $\alpha 3$ KO Mice**

Although synapses in  $\alpha 3$  KO ganglia are well-differentiated at the ultrastructural level, our previous study suggested that presynaptic terminals in  $\alpha 3$  KO ganglia lacked functional hemicholinium-sensitive choline transporters and were defective in ACh output (Rassadi et al., 2005). To test whether the transporters were present but did not function, we coimmunostained presynaptic terminals in 1-month-old WT and  $\alpha 3$  KO ganglia for VAChT and the high-affinity

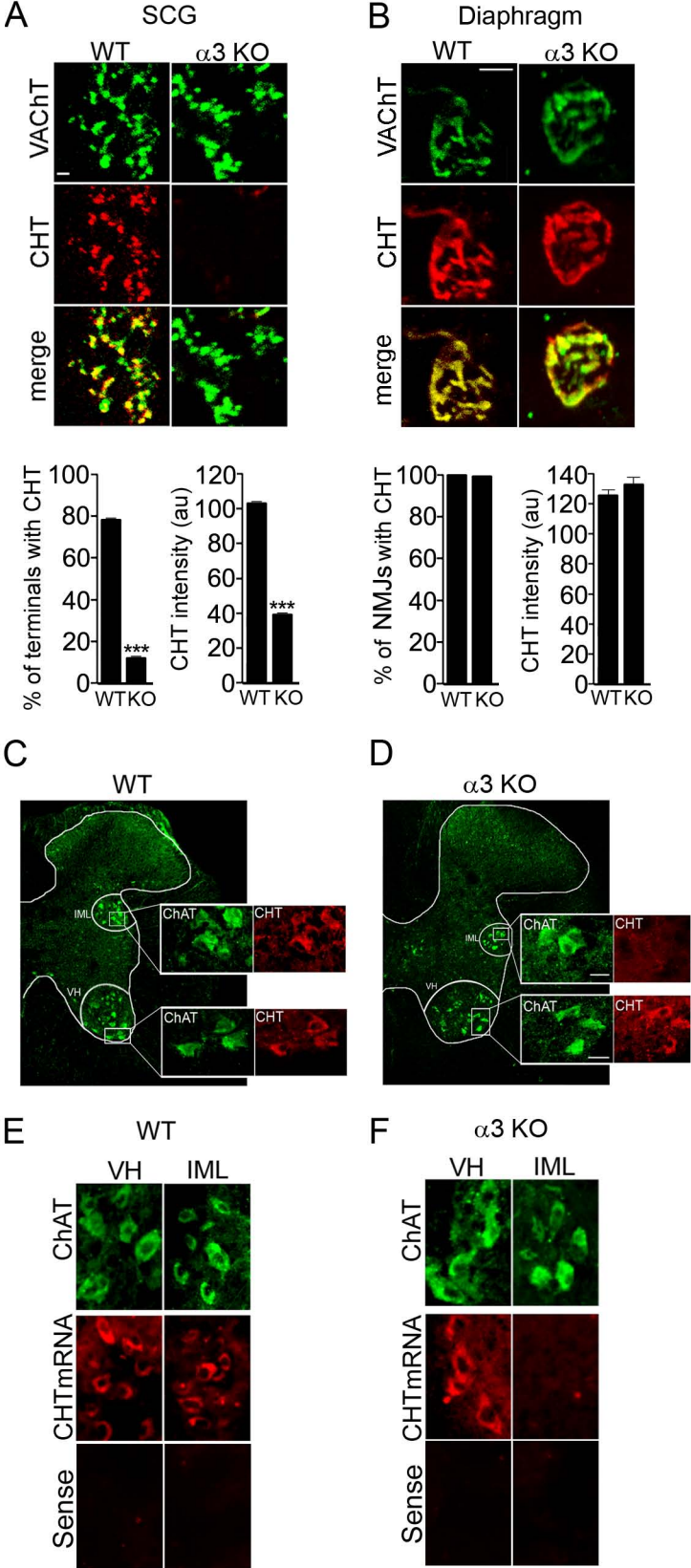


**Figure 3.2**

**FIGURE 3.2** Low Expression of CHT in Preganglionic Neurons Innervating SCG in P28  $\alpha 3$  KO Mice. **A** Immunostaining SCG from P28 WT and  $\alpha 3$  KO mice for VACHT (top; green), CHT (middle; red); colocalization of VACHT and CHT (bottom, merged). Scale bar, 1.0  $\mu$ m. The graphs show the percentage of over 3000 VACHT-positive terminals in WT SCG (n = 8) and  $\alpha 3$  KO ganglia (n = 8) that contain CHT immunofluorescence (left); the average CHT intensity excluding CHT-negative terminals is shown on the right. There is a significant reduction in the percentage of terminals with CHT and in the average CHT intensity of nerve terminals in  $\alpha 3$  KO SCG compared to those in WT SCG ( $^{***}p < 0.0001$ ). **B** Immunostaining neuromuscular junctions (NMJ) in diaphragms of P28 WT and  $\alpha 3$  KO mice for VACHT (green) and CHT (red). Scale bar, 10  $\mu$ m. The graphs show the proportion of VACHT-positive terminals (n = 50) in WT diaphragms (n = 6) and  $\alpha 3$  KO diaphragms (n = 8) that contain CHT immunofluorescence (left) and the average intensity of this CHT fluorescence (right). There is no significant difference ( $p > 0.2$ ) between the percent of terminals that contain CHT or average CHT intensity in P28 WT and  $\alpha 3$  KO diaphragms. **C** and **D** Thoracic cross-sections of a P28 WT (C) and P28  $\alpha 3$  KO (D) spinal cord double-stained for choline acetyltransferase (ChAT; green) and CHT (red). The low-power images show the location of sympathetic preganglionic neurons in the intermediolateral nucleus (IML) and motor neurons in the ventral horn (VH). The insets show high-power images of the same section: upper row, IML; lower row, VH. ChAT and CHT staining in the VH of both WT and  $\alpha 3$  KO are similar, whereas ChAT and CHT stains the IML of WT, but only ChAT stains the IML of  $\alpha 3$  KO. Similar images were observed in spinal cords from P28 WT (n = 6) and P28  $\alpha 3$  KO (n = 9) mice. Scale bars: VH is 20  $\mu$ m and IML is 10  $\mu$ m. **E** and **F** High-power images of neurons in the ventral horn (VH) and intermediolateral nucleus (IML) from a WT spinal cord (E) and  $\alpha 3$  KO spinal cord (F) treated with fluorescently tagged antisense CHT (middle, CHT mRNA). Adjacent tissue sections were immunostained for ChAT to identify the VH and the IML (top, ChAT). Fluorescent signal from spinal tissue sections treated with sense CHT mRNA probes was very low (bottom, sense). Scale bars: VH is 20  $\mu$ m and IML is 10  $\mu$ m. Error bars represent  $\pm$  SEM.

choline transporter, CHT. Our results indicate a dramatic difference in the appearance of CHT in presynaptic terminals: in WT ganglia, over 75% of VAcHT-positive varicosities contained CHT (Figure 2A); in contrast, less than 15% of VAcHT-positive varicosities in  $\alpha 3$  KO ganglia were CHT-positive; moreover, in these few VAcHT-positive terminals, the intensity of CHT immunostaining was 3-fold less than those in WT terminals (Figure 2A).

To determine whether other cholinergic terminals in  $\alpha 3$  KO mice had low levels of CHT, we examined synapses at the neuromuscular junctions (NMJs). Because fast synaptic transmission at the neuromuscular junction is mediated by  $\alpha 1$ -containing nAChRs, in  $\alpha 3$  KO mice the NMJs function well. All presynaptic terminals in  $\alpha 3$  KO diaphragm muscle had abundant CHT staining (Figure 2B); the proportion of CHT-positive terminals and intensity of CHT staining was not significantly different from those in aged-matched WT muscle.

To address whether preganglionic neurons synthesize CHT but do not target it to their terminals, we coimmunostained spinal preganglionic neurons in the intermediate lateral horn (IML) for choline acetyltransferase (ChAT) to identify cholinergic neurons and CHT; as controls, we coimmunostained motoneurons in the ventral horn (VH). In both WT and  $\alpha 3$  KO mice, ChAT-positive motoneurons in the VH had strong CHT staining (Figures 2C and 2D;  $n = 6$ ), consistent with the presence of CHT in presynaptic terminals at NMJs. Furthermore, the preganglionic neurons in the IML of WT mice had strong CHT staining. In contrast, CHT was not detected above background in preganglionic neurons in the IML of  $\alpha 3$  KO mice (Figures 2C and 2D;  $n = 6$ ).

To determine whether the retrograde signal alters CHT gene expression in preganglionic neurons, we carried out in situ hybridization for CHT mRNA. In control spinal cord, CHT mRNA was readily detected in cholinergic ventral horn

and IML neurons ([Figure 2E](#); n = 6); on the other hand, in the spinal cord of  $\alpha 3$  KO mice, we detect CHT mRNA in cholinergic neurons in the ventral horn, but interestingly not in the IML ([Figure 2F](#); n = 6). These results indicate that CHT gene expression is regulated by signals downstream of postsynaptic activity.

### **Postnatal Appearance of CHT in WT and $\alpha 3$ KO Sympathetic Ganglia**

At 1 month, CHT in WT ganglia is high whereas in  $\alpha 3$  KO ganglia CHT is low. There are two likely scenarios for why CHT is low in  $\alpha 3$  KO ganglia: (1) the appearance of CHT is induced by intrinsic mechanisms early in development, possibly by processes involved in cholinergic differentiation of preganglionic neurons (Eiden et al., 1998; Weihe et al., 1998), and its high levels are maintained by retrograde signals downstream of postsynaptic activity; or (2) CHT levels are initially low in cholinergic terminals, and its appearance is induced by extrinsic signals downstream of postsynaptic activity. To distinguish between these two mechanisms, we examined the postnatal appearance of CHT in preganglionic terminals within the SCG. At birth, less than 20% of VAcHT-positive terminals in WT ganglia had detectable CHT immunostaining ([Figures 3A and 3B](#)). Over the next few days, this proportion as well as CHT intensity increased significantly and by P7 over 80% of the VAcHT-positive varicosities costained for CHT, and the proportion remained high for at least 1 month ([Figures 3A–3C](#)). In contrast, in  $\alpha 3$  KO ganglia, fewer than 15% of the VAcHT-positive terminals had detectable CHT immunostaining at birth, and the proportion and CHT intensity remained low over the first postnatal month ([Figures 3A–3C](#)). These results indicate that CHT levels in presynaptic terminals are low at birth and suggest that its appearance is induced during the first week by extrinsic signals downstream of postsynaptic activity.

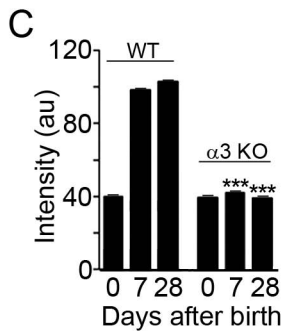
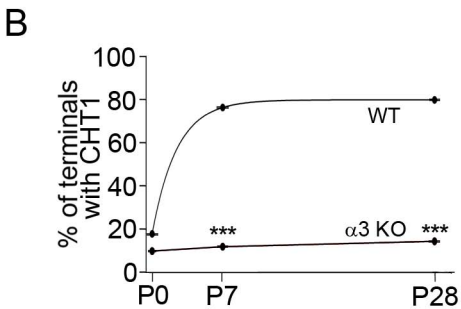
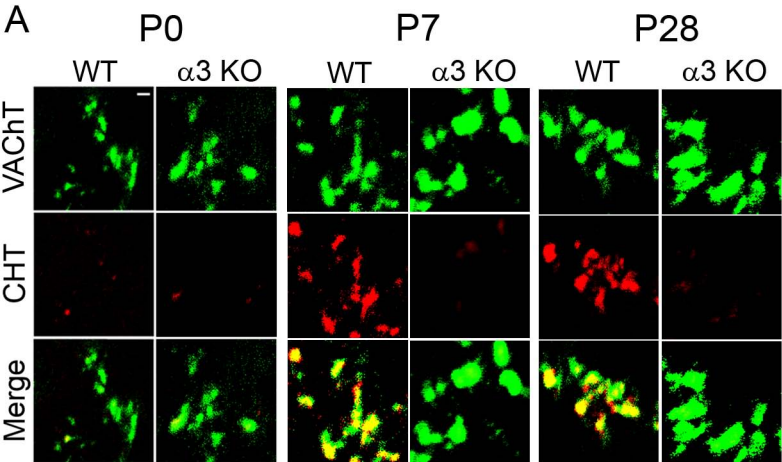


**Figure 3.3**

**FIGURE 3.3** CHT in Presynaptic Terminals in SCG from WT but Not  $\alpha 3$  KO Mice Increase over the First Postnatal Month. **A** VACht (top; green), CHT (middle; red) immunofluorescence in SCG from WT and  $\alpha 3$  KO mice at P0, at P7, and at P28. Scale bar, 1.0  $\mu$ m. **B** Percent of presynaptic terminals in WT and  $\alpha 3$  KO SCG with CHT at P0, P7, and P28. For each time point over 5000 VACht-positive terminals were analyzed in both WT (n = 8) and  $\alpha 3$  KO (n = 8) ganglia. There is a significant reduction in the percent of terminals with CHT staining in  $\alpha 3$  KO ganglia at P7 and at P28 compared to those in WT ganglia of the same age (\*\* $p < 0.0001$ ). **C** CHT intensity in presynaptic terminals increases significantly over the first postnatal month in WT SCG ( $p < 0.0001$ ; n = 3500) but not in  $\alpha 3$  KO SCG ( $p > 0.2$ ; n = 2000); CHT-negative terminals were excluded from the average intensity. Error bars represent  $\pm$  SEM.

Since CHT is crucial for the continual resynthesis and release of ACh during sustained firing, our findings predict that at birth the presynaptic terminals cannot maintain ACh release during sustained or high-frequency firing but acquire this ability during the early postnatal period. To test this prediction, we recorded intracellularly from sympathetic neurons in intact ganglia while stimulating the preganglionic nerve. (In these experiments, we added curare [5–10  $\mu$ M] to make the EPSPs subthreshold; leaving out curare had no significant effect on these results.) At birth, synapses could follow low-frequency stimulation (<1 Hz) for at least 1 min ([Figure 4A](#)); after 10 min of continuous stimulation, the EPSP amplitude was  $\sim$ 80% of control. In contrast, with higher-frequency stimulation, synapses in P0 ganglia could not keep up. When stimulated at 10 Hz, successive EPSPs gradually decreased in amplitude and were undetectable by 30–40 s ([Figure 4A](#)); this is what one would expect for synapses where the presynaptic terminals had little CHT and their releasable pool of ACh was depleted.

To quantify the decrease in EPSP amplitude over time, we repeated these experiments with synapses in ganglia from P3, P5, and P7 mice by plotting the average of ten consecutive EPSPs at 10 s intervals in a 60 s train. By P7, stimulating the preganglionic nerve at 10 Hz for 1 min caused only a small reduction in EPSP amplitude ([Figures 4B and 4C](#)). For synapses in P3 and P5 ganglia, the decrease in EPSP amplitudes was intermediate between P0 and P7 ([Figure 4D](#)). Moreover, stimulating the preganglionic nerve at 10 Hz in the presence of hemicholinium (HC-3; 1  $\mu$ M), a specific antagonist of CHT, caused the synapses in P7 ganglia to fatigue with a time course similar to those in P0 ganglia (although the HC-3-induced fatigue at P7 was not as fast as that at P0 treated with HC-3, suggesting that the block by HC-3 at P7 was not complete)

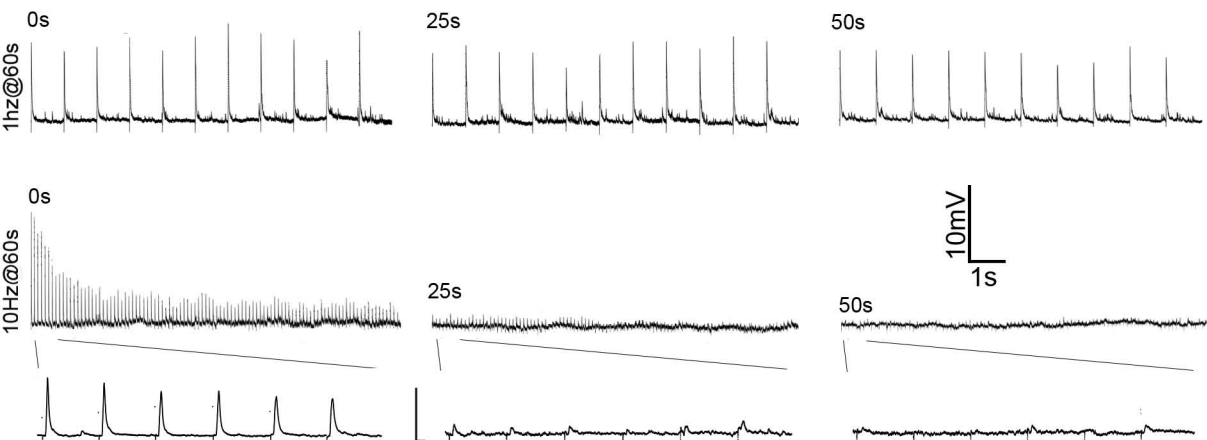
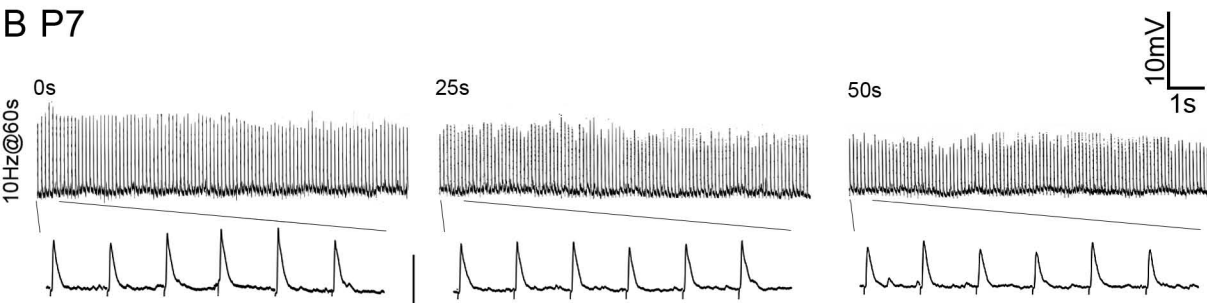
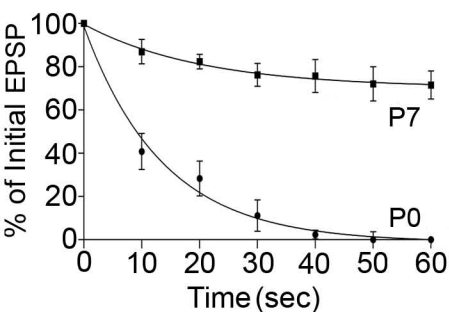
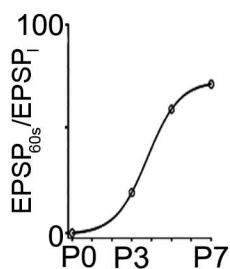
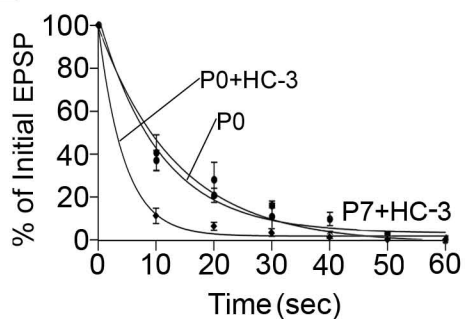
([Figure 4E](#)). Taken together, these results indicate that the ability of presynaptic terminals to maintain ACh release depends on the functional appearance of CHT and that terminals acquire CHT over the first postnatal week.

### **Viral Expression of $\alpha 3$ in $\alpha 3$ KO Mice Establishes Fast Synaptic**

#### **Transmission in Sympathetic Ganglia**

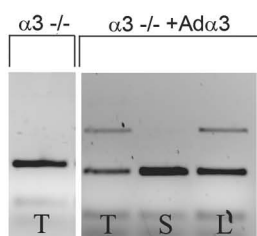
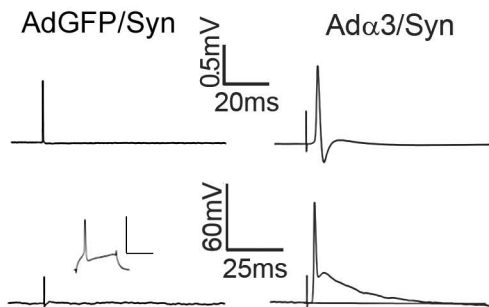
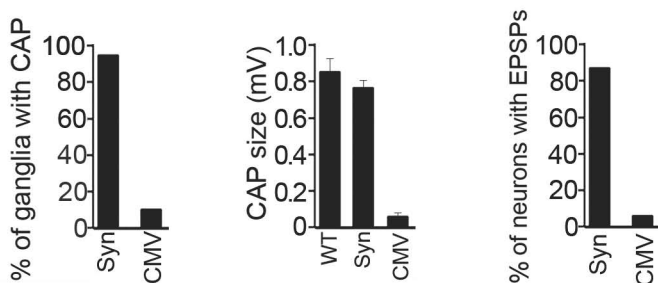
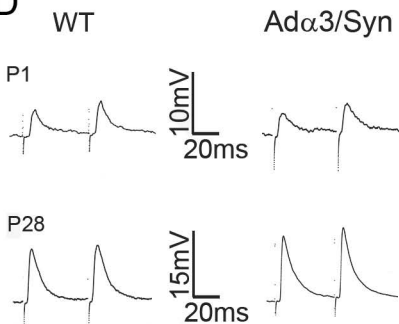
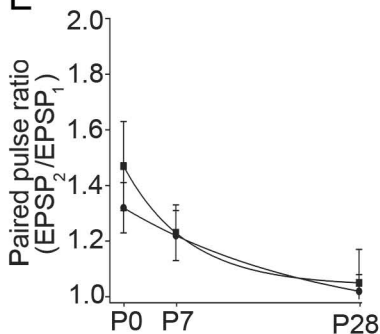
Unlike presynaptic terminals in WT ganglia, CHT is low in  $\alpha 3$  KO ganglia at birth and remains low over the first month ([Figure 3](#)). From these results, we hypothesize that the appearance of CHT in presynaptic terminals depends on a retrograde signal(s) downstream of postsynaptic activity. To test this idea directly, we used in vivo adenoviral gene transfer techniques to express the missing  $\alpha 3$  nAChR subunit and restore postsynaptic activity in  $\alpha 3$  KO ganglia. After injecting mice intraperitoneally (i.p.) with  $\alpha 3$ -containing viral vectors, we could detect viral  $\alpha 3$  in the liver but not in the spinal cord ([Figure 5A](#)), indicating that the virus stays in the periphery and does not enter the CNS.

To express  $\alpha 3$  in sympathetic neurons in vivo, we infected mice with Ad $\alpha 3$ /Syn, a replication-defective adenovirus in which the expression of the  $\alpha 3$  cDNA is driven from the synapsin (Syn) promoter (Kügler et al., 2003; Wheeler et al., 2006). Within 24 hr of infecting  $\alpha 3$  KO mice with Ad $\alpha 3$ /Syn, we obtained strong synaptic transmission in over 90% of the ganglia ([Figures 5B](#) and [5C](#)); moreover, with intracellular recording, we recorded large ( $\sim 10$  mV) nerve-evoked EPSPs from over 85% of the neurons in intact ganglia 1 day postinfection ([Figures 5B](#) and [5C](#)), and the EPSP amplitudes increased further over the next 2–3 days. These EPSPs on  $\alpha 3$  KO neurons infected with Ad $\alpha 3$ /Syn had rise times and decay times similar to those on WT neurons ([Table 1](#)), indicating that the virally expressed  $\alpha 3$  coassembles with  $\beta$  (and possibly other) subunits and

**A P0****B P7****C****D****E****Figure 3.4**

**FIGURE 3.4** The Ability of Cholinergic Nerve Terminals to Sustain High-Frequency Synaptic Transmission Develops over the First Postnatal Week and Requires the Appearance of Functional High-Affinity Choline Transporters

**A** EPSPs recorded from a neuron in intact P0 WT SCG while stimulating the preganglionic nerve at 1 Hz (top row) or 10 Hz (bottom row) for 60 s: first 10 s (left), the middle 10 s (middle), and the last 10 s (right) of the train. At 10 Hz, the first six EPSPs of each 10 s trace are shown on an expanded timescale for clarity. Presynaptic terminals are able to sustain transmission at low stimulus frequency (1 Hz) for at least 10 min but fatigue rapidly at high stimulus frequency (10 Hz). **B** EPSPs recorded from a neuron in intact P7 SCG while stimulating the preganglionic nerve at 10 Hz: first 10 s (left), the middle 10 s (middle), and the last 10 s (right). At P7, presynaptic terminals are able to sustain transmission at 10 Hz. **C** The average amplitude of ten consecutive EPSPs measured at 10 s intervals in response to a 10 Hz, 60 s stimulation and normalized to the first ten EPSPs for neurons at P0 (●) and at P7 (■). Each point represents the normalized EPSP (mean ± SEM) from over 20 neurons recorded in at least eight different WT ganglia. The solid lines in (C) and (D) represent a single-exponential fit to the data. **D** shows the normalized EPSP (mean ± SEM; n > 20 neurons in six different ganglia) for the final ten consecutive EPSPs in a 60 s train at P0, P3, P5, and P7. **E** Effects of hemicholinium-3 (HC-3). Synapses in P0 (◆) and P7 ganglia (■) fatigue within the first 30 s when stimulated in the presence of HC-3 (1 μM). Each point represents the normalized EPSP (mean ± SEM) for over 20 neurons in six different ganglia. Data from neurons in P0 SCG (●) are shown for comparison. These data demonstrate that synapses in P7 SCG require functional CHT activity to sustain transmission at 10 Hz. Error bars represent ± SEM.

**A****B****C****D****E****Figure 3.5**

**FIGURE 3.5** Rescue of Synaptic Transmission in Sympathetic Ganglia of  $\alpha 3$  KO Mice with Adenoviruses Containing Full-Length  $\alpha 3$  cDNA. **A** Amplified PCR products from DNA extracted from tail tissue (T) of a P0  $\alpha 3$  KO mouse before (left lane) and 48 hr after infection (right lane) with Ad $\alpha 3$ /Syn or from DNA extracted from spinal cord (S) or liver (L) 48 hr after infection (right lanes). Adenoviral vectors administered i.p. infect peripheral tissues but not the CNS or spinal cord. **B** Synapsin promoter drives strong  $\alpha 3$  expression in sympathetic neurons. Extracellular CAP (upper traces) and EPSPs (lower traces) recorded in sympathetic ganglia from P0  $\alpha 3$  KO mice infected with AdGFP/Syn and with Ad $\alpha 3$ /Syn measured 24 hr later.  $\alpha 3$  KO mice infected with Ad $\alpha 3$ /Syn recovered strong synaptic transmission through autonomic ganglia. **C** Proportion of ganglia with CAPs (left), the peak amplitude of the CAP (middle), and the proportion of SCG neurons with EPSPs (right) in WT,  $\alpha 3$  KO mice infected with Ad $\alpha 3$ /Syn, and  $\alpha 3$  KO mice infected with AdGFP/Syn measured 24 hr later. **D** and **E** Paired-pulse facilitation is normal at synapses rescued with Ad $\alpha 3$ /Syn. (D) Example of two EPSPs evoked 40 ms apart on SCG neurons from WT mice (left) and  $\alpha 3$  KO mice 24 hr postinfection with Ad $\alpha 3$ /Syn (right) at P1 and P28. (E) The average paired-pulse ratio was measured at P0 ( $n = 25$ ), P7 ( $n = 23$ ), and P28 ( $n = 27$ ) for synapses in WT SCG (■) or for rescued synapses in  $\alpha 3$  KO SCG (●) 24 hr postinfection with Ad $\alpha 3$ /Syn. There is no significant difference ( $p > 0.2$ ) in paired-pulse facilitation between synapses in WT SCG and those rescued with Ad $\alpha 3$ /Syn. This graph shows that excitation-secretion coupling in presynaptic terminals develops normally at silent synapses in  $\alpha 3$  KO SCG. Error bars represent  $\pm$  SEM.

**TABLE 3.1** EPSP Rising Time Constant, Decay Time Constants, and Paired-Pulse Ratio Are Similar between Neurons in Ganglia from WT and Rescued Mice

	<b>Rising Tau (ms)</b>	<b>Decay Tau (ms)</b>
P0 WT	1.41 ± 0.10	6.32 ± 0.32
P7 WT	1.2 ± 0.15	5.49 ± 0.38
Rescue at P0 (7 days after infection)	1.08 ± 0.12	5.21 ± 0.29

the receptors are targeted appropriately to synapses; furthermore, the EPSP rise and decay times suggest that ACh is released from the presynaptic terminals rapidly and cleared from the synaptic cleft normally. Further, we observed no significant difference in paired-pulse facilitation between terminals at these new functional synapses in  $\alpha 3$  KO ganglia and those in WT ganglia of similar age (Figure 5D), suggesting that excitation-secretion coupling in presynaptic terminals at these synapses is normal. Taken together, these results demonstrate that we can establish functional cholinergic synapses in  $\alpha 3$  KO ganglia within 24 hr of infecting mice with  $\alpha 3$ -expressing adenoviral vectors.

### **Establishing Postsynaptic Activity in $\alpha 3$ KO Ganglia Induces the Appearance of CHT Presynaptically**

To determine whether postsynaptic activity causes the appearance of CHT presynaptically, we infected P1  $\alpha 3$  KO mice with Ad $\alpha 3$ /Syn and recorded nerve-evoked EPSPs from sympathetic neurons in intact ganglia 24 hr later. With 10 Hz stimulation, the successive EPSPs gradually decreased in amplitude during the first 10 s and eventually became undetectable by  $\sim 40$ – $50$  s (Figures 6A and 6B), consistent with a depletion of the releasable pool of ACh. Moreover, we immunostained the ganglia and observed that CHT protein in presynaptic terminals was low (Figure 6F), similar to synapses in WT ganglia at birth (Figures 3A–3C). Next, we examined synapses in infected  $\alpha 3$  KO littermates 7 days postinfection to determine whether these synapses required a similar maturation time as those in WT ganglia. Stimulating synapses at 10 Hz for 1 min resulted in little depression of the nerve-evoked EPSPs (Figures 6A and 6C); equally relevant, the presynaptic terminals in these ganglia had abundant CHT (Figure 6F). These results indicate that a few days of postsynaptic activity is

sufficient to increase CHT levels in presynaptic terminals in rescued  $\alpha 3$  KO ganglia.

An alternative interpretation of these rescue experiments, however, is that the postsynaptic nAChRs produce a signal for the presynaptic appearance of CHT. To distinguish whether the signal for CHT expression originates from the receptor or a retrograde signal downstream of postsynaptic activity, we virally expressed receptors with a reduced single-channel conductance. To express such receptors, we mutated  $\alpha 3$  to change the glutamic acid (E) residue at the intracellular gate of the receptor channel (position 240) to alanine (A); these glutamic acid residues are present on all nAChR subunits and form the intermediate ring of negative charges at the receptor pore. Reducing the negative charge at the intermediate ring reduces the single-channel conductance of the receptors  $\sim 10$ - to  $12$ -fold (Imoto et al., 1988; Haghghi and Cooper, 2000).

$\alpha 3^{E240A}$  expressed well in sympathetic neurons, and over 80% of the neurons had nerve-evoked EPSPs, similar to the proportion infected with WT  $\alpha 3$  cDNA; however, the nerve-evoked EPSPs at synapses with  $\alpha 3^{E240A}$ -containing nAChRs were  $\sim 15$ -fold smaller than those at synapses with WT  $\alpha 3$ -containing nAChRs: at synapses rescued with  $\alpha 3^{E240A}$ -containing nAChRs, the mean EPSPs was  $1.15 \text{ mV} \pm 0.053$  ( $n = 65$ ), and at WT synapses, the mean EPSPs was  $20.1 \text{ mV} \pm 0.56$  ( $n = 96$ ; see [Figure 6D](#)). Importantly, presynaptic terminals at synapses with these conductance mutant nAChRs lacked functional CHT. One week postinfection, the EPSPs at these  $\alpha 3^{E240A}$  synapses fatigued rapidly when stimulated at 10 Hz (see [Figure 6E](#)), comparable to terminals at synapses in WT ganglia at P0 or WT P7 treated with HC-3. Moreover, by immunostaining  $\alpha 3^{E240A}$ -expressing ganglia for CHT, we show that presynaptic terminals have low levels of CHT protein, comparable to those at synapses in  $\alpha 3$  KO ganglia

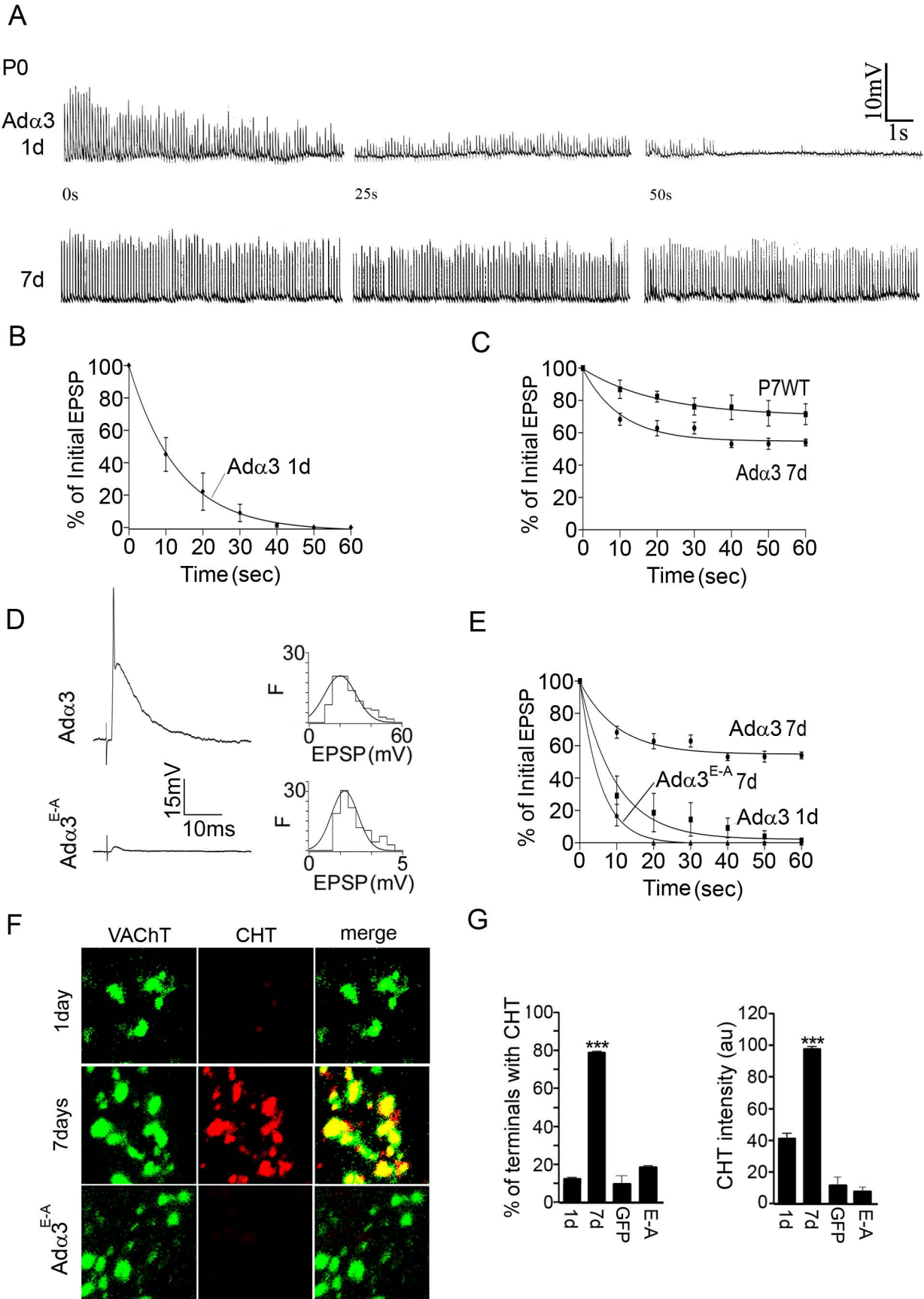


Figure 3.6

**FIGURE 3.6** Postsynaptic Activity Causes the Appearance of Functional High-Affinity Choline Transporters in Presynaptic Terminals. **A** EPSPs recorded from neurons in an intact sympathetic ganglia from a P0  $\alpha 3$  KO mouse infected with Ad $\alpha 3$ /Syn 1 day (top row) and 7 days (bottom row) postinfection: the preganglionic nerve was stimulated at 10 Hz for 60 s: first 10 s (left), the middle 10 s (middle), and the last 10 s (right). **B** EPSPs on sympathetic neurons in SCG from P0  $\alpha 3$  KO mice 1 day postinfection (Ad $\alpha 3$  1d) in response to a 10 Hz train delivered to the preganglionic nerve for 60 s: average amplitudes of ten consecutive EPSPs at 10 s intervals, normalized to the average of the first ten EPSPs (mean  $\pm$  SEM); each point is the average of  $\sim$ 50 neurons from eight to ten ganglia. **C** EPSPs on sympathetic neurons in SCG from P0  $\alpha 3$  KO mice 7 days postinfection with Ad $\alpha 3$ /Syn (Ad $\alpha 3$  7d) in response to a 10 Hz train delivered to the preganglionic nerve for 60 s: average amplitudes of ten consecutive EPSPs at 10 s intervals, normalized to the average of the first ten EPSPs (mean  $\pm$  SEM); each point is the average of  $\sim$ 50 neurons from eight to ten ganglia. Results from neurons in P7 WT SCG (Figure 4C) are shown for comparison. **D** Mutating glutamic acid residues in  $\alpha 3$  reduces the size of EPSPs without affecting expression levels. EPSPs on sympathetic neurons in SCG from P0  $\alpha 3$  KO mice 7 days postinfection with either Ad $\alpha 3$ /Syn (top, Ad $\alpha 3$ ) or with Ad $\alpha 3^{E-A}$ /Syn (bottom, Ad $\alpha 3^{E-A}$ ). The histograms to the left show the distribution of EPSP amplitudes ( $n = 95$  for Ad $\alpha 3$ /Syn and  $n = 65$  Ad $\alpha 3^{E-A}$ /Syn). The average EPSP amplitude is reduced  $\sim$ 15-fold. **E** EPSPs on sympathetic neurons in SCG from P0  $\alpha 3$  KO mice 1 day, 7 days postinfection with Ad $\alpha 3$ /Syn (Ad $\alpha 3$  7d) and 7 days postinfection with Ad $\alpha 3^{E-A}$ /Syn (Ad $\alpha 3^{E-A}$  7d) in response to a 10 Hz train delivered to the preganglionic nerve for 60 s: average amplitudes of ten consecutive EPSPs at 10 s intervals, normalized to the average of the first ten EPSPs (mean  $\pm$  SEM); each point is the average of  $\sim$ 50 neurons from eight to ten ganglia. Postsynaptic activity at synapses that express the conductance mutant  $\alpha 3^{E-A}$  cannot restore functional choline transporters in the presynaptic terminals, indicating that strong postsynaptic activity is required for the appearance of functional CHT. **F** Immunostaining SCG from P0  $\alpha 3$  KO 1 day and 7 days postinfection with Ad $\alpha 3$ /Syn, and from P0  $\alpha 3$  KO 7 days postinfection with Ad $\alpha 3^{E-A}$ /Syn for VAcHT, (left; green), CHT (middle; red). Scale bar, 1.0  $\mu$ m. **G** Reinstating postsynaptic activity causes a significant increase in the percentage (left) of VAcHT-positive terminals with CHT ( $p < 0.0001$ ) and the mean CHT intensity (right) within CHT-positive terminals ( $p < 0.001$ ). Over 4000 VAcHT-positive terminals were analyzed in ten different  $\alpha 3$  KO ganglia for each condition: 1 day and 7 days postinfection with Ad $\alpha 3$ /Syn, 7 days postinfection with Ad $\alpha 3^{E-A}$ /Syn, and AdGFP/Syn. Error bars represent  $\pm$  SEM.

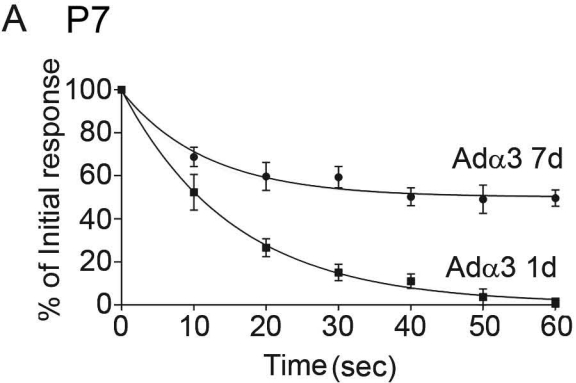
(see [Figure 6F](#)). Therefore, even though  $\alpha 3^{E240A}$ -containing nAChRs were capable of mediating small 0.5–3 mV EPSPs, neither the receptors nor the small EPSPs were sufficient to induce the appearance of CHT in the presynaptic terminals. These results rule out the possibility that the transsynaptic signal originates from the receptors; rather, they indicate that the appearance of CHT in presynaptic terminals requires a retrograde signal downstream of strong postsynaptic activity.

Restoring synaptic activity to  $\alpha 3$  KO ganglia at P1 mimicked the developmental appearance of CHT in WT ganglia. Next, we asked whether the first postnatal week was a critical period for inducing the appearance of CHT in presynaptic terminals. To address this, we expressed  $\alpha 3$  in  $\alpha 3$  KO mice at P7 and at P21 and recorded nerve-evoked EPSPs at different times postinfection. At 24 hr, the nerve-evoked EPSPs on sympathetic neurons from virally infected P7 and P21  $\alpha 3$  KO mice were similar to those on WT sympathetic neurons at P0; with 10 Hz stimulation, the EPSPs gradually decreased in amplitude and became undetectable by  $\sim 40$  s ([Figure 7A](#)), and CHT protein in presynaptic terminals was low ([Figures 7C and 7D](#)). When examined 7 days after restoring synaptic activity at P7 or P21, however, the presynaptic terminals maintained release during high-frequency stimulation ([Figure 7B](#)) and the presynaptic terminals contained high levels of CHT ([Figures 7C and 7D](#)). Taken together, these results indicate that postsynaptic activity is the major determinant for the appearance of CHT in presynaptic terminals.

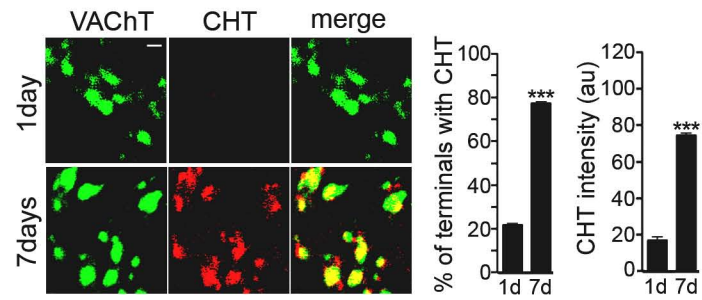
### **Postsynaptic Activity Is Required for the Continual Appearance of CHT in Presynaptic Terminals**

Unexpectedly, we observed that rescue of fast nicotinic synaptic transmission in  $\alpha 3$  KO SCG with Ad $\alpha 3$ /Syn lasted for only a few weeks. For example, we infected 20  $\alpha 3$  KO mice with Ad $\alpha 3$ /Syn at P1 and tested them at various times. We found that ganglia from all six mice tested 7–9 days postinfection had large nerve-evoked compound action potentials (CAPs) and all 54 neurons had EPSPs  $>10$  mV ([Figure 8A](#)). On the other hand, when we examined ganglia in the same series 3 weeks ( $n = 6$ ) and 7 weeks ( $n = 8$ ) postinfection, none had detectable CAPs ( $n = 14$ ) and 0/45 neurons had detectable nerve-evoked EPSPs ([Figure 8A](#)); nonetheless, all neurons had nerve-evoked muscarinic responses ([Figure 8B](#)), demonstrating that the preganglionic terminals were capable of ACh release. Therefore, it appears that Ad $\alpha 3$ /Syn stopped expressing  $\alpha 3$  after  $\sim 14$  days, and consequently the synapses stopped functioning. A similar attenuation of viral gene expression from the Syn promoter had been observed in dopaminergic neurons in the adult CNS (Kügler et al., 2003).

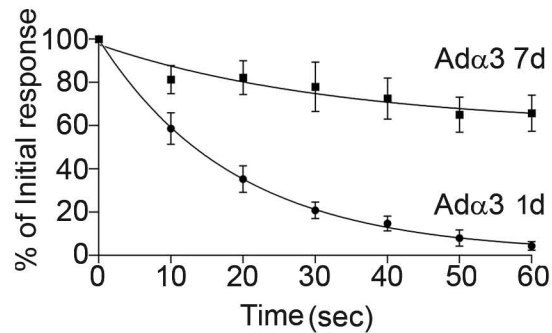
Although the mechanism for this selective attenuation of activity from the Syn promoter is unclear, we exploited this property to ask what happens to CHT levels in presynaptic terminals when active synapses revert to electrophysiologically silent synapses. Therefore, we immunostained the terminals for CHT after the electrophysiological experiments in [Figure 8A](#). Although none of the ganglia from mice 3 weeks postinfection had detectable fast synaptic transmission, over 75% of the presynaptic terminals in the SCG had high levels of CHT, as did those in ganglia 7–9 days postinfection ([Figures 8B–8D](#)). In contrast, less than 25% of the presynaptic terminals in ganglia 7 weeks postinfection had detectable CHT ([Figures 8B–8D](#)). These results indicate that



**B P7**



**C P21**



**D P21**

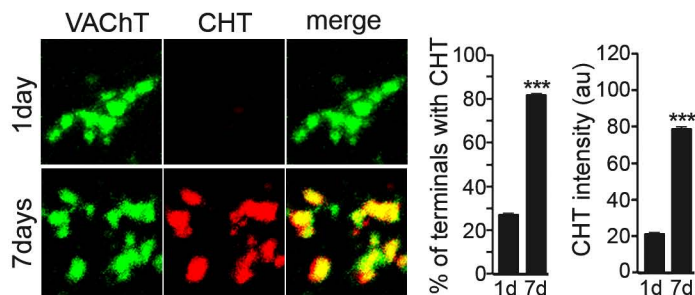


**Figure 3.7**

**FIGURE 3.7** Reinstating Synaptic Activity at P7 and at P21 Induces the Appearance of CHT in Presynaptic Terminals. **A** and **C** EPSPs on sympathetic neurons in ganglia from P7  $\alpha 3$  KO mice (A) or P21  $\alpha 3$  KO mice (C) infected with Ad $\alpha 3$ /Syn for 1 day (Ad $\alpha 3$  1d) and 7 days (Ad $\alpha 3$  7d) in response to a 10 Hz train for 60 s: average amplitudes of ten EPSPs (mean  $\pm$  SEM); each point is the average of  $\sim 25$  neurons from eight to ten ganglia. **B** and **D** Presynaptic terminals in SCG from P7  $\alpha 3$  KO mice (B) or P21  $\alpha 3$  KO mice (D) infected with Ad $\alpha 3$ /Syn for 1 day or 7 day immunostained for VAcHT (left; green) and CHT (middle; red). Scale bar, 1  $\mu$ m. The graphs show the percentage of VAcHT-positive terminals with CHT (left; \*\*\*p < 0.0001) and the average CHT intensity (right; \*\*\*p < 0.001). Over 2700 terminals in nine different ganglia were analyzed for both 1 day (1d) and 7 days (7d) postinfection. These data suggest that there is no critical period for the induction of CHT in presynaptic terminals by signals downstream of postsynaptic activity. Error bars represent  $\pm$  SEM.

continuous postsynaptic activity is required to maintain CHT levels in presynaptic terminals.

## **DISCUSSION**

Using sympathetic ganglia from  $\alpha 3$  KO outbred mice, we demonstrate that electrophysiologically silent synapses develop and persist for several weeks in the absence of postsynaptic activity. While these synapses appear morphologically normal, the presynaptic terminals are functionally immature and cannot output ACh in response to high-frequency stimulation. This defect in transmitter output occurs, in large part, because the terminals lack the high-affinity choline transporter, CHT. Without CHT, repetitive firing or high-frequency trains at developing synapses deplete the presynaptic terminals of their releasable pool of ACh and fast synaptic transmission fails. First we discuss our results that electrophysiologically silent synapses persist for several weeks in vivo, and then we discuss our findings linking signal(s) down stream of postsynaptic activity to the appearance of CHT in presynaptic terminals.

### **Electrophysiologically Silent Synapses Persist without Postsynaptic**

#### **Activity**

Synaptogenesis occurs by both activity-independent and activity-dependent mechanisms (Garner et al., 2006; Sanes and Lichtman, 1999; Tao and Poo, 2001), yet the relative contribution of these mechanisms to the stabilization and persistence of synapses is not fully understood (Craig et al., 2006). We started these experiments with the expectation that synapses must be active to mature and persist, whereas inactive synapses remain immature and

are eventually eliminated, a view suggested by several recent reviews on synapse formation (Cohen-Cory, 2002; Flavell and Greenberg, 2008) and by recent experiments at the neuromuscular junction, which demonstrate that when active and inactive synapses coexist on the same postsynaptic cell, the active synapses persist and the inactive synapses are eliminated (Buffelli et al., 2003). On the one hand, our results are consistent with this view: we show that for cholinergic synapses in SCG, synapses must be active to mature. On the other hand, we show that synapses do not necessarily need to be active to persist; instead, our results show that when all the synapses to a postsynaptic neuron are inactive, these inactive synapses are maintained.

Presumably, cholinergic nicotinic synapses on sympathetic neurons are maintained by synaptic adhesion molecules through activity-independent mechanisms, thereby allowing these synapses to persist without postsynaptic activity. The identity of these cell adhesion molecules at neuronal nicotinic synapses is incomplete. One molecule may be L1-CAM, or a related family member, given that L1-CAM is involved in aligning pre- and postsynaptic structures at synapses in chick ciliary ganglia (Triana-Baltzer et al., 2006), similar to its role at the neuromuscular junction (Landmesser et al., 1988). Other synaptic adhesion molecules may be members of the neuroligin-neurexin family, since neuroligin-neurexin interactions guide synapse formation among chick ciliary neurons in culture (Conroy et al., 2007), similar to their role at mammalian glutamatergic synapses (Craig and Kang, 2007), although more work is needed before one can be certain that neuroligin-neurexin interactions occur at nicotinic synapses on neurons *in vivo*.

The postsynaptic complex at synapses in sympathetic ganglia contains the scaffolding proteins, PSD93 and PSD95, as well as GKAP/SAPAP and

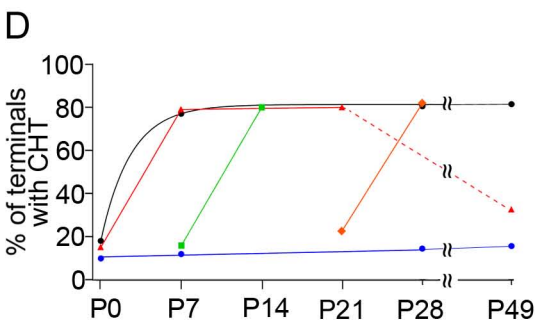
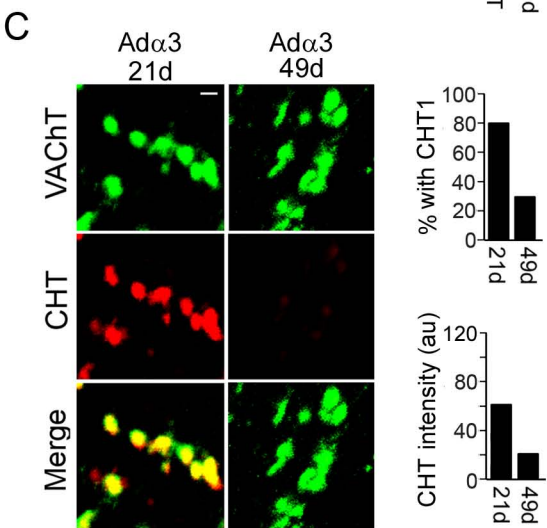
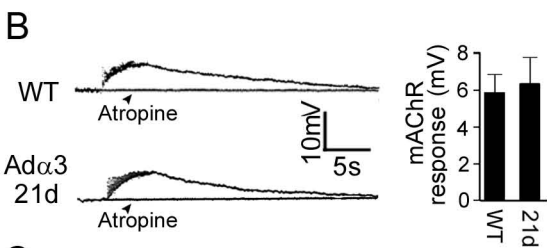
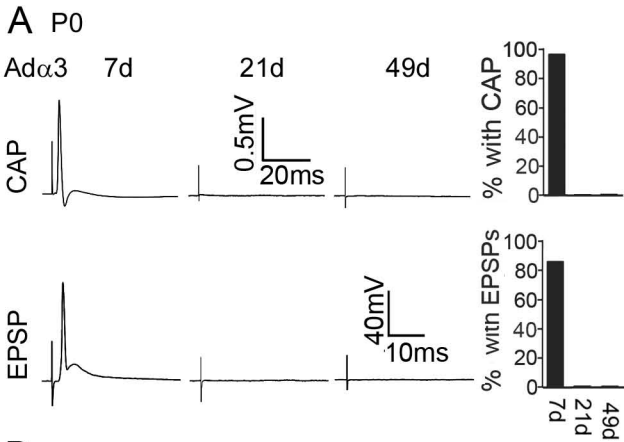


**Figure 3.8**

**FIGURE 3.8** Continuous Postsynaptic Activity Is Required to Maintain CHT Expression in Presynaptic Terminals. **A** CAPs (upper) recorded from the sympathetic trunk and EPSPs (lower) recorded from sympathetic neurons in SCG from P0  $\alpha 3$  KO mice infected with Ad $\alpha 3$ /Syn for 7 days (7d), 21 days (21d), or 49 days (49d). Synaptic transmission in SCG is present 1 week postinfection but absent 3 weeks and 7 weeks postinfection, indicating that the expression from Ad $\alpha 3$ /Syn is transient. The graphs on the left summarize the percent of ganglia with CAPs and the percent of neurons with EPSPs at 7d, 21d, and 49d (~15 neurons and 5 animals for each time point). **B** Normal muscarinic responses at 21 days postinfection with Ad $\alpha 3$ /Syn (Ad $\alpha 3$  21d) indicate that the absence of synaptic transmission is due to the lack of postsynaptic receptors. Stimulating the preganglionic nerve at 20 Hz for 2 s evoked similar muscarinic responses on a sympathetic neuron from a P21 WT mouse (top trace) and on a sympathetic neuron from a P21  $\alpha 3$  KO mouse infected with Ad $\alpha 3$ /Syn at P0 (bottom trace). The muscarinic responses were reversibly blocked by 1  $\mu$ M atropine. The graph on the left shows the average muscarinic response for ~25 sympathetic neurons from 5 P21 WT mice and ~30 sympathetic neurons in four P21  $\alpha 3$  KO mice infected with Ad $\alpha 3$ /Syn at P0. **C** Immunostaining SCG from P0  $\alpha 3$  KO mice infected with Ad $\alpha 3$ /Syn for 1 week and 7 weeks for VAcHT (top; green) and CHT (middle; red). Scale bar, 1  $\mu$ m. The graphs show the proportion of terminals that contain CHT (left) and the average CHT fluorescence intensity in CHT-positive terminals (right). The loss of postsynaptic activity for 3–4 weeks causes a significant reduction in the percentage of terminals with CHT (left, \*\*\*  $p < 0.0001$ ) and the average CHT intensity in CHT-positive terminals (right, \*\*\*  $p < 0.001$ ). Over 2000 terminals in six different ganglia were analyzed for both 1 week and 7 weeks postinfection. **D** Summary of the proportion of CHT-positive terminals in WT and  $\alpha 3$  KO SCG at ages from P0 to P50: WT mice (black),  $\alpha 3$  KO mice (blue), and P0  $\alpha 3$  KO mice infected with Ad $\alpha 3$ /Syn at P0 (red), P7 (green), and P21 (orange). Reinstating synaptic transmission in SCG of  $\alpha 3$  KO mice induces the appearance of CHT in presynaptic terminals, but when Ad $\alpha 3$ /Syn stops expressing  $\alpha 3$  after 2–3 weeks, synaptic transmission stops and CHT in presynaptic terminals decreases. These data indicate that signals downstream of postsynaptic activity are required to induce and maintain expression of CHT in presynaptic terminals. Error bars represent  $\pm$  SEM.

Shank/ProSap (Brenman et al., 1996; Conroy et al., 2003; Parker et al., 2004), similar to glutamatergic synapses in the CNS (Kim and Sheng, 2004; Li and Sheng, 2003). Over 90% of these postsynaptic PSD93 clusters colocalized with the presynaptic marker, VAcHT, in intact ganglia and serve as useful markers for the location of synapses. The role for this PSD93-GKAP-Shank complex at nicotinic synapses is not well understood. One of its functions could be to anchor synaptic adhesion molecules required for initiating synapse formation and allowing synapses to persist without activity. For example, the postsynaptic complex becomes unstable when sympathetic ganglia are denervated in PSD93 null mice (Parker et al., 2004). Another role for this scaffolding complex could be to localize signaling molecules like postsynaptic receptors, calcium-calmodulin kinase II, and nitric oxide synthase to the postsynaptic domain, similar to the role for this complex at glutamatergic synapses (Kim and Sheng, 2004).

It is not clear what regulates the formation of this PSD93-GKAP-Shank complex under the postsynaptic membrane at cholinergic-nicotinic synapses on sympathetic neurons. In  $\alpha 3$  KO ganglia, the complex forms at electrophysiologically silent synapses; therefore, the targeting and clustering of the molecules that make up this complex do not require signals downstream of the postsynaptic nAChRs, such as membrane depolarization or calcium influx.

How nAChRs are targeted and anchored in the postsynaptic membrane at neuronal synapses is poorly understood (Rosenberg et al., 2002; Parker et al., 2004; Williams et al., 1998). Expressing  $\alpha 3$  in sympathetic neurons in  $\alpha 3$  KO mice rapidly rescues fast synaptic transmission, most probably by converting silent synapses to active synapses. These results indicate that sympathetic neurons in  $\alpha 3$  KO mice retain the ability to process  $\alpha 3$  transcripts properly, including synthesizing  $\alpha 3$  subunits, coassembling them with  $\beta$  (and possibly

other) subunits, and folding the coassembled subunit proteins into  $\alpha 3$ -containing nAChRs, and targeting these newly synthesized receptors appropriately to the postsynaptic membrane. The rise and decay kinetics of the EPSPs at the rescued synapses in  $\alpha 3$  null ganglia are similar to those for EPSPs at synapses in WT ganglia, suggesting that the newly synthesized nAChRs are properly aligned to the presynaptic release sites and that the evoked ACh is cleared from the synapse normally.

Moreover, paired-pulse facilitation at these rescued synapses is similar to that at synapses in WT ganglia, indicating that the presynaptic terminals release transmitter normally in response to single action potentials. These findings are consistent with previous work showing normal vesicle recycling in presynaptic terminals at silent NMJ in paralytic zebrafish mutants (Li et al., 2003). That presynaptic terminals at these silent synapses release transmitter normally in  $\alpha 3$  null sympathetic ganglia indicates that appropriate targeting and organization of molecules in presynaptic terminals needed for excitation-secretion coupling, with the exception of CHT, do not require retrograde signals down stream of postsynaptic activity.

### **Expression of the High-Affinity Choline Transporter Requires a Retrograde Signal(s) Downstream of Postsynaptic Activity**

At birth, synapses in sympathetic ganglia are functionally immature and fatigue rapidly with repetitive stimulation. Over the first few postnatal days, these synapses mature and sustain transmission even when stimulated at high frequency or for prolonged periods. This conversion from a readily fatigable synapse to one that can sustain transmission comes about, in large part, because the presynaptic terminals acquire a HC-3-sensitive, high-affinity choline

uptake mechanism. A similar developmental process occurs at developing neuromuscular junctions (Letinsky, 1974; Pilar et al., 1981). As such, synapses in newborn sympathetic ganglia act physiologically as a low-pass filter, allowing inputs to excite the postsynaptic neurons if they arrive at low frequency but not if they arrive at high frequency; this may be a common situation as functional circuits become established (Abrahamsson et al., 2005). It is not clear what physiological role this filtering mechanism serves. One role may be to ensure that developing neurons do not become overstimulated until they have matured sufficiently to handle the excessive calcium loads that result from high-frequency excitatory synaptic activity; that is, for developing neurons, a little synaptic stimulation may be beneficial but excess synaptic stimulation could be detrimental to their survival. In the case of sympathetic neurons, we speculate that as the postsynaptic neurons receive functional innervation and mature over the first postnatal week, they become competent to handle synaptic activity at higher frequencies and communicate this to the presynaptic terminals through a retrograde signal. As functional autonomic circuits become established, this retrograde signal(s) acts on the presynaptic terminals to induce CHT, which allows the terminals to resynthesize ACh and prevent it from becoming depleted of transmitter when stimulated at higher frequencies.

In WT mice, we show that CHT increases dramatically over the first postnatal week in presynaptic terminals in sympathetic ganglia. In contrast, in  $\alpha 3$  KO SCG, CHT levels are low at birth and remain low for at least 1 month of postnatal development. Furthermore, when we rescued fast synaptic transmission in SCG of  $\alpha 3$  KO mice by overexpressing  $\alpha 3$  cDNA, the synapses recapitulate those in WT ganglia: CHT levels increase in presynaptic terminals in a few days and synapses mature in two steps: first, electrophysiologically silent

synapses progress to functional synapses that fatigue readily, and then to functional synapses that can sustain transmission at high frequencies. Rescuing synaptic transmission by overexpressing mutant  $\alpha 3^{E240A}$  supports the idea that a retrograde signal originates downstream of strong postsynaptic activity to instruct presynaptic terminals to increase their levels of CHT. The nature of this signal remains elusive, but it seems reasonable to speculate that it involves depolarization-induced calcium influx.

CHT is synthesized in the soma and targeted to a subset of synaptic vesicles in the presynaptic terminal (Ferguson et al., 2003; Ribeiro et al., 2003; Ribeiro et al., 2005). We demonstrate that CHT is not detectable in preganglionic cell bodies in  $\alpha 3$  null mice, suggesting that the lack of CHT in terminals is not solely because of inappropriate targeting of CHT, as described for cholinergic terminals in mice null for amyloid precursor proteins (Wang et al., 2007). Instead, our in situ hybridization experiments for CHT mRNA demonstrate that the retrograde signal regulates CHT gene expression.

In our rescue experiments, the transient expression from the Syn promoter allowed us to conclude that postsynaptic neurons must remain active for CHT to be continually expressed presynaptically. Two weeks after expressing  $\alpha 3$  cDNA in sympathetic neurons, activity from the Syn promoter decreased, and these active synapses reverted to their electrophysiologically silent status. (The reason for the transient expression from the Syn promoter is unclear but may be related to its regulation in catecholaminergic neurons (Kügler et al., 2003). Shortly after transmission stopped, CHT in the preganglionic terminals was high, but over the subsequent 2–3 weeks of inactivity, CHT levels drop significantly. These results indicate that the maintenance of CHT levels in presynaptic terminals requires a continuous signal downstream of postsynaptic activity.

Consistent with this, when motor axons to muscle are cut, CHT mRNA decreases in the motorneurons and reappears once their axons have successfully remade functional contact with muscle (Oshima et al., 2004).

Historically, much of what is known about ACh synthesis and release from cholinergic nerve terminals in the CNS were first worked out in preganglionic terminals in sympathetic ganglia, particularly the crucial role that high-affinity choline transport plays in cholinergic transmission (Birks and MacIntosh, 1961; Tuček, 1978). If our results hold true for cholinergic terminals in the CNS, it implies that certain ACh insufficiency diseases result from perturbations in activity-dependent retrograde signals that regulate CHT expression.

**CHAPTER 4:**  
**MITOCHONDRIAL REACTIVE OXYGEN SPECIES INACTIVATE NEURONAL  
NICOTINIC ACETYLCHOLINE RECEPTORS AND INDUCE LONG-TERM  
DEPRESSION OF FAST NICOTINIC SYNAPTIC TRANSMISSION**

**FOREWORD**

**Background and Rationale**

Neuronal nAChRs on sympathetic neurons are targeted to postsynaptic domains that are rich in mitochondria, potentially exposing these receptors to reactive oxygen species (ROS) generated by oxidative phosphorylation. Given that many diseases that produce dysautonomias also increase cytosolic ROS and given that ROS are known to modify some types of ion channels, it raises the question of whether elevations in cytosolic ROS alter the function of nAChRs. In this study V. Campanucci and I examine the effects of cytosolic ROS on the function of nAChRs.

**Hypothesis**

I predict that elevated cytosolic ROS will disrupt the function of nAChRs.

**Experimental Outline**

To examine the effects of ROS on nAChR function I will elevate ROS in cultured sympathetic neurons and simultaneously measure changes in cytosolic ROS levels and whole-cell ACh-evoked currents. To examine the effects of ROS on nAChR function *in vivo* I will (1) record synaptic transmission on sympathetic neurons in intact ganglia with antimycin A in my electrodes to poison the

mitochondria and elevate ROS. (2) record synaptic transmission from intact ganglia from mice treated with anti-NGF antibodies as a way to non-invasively elevate ROS in sympathetic neurons

**ABSTRACT**

Neuronal nicotinic acetylcholine receptors (nAChRs), ligand-gated ion channels implicated in a variety of cognitive, motor, and sensory behaviours, are targeted to compartments rich in mitochondria, particularly postsynaptic domains and presynaptic terminals, exposing these receptors to reactive oxygen species (ROS) generated by oxidative phosphorylation. In addition, these receptors can become exposed to ROS during the progression of certain neurodegenerative diseases. Because ROS are known to modify several membrane proteins, including some types of ion channels, it raises the question of whether elevations in cytosolic ROS alter the function of nAChRs. To address this, we elevated ROS in cultured sympathetic neurons, directly by perfusing neurons intracellularly with ROS, indirectly by blocking the mitochondrial electron transport chain, or noninvasively by transient NGF removal; we then simultaneously measured changes in cytosolic ROS levels and whole-cell ACh-evoked currents. In addition, we elevated cytosolic ROS in postganglionic neurons in intact ganglia and measured changes in nerve-evoked EPSPs. Our experiments indicate that mild elevations in cytosolic ROS, including that produced by transient interruption of NGF signaling, induce a use-dependent, long-lasting rundown of ACh-evoked currents on cultured sympathetic neurons and a long-lasting depression of fast nerve-evoked EPSPs. We show that these effects of cytosolic ROS are specific to nAChRs on neurons and do not cause rundown of ACh-evoked currents on muscle. Our results demonstrate that elevations in cytosolic ROS inactivate neuronal nAChRs in a use-dependent manner and suggest that mild oxidative stress impairs mechanisms mediated by cholinergic nicotinic signaling at neuronal–neuronal synapses.

## INTRODUCTION

Neuronal nicotinic acetylcholine receptors (nAChRs), members of a large family of neurotransmitter-gated ion channels, are expressed widely throughout the nervous system and are implicated in several physiological mechanisms, including sensory processing, pain perception, and reinforcing behavior to nicotine (Picciotto, 2003; Champtiaux and Changeux, 2004; Laviolette and van der Kooy, 2004; Dani and Bertrand, 2007). That nAChR signaling is crucial for these behaviors has been confirmed by recent studies on animals carrying gain-of-function or loss-of-function mutations in neuronal nAChR subunit genes (Cordero-Erausquin et al., 2000; Picciotto et al., 2001; Wang et al., 2002; Tapper et al., 2004; Maskos et al., 2005). How neuronal nAChRs alter the function of neural circuits depends primarily on where the receptors are located: on some neurons, such as those in peripheral sympathetic ganglia, nAChRs are targeted to the soma-dendritic domain where they mediate fast excitatory synaptic transmission (De Biasi, 2002; Skok, 2002); on other neurons, particularly those in the CNS, nAChRs are targeted to preterminal axons or presynaptic terminals where they modify GABA or glutamate transmitter release (Gray et al., 1996; Role and Berg, 1996; Broide and Leslie, 1999; MacDermott et al., 1999; Sher et al., 2004; Gotti et al., 2006). Because of the difficulties in recording directly from nAChRs on nerve terminals, however, we know little about the precise manner by which nAChR-mediated depolarizations modulate presynaptic transmitter release. However, considerable progress has been made in understanding these receptors at the molecular level, and the structural determinants involved in ligand-binding, ion permeation through the receptor pore, and receptor desensitization are becoming clearer (Corringer et al., 2000; Karlin, 2002; Unwin,

2005; Purohit et al., 2007). Moreover, a number of studies indicate that second messenger pathways modify the desensitization properties of the receptor, partly by phosphorylating receptor subunits (Swope et al., 2006; Quick and Lester, 2002; Giniatullin et al., 2005; Guo and Lester, 2007); however, the intracellular regulatory pathways that produce these receptor-modifying actions are not fully understood.

Because most nAChRs on cholinceptive neurons are targeted to compartments rich in mitochondria, such as presynaptic terminals and postsynaptic compartments, potentially, these receptors are exposed to reactive oxygen species (ROS) generated by oxidative phosphorylation, particularly during periods of strong electrical activity. Our interest is whether increases in the oxidative strength of the cytosol, as occurs during the overproduction of ROS, modify receptor function. Elevations in cytosolic ROS levels are associated with several diseases (Coyle and Puttfarcken, 1993; Smith et al., 1996; Mattson, 2004; Lin and Beal, 2006; Mancuso et al., 2006; Savitt et al., 2006) and are known to alter the function of several membrane proteins including certain ion channels (Park et al., 1995; Ichinari et al., 1996; Annunziato et al., 2002; Dröge, 2002; Liu and Gutterman, 2002; Tang et al., 2004; Gamper et al., 2006); yet, we have no information whether elevations in cytosolic ROS alter the function of neuronal nAChRs. Given the connection between ROS and disease, if elevations in cytosolic ROS alter the function of neuronal nAChRs, the resulting effects on synaptic transmission could have serious consequences for ROS-related diseases, including associated dysautonomias, particularly if fast nicotinic synapses in the autonomic nervous system are impaired. Consequently, we set out to determine whether changes in the oxidative status of the cytosol produce changes in nAChR function and cholinergic nicotinic synaptic transmission.

Our study started with an unexpected finding: while recording ACh-evoked currents on cultured sympathetic neurons, we observed that nAChRs on neurons in short-term cultures entered into a long-lasting, nonconducting state that caused a specific rundown of the ACh-evoked currents, whereas on neurons in long-term cultures the ACh-evoked currents were stable. This finding suggested that the functional state of nAChR on these neurons depends on some intracellular regulatory process. Here, we demonstrate that elevated mitochondrial ROS, achieved either by blocking mitochondrial electron transport chain complex III or by transiently withdrawing growth factors, induce nAChRs to adopt a long-lasting, inactivated state in a use-dependent manner and cause long-term depression of synaptic transmission in intact sympathetic ganglia. Our findings link the functional state of nAChRs on neurons to cytosolic ROS levels; equally relevant, our results imply that, during diseases involving mitochondrial dysfunction and/or oxidative stress, cholinergic nicotinic signaling mechanisms and autonomic regulation of homeostasis are impaired.

## **METHODS AND MATERIALS**

### **Primary Cultures**

Superior cervical ganglion (SCG) neurons were cultured from neonatal [postnatal day 1 (P1) to P3] mice (C57 black or CD1 strains; Charles River, St. Constant, Quebec, Canada) and rats (Sprague Dawley; Charles River) as previously described (McFarlane and Cooper, 1992). Briefly, ganglia were removed under sterile conditions and enzymatically dissociated at 37°C in HBSS containing trypsin (180–200 U/ml; Worthington, Freehold, NJ) and buffered with HEPES (adjusted to pH 7.4 with NaOH). The resulting cell suspension was

washed twice in serum-containing medium to inactivate the trypsin and plated on laminin-coated coverslips attached to modified 35 mm tissue culture dishes. The neurons were grown in media consisting of L-15 supplemented with vitamins, cofactors, penicillin–streptomycin, 5% rat serum, and NGF (40 ng/ml). Cultures were maintained at 37°C in a humidified atmosphere of 95% air–5% CO<sub>2</sub> and fed every 3 d with growth media. To eliminate non-neuronal cells, cultures were treated with cytosine arabinoside (10 μM; Sigma, St. Louis, MO) from day 2 to 4. For NGF withdrawal experiments, cultures were washed twice with growth media without NGF and maintained in growth media without NGF for 6–72 h.

To culture skeletal myotubes, we removed pectoral muscles from neonatal mice under sterile conditions, cut them into 1–2 mm pieces, and enzymatically dissociated them at 37°C in HBSS containing trypsin (180–200 U/ml; Worthington), buffered with HEPES (adjusted to pH 7.4 with NaOH). The resulting cell suspension was washed twice in serum-containing medium and plated on laminin-coated coverslips. The myoblasts were grown in media consisting of L-15 supplemented with vitamins, cofactors, penicillin–streptomycin, 10% horse serum, and maintained at 37°C in a humidified atmosphere of 95% air–5% CO<sub>2</sub> and fed every 3 d with growth media. After 3–5 d, the myoblasts fused to form myotubes; we selected the smallest myotubes for electrophysiological experiments.

### **Whole-Cell Recording**

ACh-evoked currents were measured with whole-cell patch-clamp techniques. Membrane currents were recorded with a VE-2 amplifier (Alembic Instruments, Montreal, Quebec, Canada) at room temperature, sampled at 500 Hz, and stored on a Pentium II-based personal computer and filtered off-line.

Recording electrodes had resistances of 2–5 M $\Omega$ , and series resistance was compensated from 70 to >98%. Patchkit software (Alembic) was used for stimulation and data acquisition and currents were filtered and analyzed off-line with Origin (OriginLab, Northampton, MA) or Igor (WaveMetrics, Lake Oswego, OR) software. Recording electrodes were filled with the following solution (in mM): 65 KF, 55 KAc, 5 NaCl, 0.2 CaCl<sub>2</sub>, 1 MgCl<sub>2</sub>, 10 EGTA, 2 MgATP, and 10 HEPES, and pH was adjusted to 7.2 with KOH. Cultured neurons were perfused continuously at 1 ml/min with control perfusion solution consisting of the following (in mM): 140 NaCl, 5.4 KCl, 0.33 NaH<sub>2</sub>PO<sub>4</sub>, 0.44 KH<sub>2</sub>PO<sub>4</sub>, 2.8 CaCl<sub>2</sub>, 0.18 MgCl<sub>2</sub>, 10 HEPES, 5.6 glucose, 2 glutamine, and 5  $\mu$ g/ml phenol red; pH was adjusted to 7.4 with NaOH. ACh (100  $\mu$ M) was dissolved in the perfusion solution and applied by pressure ejection from pipettes with tip diameters of 2–5  $\mu$ m positioned 20–30  $\mu$ m from the cell body (Mandelzys et al., 1995). In some experiments, atropine (1  $\mu$ M; Sigma) was added to the perfusion solution. Voltage-gated Na<sup>+</sup> currents were measured in control perfusion solution; we acquired the data at 50 kHz and filtered off-line. When measuring voltage-gated K<sup>+</sup> currents, we added 1  $\mu$ M TTX (Alomone Labs, Jerusalem, Israel) and 200  $\mu$ M CdCl<sub>2</sub> (Sigma) to the perfusion solution. For K<sup>+</sup> currents, we acquired the data at 5 kHz and filtered off-line. All activators and inhibitors of second messenger pathways were applied to individual neurons through the patch pipette.

To increase cytosolic ROS directly in individual neurons, we used two methods: (1) we dissolved 1  $\mu$ M antimycin-A (Sigma) in 100% EtOH [at 1:1000 (v/v) dilution] and added it to neurons through the recording electrode; or (2) we generated ROS from a Fenton reaction and introduced them into neurons through the recording electrode. To generate ROS from the Fenton reaction, we added 10 mM H<sub>2</sub>O<sub>2</sub> to a solution containing 44 mM-ascorbate and 1 mM FeCl<sub>3</sub>·6H<sub>2</sub>O at a

1:20 (v/v) dilution; this solution was added to the recording electrode solution (see above) at a 1:10 (v/v) dilution. We remade solutions for the Fenton reaction every 30 min from powdered ingredients at room temperature. To control for the EtOH in the antimycin-A experiments, we recorded from neurons with electrodes containing EtOH at 1:1000 (v/v) dilution but without the antimycin-A, and to control for the low ionic strength of the Fenton-containing electrode solution, we diluted the solution in the recording electrode with H<sub>2</sub>O at 1:10 (v/v); neither the added EtOH (n = 6) nor the lower ionic strength of the Fenton-containing solution (n = 6) had any detectable effects on the ACh-evoked currents.

As a measure of rundown of the ACh-evoked currents we plotted the ratio of the peak current (I) in response to the 30th application (I<sub>30</sub>) in a series to the peak current in response to the first application (I<sub>1</sub>) in the series. To quantify receptor desensitization, we fit the falling phase of the ACh-evoked currents during the ACh application to a single or double exponential function using Igor software (WaveMetrics).

Whole-cell recordings from neuronal  $\alpha 4\beta 2$  receptors and muscle  $\alpha 1\beta 1\delta \epsilon$  receptors in *Xenopus* oocytes. *Xenopus* oocytes were defolliculated and prepared as described by Bertrand et al. (1991). We injected 1–3 ng of cDNAs coding for neuronal nAChR subunits  $\alpha 4$  and  $\beta 2$ , or muscle  $\alpha 1$ ,  $\beta 1$ ,  $\delta$ , and  $\epsilon$  subunits into the nucleus of oocytes. Oocytes were incubated at 19°C for 2–5 d before recording.

To measure the macroscopic ACh-evoked currents on oocytes, we used two-electrode voltage-clamp techniques (Bertrand et al., 1991). These experiments were performed at room temperature (22–24°C) using a standard voltage-clamp amplifier (Alemic Instruments). During the recordings, oocytes were perfused with control perfusion solution or agonist solutions at 10–20

ml/min; the switch from one solution to another was performed manually. Currents were sampled at 100–350 Hz on-line with a Pentium-based PC computer (with a 64 kilobyte cache and A/D card; Omega, Stamford, CT) and filtered off-line. The program Patchkit (Alembic) was used for stimulation and data acquisition. Recording electrodes had tip diameters of 10–15  $\mu\text{m}$  and were filled with 1 M KAc. To test the effects of mitochondrial ROS, antimycin-A (100  $\mu\text{M}$ ) was added to the electrode-filling solution. Control experiments were performed by adding 100% EtOH [at 1:1000 (v/v) dilution] to the electrode solution ( $n = 6$ ). The external perfusion solution contained 96 mM NaCl, 2 mM KCl, 1 mM  $\text{NaH}_2\text{PO}_4$ , 1 mM  $\text{BaCl}_2$ , 10 mM HEPES, and 1  $\mu\text{M}$  atropine; pH was adjusted with NaOH to 7.4–7.5.

### **Intracellular ROS Measurement**

To monitor changes in cytosolic ROS, we used the redox-sensitive dye CM- $\text{H}_2\text{DCFDA}$  (Molecular Probes, Burlington, Ontario, Canada), an acetoxymethyl (AM) ester. Cultures were incubated for 40 min at 37°C with medium containing CM- $\text{H}_2\text{DCFDA}$  (10  $\mu\text{M}$ ) and subsequently washed five times with control perfusion solution (see above). The cultures were then placed on the stage of an inverted microscope (Axiovert 200 M; Zeiss, Oberkochen, Germany) and viewed through a 40x (1.3 numerical aperture) or 63x (1.4 numerical aperture) Plan Neofluor oil-immersion objective (Zeiss) at room temperature and continuously perfused throughout the experiment as described for whole-cell recordings. To obtain fluorescent images, we excited the cultures with 450–480 nm wavelength for 200 ms from a 150 W xenon arc lamp (LAMBDA DG-4; Sutter Instruments, Novato, CA) and collected 510–550 nm wavelength emissions (filter

set 31001; Chroma Technology, Brattleboro, VT) with a cooled CCD camera (CoolSnap HQ; PhotoMetrics, Tucson, AZ) controlled by Metafluor or MetaMorph softwares (Universal Imaging, West Chester, PA). For neurons treated with antimycin-A or Fenton reaction, we quantified changes in CM-H<sub>2</sub>DCFDA fluorescence over time by acquiring images every 25 s; for each image, we defined regions of interest (neuronal cell body, excluding the nucleus) on a differential interference contrast image and transferred these regions to the fluorescent images of the same field. The control fluorescence intensity (minus the background),  $F$ , was determined from neurons before establishing whole-cell patch configurations and from neighboring untreated neurons. For each neuron, we subtracted its mean fluorescent intensity (minus background) from  $F$  to obtain the change in fluorescent intensity ( $\Delta F$ ) and expressed it as  $\Delta F/F$ . To monitor changes in cytosolic ROS during NGF withdrawal experiments, we defined regions of interest as above, acquired Z stack planes at 1  $\mu\text{m}$  intervals to find the plane with the maximum mean pixel intensity for each neuron, and then calculated  $\Delta F/F$ ; in these experiments,  $F$  was the mean fluorescent intensity (after subtracting background) for neurons in control cultures with NGF. A total of >450 neurons were measured, >50 neurons in each condition.

### **Antioxidant Treatment**

To load neurons with ascorbate, we incubated neurons with ascorbate oxidase and L-ascorbate to circumvent in vitro artifacts associated with the poor transport and prooxidant effects of ascorbate (Buettner and Jurkiewicz, 1996; Clement et al., 2001). To do this, neurons were incubated for 30 min at 37°C in freshly prepared ascorbate (0.55 mM) and 0.5 U/ml ascorbate oxidase (Frank et

al., 2006). Ascorbate oxidase converts L-ascorbate to dehydroascorbate (DHA), which is transported through the facilitative glucose transporter and quickly converted to ascorbate. In other experiments, the antioxidant  $\alpha$ -lipoic acid (100  $\mu$ M) was dissolved in intracellular solution, treated with 1000 U/ml catalase for 1 h at 37°C (Vincent et al., 2005), and used as the recording solution during whole-cell recording.

Extracellular and intracellular recordings from intact SCGs. SCGs were dissected rapidly from neonatal rat and mice pups (P3–P7), pinned down with minutia pins in a recording chamber (1.5 ml volume) mounted on a fixed stage, and viewed with a dissecting microscope (SMZ-10; Nikon, Tokyo, Japan); the tissue was perfused continuously at 3–4 ml/min with oxygenated Ringer's solution at 36–37°C. To stimulate the preganglionic nerve, the cervical sympathetic trunk was connected to a stimulator (4710 ORTEC dual channel; EG&G, Gaithersburg, MD) with a suction electrode and stimulated with brief (0.1–0.3 ms) voltage pulses. For extracellular compound action potentials, the postganglionic trunk was connected to an AC differential amplifier (DP-301; Warner Instruments, Hamden, CT) with a suction electrode; the postganglionic compound action potentials were amplified, filtered at 100 Hz (low-pass cutoff) and 1 kHz (high-pass cutoff), digitized at 10 kHz, and stored on a Pentium II-based computer. To record intracellularly from individual SCG neurons, we used 50–70 M $\Omega$  glass microelectrodes (G150F-4; Warner Instruments) made with a DMZ universal puller (Zeitz Instruments, Munich, Germany) as described previously (Rassadi et al., 2005). Stable intracellular recordings were achieved with a high inertial precision microdrive (Inchworm 8200; EXFO, Vanier, Quebec, Canada) attached to a micromanipulator (SM11; Narshige, Tokyo, Japan) that drove the electrode through the ganglion. The recording electrode was filled with 1 M KAc and

connected by a thin silver chlorided wire to the head stage of an Axoclamp 2A amplifier (Molecular Devices, Sunnyvale, CA) used in current-clamp mode; depolarizing or hyperpolarizing constant current pulses were applied through the recording electrode. Membrane potentials were sampled, displayed, and stored on a Pentium II-based personal computer. Stimulation and acquisition was done with Patchkit software (Alembic), and the data were analyzed off-line with Igor. To elevate mitochondrial ROS in individual neurons, we added antimycin-A (100  $\mu$ M) to the recording electrode; as control, we recorded from neurons with the identical solution without antimycin-A. To test the effects of transient interruption in NGF signaling on ganglionic transmission, we injected neonatal mice intraperitoneally with anti-NGF antibodies (Sigma) (2.5  $\mu$ l of 3 mg/ml stock per gram of body weight) or control IgG (Cederlane Lab, Burlington, Ontario, Canada) (2.5  $\mu$ l of 2.5 mg/ml stock per gram of body weight). Usually, the evoked EPSPs were suprathreshold, and therefore to measure the changes in EPSP amplitudes accurately, in some experiments, we added curare (10  $\mu$ M) to the perfusion solution. Only neurons with membrane potentials greater than  $-40$  mV were included in this study.

### **Statistics**

To determine the statistical significance for differences in (1) the  $I_{30}/I_1$  ratios and (2) the mean fluorescent intensities, we used a nonparametric test (Mann–Whitney). To determine the statistical significance for differences in cell numbers among different conditions in the NGF withdrawal experiments, we used ANOVA, and for EPSP amplitudes, we used Student's t test.

All procedures for animal handling were performed according to the guidelines of the Canadian Council on Animal Care.

## RESULTS

Our overall interests are in cytoplasmic factors that influence the functional properties of nAChRs on neurons. The present study began by observing that the ACh-evoked currents on sympathetic neurons in short-term cultures (1–3 d) run down irreversibly, as if the AChRs were trapped in a long-lasting inactivated state. This unexpected rundown of ACh-evoked currents has not been well described and suggested to us that some unappreciated regulatory mechanism controls the function of nAChRs on neurons. Therefore, first we characterized this rundown, and then we focused our investigation on its underlying cause.

### **Rundown of ACh-Evoked Currents on Sympathetic Neurons in Short-Term Cultures**

Repeated application of ACh (100  $\mu$ M) to rodent sympathetic neurons in short-term cultures (1–3 d) resulted in a steady decline of the ACh-evoked currents; when ACh was applied for 1 s at 15 s intervals, the peak ACh-evoked inward current declined to <10% of the initial response in  $\sim$ 2–3 min (Fig. 1A). In contrast, when repeatedly applying ACh to neurons in long-term cultures (>10 d), we observed no significant decline in the ACh-evoked currents (Fig. 1A).  $\alpha$ -Bungarotoxin had no detectable effect on these currents ( $n = 6$ ) (data not shown), indicating that the currents in Figure 1A are likely mediated by  $\alpha$ 3 $\beta$ 4-containing receptors. Equally noteworthy, once the ACh-evoked current on neurons in short-term cultures had run down, it never recovered, even after washing with ACh-free solution for 30 min (Fig. 1A).

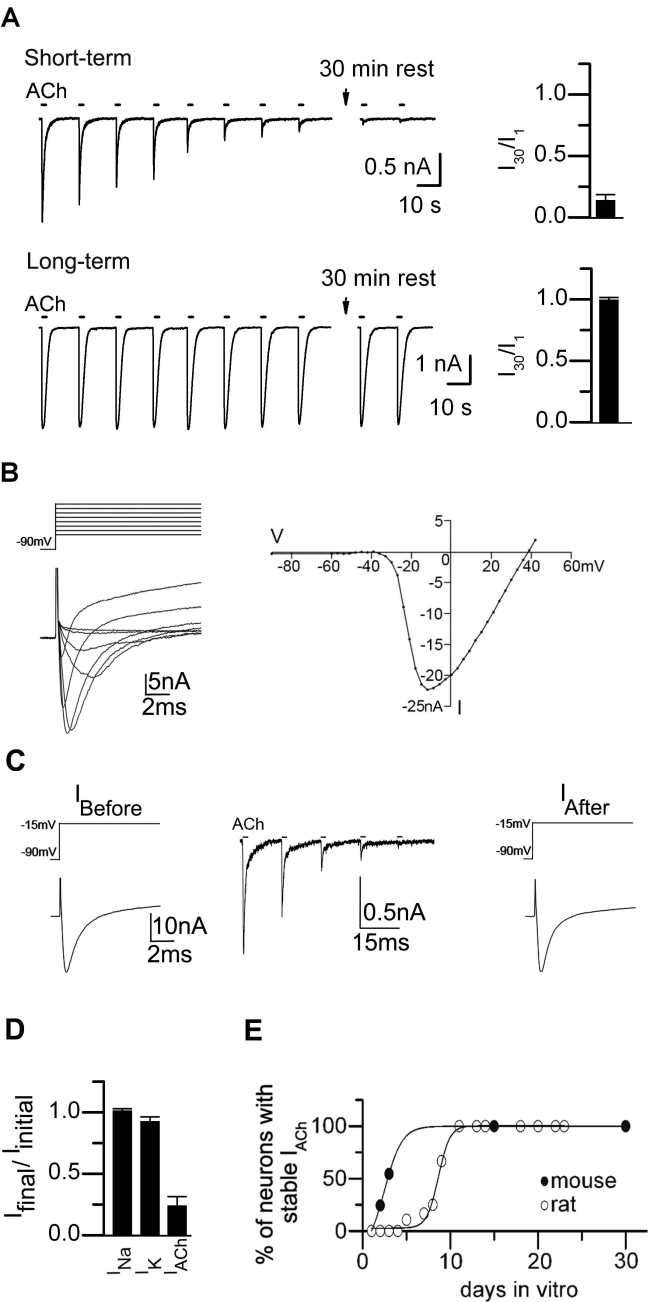


**Figure 4.1**

**FIGURE 4.1.** Rundown of ACh-evoked currents on sympathetic neurons in short-term cultures. **A** ACh-evoked currents from neonatal mouse SCG neurons in culture for 2 d (short-term) or in culture for 10 d (long-term) in response to a series of 1 s ACh (100  $\mu$ M) applications delivered at 15 s intervals. The bar graph on the right shows the mean ratio of the 30th ACh-evoked current to the first in the series ( $I_{30}/I_1$ ) for neurons in short-term culture ( $n = 7$ ) and neurons in long-term culture ( $n = 6$ ). Each bar is the mean  $I_{30}/I_1 \pm$  SE. The ACh-evoked currents on neurons in short-term culture run down rapidly, and never recovered, even after washing with ACh-free solution for 30 min; whereas those on neurons in long-term culture are stable. **B** Left, Superimposed voltage-gated inward  $\text{Na}^+$  currents ( $I_{\text{Na}}$ ) and outward  $\text{K}^+$  currents ( $I_{\text{K}}$ ) measured from a neuron in short-term culture in response to a series of voltage steps from  $-90$  mV holding potential delivered at 3 mV increments to  $+40$  mV. Only every fourth trace starting at  $-60$  mV is shown for clarity. The currents have not been corrected for leakage. Right, The corresponding peak  $I_{\text{Na}}$ -voltage relationship. **C** The peak  $I_{\text{Na}}$  recorded from a neuron in short-term culture in response to voltage steps from  $-90$  to  $-15$  mV before (left) and after (right) rundown of ACh-evoked currents (middle). The ACh-evoked currents run down but the sodium currents do not. **D** Bar graph shows the ratio of the peak  $I_{\text{Na}}$  and  $I_{\text{K}}$  on neurons in short-term culture before and after rundown of the ACh-evoked currents (mean  $\pm$  SE;  $n = 7$ ). There was no significant difference in the peak  $I_{\text{Na}}$  or  $I_{\text{K}}$  before and after rundown of the ACh-evoked currents. **E** The proportion of neurons with stable ACh-evoked currents on rat ( $\odot$ ) and mouse ( $\bullet$ ) SCG neurons in sister cultures as they developed in culture over time. ACh-evoked currents in response to a series of ACh applications were measured on at least 10 neurons selected at random in a given culture; each point represents the proportion of neurons in a given culture with stable ACh-evoked currents.

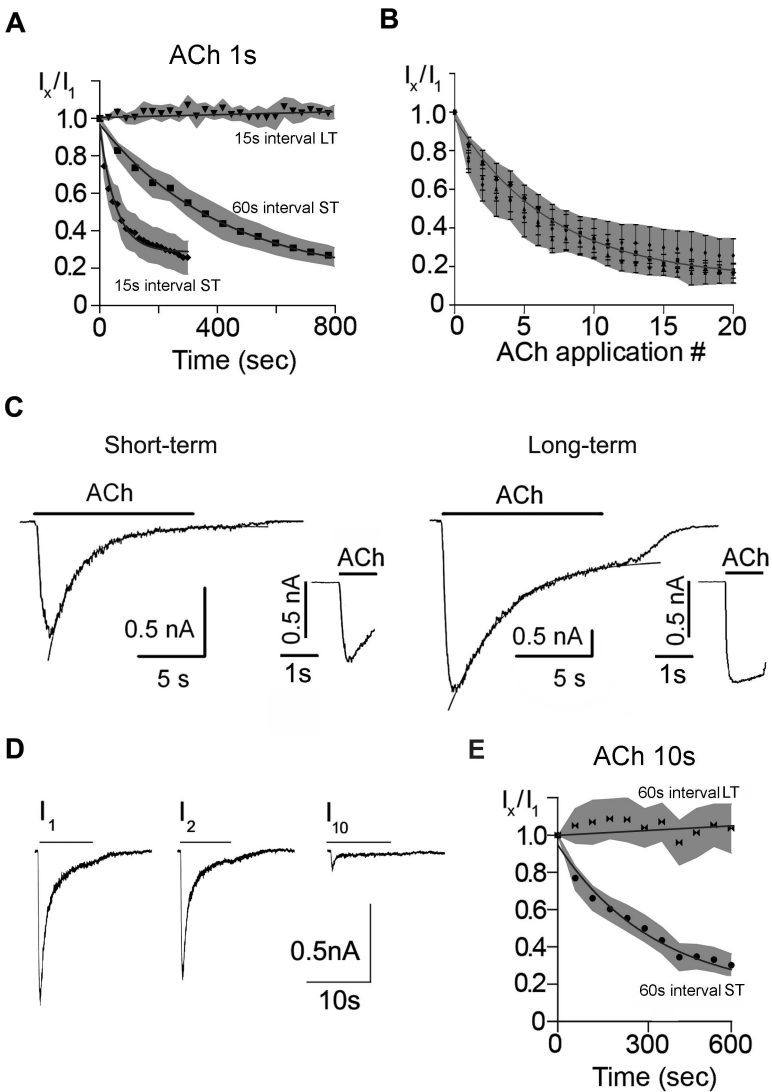


**Figure 4.2**

**FIGURE 4.2.** Use-dependent rundown of ACh-evoked currents on sympathetic neurons in short-term cultures. **A** ACh-evoked currents were measured in response to a series of 1 s ACh (100  $\mu$ M) applications delivered at 15 s intervals ( $\blacklozenge$ ) ( $n = 9$ ) and at 60 s intervals ( $\blacksquare$ ) ( $n = 8$ ) for neurons in culture for 2 d (short-term) and at 15 s intervals ( $\blacktriangledown$ ) ( $n = 6$ ) for neurons in culture for 10 d (long-term).  $I_x/I_1$  is the ratio of the  $x$ th response to the first response in a series. Each point is the mean; only every second ratio of the time series is shown for clarity. The solid lines are exponential fits to the data and the gray shaded area is the SE. The  $I_x/I_1$  ratio decreases by 50% in 78 s when ACh is delivered at 15 s intervals and 282 s when delivered at 60 s intervals. **B** The average  $I_x/I_1$  ratio versus application number from the data in A and D: 1 s ACh (100  $\mu$ M) at 15 s intervals ( $\blacklozenge$ ) ( $n = 9$ ), and at 60 s intervals ( $\blacksquare$ ) ( $n = 8$ ), and 10 s ACh (100  $\mu$ M) at 60 s intervals ( $\bullet$ ) (mean  $\pm$  SE). The solid line is an exponential fit to the data and the gray shaded area is the SE. The  $I_x/I_1$  ratio decreases by  $1/e$  in approximately six applications independent of the interval between ACh applications or ACh duration. **C** ACh-evoked currents on neurons in short-term culture desensitize more rapidly than those in long-term cultures. Examples of ACh-evoked currents from neonatal mouse SCG neurons in short-term or long-term culture in response to ACh (100  $\mu$ M) applied for 10 s. The inset shows the current at a faster time base in response to a 1 s application. For the neuron in short-term culture, the current evoked by a 10 s ACh application was fit with a double exponential function of  $\tau_f = 1.15$  s and  $\tau_s = 3.6$  s; for the neuron in long-term culture, the current was fit with a single exponential function of  $\tau = 3.4$  s (solid lines). **D** ACh-evoked currents from neonatal mouse SCG neurons in short-term culture in response to a series of 10 s ACh (100  $\mu$ M) applications delivered at 60 s intervals. The ACh-evoked current in response to the first application ( $I_1$ ) desensitized by over 95% and recovered by >70% in 60 s (second response;  $I_2$ ) but ran down by the 10th application ( $I_{10}$ ). **E** Average responses to a series of 10 s ACh (100  $\mu$ M) applications delivered at 60 s intervals for neurons in short-term ( $\bullet$ ) ( $n = 6$ ) and neurons in long-term culture ( $\blacktriangledown$ ) ( $n = 6$ ). Each point is the mean  $I_x/I_1$  ratio. The solid lines are exponential fits to the data, and the gray shaded area is the SE. There is no significant difference in the time course for the decrease in ratio when ACh is applied at for 10 s at 60 s intervals compared with ACh applied for 1 s at 60 s intervals (A). ST refers to short-term cultures, and LT refers to long-term cultures.

This striking and unexpected long-lasting rundown of ACh-evoked currents from neurons in short-term cultures was not caused by a generalized change in the neurons. We observed no significant difference in the voltage-gated  $\text{Na}^+$  currents before and after rundown of the ACh-evoked currents (Fig. 1 B–D), or in the voltage-gated  $\text{K}^+$  currents (Fig. 1D). Importantly, these results indicate that rundown of the ACh-evoked currents was not attributable to a generalized, nonspecific change in the neurons during whole-cell recording.

Over a few days in culture, the proportion of neurons with stable ACh-evoked currents increased. To quantify this conversion, we sampled neurons in sister cultures for stable ACh-evoked currents at different times after plating. To judge whether the ACh-evoked currents were stable, we delivered a series of ACh applications at 15 s intervals: If the response to the 30th application ( $I_{30}$ ) was at least 80% of the initial response ( $I_1$ ), we classified the neuron as having stable ACh-evoked currents. For the first 24 h after plating, the proportion of neurons with stable ACh-evoked currents was very low (<5%); thereafter, the proportion increased sigmoidally, and by 10 d after plating, 100% of the neurons had stable ACh-evoked currents (Fig. 1E). Moreover, the transition to neurons with stable ACh-evoked currents occurred significantly faster on sympathetic neurons from mice (within 2–3 d) compared with those from rats (7–10 d) (Fig. 1E). These results suggest that, as neonatal rodent sympathetic neurons develop in culture, some maturation process stabilizes their ACh-evoked currents.

The rundown of ACh-evoked currents from neurons in short-term cultures depends on receptor activation. When ACh was applied at 15 s intervals, the ACh-evoked current decreased by 50% in  $1.3 \pm 0.66$  min ( $n = 6$ ) (Fig. 2A); whereas the ACh-evoked current took approximately fourfold longer to decrease by 50% when ACh was applied consecutively at 60 s intervals ( $4.7 \pm 0.81$  min;  $n$

= 6) (Fig. 2A). However, when the peak ACh-evoked currents were plotted against the absolute number of ACh applications for both the 15 s series and 60 s series, the decline of the ACh-evoked currents were comparable; the plot of the  $I_{\text{ACh}}$  versus agonist applications decayed as a single exponential function, indicating that it requires approximately six consecutive ACh applications to inactivate the current by two-thirds (Fig. 2B). These results demonstrate a use dependence to the rundown: the more the receptors are activated, the greater the rundown of the ACh-evoked currents.

This rundown of ACh-evoked currents does not result from an inability to recover from desensitization. The ACh-evoked currents on neurons in short-term cultures desensitized approximately three times faster than those on neurons in long-term cultures (Fig. 2C); with 10 s applications to neurons in short-term cultures, 85% of the evoked current decayed as a single exponential function with a time constant ( $\tau_d$ ) of  $1.36 \pm 0.29$  s ( $n = 8$ ), and the remaining 15% decayed with a  $\tau_d$  of  $3.95 \pm 0.32$  s ( $n = 8$ ); whereas for neurons in sister cultures for >2 weeks (long-term cultures), the ACh-evoked currents decayed with a single exponential time course ( $\tau_d = 4.13 \pm 0.68$  s;  $n = 10$ ) (Fig. 2C). Most nAChRs on neurons in short-term cultures recover rapidly from desensitization; a second ACh application given 60 s after a long (10 s) desensitizing pulse evoked ACh currents that were ~70% of those evoked by the first (Fig. 2D). With successive ACh applications, however, ACh-evoked currents ran down with a time course similar to that induced by successive 1 s ACh applications (compare Fig. 2E), indicating that rundown does not depend on the extent of desensitization. However, successive long, desensitizing ACh applications to neurons in long-term cultures did not induce any significant rundown of the ACh-evoked currents (Fig. 2E).

These results indicate that the long-lasting rundown of ACh-evoked currents depends on a mechanism other than receptor desensitization.

### **Increasing the Antioxidant Content of the Cytosol Prevents Rundown of ACh-Evoked Currents on Neurons in Short-Term Cultures**

Rundown of ACh-evoked currents on neurons in short-term cultures was not affected by activating protein kinase A (PKA) or PKC, inhibiting PKA, PKC, tyrosine phosphorylation, or preventing elevations in intracellular  $\text{Ca}^{2+}$  (Fig. 3 A–C). In addition, none of these treatments induced rundown of ACh-evoked currents on neurons in long-term cultures (Fig. 3 D–F). Together, these results suggest that the rundown of ACh-evoked currents involves a process that does not depend directly on PKA, PKC, tyrosine kinase, or  $\text{Ca}^{2+}$  second messenger pathways.

Next, we asked whether shifts in the intracellular thio/disulfide redox state toward more oxidative conditions could underlie the rundown of the ACh-evoked currents from neurons in short-term cultures (Park et al., 1995; Annunziato et al., 2002; Tang et al., 2004; Gamper et al., 2006). To test this, we cultured neurons in media containing ascorbate and ascorbate oxidase to increase the reducing power of the cytosol (Frank et al., 2006). Unlike ACh-evoked currents on neurons in control sister cultures, all (eight of eight) neurons in short-term cultures incubated with ascorbate and ascorbate oxidase had stable ACh-evoked currents (i.e.,  $I_{30}/I_1$  was  $>0.80$ ) (Fig. 3G). In addition, we found that adding the antioxidants  $\alpha$ -lipoic acid and catalase to the recording electrode (see Materials and Methods) also prevented rundown of ACh-evoked currents on neurons in short-term cultures (Fig. 3G). These results suggest strongly that oxidative conditions of the

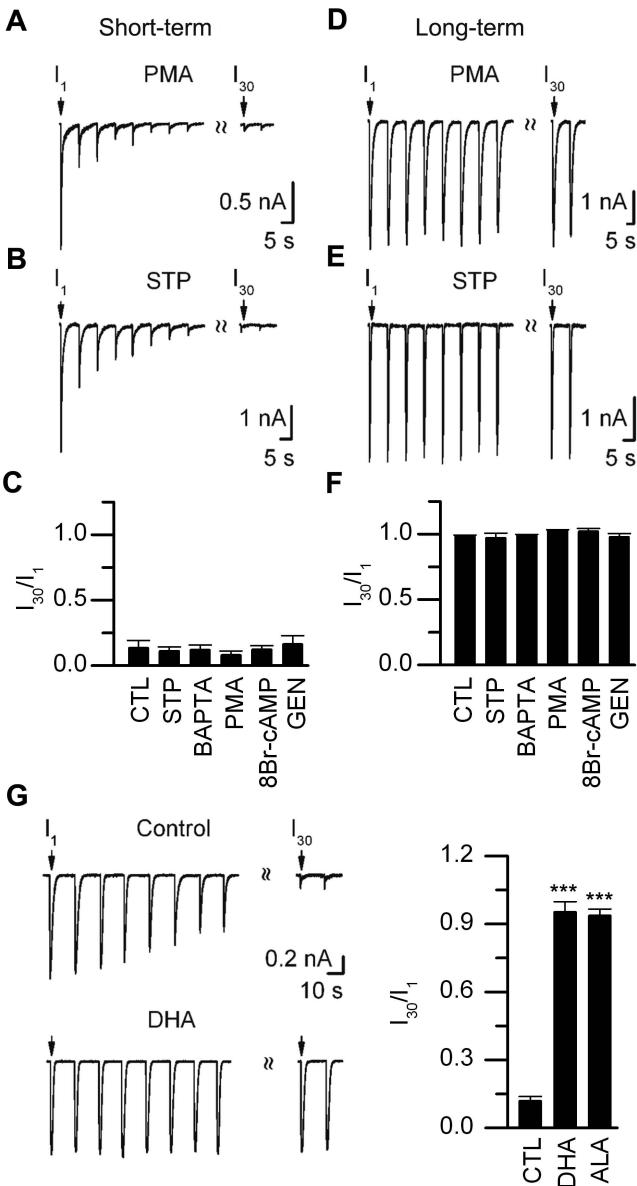


**Figure 4.3**

**FIGURE 4.3.** Rundown of ACh-evoked currents is prevented by antioxidants. **A** and **B** ACh-evoked currents from neonatal mouse SCG neurons in culture for 2 d (short-term) in response to a series of 1 s ACh (100  $\mu$ M) applications delivered at 15 s intervals when PMA (5  $\mu$ M) (**A**) or staurosporine (STP; 100 nM) (**B**) was included in the recording electrode. **C**  $I_{30}/I_1$  ratio for neurons in short-term culture for control (CTL) (n = 6), staurosporine (STP) (100 nM; n = 6), BAPTA (10 mM; n = 7), PMA (5  $\mu$ M; n = 6), genistein (10  $\mu$ M; n = 6), or 8-bromo-cAMP (250  $\mu$ M; n = 7). Each bar is the mean  $I_{30}/I_1 \pm$  SE. **D** and **E** ACh-evoked currents from neonatal mouse SCG neurons in culture for 10 d (long-term) in response to a series of 1 s ACh (100  $\mu$ M) applications delivered at 15 s intervals when PMA (5  $\mu$ M) (**D**) or staurosporine (STP; 100 nM) (**E**) was included in the recording electrode. **F** The  $I_{30}/I_1$  ratio for neurons in long-term culture for control (CTL) (n = 6), staurosporine (STP) (100 nM; n = 7), BAPTA (10 mM; n = 6), PMA (5  $\mu$ M; n = 7), genistein (10  $\mu$ M; n = 6), or 8-bromo-cAMP (250  $\mu$ M; n = 7). Each bar is the mean  $I_{30}/I_1 \pm$  SE; for control, BAPTA, and PMA experiments, the SEs are too small to resolve. **G** ACh-evoked currents from two neonatal rat SCG neurons in response to a series of 1 s ACh (100  $\mu$ M) applications delivered at 15 s intervals, one in control culture for 4 d and the other in a sister culture for 4 d but treated with antioxidants (DHA) (see Materials and Methods) 24 h before. The graph on the right shows the mean  $I_{30}/I_1$  ratio  $\pm$  SE for control (CTL) (n = 11) and neurons in sister cultures treated with the antioxidants, DHA (n = 8), or  $\alpha$ -lipoic acid (ALA) plus catalase (n = 6). \*\*\*p < 0.001.

cytosol induce long-lasting, use-dependent rundown of ACh-evoked currents on neurons.

### **Elevations in Cytosolic ROS Induce Long-Lasting, Use-Dependent Inactivation of Neuronal nAChRs**

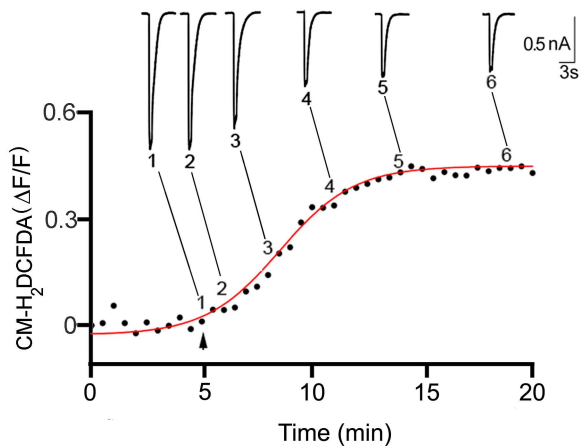
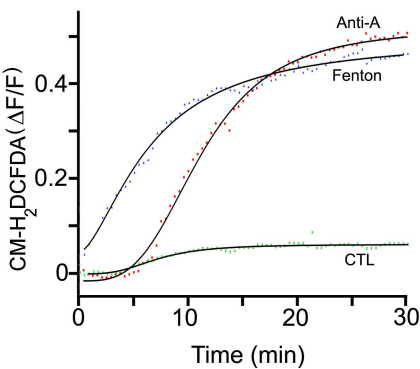
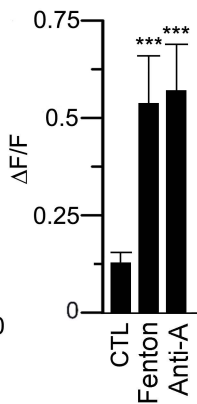
To test whether elevations in cytosolic ROS induce rundown of the ACh-evoked currents on neurons in long-term cultures, we generated ROS from a Fenton reaction (see Materials and Methods) and added them to neurons through the patch electrode. To monitor changes in cytosolic ROS over time, we loaded neurons with the fluorescent ROS indicator dye, CM-H<sub>2</sub>DCFDA. In all neurons recorded with ROS-containing electrodes, we observed an increase in ROS-induced fluorescence; the fluorescence started to increase within minutes after establishing whole-cell recording and reached a plateau by 10–15 min (Fig. 4A,B). On average,  $\Delta F/F$  increased to  $0.55 \pm 0.05$  ( $n = 7$ ) (Fig. 4C), whereas for neighboring neurons recorded with control intracellular solution,  $\Delta F/F$  was  $0.12 \pm 0.03$  ( $n = 6$ ) (Fig. 4C).

To test the effects of cytosolic ROS on the ACh-evoked currents, we recorded from neurons in long-term cultures with electrodes containing ROS generated from a Fenton reaction and simultaneously imaged changes in fluorescence and monitored ACh-evoked currents. Delivering a series of ACh applications, we found that, as ROS increased, the responses to ACh decreased (Fig. 4A), whereas for neighboring neurons recorded with electrode containing control solution, the ACh-evoked currents were stable. These results indicate that elevating ROS in the cytosol induces rundown of ACh-evoked currents.

In the experiment above, however, we applied ACh repeatedly to neurons as cytosolic ROS was increasing, making it difficult to know whether this ROS-induced rundown of ACh-evoked currents required receptor activation. To address this, we recorded from neurons with ROS-containing electrodes, waited 15 min for cytosolic ROS to reach its plateau, and then applied ACh repeatedly. The first response in the series was not significantly different from evoked currents on the neighboring control neurons, indicating that elevations in ROS by themselves do not have a detrimental affect on the receptors. However, when we delivered a series of ACh pulses to neurons with elevated ROS, the evoked current ran down rapidly (Fig. 5A); the ACh-evoked current amplitude in response to the 30th application was <15% of the response to the first (Fig. 5A,B). This ROS-induced rundown of ACh-evoked current did not recover for at least an additional 20–30 min. In contrast, the ACh-evoked currents were stable on neighboring neurons recorded with electrodes containing control solution (Fig. 5A,B). These results indicate that elevations in cytosolic ROS must be paired with receptor activation to induce a long-lasting rundown of the ACh-evoked currents.

### **Mitochondrial ROS Induces Long-Lasting, Use-Dependent Rundown of Neuronal nAChRs**

Physiologically, an important source of ROS comes from the mitochondrial electron transport chain generated as by-products of oxidative phosphorylation (Nicholls and Budd, 2000). Therefore, we asked whether mitochondrial ROS inactivate neuronal nAChRs. To address this, we inhibited complex III of the electron transport chain by adding antimycin-A (1  $\mu$ M) through the recording electrode to neurons in long-term cultures, and simultaneously monitored changes in CM-H<sub>2</sub>DCFDA fluorescence and membrane currents over

**A****B****C****Figure 4.4**

**FIGURE 4.4.** Cytosolic ROS induces rundown of ACh-evoked currents. **A** SCG neuron in culture for 14 d was loaded with CM-H<sub>2</sub>DCFDA and fluorescent images were obtained every 25 s and expressed as  $\Delta F/F$ ; the increase in fluorescence was described by a Hill function (solid line). At the arrow, ROS generated from a Fenton reaction was introduced into the neuron through the recording electrode, and a series of 1 s ACh (100  $\mu$ M) applications were delivered to the neuron at 15 s intervals to measure the ACh-evoked currents. The inset shows six selected ACh-evoked currents from the series, each obtained at different times indicated by the numbers and lines next to the curve showing the increase in ROS-induced fluorescence. **B** Example of the change in ROS-induced fluorescence in neurons in culture for 16 d when loaded acutely through the recording electrode with either ROS generated from the Fenton reaction, antimycin-A (1  $\mu$ M) or control (CTL). The increase in fluorescence was described by a Hill function (solid line). **C** The average increase in ROS-induced fluorescence for neurons in culture for 15–18 d in control (n = 6), or loaded with ROS generated from a Fenton reaction (n = 7), or antimycin-A (1  $\mu$ M; n = 7). The bars show the mean  $\Delta F/F$  plateau  $\pm$  SE recorded from neurons with control solution or when generating ROS from a Fenton reaction or antimycin-A. \*\*\*p < 0.001.

time. After blocking complex III with antimycin-A, ROS increased with a delay of 3–5 min after establishing whole-cell recording and reached a plateau by 15–20 min (Fig. 4B); on average,  $\Delta F/F$  increased to  $0.58 \pm 0.12$  ( $n = 12$ ), comparable with that in neurons perfused intracellularly with ROS from the Fenton reaction (Fig. 4C).

To determine whether elevations in mitochondrial ROS induced rundown of the ACh-evoked currents, we gave a series of ACh pulses to neurons after  $\Delta F/F$  had reached a plateau (15–20 min). The ACh-evoked current in response to the first ACh pulse was not significantly different from those on control neurons; however, we observed rundown of the ACh-evoked currents with subsequent applications; the ACh-evoked current amplitude in response to the 30th application was  $\sim 25\%$  of the response to the first (Fig. 5A,B). These results indicate that mild elevations in ROS from mitochondria are sufficient to induce an irreversible, use-dependent rundown of ACh-evoked currents. Moreover, the rundown of ACh-evoked currents induced by antimycin-A does not depend directly on PKA, PKC, tyrosine kinase, or  $Ca^{2+}$  second messenger pathways (Fig. 5C).

To rule out the possibility that elevating cytosolic ROS produced nonspecific changes in membrane currents, we measured voltage-gated  $K^+$  currents before (within 2 min of whole-cell recording) and after elevations in ROS and rundown of ACh-evoked currents ( $>20$  min). We observed no change in either the voltage-gated  $K^+$  currents, or in the holding current before and after increase in cytosolic ROS (Fig. 5D). These results indicate that elevations in ROS do not cause a generalized rundown of other membrane currents.

## **Mitochondrial ROS Induce Long-Lasting, Use-Dependent Rundown of $\alpha 4\beta 2$**

### **nAChRs**

To determine whether other nAChR subtypes expressed on neurons are inactivated by elevations in mitochondrial ROS, we examined  $\alpha 4\beta 2$  receptors expressed in *Xenopus* oocytes. When recording from oocytes expressing  $\alpha 4\beta 2$  receptors, brief (~2–3 s) applications of ACh (0.5  $\mu$ M) evoked large 3–4  $\mu$ A inward currents (Fig. 6A). These currents were stable for at least 30 min when recording from oocytes with electrodes containing control solution and ACh (0.5  $\mu$ M; 2–3 s) was applied at 1 min intervals (Fig. 6A). In contrast, when recording from oocytes with electrodes containing antimycin-A (100  $\mu$ M), the ACh-evoked currents ran down in a use-dependent manner after a delay of 10–15 min (Fig. 6A). These results suggest that elevations in mitochondrial ROS lead to the inactivation of  $\alpha 4\beta 2$  receptors, similar to endogenous nAChRs on sympathetic neurons.

## **Muscle nAChRs are not Inactivated by Cytosolic ROS**

To determine whether nAChRs on muscle were similarly affected by elevations in cytosolic ROS, we examined muscle  $\alpha 1\beta 1\delta\epsilon$  receptors expressed in *Xenopus* oocytes. In contrast to ACh-evoked currents from neuronal nAChRs when recording with electrodes containing antimycin-A, the ACh-evoked currents from oocytes expressing  $\alpha 1\beta 1\delta\epsilon$  receptors were stable for at least 30 min (Fig. 6B).

In addition, we recorded endogenous ACh-evoked currents from cultured mice myotubes. First, we loaded myotubes with CM-H<sub>2</sub>DCFDA, and then introduced ROS into individual myotubes through the recording electrode. The resting ROS-induced fluorescence was considerably higher in myotubes

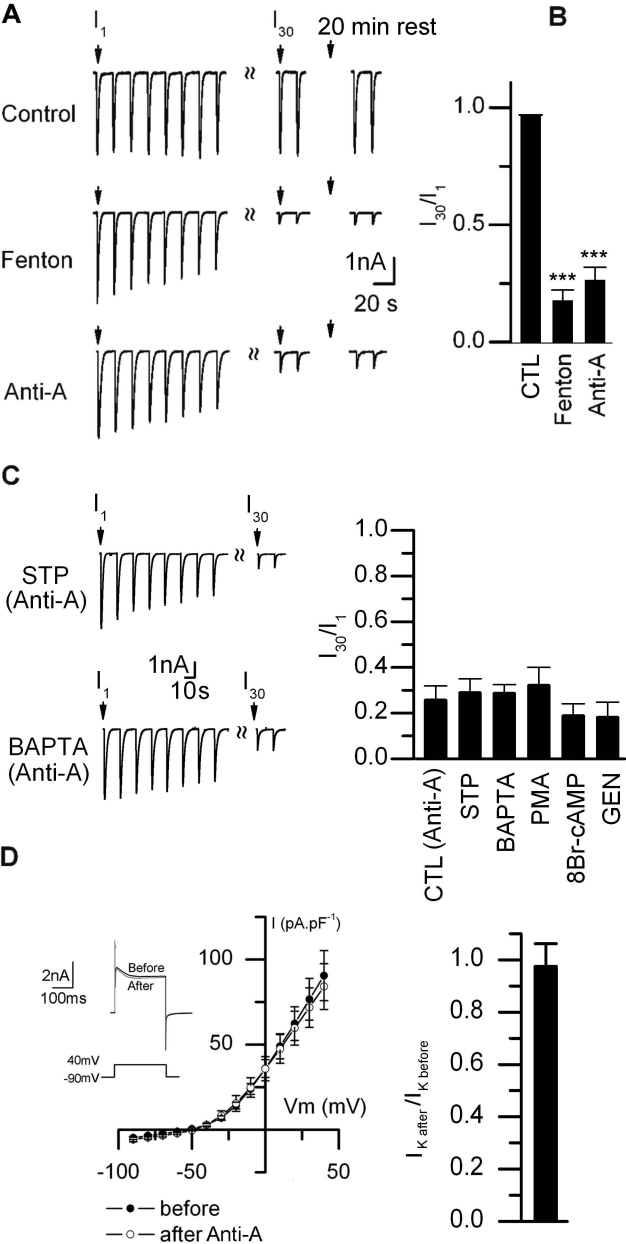


**Figure 4.5**

**FIGURE 4.5.** Mitochondrial ROS induces rundown of ACh-evoked currents. **A** ACh-evoked currents in response to repetitive ACh (100  $\mu$ M) applications at 15 s intervals from the three neurons in Figure 4B, control (top), Fenton reaction (middle), or antimycin-A (lower). **B**  $I_{30}/I_1$  ratio (mean  $\pm$  SE) for neurons loaded with control (CTL) (n = 12), Fenton reaction (n = 6), or antimycin-A (1  $\mu$ M; n = 12). The SE for CTL are too small to resolve. **C** Left, ACh-evoked currents from two neurons in culture for 16 d recorded with electrodes containing antimycin-A (1  $\mu$ M) and either staurosporine (STP) (100 nM) or BAPTA (10 mM). Right,  $I_{30}/I_1$  ratio for neurons in long-term cultures recorded with electrodes containing antimycin-A (1  $\mu$ M) plus control [CTL (anti-A)] (n = 12), staurosporine (STP) (100 nM; n = 6), BAPTA (10 mM; n = 7), PMA (5  $\mu$ M; n = 5), genistein (10  $\mu$ M; n = 6), or 8-bromo-cAMP (250  $\mu$ M; n = 6). None of these treatments prevented rundown by antimycin-A. **D** Left, The current–voltage relationship for voltage-gated  $K^+$  currents ( $I_K$ ) before and after inducing rundown of ACh-evoked currents. The inset shows outward  $K^+$  currents from a neuron perfused intracellularly with antimycin-A; the outward  $K^+$  currents were evoked by voltage steps from  $-90$  to  $+40$  mV within 2 min after establishing whole-cell recording (before) and 20 min later (after). The currents were not corrected for leakage. On the right is the ratio of  $I_K$  at  $+40$  mV before and after inducing rundown of ACh-evoked currents with antimycin-A (mean  $\pm$  SE; n = 6). There is no significant difference in the amplitude or voltage dependence of  $I_K$  or the holding current before and after inducing rundown of ACh-evoked currents. \*\*\*p < 0.001.

compared with neurons; nonetheless, we observed no significant rundown of the ACh-evoked currents in response to a series of 10 s ACh applications every 5 min, even after applying ACh repeatedly for up to 50 min (Fig. 6C). These results indicate that ROS does not inactivate muscle nAChRs.

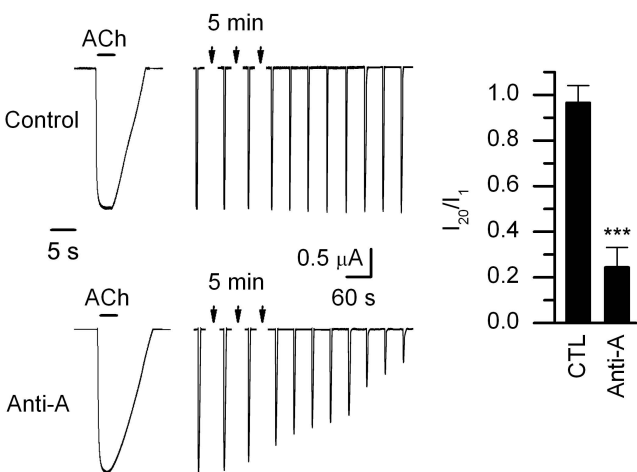
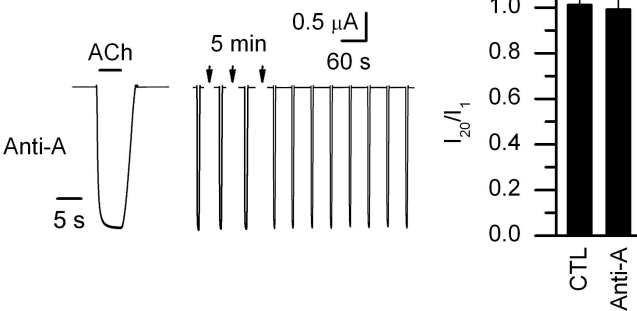
Transient elevation of mitochondrial ROS by disruption in NGF signaling  
In the above experiments, we elevated cytosolic ROS by introducing ROS directly into neurons or by inhibiting electron transport chain complex III with antimycin-A. Next, we asked whether we could induce a long-lasting inactivation of nAChRs on SCG neurons by elevating mitochondrial ROS noninvasively by transiently disrupting NGF signaling (Kirkland and Franklin, 2001; Kirkland et al., 2002).

To address this, first we withdrew NGF from neonatal sympathetic neurons in long-term cultures for various times and measured elevations in cytosolic ROS with CM-H<sub>2</sub>DCFDA fluorescence. ROS-induced fluorescence changed little during the first 6 h without NGF; by 18 h without NGF, however,  $\Delta F/F$  increased to  $0.81 \pm 0.03$  ( $n = 152$ ) (Fig. 7B), comparable with that achieved by antimycin-A or ROS from a Fenton reaction (Fig. 4C). This increase in cytosolic ROS at 18 h occurred without detectable change in neuronal morphology (when viewed with phase optics), or affect on neuronal survival (Fig. 7A,C). Moreover, when NGF was added back to these cultures, the neurons continued to grow for at least 2 weeks. In contrast, at 48 h without NGF,  $\Delta F/F$  increased to  $3.12 \pm 0.16$  ( $n = 162$ ) (Fig. 7B), and after 72 h without NGF these cultures had significantly fewer neurons and many of those that remained were in poor health when examined 1 week after adding back NGF (Fig. 7C). These results indicate that a 18 h transient disruption in NGF signaling causes relatively mild elevations in cytosolic ROS, elevations comparable with those achieved with antimycin-A, but importantly, not sufficient to affect neuronal growth or survival.

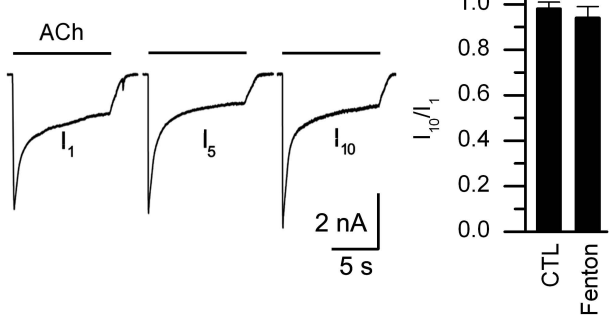
To address whether this mild increase in ROS after 18 h of NGF withdrawal induced a use-dependent rundown of ACh-evoked currents, we simultaneously measured ROS-induced fluorescence and ACh-evoked currents. The first ACh-evoked current on neurons without NGF for 18 h was not significantly different from that on neurons in sister cultures maintained continuously in NGF; however, when we delivered a series of consecutive ACh applications, the ACh-evoked currents ran down rapidly: the response to the 30th application ( $I_{30}$ ) was <20% of the first ( $I_1$ ) (Fig. 7E,G). However, for neurons in sister cultures maintained continuously in NGF, the ACh-evoked currents were stable (Fig. 7D,G). In addition, when we measured ACh-evoked currents on neurons 5 d after a transient 18 h disruption, we observed that the ROS-induced fluorescence had returned to control levels, and that the ACh-evoked currents were stable (Fig. 7G). These results indicate that a disruption in growth factor signaling can induce a long-lasting, use-dependent inactivation of ACh-evoked currents on neonatal sympathetic neurons.

Moreover, we observed no significant difference in the voltage-gated inward  $\text{Na}^+$  or outward  $\text{K}^+$  currents before and after rundown of the ACh-evoked currents (Fig. 7H). These results indicate that an 18 h disruption in NGF signaling does not cause a generalized, nonspecific change in membrane currents.

To determine that transient disruptions in NGF signaling cause rundown of the ACh-evoked currents through a mechanism involving ROS, we withdrew NGF for 18 h and simultaneously increased the antioxidant activity of the cytosol by adding ascorbate and ascorbate oxidase to the cultures. Treating these NGF-deprived neurons with ascorbate and ascorbate oxidase prevented any significant change in ROS-induced fluorescence; equally relevant, ACh-evoked currents on these 18 h NGF-deprived neurons were stable (Fig. 7F,G). These results indicate

**A** $\alpha 4\beta 2$  receptors**B** $\alpha 1\beta 1\delta \epsilon$  receptors**C**

Myocytes

**Figure 4.6**

**FIGURE 4.6.** ROS induced rundown of ACh-evoked currents is specific for nAChRs on neurons and does not inactivate muscle nAChRs. **A**  $\alpha 4\beta 2$  receptors. On the left are ACh-evoked currents from  $\alpha 4\beta 2$ -expressing oocytes recorded with an electrode containing control (top) or antimycin-A (lower). ACh (0.5  $\mu\text{M}$ ) was applied repeatedly every 1 min. The left-most traces are the ACh-evoked currents on an expanded timescale. On the right is the  $I_{20}/I_1$  ratio for  $\alpha 4\beta 2$ -expressing oocytes recorded with electrodes containing control solutions (n = 7) or electrodes containing antimycin A (n = 8). Currents were obtained after 20–30 min to allow time for antimycin-A to act. **B**  $\alpha 1\beta 1\delta\epsilon$  receptors. Left, ACh-evoked currents (10  $\mu\text{M}$  every min) from  $\alpha 1\beta 1\delta\epsilon$ -expressing oocytes recorded with an electrode containing antimycin-A. Right, the  $I_{20}/I_1$  ratio for  $\alpha 1\beta 1\delta\epsilon$ -expressing oocytes recorded with electrodes containing antimycin-A (n = 8). Currents were obtained after 20–30 min to allow time for antimycin-A.  $\alpha 1\beta 1\delta\epsilon$  receptors do not rundown in oocytes containing antimycin-A. **C** Myotubes. ACh-evoked currents from a mouse myotube in culture for 5 d and recorded with an electrode containing ROS generated from the Fenton reaction. ACh (10  $\mu\text{M}$ ) was applied for 10 s every 5 min. The figure shows the first, fifth, and 10th records of the series. On the right is the  $I_{10}/I_1$  ratio for myotubes recorded with electrodes containing control solutions (n = 5) or electrodes containing ROS from the Fenton reaction (n = 6). \*\*\*p < 0.001.

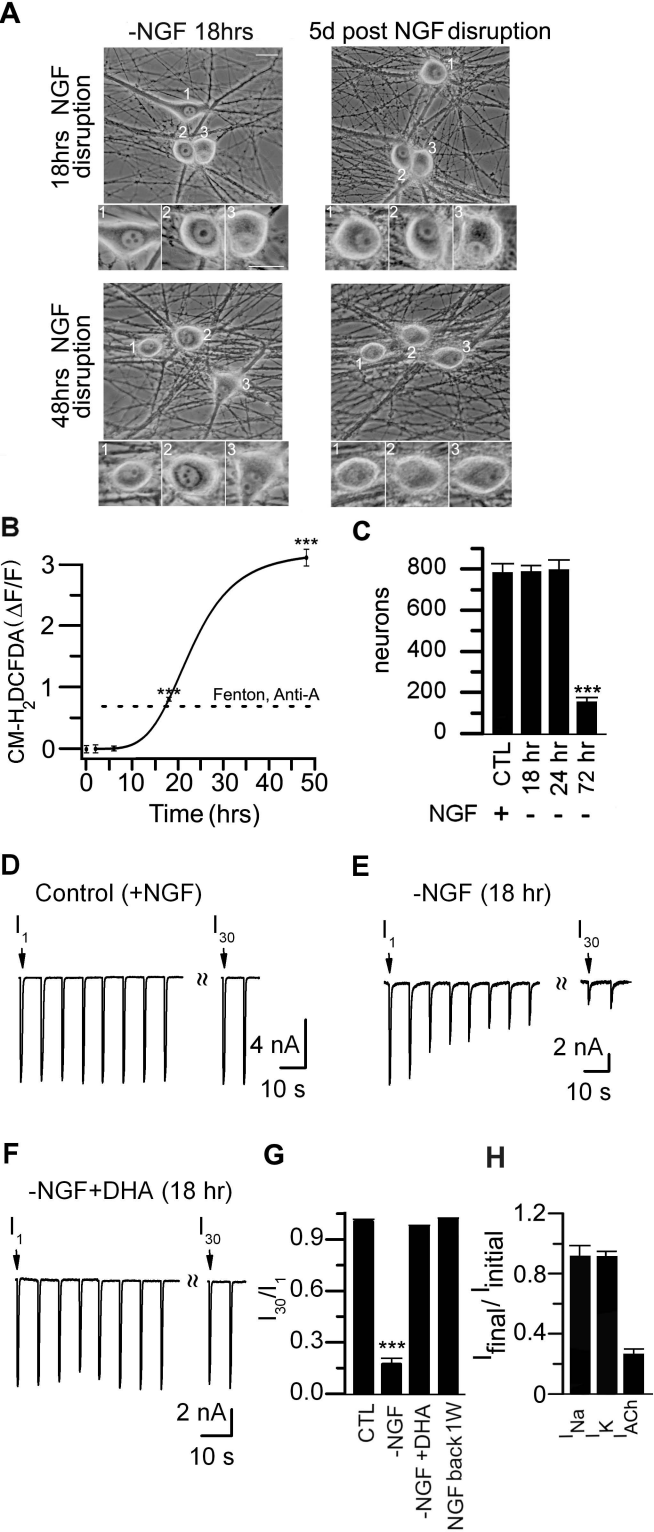


**Figure 4.7**

**FIGURE 4.7.** Transient interruption in nerve growth factor signaling increases cytosolic ROS and causes rundown of ACh evoked currents. **A** Phase micrographs of sympathetic neurons in culture for 2 weeks. NGF was removed for 18 h (top) or 48 h (bottom). The micrographs were taken at 18 h after removing NGF (left) and the same field retaken 5 d (right) after replacing NGF. The insets are magnified images of the cell bodies in each field. After 18 h without NGF followed by 5 d with NGF, the neurons have phase-bright nuclei, clearly visible nucleoli; however, after 48 h without NGF, the neurons are in poorer health. **B**  $\Delta F/F$  measurements from sympathetic neurons before and after being deprived of NGF for 2, 6, 18, and 48 h (>50 neurons were measured at each time point). Neurons were loaded with CM-H<sub>2</sub>DCFDA for 1 h and then imaged. The fluorescence remained near basal levels for the first 6 h; after 18 h of NGF removal, the increase in  $\Delta F/F$  was comparable with that induced by ROS from the Fenton reaction or antimycin-A (dotted line). The solid line is a Hill function. **C** Number of neurons per culture before (CTL) (n = 80) and 5 d after a transient removal of NGF for 18 h (n = 150), 24 h (n = 53), or 48–72 h (n = 109). A transient interruption in NGF signaling for 18 h had no significant effect on neuronal survival. **D–F**, ACh-evoked currents in response to a series of 1 s ACh (100  $\mu$ M) applications delivered at 15 s intervals from a control (+NGF) neonatal mouse SCG neuron (D) in culture for 10 d, one in a sister culture deprived of NGF for 18 h (E), and one in a sister culture deprived of NGF for 18 h but pretreated with antioxidants (DHA) for 24 h at 6 h before NGF removal (F). **G**,  $I_{30}/I_1$  ratio for neurons from control (CTL) (n = 7), 18 h after NGF removal (–NGF) (n = 14), 18 h after NGF removal with antioxidants (–NGF + DHA) (n = 6), and 1 week after a transient 18 h NGF withdrawal (n = 6). The SEs are too small to resolve. **H**, Bar graph showing the ratio of the peak  $I_{Na}$  and  $I_K$  (mean  $\pm$  SE; n = 7) before and after rundown of the ACh-evoked currents on neurons 18 h after removal of NGF. There was no significant difference in the peak  $I_{Na}$  or  $I_K$  before and after rundown of the ACh-evoked currents. \*\*\*p < 0.001.

that the transient removal of NGF causes a use-dependent rundown of the ACh-evoked currents by elevating cytosolic ROS.

### **Elevation of Mitochondrial ROS Leads to Long-Term Depression of Fast Nicotinic Synaptic Transmission in Intact Ganglia**

Our results with cultured sympathetic neurons indicate that elevations in mitochondrial ROS induce a long-lasting, use-dependent rundown of ACh-evoked currents. If extended to neurons *in vivo*, these findings predict that acute elevation in cytosolic ROS in sympathetic neurons in intact ganglia would cause a use-dependent, long-lasting inactivation of the postsynaptic nicotinic receptors and depress fast nicotinic synaptic transmission. To test this prediction, we used intracellular recordings to measure nerve-evoked fast nicotinic EPSPs on sympathetic neurons in intact ganglia from neonatal mice after inhibiting complex III in the recorded neuron with antimycin-A.

In control recordings, a maximal stimulus to the preganglionic nerve evoked large (~15 mV) suprathreshold EPSPs on sympathetic neurons. The evoked action potential obscures the peak of the EPSPs; therefore, for accurate measurements of changes in the peak amplitude of the nerve-evoked EPSPs, we partially blocked the postsynaptic nAChRs with curare (10  $\mu$ M) to make the EPSPs subthreshold. In control neurons, when stimulating the preganglionic nerve at 1 Hz for 60 s we observed no significant change in the amplitude of the nerve-evoked EPSPs (Fig. 8A). To test whether acute elevations in cytosolic ROS in sympathetic neurons affect synaptic transmission, we recorded from neurons in intact ganglia with electrodes containing antimycin-A and waited 20 min for it to diffuse into the neuron before stimulating the preganglionic nerve. In all 20 neurons recorded with electrodes containing antimycin-A, the initial EPSPs

were not significantly different from control neurons; however, when stimulating the preganglionic nerve at 1 Hz for 60 s, we observed a steady depression of nerve-evoked EPSPs which leveled off at ~50% of the initial amplitude (Fig. 8A,B). There was no change in resting potential or input resistance during this 60 s stimulation; moreover, this depression lasted for as long as we could record from the neuron (usually at least ~50 min). In contrast, we observed no depression of the nerve-evoked EPSPs on neurons recorded without antimycin-A in the electrode solution (all other components were identical) (Fig. 8A,B). These results indicate that acute elevations in mitochondrial ROS in postsynaptic sympathetic neurons can produce a long-lasting depression of the nerve-evoked EPSPs in sympathetic ganglia.

### **Transient Disruption in NGF Signaling Leads to Long-Term Depression of Fast Nicotinic Synaptic Transmission in Intact Ganglia**

We have shown above that transient withdrawal of NGF signaling elevates cytosolic ROS and causes a use-dependent rundown of the ACh-evoked currents on cultured sympathetic neurons. Therefore, we asked whether a transient disruption in NGF signaling in vivo would depress fast EPSPs in sympathetic ganglia. To address this, we injected neonatal mice with either anti-NGF antibodies or control IgG antibodies and measured the nerve-evoked fast EPSPs on sympathetic neurons in intact ganglia 48 h later. In ganglia from mice injected with control IgG antibodies, stimulating the preganglionic nerve evoked suprathreshold EPSPs that were not significantly different in amplitude from those on neurons in ganglia from control mice (Fig. 8C,D). However, in ganglia from mice injected with anti-NGF antibodies 48 h earlier, the nerve-evoked EPSPs

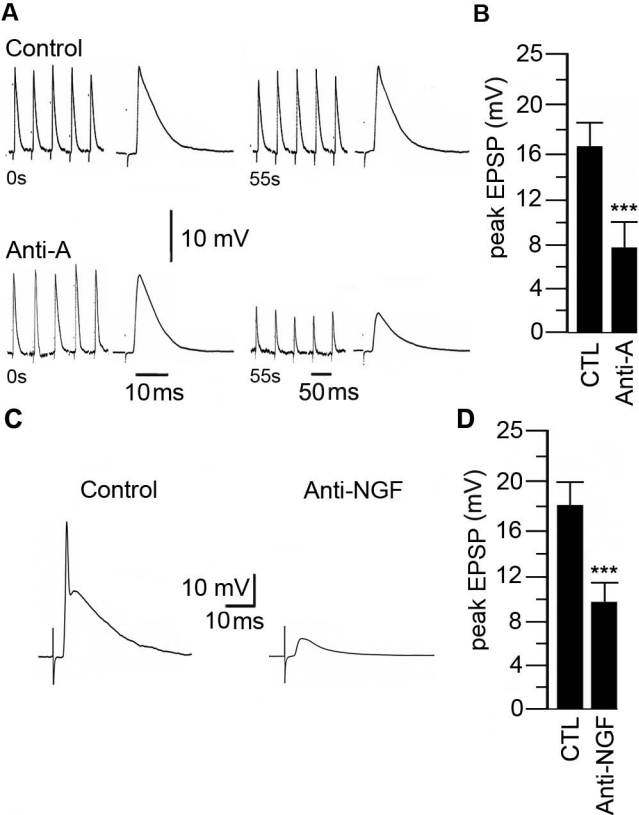


**Figure 4.8**

**FIGURE 4.8.** Elevated ROS in sympathetic neurons in intact ganglia depress fast synaptic transmission. **A**, The first and last five consecutive EPSPs produced by stimulating the preganglionic nerve at 1 Hz for 60 s and recording intracellularly from neurons with electrodes containing control solution (top) or antimycin-A (100  $\mu$ M) (bottom); the expanded trace at the end of each series represents the average EPSP. The EPSPs were made subthreshold by adding curare (10  $\mu$ M). Note: The timescale for the average EPSPs is 10 ms and 50 ms for the five consecutive EPSPs. **B**, The average peak EPSP for the last five EPSPs recorded with electrodes containing control (n = 20) or antimycin-A (n = 20). **C**, EPSPs from sympathetic neurons in ganglia from P28 mice injected with control IgG or anti-NGF antibodies (20 ng/ml; 2.5  $\mu$ l/g) for 2 d. **D**, The average peak EPSP for sympathetic neurons from control (n = 20) and anti-NGF-treated (n = 20) mice. \*\*\*p < 0.001.

were all subthreshold and their amplitudes were ~50% smaller than in control ganglia (Fig. 8C,D). We observed no significant difference in resting potential or input resistance among neurons in ganglia from mice injected with anti-NGF compared with those in control ganglia. These results suggest that transient disruption of NGF signaling depresses cholinergic–nicotinic synaptic transmission in sympathetic ganglia.

## DISCUSSION

In this study, we uncovered a new mechanism that inactivates nAChRs on neurons. We show that relatively mild shifts in the intracellular thiol/disulfide redox state toward more oxidative conditions induce a rundown of ACh-evoked currents. Once the ACh-evoked currents run down, they do not recover for at least 1 h; it is as if the receptors become trapped in a long-lasting inactivated state. This ROS-induced rundown of ACh-evoked currents is specific to neuronal nAChRs, because elevating ROS had no detectable effect on muscle nAChRs.

In previous work (De Koninck and Cooper, 1995), we measured gene expression of sympathetic neurons developing in culture. We found that these neurons express five nicotinic receptor transcripts: mRNA for  $\alpha 3$  and  $\beta 4$  are the most abundant and increase over the first week in culture; mRNA for  $\beta 2$  and  $\alpha 5$  are several fold lower and remain constant, whereas mRNA for  $\alpha 7$  is initially high but falls rapidly within 1–2 d in culture and remains low. Although there are no dramatic changes in nAChR subunit gene expression in rodent sympathetic neurons in culture, we cannot conclude definitively that the subunit composition of the receptors stays constant. Nonetheless, whatever the exact subunit

composition, nAChRs on neurons both in short-term cultures and in long-term cultures are inactivated by cytosolic ROS in a use-dependent manner.

Cytosolic ROS, by themselves, do not trap resting receptors in an inactivated state: elevated ROS must be paired with receptor activation to induce rundown of ACh-evoked currents. We are uncertain of the underlying mechanisms. Our preliminary evidence suggests that cysteine residues in the M1–M2 linker are oxidized by ROS and lock the receptor in an inactive configuration (Campanucci and Cooper, 2007); we speculate that these residues are buried or hidden when the receptor is in the resting state and only become exposed to ROS during activation as the receptor undergoes the conformational change to the open state. Importantly, this relationship between increases in cytosolic ROS and nAChR inactivation extends to fast nicotinic transmission in sympathetic ganglia; increasing ROS in sympathetic neurons depresses nerve-evoked EPSPs in intact ganglia.

Fast nicotinic EPSPs in sympathetic ganglia link the activity of various CNS nuclei to sympathetic nerve activity and are crucial for maintaining peripheral homeostasis. Therefore, our findings that elevated ROS in sympathetic neurons depress ganglionic transmission have relevance to sympathetic insufficiencies experienced during diseases associated with mitochondrial dysfunction and oxidative stress, such as Parkinson's disease and diabetes. For example, ~20–30% of patients with diabetes have cardiovascular autonomic neuropathy (Vinik et al., 2003; Savitt et al., 2006), and ~20–50% of patients with Parkinson's disease experience dysautonomia, especially orthostatic hypotension, which increases the incidence of accidental trauma (Goldstein, 2003). The cause of dysautonomia in patients with Parkinson's disease or diabetes is not known, but if mitochondrial dysfunction and/or oxidative stress

associated with these diseases occurs in sympathetic neurons, our results suggest that the elevated cytosolic ROS would disrupt ganglionic synaptic transmission, thereby producing dysautonomic symptoms.

Sympathetic neurons, in particular, are vulnerable to oxidative damage because tyrosine hydroxylase and monoamine oxidase produce  $H_2O_2$  as normal by-products of their activities (Coyle and Puttfarcken, 1993), and because catecholamines auto-oxidize to produce  $H_2O_2$  which decomposes to the highly reactive hydroxyl radical, a process accelerated by  $Fe^{2+}$  (Halliwell, 2006). Our results predict that if ROS are elevated in sympathetic neurons of patients with diseases related to mitochondrial dysfunction and/or oxidative stress, ganglionic transmission will be depressed, and these patients will experience sympathetic insufficiencies, such as poorly regulated blood pressure, cardiac arrhythmias, and perturbations in other homeostatic control processes.

The major symptoms of Parkinson's disease result from a selective loss of dopaminergic neurons in the substantia nigra pars compacta (Beal, 2003; Dauer and Przedborski, 2003; Abou-Sleiman et al., 2006). Many of these substantia nigra neurons express  $\alpha 4\beta 2$ -containing and  $\alpha 6\beta 2$ -containing nAChRs (Zoli et al., 2002; Champtiaux et al., 2003), and our results indicate that elevated ROS trap  $\alpha 4\beta 2$  nAChRs in a long-lasting inactivated state, similar to nAChRs on sympathetic neurons. We speculate that, during the early progression of Parkinson's disease, oxidative stress in dopaminergic nigral neurons induces long-lasting inactivation of these  $\alpha 4\beta 2$ -containing and  $\alpha 6\beta 2$ -containing nAChRs, and contributes, in part, to the movement disorders and cognitive deficits experienced by Parkinson's patients.

In the CNS, most nAChRs are located presynaptically where they enhance transmitter release, an important process that underlies many forms of synaptic plasticity (MacDermott et al., 1999; Dani and Bertrand, 2007). These presynaptic compartments are rich in mitochondria, and therefore presynaptic nAChRs could be subjected to elevated levels of cytosolic ROS, particularly generated by the mitochondrial electron transport chain during periods of high activity (Nicholls and Budd, 2000). Because of the difficulties in recording directly from nAChRs on nerve terminals, we know little about the exact manner that nAChR-mediated depolarization and  $Ca^{2+}$  influx, in concert with normal impulse activity, modulate presynaptic transmitter release, or whether fluctuations in cytosolic ROS occur. But if cytosolic ROS levels do increase, they would inactivate these presynaptic receptors and reduce the effects of ACh at these synapses.

We show that transient interruption of NGF signaling induces rundown of ACh-evoked currents on sympathetic neurons by increasing cytosolic ROS without affecting neuronal survival. It is unclear how much circulating NGF fluctuates in vivo, or whether and by how much circulating NGF decreases during disease. Our results suggest that a transient drop in circulating NGF during disease, or therapeutic treatment with anti-NGF antibodies, would depress synaptic transmission in sympathetic ganglia and lead to sympathetic insufficiencies and exacerbate the disease condition. This unexplored area deserves additional investigation.

In young cultured neurons, ROS out balances the antioxidant activities of ROS scavengers, shifting the thio/disulfide redox state of the cytosol toward oxidative conditions and causes the ACh-evoked currents to run down. It is known that oxidative conditions trigger redox signaling mechanisms, including

increased signaling through tyrosine kinase pathways by suppressing tyrosine phosphatase activity (Dröge, 2002). Tyrosine kinase pathways are crucial for the growth and survival of neurons (Huang and Reichardt, 2003). Therefore, we speculate that the mild shifts in the intracellular thiol/disulfide redox state toward more oxidative conditions in young neurons may help them to survive in culture, particularly during the early stages when recovering from the trauma of axotomy and enzymatic dissociation. However, ACh-evoked depolarizations, and the related increase in calcium influx, together with elevated ROS could trigger excitotoxicity and cell death. Therefore, the ROS-induced rundown of ACh-evoked currents could act as a protective mechanism to prevent overexcitation, excess calcium influx, and cell death.

Our results have uncovered a cellular mechanism that regulates the function of neuronal nAChRs; however, they also raise a number of questions. For example: How do ROS inactivate neuronal nAChRs? Do ROS act on the receptors directly, or do they act through intermediators? How do nAChRs recover from ROS-induced rundown? Are the receptors removed from the membrane and destroyed, or are receptors restored to their resting state by intracellular reducing agents. Answers to these questions must await additional work.

**CHAPTER 5:**  
**HYPERGLYCEMIA PRODUCES DYSAUTONOMIAS BY INACTIVATING**  
**NEURONAL NICOTINIC ACETYLCHOLINE RECEPTORS**

**FOREWORD**

**Background and Rationale**

In chapter 2, V. Campanucci and I show that (1) mild elevations in cytosolic ROS produce a use-dependent, long-lasting inactivation of nAChRs on sympathetic neurons; (2) Elevations in cytosolic ROS are able to depress synaptic transmission *in vivo*. In this study V. Campanucci and I (1) uncover the molecular mechanism of ROS-induced nAChR inactivation and (2) generalize our finding that ROS depresses synaptic transmission to dysautonomias that result from diabetes.

**Hypothesis**

I predict that (1) Hyperglycemia elevates ROS in sympathetic neurons and inactivates nAChRs; and that (2) ROS attacks a highly conserved ring of cysteine residues in the channel pore to inactivate nAChRs; and that (3) Diabetes-induced elevations in cytosolic ROS, attack inactivate nAChRs, depress synaptic transmission through sympathetic ganglia and produce dysautonomias.

**Experimental Outline**

I will test these hypotheses by first increasing glucose concentrations in extracellular media and measuring ACh evoked currents. If these currents are depressed then I will examine synaptic transmission on sympathetic neurons

from mouse models of type1 and type2 diabetes. To determine whether cysteine residues in the channel pore are attacked by ROS to inactivate nAChRs; I will record from cultured  $\alpha 3$ -null neurons infected with adenoviruses that express  $\alpha 3$  subunits with the cysteines mutated to alanines. If these cys-less  $\alpha 3$  nAChRs are protected from ROS, then I will infect diabetic  $\alpha 3$  KO mice with adenoviruses that express cys-less  $\alpha 3$  subunits and measure synaptic transmission. Finally I will measure two body processes that depend on functional autonomic nerves, thermogenesis and heart rate, in type 1 diabetic mice, type 2 diabetic mice and type 1 diabetic  $\alpha 3$  KO mice that express mutated  $\alpha 3^{c-a}$  nAChRs.

**ABSTRACT**

Most people with diabetes develop a wide range of abnormalities and unique syndromes that adversely affect their quality of life and life expectancy. Although it is not fully understood how these multi-system abnormalities progress, it seems likely that they involve a disruption in the complex way these systems are regulated. To learn more, we focused on the autonomic nervous system, mainly because it regulates the function of many systems affected in diabetics, particularly the heart and the circulation. Using different diabetic mouse models, we demonstrate that hyperglycemia elevates reactive oxygen species (ROS) in sympathetic neurons and causes rapid inactivation of nicotinic ACh receptors (nAChRs), receptors that mediate fast synaptic transmission in autonomic ganglia. Consequently, synaptic transmission in autonomic ganglia is depressed and mice develop dysautonomia, including poor autonomic control of heart rate. Moreover, our experiments show that ROS inactivates nAChRs by oxidizing highly conserved Cys residues located at the inner mouth of the receptor's pore, demonstrating the molecular mechanism linking hyperglycemia and dysautonomias. Our results suggest that early hyperglycemia-induced autonomic insufficiencies act together with high circulating levels of glucose to damage tissues, producing microvascular and cardiovascular complications that enhance the progression of system-wide abnormalities that occur in people with diabetes.

## INTRODUCTION

Diabetes, a disease characterized by chronic elevation of plasma glucose, results from insufficient insulin production or from insulin resistance. If left unchecked, this elevated glucose, or hyperglycemia, damages the cardiovascular system, the retina, the kidney, and the peripheral nerves (Vinik and Zeigler, 2007; Calcutt et al., 2009); as a result, many diabetics develop nephropathies (Singh et al., 2008), have visual impairments (Lorenzi and Gerhardinger, 2001), experience uncontrolled pain (Ziegler, 2008), and are predisposed to life-threatening myocardial infarctions, cardiac arrhythmias and stroke that seriously affect their quality of life and shorten their life expectancy (Vinik et al., 2003). The severity of these diabetic-related syndromes has prompted much research on factors that contribute to the progression of these systemwide abnormalities. Many organs are damaged directly by hyperglycemia. For example, studies in animals and in cell culture demonstrate that hyperglycemia induces early pathological changes to vasculature endothelial cells by elevating cytosolic reactive oxygen species (ROS), indicating that abnormal blood flow and increased vascular permeability contribute to the hyperglycemia-related damage of many tissues and organs (Brownlee, 2005; Brownlee, 2001). In addition to these local microvascular pathologies, diabetics develop macrovascular diseases that affect blood flow in arteries to the heart and brain (Calcutt et al., 2009; Aaron, 2006). Because of hyperglycemia's detrimental effects on the circulation, an emerging idea is that early disruptions in blood flow play an important role in how several diabetes-related syndromes progress (Brownlee, 2005; Orasanu and Plutzky, 2006).

Less clear is the role of the autonomic nervous system in the early progression of these diabetes-related syndromes. The autonomic nervous system innervates all internal organs, including the heart and the blood vessels, and regulates the circulation. Furthermore, the majority of people suffering from diabetes develop dysautonomias and autonomic neuropathies; among the most common and the most troubling are those that adversely affect vascular dynamics because they can cause malignant arrhythmogenesis and sudden cardiac death (Vinik and Zeigler, 2007; Vinik et al., 2003). Given this, it is reasonable to suppose that a decrease in the function of the autonomic nervous system contributes in important ways to the progression of system-wide diabetic disorders. Yet surprisingly, the functional activity of autonomic nerves during the early phase of diabetes is rarely examined in detail.

Briefly, activity in autonomic nerves is governed largely by signals originating in various CNS structures, as well as from peripheral mechano- and chemoreceptors; these signals converge directly or indirectly onto preganglionic neurons in the spinal cord and are relayed to peripheral organs through excitatory cholinergic nicotinic synapses in paravertebral and prevertebral autonomic ganglia. Clinically, diabetic autonomic neuropathies are detected after long-term hyperglycemia, and are thought to be produced by nerve injury secondary to hyperglycemia-induced damage to the circulation (Vinik et al., 2003). On the other hand, hyperglycemia elevates ROS in autonomic neurons soon after the neurons are exposed to high extracellular glucose (Tomlinson and Gardiner, 2008); moreover, we demonstrated recently that mild elevation in cytosolic ROS inactivates postsynaptic nAChRs on sympathetic neurons and depresses synaptic transmission (Campanucci et al., 2008). These observations, therefore, raise the question: does hyperglycemia inactivate nAChRs on

autonomic neurons and cause long-term depression of synaptic transmission in autonomic ganglia? If so, does this hyperglycemia-induced depression of synaptic transmission produce autonomic hypofunction or cardiovascular dysautonomias that could accelerate the progression of diabetic complications?

## **METHODS AND MATERIALS**

### **Animals**

In most experiments we used C57BL/6/J - CD+ mixed-background colony. For experiments on mice with a disruption in leptin signaling we used heterozygote and homozygote Ob (B6.V-Lepob/J) and Db (BKS.Cg-*Dock7m* +/+ *Leprdb*/J) mice purchased from Jackson Laboratory (Bar Harbor, ME). For gene transfer experiments, we used outbred  $\alpha 3$  KO mice produced by mating C57BL/6/J  $\alpha 3$ +/- males (gift from Dr. A. Beaudet, Baylor College of Medicine) to CD+ females (Charles River, St. Constant, Quebec) and then mated the F1 heterozygotes to produce  $\alpha 3$  KO mice on a mixed C57BL/6/J - CD+ background. All genotyping of pups was done by PCR (Xu et al., 1999). Most experiments were done with superior cervical ganglia (SCG) from neonatal pups (P0–P14) and young adults (P21–P60) mice, except for those with Ob and Db mice who were 4-6 month old. To model type I diabetes we starved WT pups (P4-7) for ~2hrs, injected them with streptozotocin (STZ, 40mg/Kg) and put them back with their mother. The next day ~80% of pups had blood glucose > 22mM which remained elevated for at least 2 months, indicating that most, if not all,  $\beta$ -cells had been destroyed. For some experiments we anaesthetized young mice (P21-P39) mice with ketamine, and implanted a time release insulin pellet under the skin (2U/24 hour/implant, LinShin, Toronto), and injected them the next day with STZ (40-60 mg/Kg).

### **Primary Cultures**

Superior cervical ganglion (SCG) neurons were cultured from neonatal postnatal day 1 (P1) to P3 mice (C57 black or CD1 strains; Charles River, St. Constant, Quebec, Canada) as previously described (MacFarlane and Cooper, 1992). Briefly, ganglia were removed under sterile conditions and enzymatically dissociated at 37°C in HBSS containing trypsin (180–200 U/ml; Worthington, Freehold, NJ) and buffered with HEPES (adjusted to pH 7.4 with NaOH). The resulting cell suspension was washed twice in serum-containing medium to inactivate the trypsin and plated on laminin-coated coverslips attached to modified 35 mm tissue culture dishes. The neurons were grown in media consisting of L-15 supplemented with vitamins, cofactors, penicillin–streptomycin, 5% rat serum, 5mM glucose, and NGF (25 ng/ml). Cultures were maintained at 37°C in a humidified atmosphere of 95% air–5% CO<sub>2</sub> and fed every 3 d with growth media. To eliminate non-neuronal cells, cultures were treated with cytosine arabinoside (10 µM; Sigma, St. Louis, MO) from day 2 to 4. For high glucose experiments, week-old cultures were fed with growth media containing 25mM glucose for an additional 1 week before measuring ACh-evoked currents. To rule out a direct effect of STZ on ACh-evoked currents, in some experiments, neurons were cultured in 1mM STZ for 1 week before recording; we also applied STZ (1mM) acutely to neurons while recording ACh-evoked currents. In other controls we recorded ACh-evoked currents from neurons cultured in 3ng/mL insulin added for 1 week together with 25 mM glucose.

### **Whole Cell Recording**

ACh-evoked currents were measured with whole-cell patch-clamp techniques. Membrane currents were recorded with a VE-2 amplifier (Alembic Instruments, Montreal, Quebec, Canada) at room temperature, sampled at 500 Hz, and stored on a Pentium II-based personal computer. Recording electrodes had resistances of 2–5 M $\Omega$ , and series resistance was compensated from 70 to >98%. Patchkit software (Alembic) was used for stimulation and data acquisition and currents were filtered and analyzed off-line with Igor (WaveMetrics, Lake Oswego, OR) software. Recording electrodes were filled with the following solution (in mM): 65 KF, 55 KAc, 5 NaCl, 0.2 CaCl<sub>2</sub>, 1 MgCl<sub>2</sub>, 10 EGTA, 2 MgATP, and 10 HEPES, and pH was adjusted to 7.2 with KOH. In some experiments, the antioxidant  $\alpha$ -lipoic acid (100  $\mu$ M) was dissolved in intracellular solution, treated with 1000 U/ml catalase for 1 h at 37°C, and used as the recording solution during whole-cell recording. Cultured neurons were perfused continuously at 1 ml/min with control perfusion solution consisting of the following (in mM): 140 NaCl, 5.4 KCl, 0.33 NaH<sub>2</sub>PO<sub>4</sub>, 0.44 KH<sub>2</sub>PO<sub>4</sub>, 2.8 CaCl<sub>2</sub>, 0.18 MgCl<sub>2</sub>, 10 HEPES, 5.6 glucose, 2 glutamine, and 5  $\mu$ g/ml phenol red; pH was adjusted to 7.4 with NaOH. ACh (100  $\mu$ M) was dissolved in the perfusion solution and applied by pressure ejection from pipettes with tip diameters of 2–5  $\mu$ m positioned 20–30  $\mu$ m from the cell body. In some experiments, atropine (1  $\mu$ M; Sigma) was added to the perfusion solution. As a measure of rundown of the ACh-evoked currents we plotted the ratio of the peak current ( $I$ ) in response to the 30th application ( $I/30$ ) in a series to the peak current in response to the first application ( $I/1$ ) in the series.

### **Intracellular ROS Measurements**

We used the redox-sensitive dye CM-H2DCFDA to monitor changes in cytosolic ROS (12). Briefly, cultures were incubated for 40-60 min at 37°C with medium containing CMH2DCFDA (10  $\mu$ M) and subsequently washed five times with control perfusion solution (see above). The cultures were then placed on the stage of an inverted microscope (Axiovert 200 M; Zeiss, Oberkochen, Germany) and viewed through a 40x (1.3 numerical aperture) Plan Neofluor oil-immersion objective (Zeiss) at room temperature. To obtain fluorescent images, we excited the cultures with 450–480 nm wavelength for 200 ms from a 150 W xenon arc lamp (LAMBDA DG-4; Sutter Instruments, Novato, CA) and collected 510–550 nm wavelength emissions (filter set 31001; Chroma Technology, Brattleboro, VT) with a cooled CCD camera (CoolSnap HQ; PhotoMetrics, Tucson, AZ) controlled by MetaMorph software (Universal Imaging, West Chester, PA). For each image, we defined regions of interest (neuronal cell body, excluding the nucleus) on a differential interference contrast image and transferred these regions to the fluorescent images of the same field. Images were digitized in 8-bits and for each neuron, mean fluorescent intensity (minus background) is expressed in 256 arbitrary units of grey.

### **Extracellular and Intracellular Recording**

SCGs were dissected rapidly from mice, pinned down with minutia pins in a recording chamber (1.5 ml volume) mounted on a fixed stage, and viewed with a dissecting microscope (SMZ-10; Nikon, Tokyo, Japan); the tissue was perfused continuously at 3–4 ml/min with oxygenated Ringer's solution at 36–37°C. To stimulate the preganglionic nerve, the cervical sympathetic trunk was connected to a stimulator (4710 ORTEC dual channel; EG&G, Gaithersburg, MD) with a suction electrode and stimulated with brief (0.1–0.3 ms) voltage pulses. For

extracellular compound action potentials, the postganglionic trunk was connected to an AC differential amplifier (DP-301; Warner Instruments, Hamden, CT) with a suction electrode; the postganglionic compound action potentials were amplified, filtered at 100 Hz (low-pass cutoff) and 1 kHz (high-pass cutoff), digitized at 10 kHz, and stored on a Pentium II-based computer. To record intracellularly from individual SCG neurons, we used 50–70 M $\Omega$  glass microelectrodes (G150F-4; Warner Instruments) made with a DMZ universal puller (Zeitz Instruments, Munich, Germany) as described previously. Stable intracellular recordings were achieved with a high inertial precision microdrive (Inchworm 8200; EXFO, Vanier, Quebec, Canada) attached to a micromanipulator (SM11; Narshige, Tokyo, Japan) that drove the electrode through the ganglion. The recording electrode was filled with 1 M KAc and connected by a thin silver chlorided wire to the head stage of an Axoclamp 2A amplifier (Molecular Devices, Sunnyvale, CA) used in current-clamp mode; depolarizing or hyperpolarizing constant current pulses were applied through the recording electrode. Membrane potentials were sampled, displayed, and stored on a Pentium II-based personal computer. Stimulation and acquisition was done with Patchkit software (Alembic), and the data were analyzed off-line with Igor. Only neurons with membrane potentials greater than  $-40$  mV were included in this study. To quantify the depression of synaptic transmission in mice with hyperglycemia we gave a series of stimuli to the preganglionic nerve at 1Hz and collected  $\sim 40$  EPSPs per neuron. Then we integrated and averaged these EPSPs to determine the average EPSP area for a given neuron.

### **Heart Rate and Temperature Measurements**

In most experiments, we used a MouseOX (STARR Life Science Corp, Oakmont, PA) heart monitor system to measure heart rate. Briefly, we restrained mice in a heated tube, clamped an LED pulse oximeter on the tail vein, and used MouseOx software to convert infrared absorbance measurements into heart rate. In some experiments, we measured heart rates by placing mice inside a modified cylindrical plastic tube that contained a 12 electrode array coated with Ten20 conductive jelly (D.O. Weaver and Co, Aurora, USA) and acquired electrocardiograms. These 3-lead ECG signals were amplified by a DAM 50 differential amplifier (WPI, Sarasota, Florida), digitized by a PCIe-6259 A/D card (National instruments), and acquired by NClamp software running in IGOR (Wavemetrics, Inc., Lake Oswego, OR). To measure the ability of mice to maintain core temperature we placed mice in a cold room at 4°C and measured their body temperature using a small flexible rectal thermometer. Temperature-loss experiments were stopped at 3.5 hours.

### **Adenoviruses**

Full-length  $\alpha 3$  neuronal nAChR subunit cDNA was ligated into pAdTrack-cytomegalovirus(Ad $\alpha 3$ /CMV) or pAdTrack-synapsin 1 (Ad $\alpha 3$ /Syn), and replication-deficient viral vectors were made according to He et al. (1998). All viruses were titered in duplicate with the cytopathic effect method (. Neonatal animals (P0–P21) and young adult (P28–P42)  $\alpha 3$  KO animals were infected with Ad $\alpha 3$ /Syn or Ad $\alpha 3$ C-A/Syn adenovirus by injecting the vectors intraperitoneal (50–100  $\mu$ l at 10<sup>7</sup> pfu dissolved in L15) for pups younger than P10; for older mice, we injected virus i.v. through the tail vein (Krishnaswamy and Cooper, 2009). For Ad $\alpha 3$ C-A/Syn, we mutated  $\alpha 3$  at position 239 using Quick-Change

Site-Directed Mutagenesis kit (Stratagene, La Jolla, CA) and verified the change by sequencing before building the viral construct.

### **Statistics**

To determine the statistical significance for differences in the mean fluorescent intensities, heart rates and core temperature measurements we used the Student's T-test; for comparisons of the  $I_{30}/I_1$  ratios or EPSP areas we used the non-parametric Mann-Whitney test. All procedures for animal handling were performed according to the guidelines of the Canadian Council on Animal Care.

## **RESULTS**

### **Hyperglycemia Inactivates Nicotinic Acetylcholine Receptors on Autonomic**

#### **Neurons**

To test whether hyperglycemia inactivates nAChRs on autonomic neurons, we grew neonatal mouse sympathetic neurons in culture initially for 1 week in media containing normal 5 mM glucose, and then we elevated glucose to 25 mM for 1 week to mimic conditions in diabetics and investigated the function of nAChRs electrophysiologically with whole-cell voltage clamp. For neurons maintained in 5 mM glucose throughout (controls), repeatedly applying ACh (100  $\mu$ M for 1 sec) at 15 sec intervals for 5-10 mins evoked large inward currents of constant amplitude (Fig. 1A); the peak current amplitude of the 30<sup>th</sup> application was close to that of the first ( $I_{30}/I_1$ )(Fig. 1B). In contrast, for neurons exposed to 25 mM glucose during the 2<sup>nd</sup> wk, repeatedly applying ACh at 15 sec intervals caused a use-dependent run-down of the ACh-evoked currents (Fig. 1A); the peak current amplitude of the 30<sup>th</sup> application was less than 30% of the first (Fig. 1B) and did not recover for at least 1 hr.

This use-dependent run-down was similar to what we observed when intracellular ROS becomes elevated (Campanucci et al., 2008). Therefore, we investigated whether hyperglycemia elevates ROS in sympathetic neurons. To measure changes in intracellular ROS we used the ROS indicator dye CM-H2DCFDA. The average DCFDA fluorescence was ~2-fold greater in neurons maintained in 25 mM glucose ( $2378 \text{ a.u} \pm 300$ ;  $n=50$ ) vs those in 5 mM ( $1288 \text{ a.u} \pm 123$ ;  $n=50$ ), indicating that hyperglycemia caused a mild elevation in ROS in these neurons (Fig. 1C). To determine whether this elevation in hyperglycemia-induced ROS causes nAChRs to inactivate, we treated neurons with the antioxidant  $\alpha$ -lipoic acid (100  $\mu\text{M}$ ) and catalase (1000 units/ml) when we elevated glucose to 25 mM, or simply added  $\alpha$ -lipoic acid and catalase to our recording electrode; in either case,  $\alpha$ -lipoic acid prevented run-down of the ACh-evoked currents (Fig. 1A). These results indicate that hyperglycemia acts through ROS to induce rundown of the ACh evoked currents.

### **Hyperglycemia Depresses Synaptic Transmission in Sympathetic Ganglia**

The results from cultured sympathetic neurons indicate that elevated extracellular glucose causes nAChRs to undergo long-lasting inactivation. If hyperglycemia has similar effects in vivo, we predict that hyperglycemia will depress transmission in autonomic ganglia. To test this, we made neonatal mice (ages 10-14 days postnatal) diabetic by injecting them with streptozotocin (STZ; 40-60 mg/kg i.p.), a drug that destroys insulin-producing pancreatic beta cells (Junod et al., 1969; Lenzen, 2008). Two to three days after STZ injection, blood glucose concentrations increased from 5-7 mM to 22-30 mM in 26 of 30 mice and remained above 25 mM for at least an additional 2 months.

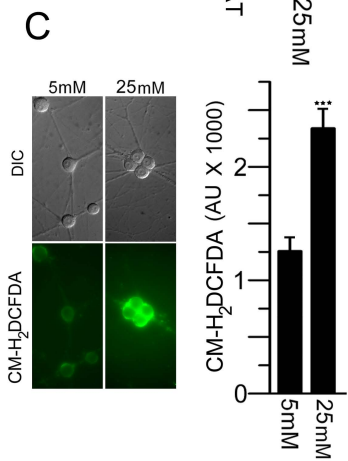
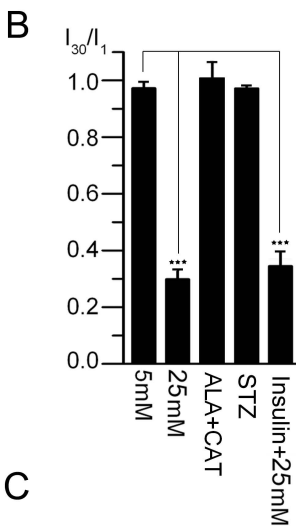
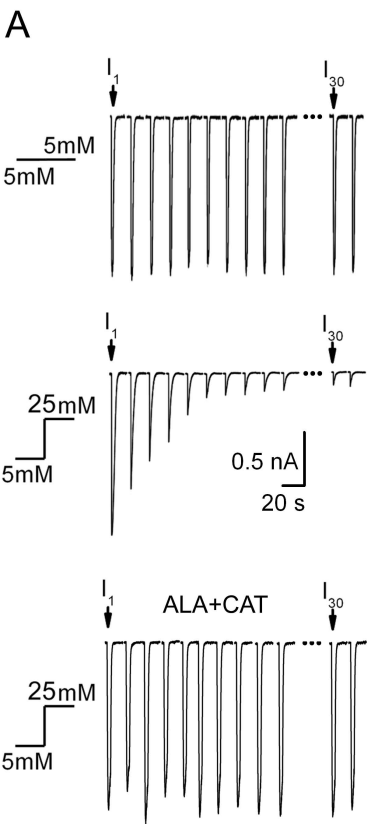


**Figure 5.1**

**FIGURE 5.1.** Increasing glucose to 25mM elevates ROS in sympathetic neurons and produces a usedependent rundown of ACh-evoked currents. **A.** Currents evoked by a series of 1 s ACh (100  $\mu$ M) applications delivered at 15 s intervals on neonatal mouse SCG neurons cultured in 5mM glucose for the 1st week, and then 1 week in 5 mM glucose (top), 1 week in 25mM glucose (middle), or 1 week in 25mM glucose and perfused intracellularly with the antioxidants  $\alpha$ -lipoic acid and catalase (bottom). The ACh-evoked currents on neurons exposed to 25mM glucose run down rapidly, and never recovered, even after washing with ACh-free solution for 30 min, whereas those exposed to 25mM glucose and perfused intracellularly with antioxidants  $\alpha$ -lipoic acid and catalase are stable. Every 4th trace is shown for clarity. **B.** Ratio of the 30th ACh-evoked current to the first in the series ( $I_{30}/I_1$ ) for neurons cultured in 5mM glucose for the 1st week, and then 1 week in 5 mM glucose ( $n = 7$ ), 1 week in 25mM glucose ( $n = 14$ ), 1 week in 25mM glucose and perfused intracellularly with the antioxidants  $\alpha$ -lipoic acid and catalase ( $n = 21$ ), 1 week in 5 mM glucose together with STZ (1 mM) ( $n = 15$ ), and 1 week in 25 mM glucose together with insulin (3U/ml) ( $n = 8$ ). Each bar is the mean  $I_{30}/I_1 \pm$  s.e.m; \*\*\* refers to  $p < 0.001$ . **C.** Phase contrast and fluorescent images of neurons cultured in 5mM glucose for 2 weeks, or in 5mM glucose for a week followed by 25mM glucose for a week, and loaded with CM-H2DCFDA for 1 h. The graph show the average increase in ROS-induced fluorescence in arbitrary units for neurons cultured in 5mM glucose for 2 weeks ( $n=30$ ) or in 5mM glucose for a week followed by 25mM glucose for a week ( $n = 30$ ). Each bar is the mean  $\pm$  s.e.m; \*\*\* refers to  $p < 0.001$ .

To measure synaptic transmission in intact ganglia, we stimulated the preganglionic nerve and recorded the compound action potential (CAP) from the postganglionic sympathetic nerve trunk. As early as 1 week after making mice hyperglycemic (blood glucose greater than 22 mM), the CAP was reduced by 50-60% compared to controls, and remained significantly reduced for at least 4-6 weeks (Fig. 2A), indicating that elevated blood glucose depresses synaptic transmission. To rule out some unanticipated action of STZ on synaptic transmission, we exogenously supplied insulin through a slow-release pellet (2U/24hr/pellet) to mice at the time of STZ treatment; chronic insulin treatment maintained blood glucose below 7 mM in STZ-treated mice (n=6), and prevented the decrease in the CAP (Fig. 2C).

The reduced CAP in hyperglycemic mice suggests that elevated blood glucose depresses synapses on postganglionic sympathetic neurons. To test this directly, we recorded from individual sympathetic neurons in intact ganglia with intracellular electrodes while stimulating the preganglionic nerve. A maximal stimulus to the preganglionic nerve evoked large suprathreshold excitatory postsynaptic potentials (EPSPs) from sympathetic neurons in intact ganglia from control mice (Fig. 2B). In contrast, the nerve evoked EPSPs were dramatically reduced in amplitude on sympathetic neurons in ganglia from mice 1 week after becoming hyperglycemic (Fig.2B,D), and over 60% of neurons had subthreshold EPSPs. The EPSPs became depressed within 2-3 days of hyperglycemia and remained significantly depressed for at least 4-6 weeks (Fig. 2B,D). On the other hand, in ganglia from mice treated simultaneously with STZ and a slow-release insulin pellet, and whose blood glucose was < 7 mM, the nerve-evoked EPSPs were not significantly different from those in ganglia of untreated, aged-matched control mice (Fig. 2C,D). These results, taken together with those from

sympathetic neurons in culture, indicate that hyperglycemia elevates ROS in sympathetic neurons which promote a use-dependent inactivation of postsynaptic nAChRs and causes a long-lasting depression of synaptic transmission in sympathetic ganglia.

In control ganglia, when stimulating the preganglionic nerve with brief trains, each preganglionic AP evoked a suprathreshold EPSP on the postsynaptic sympathetic neuron and there was 1-1 firing between the preganglionic input and postganglionic neuron. On the other hand, because hyperglycemia depresses synaptic transmission, the normal input-output relationship between pre- and postganglionic firing became disrupted; when we stimulated the preganglionic nerve in ganglia from hyperglycemic animals, either the nerve-evoked EPSPs were subthreshold (60% of sympathetic neurons) and these EPSPs remained subthreshold during the burst, or the EPSPs were suprathreshold and in 20% of these neurons the EPSP rapidly became subthreshold within 6-10 stimuli and remained subthreshold for the duration of the burst. These results indicate that hyperglycemia reduces the firing activity of postganglionic sympathetic nerves.

### **Sympathetic Hypofunction in Hyperglycemic Mice**

We expected that the reduced firing activity of postganglionic sympathetic nerves in hyperglycemic mice would result in sympathetic hypo-function or dysautonomias. To test this, we evaluated sympathetic function by non-invasively measuring heart rate and thermoregulation, two physiological processes that depend on intact sympathetic function (Axelsson, 1971; Bachman et al., 2002). For effects of sympathetic nerve activity on heart rate (sympathetic drive), first we treated mice with atropine (1 mg/Kg i.p.) to block muscarinic receptors, then we



**FIGURE 5.2.** Hyperglycemia depresses fast synaptic transmission in sympathetic ganglia. **A.** Compound action potentials (CAPs) recorded from a sympathetic ganglion in a control P21 mouse (serum glucose ~ 5 mM) (left) and P21 mouse made hyperglycemic at P7 (serum glucose ~ 25mM)(right). Hyperglycemia reduced the CAP by approximately 65-70%. **B.** Nerve-evoked excitatory postsynaptic potentials (EPSPs) recorded intracellularly from sympathetic neurons from control mice at 1 week (top), 2 weeks (middle) and 1 month (bottom) after injection with control sodium citrate buffer at P2-P4 (left column, serum glucose 5-7 mM) or from mice 1 wk, 2 wk, and 4 wk after becoming hyperglycemic at P3-P4 (right column, serum glucose 25-30 mM). Hyperglycemia depresses fast synaptic transmission. **C.** CAPs and EPSPs recorded from month-old mice injected with STZ at P7 and simultaneously implanted with a slow-release insulin pellet (serum glucose 5-7mM). Exogenous insulin overcomes the effects STZ, maintaining blood glucose at control levels and preventing long-term depression of synaptic transmission. **D.** Average integrated EPSP sizes recorded from sympathetic neurons in mice 1 week (1w;  $n=35$ ), 2 weeks (2w;  $n=27$ ), z1 month (1mo;  $n=21$ ) after becoming hyperglycemic with STZ, or 1 month after simultaneously injecting mice with STZ and implanting them with a slow-release insulin pellet ( $n=10$ ). All values are the means  $\pm$  s.e.m expressed as a percent of control integrated EPSP ; \*\*\* represents  $p<0.001$ .

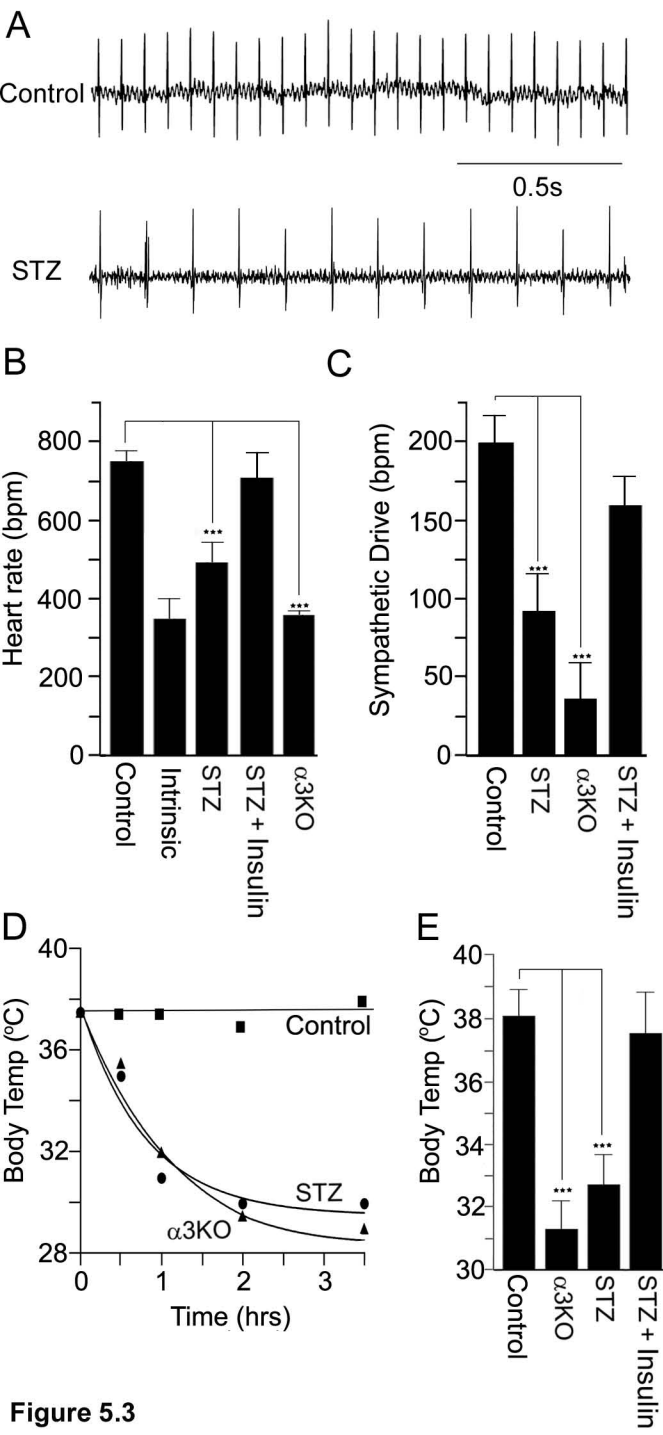


**FIGURE 5.3.** Streptozotocin-induced hyperglycemia reduces sympathetic drive to the heart and disrupts thermogenesis. **A.** Non-invasive electrocardiogram recordings of heart rate from P28 control mice (Control) and P28 mice made hyperglycemic (serum glucose 26-29 mM) at P9. Resting heart rate in mice with hyperglycemia is approximately 50% of control. **B.** Resting heart rates (beats per minute) in P21 control mice (Control;  $n=12$ ), intrinsic heart rate in P21 control mice treated with atropine and propranolol to block muscarinic and  $\beta$ -adrenergic receptors (Intrinsic;  $n=12$ ), P21 mice made hyperglycemic with STZ (STZ;  $n=18$ ) at P7; P21 mice treated simultaneously with STZ and insulin (STZ+Insulin;  $n=6$ ) at P7; P21  $\alpha 3$  KO mice ( $\alpha 3$  KO;  $n=10$ ). Resting heart rate in hyperglycemic mice is depressed and is comparable to heart rates in  $\alpha 3$  KO mice who have a non-functional autonomic nervous. Each bar is the mean bpm  $\pm$  s.e.m. \*\*\* represents  $p<0.001$ . **C.** Sympathetic drive to the heart in P21 control mice (Control;  $n=12$ ), P21 mice made hyperglycemic with STZ at P10 (STZ;  $n=15$ ); P21 mice treated simultaneously with STZ and insulin (STZ+Insulin;  $n=5$ ), and P21  $\alpha 3$  KO mice ( $\alpha 3$  KO;  $n=10$ ). Sympathetic drive is the difference between heart rates measured with atropine alone (1mg/Kg) and atropine together with propranolol (1mg/Kg). Each bar is the mean bpm  $\pm$  s.e.m. . \*\*\* represents  $p<0.001$ . **D.** Core body temperature measured for up to 3.5 hours at 40C from a P35 control mouse, a P35 mouse made hyperglycemic (serum glucose 28-29 mM) with STZ at P10, and a P35  $\alpha 3$  KO mouse. **E.** Core body temperature from control mice (Control;  $n=6$ ),  $\alpha 3$  KO mice ( $\alpha 3$  KO;  $n=6$ ), mice made hyperglycemic (serum glucose 27-31 mM) with STZ at P7 (STZ;  $n=6$ ); and mice treated simultaneously with STZ and insulin at P7 (STZ+Insulin;  $n=3$ ). Hyperglycemia depresses the sympathetic drive to brown fat and disrupts thermogenesis. Each bar is the mean  $\pm$  s.e.m. \*\*\* represents  $p<0.001$ .

measured the heart rate before and after treating mice with propranolol (1 mg/Kg i.p.), a drug that blocks the heart's  $\beta$ -adrenergic receptors. The resting, innervated heart rate in control young (4-6 wk-old) mice is approximately  $750 \pm 27$  beats per minute (bpm) (n=35) (Fig. 3A,B), whereas the intrinsic, noninnervated heart rate, determined by blocking both muscarinic and adrenergic receptors to the heart, is approximately  $350 \pm 43$  bpm (n=12) (Fig. 3B). In mice made hyperglycemic with STZ (blood glucose  $>22$  mM) for 2-3 weeks, the sympathetic drive to the heart was reduced to  $39 \pm 11$  % (n=18) of that in aged match control mice (Fig. 3A-C). Supplying insulin exogenously to mice at the time of STZ treatment prevented this decrease in sympathetic drive to the heart (Fig. 3B,C).

As a second measure of sympathetic function, we examined thermoregulation during cold exposure (Bachman et al., 2003). Sympathetic nerves prevent heat loss during cold exposure by constricting blood vessels to the skin, and by generating heat from brown adipose tissue (Cannon and Nedergaard, 2004). When control mice were placed at  $4^{\circ}\text{C}$ , their core body temperature fell by  $0.5\text{-}1^{\circ}\text{C}$  during the first 30 min and remained constant for at least 2-3 hr. In contrast, when hyperglycemic mice (blood glucose  $>22$  mM for at least 2 wk) were placed at  $4^{\circ}\text{C}$ , their core temperature dropped by  $5\text{-}8^{\circ}\text{C}$  within 2 hr, and the mice became lethargic (Fig. 3D,E). On the other hand, when the mice were treated simultaneously with STZ and insulin for 2 weeks and then placed at  $4^{\circ}\text{C}$ , we observed no significant change in core temperature from that of control mice

(Fig. 3E). Both the decrease in heart-rate and the lack of thermoregulation in hyperglycemic mice suggest that sympathetic nerve activity is low, results consistent with the depression in synaptic transmission in sympathetic ganglia.

### **Depressed Synaptic Transmission in Leptin (ob/ob) and Leptin Receptor(db/db) Mutant Mice**

Hyperglycemia is often a feature of metabolic syndromes such as obesity, and most people who are obese are also diabetic. Therefore, we extended our study to investigate synaptic transmission in sympathetic ganglia of mice that become obese because of a disruption in leptin signaling. Briefly, leptin, a multifunctional protein secreted primarily by adipocytes, has important effects on energy balance and glucose homeostasis (Spiegelman and Flier, 1996; Rosen and Spiegelman, 2006). Mice with mutations that disrupt the leptin gene (*ob/ob*) or the leptin receptors (*db/db*) become obese as well as insulin-resistant and hyperglycemic (Coleman, 1978, Zhang et al., 1994; Chen et al., 1996), making these mice a good model for type 2 diabetes.

Using adults (16-24 wk-old) *ob/ob* and *db/db* mice, we found that blood glucose ranged from 15 to >30 mM (n=12), even though insulin levels are elevated more than 10-fold (Coleman, 1978). Stimulating the preganglionic nerve to sympathetic ganglia from hyperglycemic *ob/ob* and *db/db* mice (blood glucose > 25 mM) demonstrated that both the compound action potentials and the nerve-evoked EPSPs were significantly depressed in sympathetic ganglia. Upon preganglionic nerve stimulation, the nerve-evoked EPSPs on over 60% of sympathetic neurons were subthreshold (Fig. 4A,B), and for the remainder, half the EPSPs became subthreshold within 6-12 stimuli when the preganglionic nerve fired at 10 Hz. These results, together with our results from STZ-treated mice, indicate that hyperglycemia induces a depression in synaptic transmission in sympathetic ganglia, regardless of whether the hyperglycemia results from

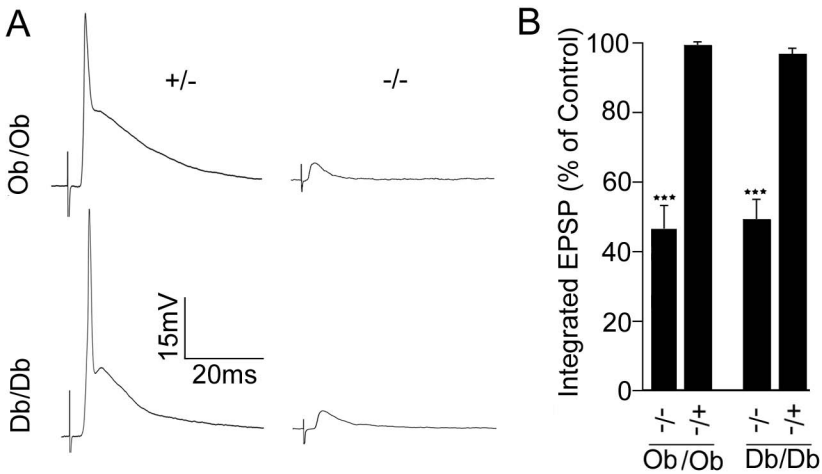


**Figure 5.4**

**FIGURE 5.4.** Hyperglycemia produced by mutations in either the leptin receptor or leptin ligand depresses synaptic transmission on autonomic neurons. **A.** Nerve-evoked excitatory postsynaptic potentials (EPSPs) recorded intracellularly from sympathetic neurons in a 4 month-old ob +/- (top) and db +/- (bottom) (left column) and ob -/- and db -/- mice (right column). **B.** Integrated EPSP sizes recorded from sympathetic neurons in 4 month-old ob -/- ( $n=25$ ), ob +/- ( $n=10$ ), db -/- ( $n=27$ ) and db +/- ( $n=10$ ) mice. Synaptic transmission in sympathetic ganglia is depressed in mice with a disruption in leptin signaling. Each bar is the mean  $\pm$  s.e.m. \*\*\* represents  $p<0.001$ .

insufficient insulin, as in type 1 diabetes, or insulin resistance, as in type 2 diabetes.

### **Hyperglycemia –Induced ROS Inactivates nAChRs Through Cys Residues at the Inner Mouth of the Channel Pore**

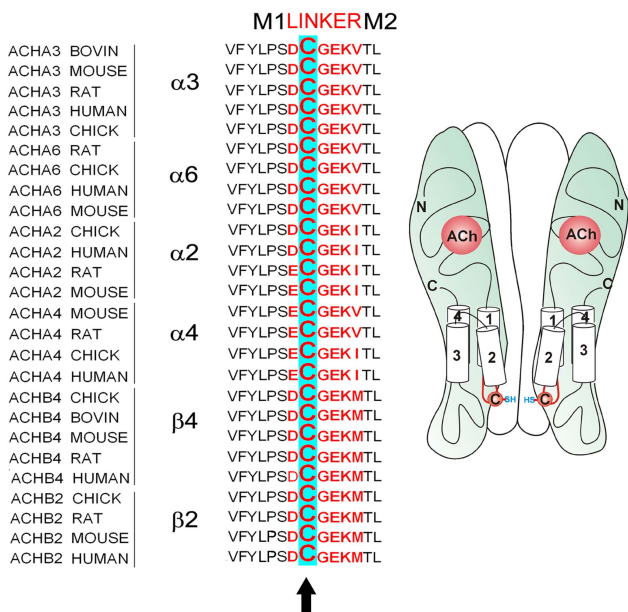
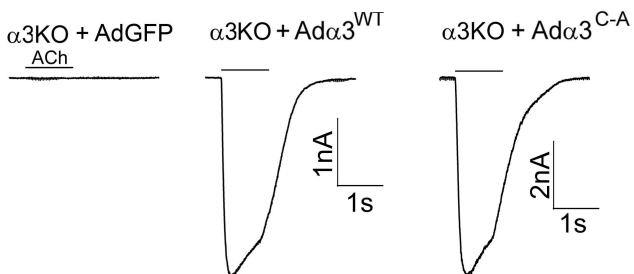
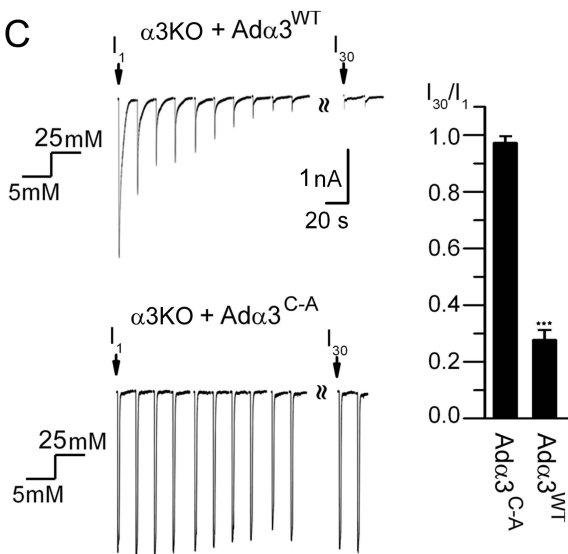
How does a mild increase in intracellular ROS cause a long-lasting, use-dependent inactivation of nAChRs on sympathetic neurons? Structurally, nAChRs subunits have 4 hydrophobic, membrane spanning domains (Dane and Bertrand, 2007); in the short intracellular linker between transmembrane domain 1 and 2 most neuronal, but not muscle, nAChRs subunits have a highly conserved Cys residue located near the inner mouth of the receptor channel (Fig. 5A), including  $\alpha 3$  and  $\beta 4$ , the main nAChRs subunits expressed by sympathetic neurons (De Koninck and Cooper, 1995; Rassadi et al., 2005; Krishnaswamy and Cooper, 2009). We postulated that ROS oxidizes these Cys residues, trapping the receptor in a long-lasting, non-conducting state. To test this, we mutated the Cys at position 239 in the  $\alpha 3$  subunit to an Ala ( $\alpha 3C239A$ ) and expressed it in cultured sympathetic neurons from  $\alpha 3$ -null mice. Sympathetic neurons null for  $\alpha 3$  ( $\alpha 3$  KO) do not have ACh-evoked currents (Fig. 5B) (Rassadi et al., 2005); however, expressing either the WT or  $\alpha 3C239A$  cDNA with adenoviral vectors rescues the ACh-evoked inward currents (Fig. 5B) (Rassadi et al., 2005), indicating that these  $\alpha 3$  subunits can co-assemble with endogenous  $\beta$  (and possibly other) subunits to form functional nAChRs. Equally important, they show that the C239A mutation in  $\alpha 3$  does not interfere with normal receptor function.

When  $\alpha 3$  KO neurons were infected with vectors expressing the WT  $\alpha 3$  subunit and exposed to 25 mM glucose, the ACh-evoked currents ran down with

repeated ACh application (Fig. 5C), similar to those on WT neurons. Interestingly, however, when  $\alpha 3$  KO neurons were infected with vectors expressing the  $\alpha 3$ C239A and exposed to 25 mM glucose, the ACh-evoked currents were stable (Fig. 5C). These results indicate that the hyperglycemia-induced ROS targets Cys 239 to produce long-lasting inactivation of the receptor.

Our results from cultured neurons, described above, imply that synapses in sympathetic ganglia of mice expressing  $\alpha 3$ C239A subunits would be resistant to hyperglycemia-induced depression. To test this, we infected neonatal (P10-P14)  $\alpha 3$  KO mice with adenoviral vectors expressing either WT or  $\alpha 3$ C239A cDNA under the control of the synapsin promoter (*Ad $\alpha 3$ /Syn* or *Ad $\alpha 3$ C239A/Syn*), a promoter that restricts expression of  $\alpha 3$  mainly to peripheral neurons (Krishnaswamy and Cooper, 2009). As control, we injected some mice with *AdGFP/Syn*. Sympathetic ganglia in  $\alpha 3$  KO mice have no synaptic transmission because the postganglionic sympathetic neurons do not have functional nAChRs (Rassadi et al., 2005; Krishnaswamy and Cooper, 2009; Fig. 5B); however, within 24 hr of expressing WT  $\alpha 3$  in  $\alpha 3$  KO mice, nicotinic synaptic transmission became functional (26; Fig. 6A). By 3-4 days post-infection, the nerve-evoked EPSPs were suprathreshold and their amplitudes were not significantly different from those in control WT mice; on the other hand, none of the ganglia from mice infected with *AdGFP/Syn* had detectable synaptic transmission. These results indicate that infecting  $\alpha 3$  KO mice with *Ad $\alpha 3$ /Syn* rescues normal synaptic transmission (Krishnaswamy and Cooper, 2009).

To test whether the C239A mutation in  $\alpha 3$  prevents synapses in sympathetic ganglia from hyperglycemia-induced long-lasting depression, we infected 24 young (P7-P10)  $\alpha 3$  KO mice with adenoviral vectors expressing either WT  $\alpha 3$  (*Ad $\alpha 3$ /Syn*),  $\alpha 3$ C239A (*Ad $\alpha 3$ C239A/Syn*) or control GFP (*AdGFP/Syn*),

**A****B****C****Figure 5.5**

**FIGURE 5.5.** Hyperglycemia-induced elevation in ROS inactivates nAChRs by oxidizing cysteine residues at the intracellular mouth of the nAChR channel. **A.** Amino acid sequence alignment of several vertebrate nAChR subunits at the intracellular region between the first (M1) and second (M2) transmembrane domains (left) and a schematic of nAChR showing location of the conserved Cys. **B.** ACh-evoked currents on P2  $\alpha 3$  KO SCG neurons cultured for 1 week and infected with adenoviruses containing GFP (AdGFP, left), full length  $\alpha 3$  (Ad $\alpha 3$ WT, middle) or with mutated  $\alpha 3$ C239A.  $\alpha 3$  KO neurons infected with AdGFP have no ACh-evoked currents, whereas adenoviruses containing  $\alpha 3$ WT or  $\alpha 3$ C-A rescues ACh sensitivity. **C.** Currents evoked by a series of 1 s ACh (100  $\mu$ M) applications delivered at 15 s intervals on neonatal  $\alpha 3$  KO mouse SCG neurons cultured in 5mM glucose for 2 weeks followed by 25mM glucose for a week, infected with either Ad $\alpha 3$ WT (top) or with Ad $\alpha 3$ C-A (bottom). Every 4th trace is shown for clarity. ACh-evoked currents on neurons that express  $\alpha 3$ WT run down rapidly; in contrast, ACh-evoked currents on neurons that express  $\alpha 3$ C-A are stable. **D.** Ratio of the 30th ACh-evoked current to the first in the series ( $I_{30}/I_1$ ) for  $\alpha 3$  KO neurons cultured in 5mM glucose for 2 weeks followed by 25mM glucose for a week infected with either Ad $\alpha 3$ C-A ( $n=25$ ) or Ad $\alpha 3$ WT ( $n=23$ ). Each bar is the mean  $I_{30}/I_1 \pm$  s.e.m. \*\*\* represents  $p < 0.001$ .

and 1 days later, we injected these mice with STZ (40-60 mg/kg): blood glucose in all 24 STZ-treated mice was elevated to >22 mM in 3 days and remained elevated for at least 1 month. After 1 and 2 weeks, we tested synaptic transmission in sympathetic ganglia.

In 8/8 mice infected with Ad $\alpha$ 3/Syn and made hyperglycemic sympathetic neurons had nerve-evoked EPSPs that were considerably reduced in amplitude (Fig. 6B), similar to EPSPs on sympathetic neurons in hyperglycemic WT mice. Most relevant, in ganglia from mice infected with Ad $\alpha$ 3C239A/Syn and hyperglycemic blood glucose levels (>22mM) all nerve-evoked EPSPs were suprathreshold and had amplitudes that were not significantly different from those in control WT mice with normal (5-7 mM) blood glucose (Fig. 6B,C). These results indicate that mutating C239 to A in  $\alpha$ 3 protects synapses in autonomic ganglia from hyperglycemia-induced depression.

Given that hyperglycemia does not induce depression of synaptic transmission in  $\alpha$ 3C239A – expressing mice, we predicted that these hyperglycemic mice would not have sympathetic hypo-function or dysautonomia. To test this, we measured functional sympathetic innervation to the heart in  $\alpha$ 3C239A –expressing hyperglycemic mice by measuring the difference in heart rate before and after propranolol (sympathetic drive). In control mice, the difference in heart rate before and after propranolol was approximately 200 beats per minute (bpm) (Fig. 6D), whereas in  $\alpha$ 3 KO mice infected with GFP (AdGFP/Syn), propranolol had no effect on heart rate since these mice have no synaptic transmission in autonomic ganglia (Krishnaswamy and Cooper, 2009). In  $\alpha$ 3 KO mice infected with WT  $\alpha$ 3 (Ad $\alpha$ 3/Syn) and made hyperglycemic (blood glucose > 22mM) the difference in heart rate before and after propranolol was approximately 100 bpm, similar to its effect on heart rate in control mice made

hyperglycemic (Fig. 6D). On the other hand,  $\alpha 3$  KO mice infected with  $\alpha 3$ C239A (Ad $\alpha 3$ C239A/Syn) and made hyperglycemic (blood glucose > 22 mM) the difference in heart rate before and after propranolol was approximately 180 bpm (Fig.6D), similar to its effect on heart rate in control mice with normal (5-7 mM) blood glucose. These results indicate that the  $\alpha 3$  C239A mutation prevents dysautonomia in hyperglycemic mice.

## DISCUSSION

Our results indicate that synapses in autonomic ganglia malfunction shortly after mice become hyperglycemic, disrupting the link between the CNS and the periphery, and thereby produce autonomic insufficiencies or dysautonomias. Within 2 days of mice becoming hyperglycemic, synapses in autonomic ganglia are depressed, and remain depressed as long as blood glucose is elevated. This immediate effect of hyperglycemia causes autonomic insufficiencies. As examples, we demonstrate that sympathetic reflexes that normally accelerate heart rate are reduced dramatically in diabetic animals, as are sympathetic reflexes involved in thermogenesis. These reduced reflex responses in hyperglycemic animals were comparable to the reduction in mice null for the  $\alpha 3$  nAChR subunit, a subunit that is essential for synaptic transmission in sympathetic ganglia (Rassadi et al., 2005; Krishnaswamy and Cooper, 2009). The hearts in these  $\alpha 3$ -null mice highlight the importance of these synapses for sympathetic function and serve as a good reference for the effects of hyperglycemia; the hearts in these  $\alpha 3$ -null mice have no functional autonomic innervation, nor can these mice maintain body temperature during cold exposure. Furthermore, we show that synaptic transmission in autonomic ganglia and

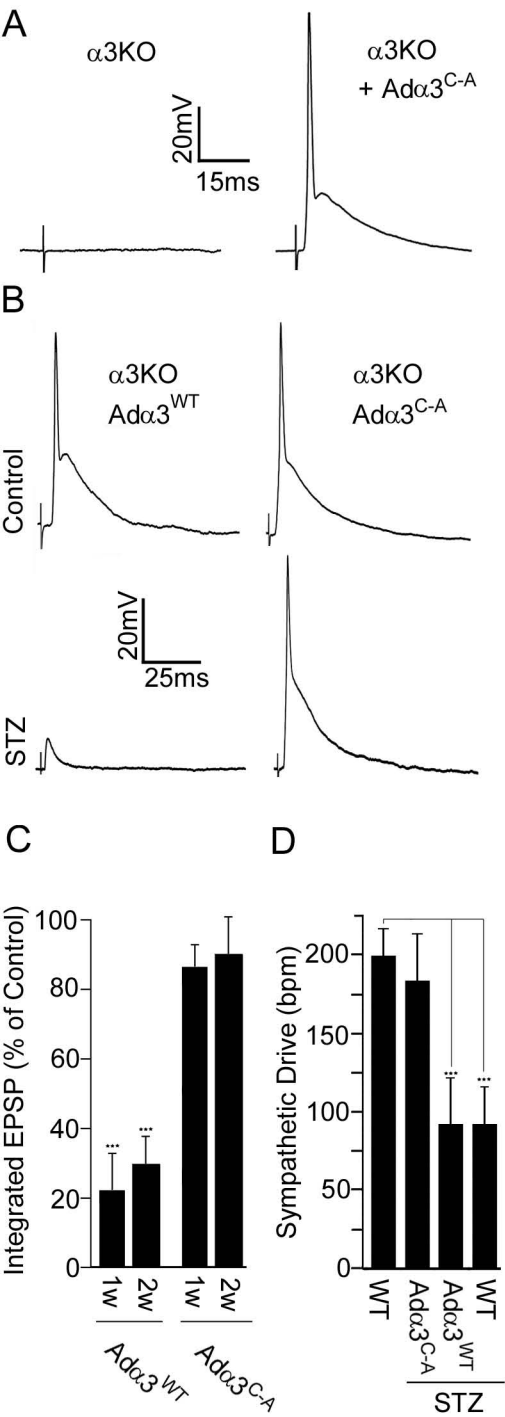


**Figure 5.6**

**FIGURE 5.6.** Synaptic transmission and sympathetic drive to the heart rate are normal in hyperglycemic mice expressing  $\alpha 3C239A$  receptors. **A.** Nerve-evoked excitatory postsynaptic potentials (EPSPs) recorded intracellularly from sympathetic neurons in intact ganglia from P14  $\alpha 3$  KO mice (left) and P14  $\alpha 3$  KO mice infected at P0 with adenoviruses that contain  $\alpha 3C-A$ . **B.** EPSPs from sympathetic neurons in P18  $\alpha 3$  KO mouse rescued with Ad $\alpha 3$ WT (left column) or rescued with Ad $\alpha 3C-A$  (right column), 2 weeks after injection with control (top) or STZ (bottom). Mice were hyperglycemic (serum glucose ~25-30mM) within 2-3 days of STZ. Synaptic transmission in autonomic ganglia from mice that express  $\alpha 3C-A$  containing nAChRs is protected from effects of hyperglycemia. **C.** Integrated EPSPs from sympathetic neurons in  $\alpha 3$  KO mice rescued with either Ad $\alpha 3$ WT or with Ad $\alpha 3C-A$ , 1 week (Ad $\alpha 3$ WT  $n=20$ , Ad $\alpha 3C-A$   $n=20$ ) or 2 weeks (Ad $\alpha 3$ WT  $n=10$ , Ad $\alpha 3C-A$   $n=18$ ) after becoming hyperglycemic (serum glucose (25-30 mM)). Each bar is the mean  $\pm$  s.e.m. \*\*\* represents  $p<0.001$ . **D.** Sympathetic drive to the heart in hyperglycemic  $\alpha 3$  KO mice rescued with either Ad $\alpha 3$ WT ( $n=6$ ) or with Ad $\alpha 3C-A$  ( $n=7$ ). Hyperglycemic WT animals ( $n=15$ ) and control sham-injected animals are shown for comparison ( $n=12$ ). Each bar is the mean bpm  $\pm$  s.e.m. \*\*\* represents  $p<0.001$ .

autonomic function is normal in hyperglycemic mice expressing the mutant C239A  $\alpha 3$  subunit. These results add strong support for our conclusion that hyperglycemia's adverse affect on synaptic transmission produces autonomic insufficiencies.

In addition, we show that synaptic transmission in autonomic ganglia is severely depressed in mice null for leptin (*ob*) or its receptors (*db*); these mice are obese as well as hyperglycemic, and also have high circulating levels of insulin (Coleman, 1978, Zhang et al., 1994; Chen et al., 1996). Therefore, it does not matter whether mice become hyperglycemic because of little or no circulating insulin, as in our experiments where we destroyed pancreatic  $\beta$  cells, or whether mice become hyperglycemic because of obesity-induced insulin resistance and have high circulating insulin; in both hyperglycemic situations, synaptic transmission in autonomic ganglia is depressed and animals suffer autonomic insufficiencies. These experiments indicate that hyperglycemia causes synaptic transmission to be depressed, independent of the circulating levels of insulin. Given that autonomic nerves innervate most peripheral tissues, including the heart, blood vessels, and the kidney, our results imply that these early hyperglycemia-induced autonomic insufficiencies act together with high circulating levels of glucose to damage tissues, producing microvascular and cardiovascular complications that lead to the progression of system-wide abnormalities that occur in people with diabetes.

We show that hyperglycemia depresses synaptic transmission by elevating cytosolic reactive oxygen species (ROS) in autonomic neurons and inactivating postsynaptic nAChRs. The elevation in cytosolic ROS in autonomic neurons during hyperglycemia is largely a result of two processes: 1) accelerated oxidative metabolism by mitochondria as intracellular glucose increases; and 2)

extra glucose processed through the polyol (or sorbitol) pathway, a process that reduces anti-oxidants and free radical scavengers (Brownlee, 2001; Tomlinson and Gardiner, 2008). Both processes elevate free radicals and shift the redox state of the cytosol towards oxidative conditions necessary to inactivate nAChRs. The effects of hyperglycemia on nAChR function is mimicked either by acutely blocking the electron transport chain complex III or by transient (1-2 days) growth factor withdrawal; both elevate mitochondrial ROS in sympathetic neurons and inactivate nAChRs (Campanucci et al., 2008). Moreover, adding anti-oxidants to the cytosol prevents the effects of high glucose on nAChR inactivation.

Increased cytosolic ROS inactivate nAChRs by interacting with a ring of highly conserved Cys residues located at the inner mouth of the receptor's pore. How the interaction between ROS and these critical Cys residues inactivate the receptor is not yet fully understood, but the most plausible scenario is that ROS oxidize these Cys residues, and promote subunits in the receptor pentamer to cross-link, trapping the channel in a non-conducting state. The normal physiological role for these highly-conserved Cys residues is not clear: they are not required for receptor activation, desensitization, or recovery from desensitization. By inactivating the receptor when oxidized, these Cys may serve to protect neurons from over-excitation by the preganglionic nerve should cytosolic ROS become elevated, perhaps during high metabolic activity, or when the neurons are transiently deprived of growth factors (Kirkland and Franklin, 2001; Campanucci et al., 2008). Interestingly these Cys are not conserved on nAChRs on skeletal muscle.

A common occurrence in those who gain weight is insulin resistance and hyperglycemia, similar to mice with a disruption in leptin signaling. We show that this obesity-linked hyperglycemia disrupts the function of synapses in autonomic

ganglia and impairs several homeostatic control mechanisms, including cold-induced thermogenesis, a reflex that depends on functional sympathetic activity to generate heat from brown adipose tissue. Brown adipose tissue, a tissue once thought restricted to rodents and human infants, but recently shown to be metabolically important in adults as well, plays an important role in energy balance (Cannon and Nedergaard, 2004; van Marken Lichtenbelt WD, et al. 2009; Virtanen et al., 2009; Cypess et al., 2009). By decreasing the metabolic activity of brown fat, this obesity-linked hyperglycemia creates an undesirable positive feedback cycle, one that reinforces weight gain by depressing synaptic transmission in sympathetic ganglia and decreasing activity of brown adipose tissue, which lowers energy expenditure and increases energy storage by white adipose, thereby producing further weight gain.

## CHAPTER 6: GENERAL DISCUSSION AND CONCLUSION

### DISCUSSION

#### **Activity-dependent Retrograde Signals Instruct Cholinergic Nerve**

#### **Terminals to Express the High-Affinity Choline Transporter**

I show that cholinergic synapses in sympathetic ganglia at birth are functionally immature and fatigue rapidly with repetitive stimulation. Over the first postnatal week, these synapses mature and sustain transmission even when stimulated at high frequency or for prolonged periods. This conversion from a readily fatigable synapse to one that can sustain transmission is produced by activity-dependent retrograde signals that instruct preganglionic neurons to express CHT at their nerve terminals. Furthermore, my rescue experiments using *in vivo* adenoviral gene-transfer strategies demonstrate that preganglionic nerve terminals require continuous activity-dependent retrograde signals to continuously express CHT. Given these results, it is possible that ACh-insufficiencies that underlie diseases such as Parkinson's disease (Dani and Bertrand, 2007), might result from disrupted activity-dependent signals that direct CHT expression in nerve terminals. However, more work is necessary to determine whether the retrograde control of CHT that I have discovered at ganglionic cholinergic synapses is common to all cholinergic synapses. There is no evidence that directly addresses this issue but several studies are consistent with my model.

At the developing NMJ, the appearance of a hemicholinium 3-sensitive high-affinity choline uptake system correlates strongly with the ability of motor nerve terminals to sustain transmission (Letinsky, 1974; Pilar et al., 1981), suggesting that CHT is expressed in motor nerve terminals after NMJs form and become active, similar to the way CHT is expressed in preganglionic nerve terminals in sympathetic ganglia. Furthermore, the levels of CHT mRNA drop in axotomized motor neurons and only reappear when motor nerves re-innervate muscle (Oshima et al., 2004), suggesting that motor neurons require continuous muscle-derived retrograde factors, perhaps activity-dependent factors, to express CHT. These results are consistent with my observation that cholinergic nerve terminals require retrograde signals to mature and express CHT, but more work will be needed to verify my idea at NMJs and identify whether these signals are produced in response to synaptic activity.

At CNS synapses, CHT levels increase to overcome insults to cholinergic signalling produced by reduced ChAT (ChAT heterozygote mice), reduced synaptic choline (AChE knockout mice) and increased ACh hydrolysis (AChE overexpressing mice) (see section 1.4.1.5). Taken together, these results indicate that CHT is increased in nerve terminals to strengthen CNS cholinergic synapses, similar to the way CHT increases in preganglionic nerve terminals to strengthen transmission at ganglionic synapses. It is attractive to think that CNS neurons in the above cases detect reduced cholinergic signalling via postsynaptic activity and release retrograde signals that increase CHT in nerve terminals to compensate. Unfortunately, the nature of these retrograde signals remains elusive.

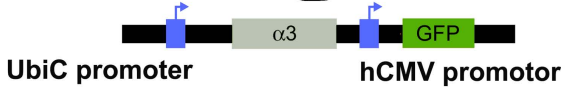
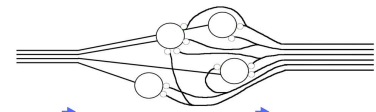
It seems reasonable to speculate that these retrograde signals are generated in response to  $Ca^{2+}$  influx produced by strong depolarization. My

rescue experiments with conductance mutant  $\alpha 3^{E240A}$  subunits support this idea, since the EPSPs on sympathetic neurons rescued with  $\alpha 3^{E240A}$  subunits were too weak to induce nerve terminals to express CHT. If this idea is true, then it is likely that retrograde signals are transcribed in response to  $Ca^{2+}$  influx. Certainly,  $Ca^{2+}$  influx through nAChRs and voltage-gated  $Ca^{2+}$  channels on cultured sympathetic neurons is strong enough to activate genes regulated by calcium response elements (CREs) (Wheeler and Cooper, 2001, 2004). One potentially suitable candidate retrograde factor could be BDNF, since the BDNF promoter contains CREs (Tao and Poo, 2001), since preganglionic nerve terminals express BDNF receptors (TrkB) and since BDNF-TrkB signaling is known to affect these nerve terminals *in vivo* (Causing et al., 1997).

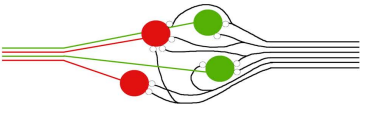
### **Electrophysiologically Silent Synapses Persist without Postsynaptic**

#### **Activity**

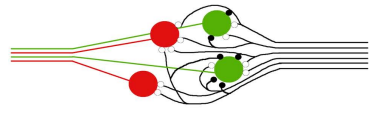
My results from sympathetic neurons in  $\alpha 3$  KO mice demonstrate that electrophysiologically silent synapses form and express several pre- and postsynaptic proteins critical for cholinergic synaptic transmission, except for CHT. These results are consistent with previous observations that indicate that the initial events in synapse formation can proceed without synaptic activity (Misgeld et al., 2002; Verhage et al., 2000; Washbourne et al., 2002). In contrast to these previous results, my results demonstrate that synapses continue to form following these initial events and persist for weeks without synaptic activity. Moreover, these electrophysiologically silent synapses form in comparable numbers to active synapses formed on WT neurons. Taken together, these results indicate that synaptic activity is not required for synapses to form and persist on sympathetic neurons. If these results are true for other synapses, such

**A**

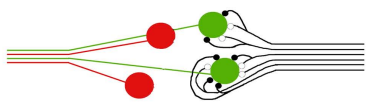
Green cells express  $\alpha 3$  and are active  
Red cells do not express  $\alpha 3$  and are inactive



No Change



Sprout



Eliminate

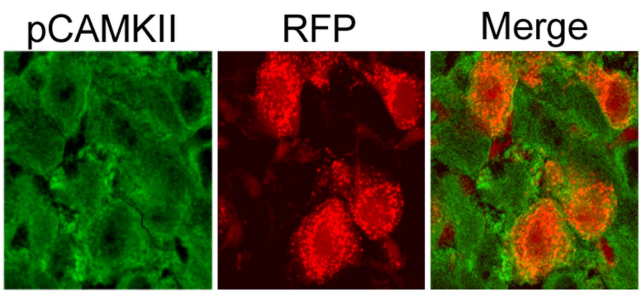
**B**

Figure 6.1

**Figure 6.1.** Sympathetic circuits constructed from active and inactive sympathetic neurons could choose one of 3 possible outcomes

Schematic of 3 possible outcomes produced by mosaic expression of  $\alpha 3$  in sympathetic neurons and mosaic expression of RFP in sympathetic neurons. **A** Only 50% of sympathetic neurons in mice hemizygous for  $\alpha 3$  will express  $\alpha 3$  subunits because of X-inactivation. Three possible outcomes if sympathetic circuits are made up of active and inactive cells: (1) Preganglionic axons innervate active and inactive sympathetic neurons equally, indicating that sympathetic circuits do not reinforce active synaptic connections; (2) Preganglionic axons only innervate active sympathetic neurons, suggesting that sympathetic circuits reinforce active synaptic connections and eliminate inactive ones; (3) Preganglionic axons innervate inactive sympathetic neurons because synapses can persist without activity but sprout to innervate active sympathetic neurons to compensate and keep sympathetic circuitry intact. Red cells denote inactive cells. Green cells denote active cells. **B** Tissue sections from the SCG of mice mice that are hemizygous for a transgene that expresses red fluorescent protein (RFP) immunostained for neuron specific marker phosphorylated CAMKII (pCAM). Approximately 50% of the pCAMKII positive SCG neurons also express RFP, indicating that the X chromosome with the RFP transgene was left active.

as those in the CNS, then it implies that many morphological synapses are not necessarily functional.

A well accepted view of developing circuits is that active synapses persist, whereas inactive or weak synapses are eliminated (Cohen-Cory, 2002; Greenberg, 2008). Several observations support this view and indicate that neural circuits selectively eliminate inactive synaptic connections (Katz and Shatz, 1996; Lichtman and Colman, 2000). For example, visual circuits that develop without input from one eye are formed almost entirely of synapses from inputs of the remaining eye (Katz and Shatz, 1996). Intuitively, it makes sense that circuits would reinforce active, useful synaptic connections over inactive useless ones. If this is so, then why do silent cholinergic synapses persist on  $\alpha 3$  KO sympathetic neurons? Perhaps these silent cholinergic synapses persist because sympathetic circuits are made up entirely of inactive synaptic connections. If sympathetic circuits were given a choice between inactive and active sympathetic neurons, then maybe they would eliminate inactive synaptic connections and consist only of preganglionic synapses formed on active sympathetic neurons.

One way to test this idea would be to study the development of synapses in mosaic sympathetic ganglia that contain  $\alpha 3$ -expressing and  $\alpha 3$ -null sympathetic neurons. This experiment has three possible outcomes (Figure 6.1A): (1) Preganglionic axons innervate active and inactive sympathetic neurons equally, indicating that sympathetic circuits do not reinforce active synaptic connections; (2) Preganglionic axons only innervate active sympathetic neurons, suggesting that sympathetic circuits reinforce active synaptic connections and eliminate inactive ones; or (3) Preganglionic axons innervate inactive sympathetic

neurons because synapses can persist without activity but sprout to innervate active sympathetic neurons to compensate and keep sympathetic circuitry intact.

This issue is exciting and I have developed a strategy to generate mosaic sympathetic ganglia that contain  $\alpha 3$ -expressing and  $\alpha 3$ -null sympathetic neurons. Briefly, I am constructing a transgene that contains the  $\alpha 3$  subunit driven by the strong human ubiquitinC (UbiC) promoter, followed by green fluorescent protein driven by the activity-dependent hCMV promoter (Wheeler and Cooper, 2001, 2004). With the help of Dr. A. Peterson's lab, this transgene will be homologously recombined into the Hypoxanthine-guanine phosphoribosyltransferase (HPRT) gene of mouse embryonic stem (ES) cells and recombinants will be selected by eliminating non-recombined clones with hypoxanthine aminopterin thymidine containing medium. Transgene positive ES cells will then be injected into 8 cell zygotes to generate 9 cell zygotes and then implanted into pseudopregnant female mice to produce transgenic  $\alpha 3$ -expressing mice. Next, I will breed the  $\alpha 3$  transgene into genomic  $\alpha 3$  heterozygote mice to generate male genomic  $\alpha 3$  heterozygotes ( $\alpha 3^{+/-}$ ) that are hemizygous for the  $\alpha 3$  transgene ( $X^{\alpha 3}Y$ ). Breeding these male ( $\alpha 3^{+/-} / X^{\alpha 3}Y$ ) mice to female genomic  $\alpha 3$  heterozygotes ( $\alpha 3^{+/-}$ ) will produce female homozygote ( $\alpha 3^{-/-}$ ) mice that are hemizygous for the  $\alpha 3$  transgene. These female hemizygotes ( $\alpha 3^{-/-} / X^{\alpha 3}Y$ ), like all female mammals, are natural mosaics since each mouse cell randomly inactivates one of the two X chromosomes. Theoretically, this should produce genomic  $\alpha 3$  KO mice that express transgenic  $\alpha 3$  subunits in 50% of their sympathetic neurons. Moreover, these  $\alpha 3$ -expressing, active cells will express GFP from the activity-dependent hCMV promoter (Figure 6.1B). My preliminary results from female mice that are hemizygous for a transgene that expresses red fluorescent protein (RFP) from

the UbiC promoter confirm this theory. SCG tissue sections from these mice show a random distribution of phosphoCAMKII –stained sympathetic neurons that express RFP (Figure 6.1B). I am currently in the process of constructing the UbiC- $\alpha$ 3 /hCMV-GFP transgene.

### **Cytosolic ROS Attack a Highly Conserved Ring of Cysteine Residues near the Channel Pore and Inactivate nAChRs**

I show that elevations in cytosolic ROS trap nAChRs in a long lasting inactivated state. Furthermore, I show that ROS trap nAChR in an inactive state by attacking a highly conserved ring of cysteine residues near the cytosolic mouth of the receptor pore (Figure 6.2A). Moreover, I show that that cytosolic ROS must be paired with receptor activation to inactivate nAChRs, suggesting that these cysteines are buried and inaccessible to ROS when nAChRs are in their resting configuration. How are these cysteines modified to inactivate nAChRs?

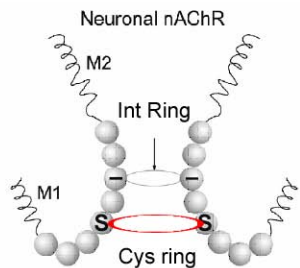
ROS are unstable, highly reactive molecules because they contain free, unpaired electrons. Commonly, these molecules react with sulphhydryl groups on the side-chains of cysteine residues and rob them of protons, leaving sulfur atoms with an unbonded, reactive electron pair (Poole and Nelson 2008). In most cells, several ROS buffering enzymes, such as glutathione reductase, keep the cytosol reduced and donate protons to neutralize these reactive sulfur atoms (Brownlee, 2001; Tomlinson and Gardiner, 2008). However, when these buffers become overwhelmed, as seen under diabetic conditions, intracellular ROS elevates and sulfur atoms on cysteines likely remain in an oxidized, reactive state. In many cases, oxidized cysteines react with each other and bond together. Given that cysteine residues from each nAChR subunit are arranged in

a ring-like structure near the receptor pore, it is likely that ROS causes these cysteines to become oxidized and crosslinked, locking nAChRs in an inactive configuration (Figure 6.2B). Alternatively, it is possible that oxidized cysteine residues crosslink to intracellular proteins, perhaps to scaffold proteins, to prevent nAChRs from changing conformation. If cysteines crosslink together within the receptor pore or if they crosslink to cytosolic proteins to inactivate nAChRs, can they be reduced to reactivate nAChRs? If not, are these inactivated nAChRs degraded and replaced with newly synthesized nAChRs? What is the fate of inactivated nAChRs?

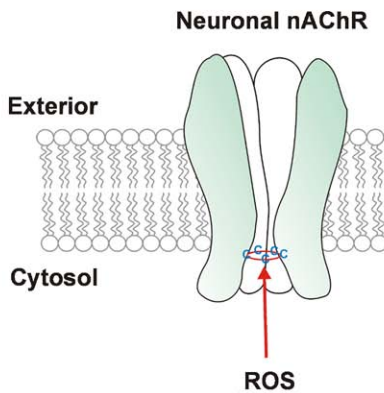
One way to study these issues would be to label ROS-inactivated receptors and monitor the recovery of ACh-evoked currents on sympathetic neurons. If ACh-evoked currents reappear on sympathetic neurons but labeled receptors disappear from the membrane, then it is likely that inactivated nAChRs are being replaced by newly synthesized, unlabelled receptors. Alternatively, if ACh-evoked currents reappear on sympathetic neurons and the number of labeled receptors at the plasma membrane remains constant, then it is likely that these inactive nAChRs are being reduced and reactivated. Normally, this experiment could be performed with microscopy and fluorescently-labeled antibodies directed against the extracellular parts of the channel. Unfortunately, this experiment is difficult to because many nAChR antibodies are not specific enough (Moser et al., 2007).

To address this difficulty, I have collaborated with Dr. E. Hawrot's group to develop knock-in mice that express mutated  $\alpha 3$ -subunits that bind the snake-venom toxin,  $\alpha$ bgt. Previous work from Hawrot's group indicates that 5 amino acids close to the extracellular binding pocket of nAChRs are critical for  $\alpha$ bgt to

A



	M1	M1-M2	M2	
α3	VFVLEPS	DGG EK	VFFQISVLLS	(rat)
α4	VFVLEPS	DGG EK	IFFQISVLLS	(rat)
β2	VFVLEPS	DGG EK	MLFQISVLLS	(rat)
β4	VFVLEPS	DGG EK	MLFQISVLLS	(rat)
γ1	VFVLEPT	DGG EK	MLFQISVLLS	
δ1	VFVLEPS	DGG EK	MLFQISVLLS	
ε	VFVLEPS	DGG EK	MLFQISVLLS	
γ	AVFLDPA	QAG QK	CEVQINVLLS	
ε	IYFLDPA	RAG QK	CEVATNVLLS	



B

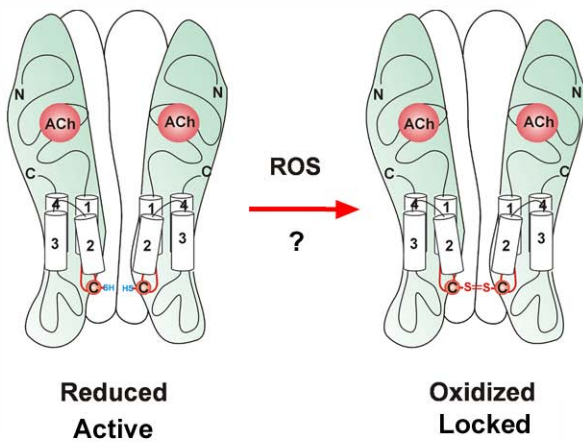


Figure 6.2

**Figure 6.2.** ROS potentially inactivates nAChRs by oxidizing a conserved group of cysteine residues in the M1-M2 linker. **A and B** Schematic drawing of the M1-M2 intracellular linker region that forms that cytosolic mouth of nAChRs. The left drawing illustrates the positions of the conserved cysteine residues that are attacked by ROS (S) and the negatively charged residues that important for inward rectification. **C** Schematic drawing of the nAChR in crosssection. This drawing illustrates my idea that these cysteines may become oxidized by ROS and then crosslink together, locking nAChRs in an inactive configuration

bind to muscle nAChRs (Levandoski, 1999). In our collaboration, they went a step further and generated knock-in mice that express  $\alpha 3$  subunits mutated to include these critical 5 amino acids ( $\alpha 3[5]$  mice) (see appendix for manuscript, Caffery et al., 2009). Our prediction was that  $\alpha 3[5]$  subunits would form functional receptors that we could then either block or label using  $\alpha$ bgt. Indeed, my intracellular recordings from sympathetic neurons in  $\alpha 3[5]$  ganglia demonstrate that functional  $\alpha 3[5]$ -containing nAChRs are targeted to synaptic domains and allow synaptic transmission to be blocked by  $\alpha$ bgt. In support of this, my imaging experiments with rhodamine-labelled  $\alpha$ bgt (rhobgt) show that >90% of rhobgt-labelled nAChR puncta colocalize with nerve terminals immunostained for VAcHT in  $\alpha 3[5]$  ganglia. These results indicate that  $\alpha 3[5]$  knock-in mice are a useful tool to study synaptic nAChRs on sympathetic neurons. With  $\alpha 3[5]$ -expressing sympathetic neurons and rhobgt, I should be in a good position to label nAChRs on live sympathetic neurons and track the fate of ROS-inactivated nAChRs.

### **Diabetes-Induced ROS Inactivates nAChRs, Depresses Synaptic**

### **Transmission and Results in Dysautonomias**

I show that elevated extracellular glucose increases cytosolic ROS in sympathetic neurons and inactivates nAChRs because ROS attacks a highly conserved ring of cysteine residues located near the cytosolic mouth of the receptor pore. Furthermore, I show that hyperglycemia-induced ROS attacks these cysteines *in vivo* to inactivate nAChRs and depress synaptic transmission through autonomic ganglia of mice with type 1 and type 2 diabetes. Fast nicotinic EPSPs in sympathetic ganglia link the activity of various CNS nuclei to

sympathetic nerve activity and are crucial for maintaining peripheral homeostasis. For this reason, depressed synaptic transmission in diabetic mice results in severe cardiovascular and thermoregulatory dysautonomias. These results are important because they potentially explain the development of dysautonomias among people who suffer from diabetes (Dyck et al., 1993, Vinik et al., 2003). Unfortunately there are no satisfactory treatments for diabetic dysautonomias. However, my results suggest that if treatments improve cholinergic-nicotinic transmission in autonomic ganglia they should lessen effects of dysautonomias and potentially improve quality of life for diabetic patients.

Among diabetic dysautonomias, diabetic cardiovascular dysautonomia is one of the most common, affecting 1 in 5 people with type 1 diabetes (Vinik et al., 2003). Diabetic cardiovascular dysautonomia is particularly troubling because it results in postural hypotension, exercise intolerance, enhanced intraoperative cardiovascular liability, an increased incidence of asymptomatic ischemia and a predisposition to malignant arrhythmogenesis and sudden cardiac death (Duby et al., 2004; Vinik et al., 2003). As a consequence, people with diabetic cardiovascular dysautonomias have a 5-year mortality rate that is five times higher than people with other types of diabetic dysautonomias (Vinik et al., 2003; Vinik and Zeigler, 2007).

The cause for these dysautonomias is poorly understood, but one idea is that they result from degenerative changes in sympathetic ganglia that disrupt synaptic transmission (Vinik et al., 2003). Consistent with this idea, sympathetic nerve endings appear dystrophic in the prevertebral superior mesenteric and celiac ganglia of patients with diabetes (Schmidt, 1996). The diseased nerve endings in these pelvic sympathetic ganglia likely depress EPSPs on sympathetic neurons and likely account for the gastrointestinal dysautonomias experienced by

people with diabetes. However, they do not explain cardiovascular dysautonomias since homeostatic control of the cardiovascular system is produced by thoracic paravertebral sympathetic ganglia. Diseased nerve endings are not present in the paravertebral ganglia that control cardiovascular function (Schmidt et al., 2008), indicating that other disease mechanisms disrupt cholinergic transmission within these ganglia. Given my results from diabetic mice and given that human nAChR subunits contain the cysteines that make nAChRs susceptible to ROS, one possibility is that human diabetic cardiovascular dysautonomias appear when ROS inactivates nAChRs on paravertebral sympathetic neurons.

Clinically, diabetic dysautonomia is thought of as a progressive, late-stage complication of diabetes, since many dysautonomias in many diabetic patients appear several years after the onset of the disease (Vinik et al., 2003). However, if ROS-induced inactivation of nAChRs happens in people with diabetes like it does in diabetic mice, then my results predict that these dysautonomias would happen much earlier in the progression of diabetes. Why do these dysautonomias develop so early in mice but only appear later in humans? One possibility is that glucose levels in people with diabetes are lower than those of diabetic mice, likely a result of insulin treatment in the case of type 1 diabetes or diet control in the case of type 2 diabetes. Since the glucose levels are lower, perhaps the levels of cytosolic ROS are lower and as a consequence ROS-induced inactivation of nAChRs proceeds slower in humans with diabetes. Another possibility is that sympathetic neurons in humans can temporarily compensate for increased ROS to keep synaptic transmission normal and only succumb to elevated ROS much later. My recent experiments (data not shown) demonstrate that synaptic transmission remains depressed in mice with diabetes

for >3mo, showing that sympathetic neurons cannot compensate for increased ROS for at least 3 months. Yet another possible explanation for the late onset of dysautonomias in humans is that ROS-induced inactivation of nAChRs puts other aspects of sympathetic circuits at risk for deterioration. For example, if too many nAChRs are inactivated by ROS then maybe synaptic activity on sympathetic neurons becomes too weak to maintain the levels of CHT in nerve terminals, resulting in even more strongly depressed cholinergic EPSPs. Clearly more work is needed to translate my findings on diabetic dysautonomias in mice to dysautonomias experienced by people with diabetes.

## CONCLUSION

In conclusion, I have discovered two new, use-dependent consequences of nAChRs signaling on the functional properties of cholinergic synapses.

1. *Nerve terminals at developing cholinergic synapses require retrograde signals that depend on postsynaptic activity in order to express CHT and sustain transmitter release.* Our model of this process is as follows:

Cholinergic synapses form on sympathetic neurons between E12-E14, however the nerve terminals at these synapses are functionally immature because they cannot sustain synaptic transmission. At birth, the sympathetic nervous system is strongly driven and retrograde signals that depend on postsynaptic activity are generated by postsynaptic neurons. These retrograde signals then act on presynaptic neurons and cause them to mature and express CHT at their nerve terminals. Once these nerve terminals have CHT they can sustain ACh release and behave in a normal, mature way (Figure 6.3A).

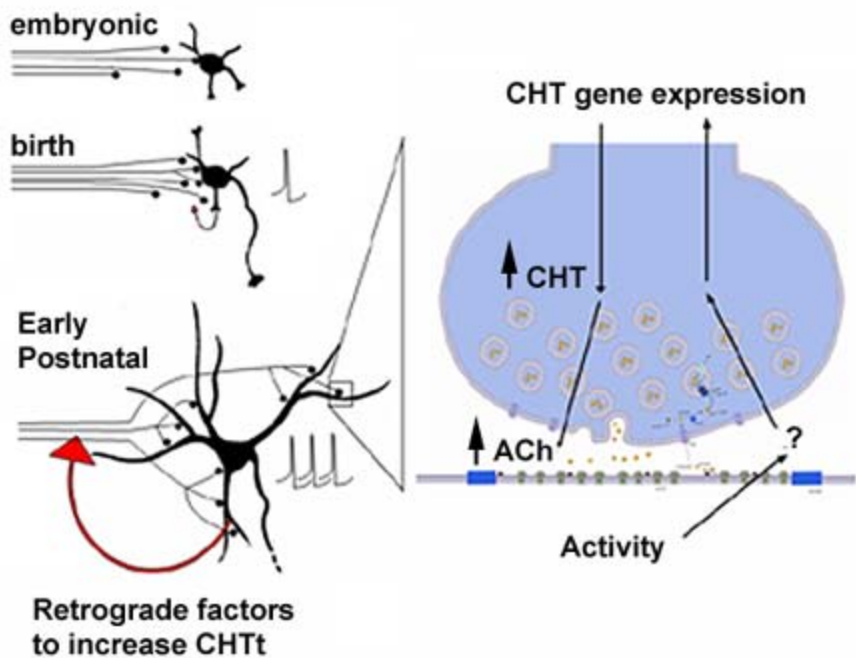
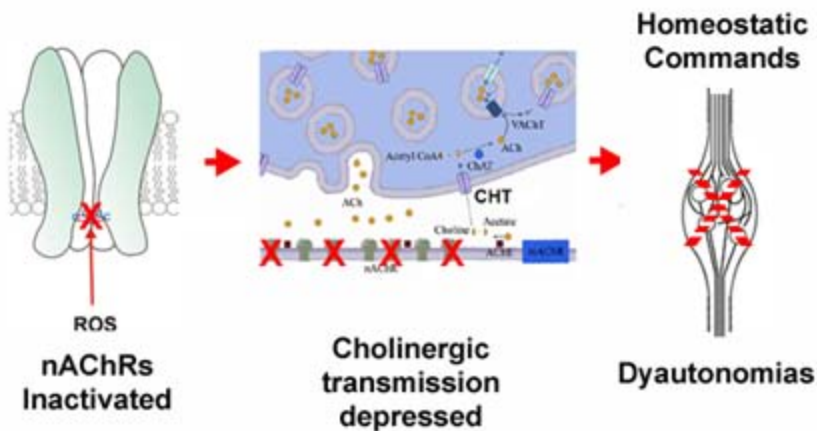
**A****B**

Figure 6.3

**Figure 6.3.** Conclusion. **A** Cholinergic synapses form on sympathetic neurons between E12-E14, however the nerve terminals at these synapses are functionally immature because they cannot sustain synaptic transmission (left). At birth, the sympathetic nervous system is strongly driven and retrograde signals that depend on postsynaptic activity are generated by postsynaptic neurons. These retrograde signals then act on nerve terminals and cause them to mature and express CHT (right). Once these nerve terminals have CHT they can sustain ACh release and behave in a normal, mature way. **B** Elevated serum glucose increases cytosolic ROS. This elevation increases the likelihood that ROS will attack a highly conserved ring of cysteine residues in the inner mouth of the receptor pore (Left). The precise modification of these cysteines is unclear, but causes nAChRs to enter a long lasting inactivated state, depressing synaptic transmission (middle). Depressed cholinergic-nicotinic transmission through sympathetic ganglia deteriorates the link homeostatic commands generated in various CNS nuclei to homeostatic control of various body processes by sympathetic nerve activity, resulting in dysautonomias (right).

2. *ROS produced by diabetic-hyperglycemia inactivates nAChRs on sympathetic ganglia, depresses synaptic transmission and causes dysautonomias.* Our model of this is as follows: Elevated serum glucose is well known to increase the production of cytosolic ROS (Tomlinson and Gardiner, 2008). This elevation increases the likelihood that ROS will attack a highly conserved ring of cysteine residues in the inner mouth of the receptor pore. The precise modification of these cysteines is unclear, but causes nAChRs to enter a long lasting inactivated state, depressing synaptic transmission. Depressed cholinergic-nicotinic transmission through sympathetic ganglia deteriorates the link between homeostatic commands generated in various CNS nuclei and homeostatic control of various body processes by sympathetic nerve activity, resulting in dysautonomias (Figure 6.3B).

## REFERENCES

- Abou-Sleiman PM, Muqit MMK, Wood NW. (2006) Expanding insights of mitochondrial dysfunction in Parkinson's disease. *Nat Rev Neurosci* 7:207–219.
- Abrahamsson T, Gustafsson B, Hanse E. (2005) Synaptic fatigue at the naive perforant path-dentate granule cell synapse in the rat. *J. Physiol.* 569:737–750.
- Albuquerque EX, Pereira EF, Alkondon M, Rogers SW. (2009) Mammalian nicotinic acetylcholine receptors: from structure to function. *Physiol Rev.* 89(1):73-120.
- Annunziato L, Pannaccione A, Cataldi M, Secondo A, Castaldo P, Di Renzo G, Tagliatela M. (2002) Modulation of ion channels by reactive oxygen and nitrogen species: a pathophysiological role in brain aging? *Neurobiol Aging* 23:819–834.
- Apparsundaram S, Ferguson SM, George AL, Blakely RD. (2000) Molecular cloning of a human, hemicholinium-3-sensitive choline transporter. *Biochem. Biophys. Res. Commun.* 276:862–867.
- Apparsundaram S, Ferguson SM, Blakely RD. (2001) Molecular cloning and characterization of a murine hemicholinium-3-sensitive choline transporter. *Biochem. Soc. Trans.* 29:711–716.
- Axelsson J. (1971) Catecholamine functions. *Ann. Rev. Physiol.* 33:1-30.
- Bachman ES, Dhillon H, Zhang CY, Cinti S, Bianco AC, Kobilka BD, Lowell BB. (2002)  $\beta$ AR signaling required for diet-induced thermogenesis and obesity resistance. *Science* 297:843-845.
- Bazalakova MH, Blakely RD. (2006) The high-affinity choline transporter: a critical protein for sustaining cholinergic signaling as revealed in studies of genetically altered mice. *Handb Exp Pharmacol.* 175:525-544.
- Beal MF. (2003) Bioenergetic approaches for neuroprotection in Parkinson's disease. *Ann Neurol* 53[Suppl 3]:S39–S47.
- Beeri R, Le Novere N, Mervis R, Huberman T, Grauer E, Changeux JP, Soreq H. (1997) Enhanced hemicholinium binding and attenuated dendrite branching in cognitively impaired acetylcholinesterase-transgenic mice. *J Neurochem* 69:2441–2451.
- Bejanin S, Cervini R, Mallet J, Berrard S. (1994) A unique gene organization for two cholinergic markers, choline acetyltransferase and a putative vesicular transporter of acetylcholine. *JBC.* 269(35):21944-7.
- Bertrand D, Cooper E, Valera S, Rungger D, Ballivet M. (1991) Electrophysiology of neuronal nicotinic acetylcholine receptors expressed in *Xenopus* oocytes following nuclear injection of genes or cDNAs. *Methods Neurosci* 4:174–193.

- Birks RI, MacIntosh, FC. (1961) Acetylcholine metabolism of a sympathetic ganglion, *J. Biochem. Physiol.* 39:787–827.
- Boulter J, O'Shea-Greenfield A, Duvoisin RM, Connolly JG, Wada E, Jensen A, Gardner PD, Ballivet M, Deneris ES, McKinnon D, Heinemann, S, Patrick J. (1990).  $\alpha$ -3,  $\alpha$ -5 and  $\beta$ -4: Three members of the rat neuronal nicotinic acetylcholine receptor-related gene family form a gene cluster. *JBC* 265:4472-4482.
- Brandon EP, Mellott T, Pizzo DP, Coufal N, D'Amour KA, Gobeske K, Lortie M, Lopez-Coviella I, Berse B, Thal LJ, Gage FH, Blusztajn JK. (2004) Choline transporter 1 maintains cholinergic function in choline acetyltransferase haploinsufficiency. *J Neurosci* 24:5459–5466.
- Brenman JL, Christopherson KS, Craven SE, McGee AW, Bredt DS. (1996) Cloning and characterization of postsynaptic density 93, a nitric oxide synthase interacting protein. *J. Neurosci.* 16:7407–7415.
- Broide RS, Leslie FM. (1999) The  $\alpha$ 7 nicotinic acetylcholine receptor in neuronal plasticity. *Mol Neurobiol* 20:1–16.
- Brown DA, Selyanko AA. (1985) Membrane currents underlying the cholinergic slow excitatory post-synaptic potential in the rat sympathetic ganglion. *J Physiol (Lond)* 365:365–387.
- Brown DA, Abogadie FC, Allen TG, Buckley NJ, Caulfield MP, Delmas P, Haley JE, Lamas JA, Selyanko AA. (1997) Muscarinic mechanisms in nerve cells. *Life Sci.* 60(13-14):1137-44.
- Brown, D.A. and Fumagalli, L., (1977) Dissociation of  $\alpha$ -bungarotoxin binding and receptor block in the rat superior cervical ganglion, *Brain Res.* 129: 165-168.
- Brownlee M. (2005) The pathobiology of diabetic complications: a unifying mechanism. *Diabetes.* 54(6):1615-25.
- Brownlee M. (2001) Biochemistry and molecular cell biology of diabetic complications. *Nature* 414:813-820.
- Brumwell CL, Johnson JL, Jacob MH. (2002) Extrasynaptic  $\alpha$ 7-nicotinic acetylcholine receptor expression in developing neurons is regulated by inputs, targets, and activity. *J Neurosci* 22:8101–8109.
- Buffelli M, Burgess RW, Feng G, Lobe CG, Lichtman JW, Sanes JR. (2003) Genetic evidence that relative synaptic efficacy biases the outcome of synaptic competition. *Nature* 424:430–434.
- Buettner GR, Jurkiewicz BA (1996) Catalytic metals, ascorbate and free radicals: combinations to avoid. *Radiat Res* 145:532–541.

- Calcutt NA, Cooper ME, Kern TS, Schmidt AM. (2009) Therapies for hyperglycaemia-induced diabetic complications: from animal models to clinical trials. *Nat. Rev. Drug Discov.* 8:417-429.
- Campanucci VA, Cooper E. (2007) Inactivation of neuronal nicotinic ACh receptors by oxidation of intracellular cysteine residues. *Soc Neurosci Abstr* 33:677-8.
- Campanucci VA, Krishnaswamy A, Cooper E. (2008) Mitochondrial reactive oxygen species inactivate neuronal nicotinic acetylcholine receptors and induce long-term depression of fast nicotinic synaptic transmission. *J Neurosci.* 28(7):1733-44.
- Cannon B, Nedergaard J. (2004) Brown adipose tissue: function and physiological significance. *Physiol. Rev.* 84:277-359.
- Carbini LA, Hersh LB. (1993) Functional analysis of conserved histidines in choline acetyltransferase by site-directed mutagenesis. *J. Neurochem.* 61:247-253.
- Carroll PT. (1994) Membrane-bound choline-O-acetyltransferase in rat hippocampal tissue is associated with synaptic vesicles. *Brain Res.* 633:112-118.
- Causing CG, Gloster A, Aloyz R, Bamji SX, Chang E, Fawcett J, Kuchel G, Miller FD. (1997) Synaptic innervation density is regulated by neuron-derived BDNF. *Neuron* 18(2):257-67.
- Champtiaux N, Changeux J-P. (2004) Knockout and knockin mice to investigate the role of nicotinic receptors in the central nervous system. *Prog Brain Res* 145:235-251.
- Chang KT, Berg DK. (1999) Nicotinic acetylcholine receptors containing  $\alpha 7$  subunits are required for reliable synaptic transmission in situ. *J Neurosci* 19:3701-3710.
- Chen H, Charlat O, Tartaglia LA, Woolf EA, Weng X, Ellis SJ, Lakey ND, Culpepper J, Moore KJ, Breitbart RE, Duyk GM, Tepper RI, Morgenstern JP. (1996) Evidence that the diabetes gene encodes the leptin receptor: identification of a mutation in the leptin receptor gene in db/db mice. *Cell* 84:491-5.
- Chiappinelli VA, Dryer SE. (1984) Nicotinic transmission in sympathetic ganglia: blockade by the snake venom neurotoxin kappa-bungarotoxin. *Neurosci Lett.* 50(1-3):239-44.
- Clement MV, Ramalingam J, Long LH, Halliwell B. (2001) The in vitro cytotoxicity of ascorbate depends on the culture medium used to perform the assay and involves hydrogen peroxide. *Antioxid Redox Signal* 3:157-163.
- Cohen-Cory S. (2002) The developing synapse: construction and modulation of synaptic structures and circuits. *Science* 298:770-776.

- Coleman DL. (1978) Obese and diabetes: two mutant genes causing diabetes-obesity syndromes in mice. *Diabetologia* 14:141–148.
- Conroy WG, Liu Z, Nai Q, Coggan JS, Berg DK. (2003) PDZ-containing proteins provide a functional postsynaptic scaffold for nicotinic receptors in neurons. *Neuron* 38:759–771.
- Conroy WG, Nai Q, Ross B, Naughton G, Berg DK. (2007) Postsynaptic neuroligin enhances presynaptic inputs at neuronal nicotinic synapses. *Dev Biol.* 307(1):79-91.
- Cooper E, Couturier S, Ballivet M. (1991) Pentameric structure and subunit stoichiometry of a neuronal nicotinic acetylcholine receptor. *Nature.* 350(6315):235-8.
- Cordero-Erausquin M, Marubio LM, Klink R, Changeux JP. (2000) Nicotinic receptor function: new perspectives from knockout mice. *Trends Pharmacol Sci* 21:211–217.
- Corringer PJ, Le Novère N, Changeux JP. (2000) Nicotinic receptors at the amino acid level. *Annu Rev Pharmacol Toxicol* 40:431–458.
- Couturier S, Bertrand D, Matter JM, Hernandez MC, Bertrand S, Millar N, Valera S, Barkas T, Ballivet M. (1990) A neuronal nicotinic acetylcholine receptor subunit( $\alpha$ 7) is developmentally regulated and forms a homo-oligomeric channel blocked by  $\alpha$ -BTX. *Neuron.* 5(6):847-56.
- Coyle JT, Puttfarcken P. (1993) Oxidative stress, glutamate, and neurodegenerative disorders. *Science* 262:689–695.
- Craig AM, Graf ER, Linhoff MW. (2006) How to build a central synapse: clues from cell culture. *Trends Neurosci.* 29:8–20.
- Craig AM, Kang Y. (2007) Neurexin-neuroligin signaling in synapse development. *Curr. Opin. Neurobiol.* 17:43–52.
- Crowley C, Spencer SD, Nishimura MC, Chen KS, Pitts-Meek S, Armanini MP, Ling LH, McMahon SB, Shelton DL, Levinson AD, Phillips HS. (1994) Mice lacking nerve growth factor display perinatal loss of sensory and sympathetic neurons yet develop basal forebrain cholinergic neurons. *Cell* 76:1001-1011.
- Cuevas J, Berg DK. (1998) Mammalian nicotinic receptors with  $\alpha$ 7 subunits that slowly desensitize and rapidly recover from  $\alpha$ -bungarotoxin blockade. *J Neurosci* 18:10335–10344.
- Cypess AM, et al. (2009) Identification and importance of brown adipose tissue in adult humans. *N Engl J Med.* 360:1509-17.

- Dani JA, Bertrand D. (2007) Nicotinic acetylcholine receptors and nicotinic cholinergic mechanisms of the central nervous system. *Annu Rev Pharmacol Toxicol.* 47:699-729.
- Dauer W, Przedborski S. (2003) Parkinson's disease: mechanisms and models. *Neuron* 39:889-909.
- Davis GW, DiAntonio A, Petersen SA, Goodman CS. (1998) Postsynaptic PKA controls quantal size and reveals a retro-grade signal that regulates presynaptic transmitter release in *Drosophila*. *Neuron* 20: 305-315.
- De Biasi M. (2002) Nicotinic mechanisms in the autonomic control of organ systems. *J Neurobiol* 53:568-579.
- De Koninck P, Cooper E. (1995) Differential regulation of neuronal nicotinic ACh receptor subunit genes in cultured neonatal rat sympathetic neurons: specific induction of  $\alpha 7$  by membrane depolarization through a  $Ca^{2+}$ /calmodulin-dependent kinase pathway. *J Neurosci.* 15(12):7966-78.
- Deutsch JA. (1971) The cholinergic synapse and the site of memory. *Science* 174:788-794.
- DiAntonio A, Petersen SA, Heckmann M, Goodman CS. (1999) Glutamate receptor expression regulates quantal size and quantal content at the *Drosophila* neuromuscular junction. *J Neurosci* 19: 3023-3032.
- Drisdell RC, Green WN. (2000) Neuronal  $\alpha$ -bungarotoxin receptors are  $\alpha 7$  subunit homomers. *J. Neurosci.* 20:133-139.
- Dröge W. (2002) Free radicals in the physiological control of cell function. *Physiol Rev* 82:47-95.
- Duby JJ, Campbell RK, Setter SM, White JR, Rasmussen, KA. (2004) Diabetic neuropathy: An intensive review. *Am J Health-Syst Pharm* 61:160-173.
- Dyck PJ, Kratz KM, Karnes JL, Litchy WJ, Klein R, Pach JM, Wilson DM, O'Brien PC, Melton LJ 3rd, Service FJ. (1993) The prevalence by staged severity of various types of diabetic neuropathy, retinopathy, and nephropathy in a population-based cohort: the Rochester Diabetic Neuropathy Study. *Neurology.* 43:817-24.
- Eiden LE. (1998) The cholinergic gene locus. *J Neurochem.* 70(6):2227-40.
- Erb C, Troost J, Kopf S, Schmitt U, Löffelholz K, Soreq H, Klein J. (2001) Compensatory mechanisms enhance hippocampal acetylcholine release in transgenic mice expressing human acetylcholinesterase. *J Neurochem* 77:638-646
- Erickson JD, Varoqui H, Schäfer MK, Modi W, Diebler MF, Weihe E, Rand J, Eiden LE, Bonner TI, Usdin TB. (1994) Functional identification of a vesicular

acetylcholine transporter and its expression from a "cholinergic" gene locus. *JBC* 269(35):21929-32.

Fagan AM, Zhang H, Landis S, Richard J, Smeyne RJ, Silos-Santiago I, Barbacid M. (1996) TrkA, but not TrkC, receptors are essential for survival of sympathetic neurons in vivo. *J Neurosci* 16: 6208–6218.

Feng G, Steinbach JH, Sanes JR. (1998) Rapsyn clusters neuronal acetylcholine receptors but is inessential for formation of an interneuronal cholinergic synapse. *J Neurosci*. 18(11):4166-76.

Fernandez HL, Moreno RD, Inestrosa NC. (1996) Tetrameric (G4) acetylcholinesterase: structure, localization, and physiological regulation. *J Neurochem*. Apr;66(4):1335-46.

Ferguson SM, Bazalakova M, Savchenko V, Tapia JC, Wright J, Blakely RD. (2004) Lethal impairment of cholinergic neurotransmission in hemicholinium-3-sensitive choline transporter knockout mice. *PNAS* 101:8762–8767.

Ferguson SM, Blakely RD. (2004) The choline transporter resurfaces: new roles for synaptic vesicles? *Mol Interv*. 4(1):22-37.

Ferguson SM, Savchenko V, Apparsundaram S, Zwick M, Wright J, Heilman CJ, Yi H, Levey AI, Blakely RD. (2003) Vesicular localization and activity-dependent trafficking of presynaptic choline transporters. *J. Neurosci*. 23:9697–9709.

Flavell SW, Greenberg ME. (2008) Signaling mechanisms linking neuronal activity to gene expression and plasticity of the nervous system. *Annu. Rev. Neurosci*. 31:563–590.

Forehand CJ. (1985) Density of somatic innervation on mammalian autonomic ganglion cells is inversely related to dendritic complexity and preganglionic convergence. *J Neurosci*. 5(12):3403-8.

Frank J, Flaccus A, Schwarz C, Lambert C, Biesalski HK. (2006) Ascorbic acid suppresses cell death in rat DS-sarcoma cancer cells induced by 5-aminolevulinic acid-based photodynamic therapy. *Free Radic Biol Med* 40:827–836.

From AM, Leibson CL, Bursi F, Redfield MM, Weston SA, Jacobsen SJ, Rodeheffer RJ, Roger VL. (2006) Diabetes in heart failure: prevalence and impact on outcome in the population. *Am. J. Med*. 119:591-599.

Gamper N, Oleg Zaika O, Yang Li Y, Martin P, Hernandez CC, Perez MC, Wang AYC, Jaffe DB, Shapiro MS. (2006) Oxidative modification of M-type K(+) channels as a mechanism of cytoprotective neuronal silencing. *EMBO J* 25:4996–5004.

Garner CC, Waites CL, Ziv NE. (2006) Synapse development: still looking for the forest, still lost in the trees. *Cell Tissue Res*. 326:249–262.

- Gautam M, Noakes PG, Moscoso L, Rupp F, Scheller RH, Merlie JP, Sanes JR. (1996) Defective neuromuscular synaptogenesis in agrin-deficient mutant mice. *Cell* 85:525–535.
- Gibbins IL, Morris JL. (2006) Structure of peripheral synapses: autonomic ganglia. *Cell Tissue Res.* 326(2):205-20.
- Gingras J, Rassadi S, Cooper E, Ferns M. (2002) Agrin plays an organizing role in the formation of sympathetic synapses. *JCB.* 158(6): 1109-18.
- Gingras J, Rassadi S, Cooper E, Ferns M. (2007) Synaptic transmission is impaired at neuronal autonomic synapses in agrin-null mice. *Dev Neurobiol.* 67(5):521-34.
- Giniatullin R, Nistri A, Yakel JL. (2005) Desensitization of nicotinic ACh receptors: shaping cholinergic signaling. *Trends Neurosci* 28:371–378.
- Glebova NO, Ginty DD. (2005) Growth and survival signals controlling sympathetic nervous system development. *Annu Rev Neurosci.* 28:191-222.
- Goldstein DS. (2003) Dysautonomia in Parkinson's disease: neurocardiological abnormalities. *Lancet Neurol* 2:669–676.
- Gotti C, Clementi F. (2004) Neuronal nicotinic receptors: from structure to pathology. *Prog Neurobiol.* 74(6):363-96.
- Gotti C, Zoli M, Clementi F. (2006) Brain nicotinic acetylcholine receptors: native subtypes and their relevance. *Trends Pharmacol Sci* 27:482–491.
- Goudou D, Verdier-Sahuque M, Rieger F. (1985) External and internal acetylcholinesterase in rat sympathetic neurones in vivo and in vitro. *FEBS* 186(1):54-8.
- Gray R, Rajan AS, Radcliffe KA, Yakehiro M, Dani JA. (1996) Hippocampal synaptic transmission enhanced by low concentrations of nicotine. *Nature* 383:713–716.
- Guo X, Lester RA. (2007) Regulation of nicotinic acetylcholine receptor desensitization by  $Ca^{2+}$ . *J Neurophysiol* 97:93–101.
- Haghighi AP, Cooper E. (2000) A molecular link between inward rectification and calcium permeability of neuronal nicotinic acetylcholine  $\alpha 3\beta 4$  and  $\alpha 4\beta 2$  receptors. *J Neurosci.* 20(2):529-41.
- Haghighi AP, Cooper E. (1998) Neuronal nicotinic acetylcholine receptors are blocked by intracellular spermine in a voltage-dependent manner. *J Neurosci.* 18(11):4050-62.
- Haghighi AP, McCabe BD, Fetter RD, Palmer JE, Hom S, Goodman CS. (2003) Retrograde control of synaptic transmission by postsynaptic CaMKII at the *Drosophila* neuromuscular junction. *Neuron* 39:255–267.

- Halliwell B. (2006) Oxidative stress and neurodegeneration: where are we now? *J Neurochem* 97:1634–1658.
- Hahm SH, Chen L, Patel C, Erickson J, Bonner TI, Weihe E, Schäfer MK, Eiden LE. (1997) Upstream sequencing and functional characterization of the human cholinergic gene locus. *J Mol Neurosci.* 9(3):223-36.
- He TC, Zhou S, da Costa LT, Yu J, Kinzler KW, Vogelstein B. (1998) A simplified system for generating recombinant adenoviruses. *Proc Natl Acad Sci USA* 95:2509–2514.
- Helekar SA, Char D, Neff S, Patrick J. (1994) Prolyl isomerase requirement for the expression of functional homo-oligomeric ligand-gated ion channels. *Neuron* 12:179–189.
- Huang EJ, Reichardt LF. (2003) Trk receptors: roles in neuronal signal transduction. *Annu Rev Biochem* 72:609–642.
- Ichinari K, Kakei M, Matsuoka T, Nakashima H, Tanaka H. (1996) Direct activation of the ATP-sensitive potassium channel by oxygen free radicals in guinea-pig ventricular cells: its potentiation by MgADP. *J Mol Cell Cardiol* 28:1867–1877.
- Imoto K, Busch C, Sakmann B, Mishina M, Konno T, Nakai J, Bujo H, Mori Y, Fukuda K, Numa S. (1998) Rings of negatively charged amino acids determine the acetylcholine receptor channel conductance. *Nature* 335:645–648.
- Iverson S, Iverson L, Saper C. (2000) The Autonomic Nervous System and the Hypothalamus. In Kandel ER, Schwartz JH, Jessel TM. (Eds.), *Principles of Neuroscience* 4<sup>th</sup> ed. McGraw-Hill: New York.
- Junod A, Lambert AE, Stauffacher W, Renold AE. (1969) Diabetogenic action of streptozotocin: relationship of dose to metabolic response. *J Clin Invest.* 48:2129-39.
- Karlin A. (2002) Emerging structure of the nicotinic acetylcholine receptors. *Nat Rev Neurosci* 3:102–114.
- Katz LC, Shatz CJ. (1996) Synaptic activity and the construction of cortical circuits. *Science* 274(5290):1133-8.
- Kim E, Sheng M. (2004) PDZ domain proteins of synapses. *Nat. Rev. Neurosci.* 5:771–781.
- Kirkland RA, Franklin JL. (2001) Evidence for redox regulation of cytochrome c release during programmed neuronal death: antioxidant effects of protein synthesis and caspase inhibition. *J Neurosci* 21:1949–1963.

- Kirkland RA, Adibhatla RM, Hatcher JF, Franklin JL. (2002) A Bax-induced pro-oxidant state is critical for cytochrome c release during programmed neuronal death. *J Neurosci* 22:6480–6490.
- Krishnaswamy A, Cooper E. (2009) An activity-dependent retrograde signal induces the expression of the high-affinity choline transporter in cholinergic neurons. *Neuron* 61(2):272-86.
- Kügler S, Kilic E, Bähr M. (2003) Human synapsin 1 gene promoter confers highly neuron-specific long-term transgene expression from an adenoviral vector in the adult rat brain depending on the transduced area. *Gene Ther.* 10:337–347.
- Lan CT, Wen CY, Tan CK, Ling EA, Shieh JH. (1995) Ultrastructural-identification of cholinergic neurons in the external cuneate nucleus of the gerbil: acetylcholinesterase histochemistry and choline acetyltransferase immunohistochemistry. *J. Neurocytol.* 24:838-852.
- Landmesser L, Dahm L, Schultz K, Rutishauser U. (1988) Distinct roles for adhesion molecules during innervation of embryonic chick muscle. *Dev. Biol.* 130:645–670.
- Lavolette SR, van der Kooy D. (2004) The neurobiology of nicotine addiction: bridging the gap from molecules to behaviour. *Nat Rev Neurosci* 5:55–65.
- Lecomte MJ, De Gois S, Guerci A, Ravassard P, Faucon Biguet N, Mallet J, Berrard S. (2005) Differential expression and regulation of the high-affinity choline transporter CHT1 and choline acetyltransferase in neurons of superior cervical ganglia. *Mol Cell Neurosci.* 28(2):303-13.
- Le Novère N, Corringer PJ, Changeux JP. (2002) The diversity of subunit composition in nAChRs: evolutionary origins, physiologic and pharmacologic consequences. *J Neurobiol.* 53(4):447-56.
- Lenzen S. (2008) The mechanisms of alloxan- and streptozotocin-induced diabetes. *Diabetologia* 51:216-26.
- Leonard S, Bertrand D. (2001) Neuronal nicotinic receptors: from structure to function. *Nicotine Tob Res.* 3(3):203-23.
- Letinsky MS. (1974) Physiological properties of developing frog tadpole nerve-muscle junctions during repetitive stimulation. *Dev. Biol.* 40:154–161.
- Levandoski MM, Lin Y, Moise L, McLaughlin JT, Cooper E, Hawrot E. (1999) Chimeric analysis of a neuronal nicotinic acetylcholine receptor reveals amino acids conferring sensitivity to alpha-bungarotoxin. *J Biol Chem.* 1999 274(37):26113-9.
- Li W, Ono F, Brehm P. (2003) Optical measurements of presynaptic release in mutant zebrafish lacking postsynaptic receptors. *J Neurosci* 23:10467–10474.

- Li Z, Sheng M. (2003) Some assembly required: the development of neuronal synapses. *Nat. Rev. Mol. Cell Biol.* 4:833–841.
- Liang S-D, Vizi ES. (1997) Positive feedback modulation of acetylcholine release from isolated rat superior cervical ganglion. *J Pharmacol Exp Ther* 280:650–655.
- Lichtman JW, Colman H. (2000) Synapse elimination and indelible memory. *Neuron* 25(2):269-78.
- Lichtman JW, Purves D. (1980) The elimination of redundant preganglionic innervation to hamster sympathetic ganglion cells in early post-natal life. *J Physiol.* 301:213-28.
- Lin MT, Beal MF. (2006) Mitochondrial dysfunction and oxidative stress in neurodegenerative diseases. *Nature* 443:787–795.
- Liu Y, Gutterman DD. (2002) The coronary circulation in diabetes: influence of reactive oxygen species on K<sup>+</sup> channel-mediated vasodilation. *Vascul Pharmacol* 38:43–49.
- Lorenzi M, Gerhardinger C. (2001) Early cellular and molecular changes induced by diabetes in the retina. *Diabetologia* 44 791-804.
- Loring RH, Sah DW, Landis SC, Zigmond RE. (1988) The ultrastructural distribution of putative nicotinic receptors on cultured neurons from the rat superior cervical ganglion. *Neuroscience* 24:1071–1080.
- MacDermott AB, Role LW, Siegelbaum SA. (1999) Presynaptic ionotropic receptors and the control of transmitter release. *Annu Rev Neurosci* 22:443–485.
- Mancuso M, Coppede F, Migliore L, Siciliano G, Murri L. (2006) Mitochondrial dysfunction, oxidative stress and neurodegeneration. *J Alzheimers Dis* 10:59–73.
- Mandelzys A, De Koninck P, Cooper E. (1995) Agonist and toxin sensitivities of ACh-evoked currents on neurons expressing multiple nicotinic ACh receptor subunits. *J Neurophysiol* 74:1212–1221.
- Mandelzys A, Pié B, Deneris ES, Cooper E. (1994) The developmental increase in ACh current densities on rat sympathetic neurons correlates with changes in nicotinic ACh receptor alpha-subunit gene expression and occurs independent of innervation. *J Neurosci.* 14(4):2357-64.
- Martinez-Murillo R, Villalba RM, Montero-Caballero MI, Rodrigo J. (1989) Cholinergic somata and terminals in the rat substantia nigra: An immunocytochemical study with optical and electron microscopic techniques. *J. Comp. Neurol.* 281:397–415.
- Maskos U, Molles BE, Pons S, Besson M, Guiard BP, Guilloux JP, Evrard A, Cazala P, Cormier A, Mameli-Engvall M, Dufour N, Cloez-Tayarani I, Bemelmans AP, Mallet J, Gardier AM, David V, Faure P, Granon S, Changeux JP. (2005)

Nicotine reinforcement and cognition restored by targeted expression of nicotinic receptors. *Nature* 436:103–107.

Mattson MP. (2004) Pathways towards and away from Alzheimer's disease. *Nature* 430:631–639.

McDonough J, Deneris E. (1997). Beta43': An enhancer displaying neural-restricted activity is located in the 3'-untranslated exon of the rat nicotinic acetylcholine receptor beta4 gene. *Journal of Neuroscience* 17:2273-2283.

McFarlane S, Cooper E. (1992) Postnatal development of voltage-gated K currents on rat sympathetic neurons. *J Neurophysiol* 67:1291–1300.

McGehee DS, Role LW. (1995) Physiological diversity of nicotinic acetylcholine receptors expressed by vertebrate neurons. *Annu Rev Physiol* 57:521–546.

Misgeld T, Burgess RW, Lewis RM, Cunningham JM, Lichtman JW, Sanes JR. (2002) Roles of neurotransmitter in synapse formation: development of neuromuscular junctions lacking choline acetyltransferase, *Neuron* 36: 635–648.

Møller M, Baeres FM. (2002) The anatomy and innervation of the mammalian pineal gland. *Cell Tissue Res.* 309(1):139-50.

Moser N, Mechawar N, Jones I, Gochberg-Sarver A, Orr-Urtreger A, Plomann M, Salas R, Molles B, Marubio L, Roth U, Maskos U, Winzer-Serhan U, Bourgeois JP, Le Sourd AM, De Biasi M, Schröder H, Lindstrom J, Maelicke A, Changeux JP, Wevers A. (2007) Evaluating the suitability of nicotinic acetylcholine receptor antibodies for standard immunodetection procedures. *J Neurochem.* 102(2):479-92.

Neff RA 3rd, Gomez-Varela D, Fernandes CC, Berg DK. (2009) Postsynaptic scaffolds for nicotinic receptors on neurons. *Acta Pharmacol Sin.* 30(6):694-701.

Nicholls DG, Budd SL. (2000) Mitochondria and neuronal survival. *Physiol Rev* 80:315–360.

Nja N, Purves D. (1977a) Specific innervation of guinea-pig superior cervical ganglion cells by preganglionic fibres arising from different levels of the spinal cord. *J. Physiol.* 264:565-583.

Nja N, Purves D. (1977b) Re-innervation of guineapig superior cervical ganglion cells by preganglionic fibres arising from different levels of the spinal cord. *J.Physiol.* 273:633-651.

Nyberg-Hoffman C, Shabram P, Li W, Giroux D, Aguilar-Cordova E. (1997) Sensitivity and reproducibility in adenoviral infectious titer determination. *Nat Med* 3:808–811.

Oda Y. (1999) Choline acetyltransferase: the structure, distribution and pathologic changes in the central nervous system. *Pathol Int.* 49(11):921-37.

- Okuda T, Haga T. (2003) High-affinity choline transporter. *Neurochem. Res.* 28:483–488.
- Okuda T, Haga T, Kanai Y, Endou H, Ishihara T, Katsura I. (2000) Identification and characterization of the high-affinity choline transporter. *Nat. Neurosci.* 3:3120–3125.
- Orasanu G, Plutzky J. (2009) The pathologic continuum of diabetic vascular disease. *Am Coll Cardiol.* 53 S35-42. (2009).
- Oshima S, Yamada K, Shirakawa T, Watanabe M. (2004) Changes of high-affinity choline transporter CHT1 mRNA expression during degeneration and regeneration of hypoglossal nerves in mice. *Neurosci Lett* 365:97–101.
- Park MK, Lee SH, Lee SJ, Ho WK, Earm YE. (1995) Different modulation of Ca-activated K channels by the intracellular redox potential in pulmonary and ear arterial smooth muscle cells of the rabbit. *Pflügers Arch* 430:308–314.
- Parker MJ, Zhao S, Brecht DS, Sanes JR, Feng G. (2004) PSD93 regulates synaptic stability at neuronal cholinergic synapses. *J Neurosci.* 24(2):378-88.
- Petersen SA, Fetter RD, Noordermeer JN, Goodman CS, DiAntonio A. (1997) Genetic analysis of glutamate receptors in *Drosophila* reveals a retrograde signal regulating presynaptic transmitter release. *Neuron* 19:1237–1248.
- Picciotto MR. (2003) Nicotine as a modulator of behavior: beyond the inverted U. *Trends Pharmacol Sci* 24:493–499.
- Picciotto MR, Caldarone BJ, Brunzell DH, Zachariou V, Stevens TR, King SL. (2001) Neuronal nicotinic acetylcholine receptor subunit knockout mice: physiological and behavioral phenotypes and possible clinical implications. *Pharmacol Ther* 92:89–108.
- Pilar G, Tuttle J, Vaca K. (1981) Functional maturation of motor nerve terminals in the avian iris: ultrastructure, transmitter metabolism and synaptic reliability. *J. Physiol.* 321:175–193.
- Polo-Parada L, Bose CM, Landmesser LT. (2001) Alterations in transmission, vesicle dynamics, and transmitter release machinery at NCAM-deficient neuromuscular junctions, *Neuron* 32:815–828.
- Polo-Parada L, Bose CM, Plattner F, Landmesser LT. (2004) Distinct roles of different neural cell adhesion molecule (NCAM) isoforms in synaptic maturation revealed by analysis of NCAM 180 kDa isoform-deficient mice. *J. Neurosci.* 24:1852–1864.
- Polo-Parada L, Plattner F, Bose C, Landmesser LT. (2005) NCAM 180 acting via a conserved C-terminal domain and MLCK is essential for effective transmission with repetitive stimulation. *Neuron* 46:917–931.

- Poole LB, Nelson KJ. (2008) Discovering mechanisms of signaling-mediated cysteine oxidation. *Curr Opin Chem Biol.* 12(1):18-24.
- Prado MA, Reis RA, Prado VF, de Mello MC, Gomez MV, de Mello FG. (2002) Regulation of acetylcholine synthesis and storage. *Neurochem Int.* 41(5):291-9.
- Purohit P, Mitra A, Auerbach A. (2007) A stepwise mechanism for acetylcholine receptor channel gating. *Nature* 446:930–933.
- Purves D, Lichtman JW. (1978) Formation and maintenance of synaptic connections in autonomic ganglia. *Physiol Rev.* 58(4):821-62.
- Purves D, Lichtman JW. (1980) Elimination of synapses in the developing nervous system. *Science.* 210:153-7.
- Purves D, Wigston DJ. (1983) Neural units in the superior cervical ganglion of the guinea-pig. *J Physiol.* 1983 Jan;334:169-78.
- Quick MW, Lester RA. (2002) Desensitization of neuronal nicotinic receptors. *J Neurobiol* 53:457–478.
- Rafuse VF, Polo-Parada L, Landmesser LT. (2000) Structural and functional alterations of neuromuscular junctions in NCAM-deficient mice. *J. Neurosci.* 20:6529–6539.
- Ramcharan EJ, Matthews MR. (1996) Autoradiographic localization of functional muscarinic receptors in the rat superior cervical sympathetic ganglion reveals an extensive distribution over non-synaptic surfaces of neuronal somata, dendrites and nerve endings. *Neuroscience* 71:797–832.
- Rassadi S, Krishnaswamy A, Pie B, McConnell R, Jacob MH, Cooper E. (2005) A null mutation for the alpha3 nicotinic acetylcholine (ACh) receptor gene abolishes fast synaptic activity in sympathetic ganglia and reveals that ACh output from developing preganglionic terminals is regulated in an activity-dependent retrograde manner. *J Neurosci* 25:8555–8566.
- Ribeiro FM, Black SA, Cregan SP, Prado VF, Prado MA, Rylett RJ, Ferguson SS. (2005) Constitutive high-affinity choline transporter endocytosis is determined by a carboxyl-terminal tail dileucine motif. *J. Neurochem.* 94:86–96.
- Ribeiro FM, Black SA, Prado VF, Rylett RJ, Ferguson SS, Prado MA. (2006) The “ins” and “outs” of the high-affinity choline transporter CHT1. *J. Neurochem.* 97:1–12.
- Rogers M, Sargent PB. (2003) Rapid activation of presynaptic nicotinic acetylcholine receptors by nerve-released transmitter. *Eur J Neurosci* 18:2946–2956.
- Role LW, Berg DK. (1996) Nicotinic receptors in the development and modulation of CNS synapses. *Neuron* 16:1077–1085.

- Role LW. (1992) Diversity in primary structure and function of neuronal nicotinic acetylcholine receptor channels. *Curr Opin Neurobiol* 2:254–262.
- Rosen ED, Spiegelman BM. (2006) Adipocytes as regulators of energy balance and glucose homeostasis. *Nature* 444:847-853.
- Rosenberg MM, Blitzblau RC, Olsen DP, Jacob MH. (2002) Regulatory mechanisms that govern nicotinic synapse formation in neurons. *J Neurobiol* 53:542–555.
- Rosenberg M, Pié B, Cooper E. (1997) Developing neonatal rat sympathetic and sensory neurons differ in their regulation of 5-HT<sub>3</sub> receptor expression. *J Neurosci*. 17:6629–6638.
- Rubin E. (1985a) Development of the rat superior cervical ganglion: ingrowth of preganglionic axons. *J Neurosci*. 5(3):685-96.
- Rubin E. (1985b) Development of the rat superior cervical ganglion: initial stages of synapse formation. *J Neurosci*. 5(3):697-704.
- Rubin E. (1985c) Development of the rat superior cervical ganglion: ganglion cell maturation. *J Neurosci*. 5(3):673-84.
- Ruit KG, Osborne PA, Schmidt RE, Johnson EM Jr, Snider WD. (1990) Nerve growth factor regulates sympathetic ganglion cell morphology and survival in the adult mouse. *J Neurosci*. 10:2412–19.
- Sanes JR, Lichtman JW. (2001) Induction, assembly, maturation and maintenance of a postsynaptic apparatus. *Nat Rev Neurosci*. 2(11):791-805.
- Sanes JR, Lichtman JW. (1999) Development of the vertebrate neuromuscular junction. *Annu Rev Neurosci* 22:389–442.
- Sargent PB. (1993) The diversity of neuronal nicotinic acetylcholine receptors. *Annu Rev Neurosci*. 16:403-43.
- Savitt JM, Dawson VL, Dawson TM. (2006) Diagnosis and treatment of Parkinson disease: molecules to medicine. *J Clin Invest* 116:1744–1754.
- Schmidt RE, Parvin CA, Green KG. (2008) Synaptic ultrastructural alterations anticipate the development of neuroaxonal dystrophy in sympathetic ganglia of aged and diabetic mice. *J Neuropathol Exp Neurol*. 67(12):1166-86.
- Schmidt RE. (1996) The neuropathology of human sympathetic autonomic ganglia. *Microscop Res Tech* 35:107-121.
- Schoch S, Deak F, Konigstorfer A, Mozhayeva M, Sara Y, Sudhof TC, Kavalali ET. (2001) SNARE function analyzed in synaptobrevin/VAMP knockout mice. *Science* 294:1117–1122.

- Sharma G, Vijayaraghavan S. (2003) Modulation of presynaptic store calcium induces release of glutamate and postsynaptic firing. *Neuron* 38:929–939.
- Sharma G, Grybko M, Vijayaraghavan S. (2008) Action potential-independent and nicotinic receptor-mediated concerted release of multiple quanta at hippocampal CA3-mossy fiber synapses. *J Neurosci.* 28(10):2563-75.
- Sher E, Chen Y, Sharples TJ, Broad LM, Benedetti G, Zwart R, McPhie GI, Pearson KH, Baldwinson T, De Filippi G. (2004) Physiological roles of neuronal nicotinic receptor subtypes: new insights on the nicotinic modulation of neurotransmitter release, synaptic transmission and plasticity. *Curr Top Med Chem* 4:283–297.
- Silver LM. (1995). *Mouse Genetics Concepts and Applications*. Oxford University Press, New York.
- Singh DK, Winocour P, Farrington K. (2008) Mechanisms of Disease: The hypoxic tubular hypothesis of diabetic nephropathy. *Nature Clinical Practice* 4 216-226.
- Skok VI. (2002) Nicotinic acetylcholine receptors in autonomic ganglia. *Auton Neurosci* 97:1–11.
- Smith LK, Carroll PT. (1993) Membrane-bound choline-O-acetyltransferase in rat hippocampal tissue is anchored by glycosyl-phosphatidylinositol. *Brain Res.* 605:155-163.
- Smith MA, Perry G, Richey PL, Sayre LM, Anderson VE, Beal MF, Kowall N. (1996) Oxidative damage in Alzheimer's. *Nature* 382:120–121.
- Smeyne RJ, Klein R, Schnapp A, Long LK, Bryant S, Lewin A, Lira SA, Barbacid M. (1994) Severe sensory and sympathetic neuropathies in mice carrying a disrupted *Trk/NGF* receptor gene. *Nature.* 364: 246-249.
- Snider WD. (1988) Nerve growth factor enhances dendritic arborization of sympathetic ganglion cells in developing mammals. *J. Neurosci.* 8:2628–34.
- Soreq H, Seidman S. (2001) Acetylcholinesterase--new roles for an old actor. *Nat Rev Neurosci.* 2(4):294-302.
- Spiegelman BM, Flier JS. (1996) Adipogenesis and obesity: rounding out the big picture. *Cell* 87:377–389.
- Sudhof TC. (2004) The synaptic vesicle cycle. *Annu Rev Neurosci*;27:509-47.
- Swope SL, Qu Z, Huganir RL. (1995) Phosphorylation of the nicotinic acetylcholine receptor by protein tyrosine kinases. *Ann NY Acad Sci* 757:197–214.

Tang XD, Garcia ML, Heinemann SH, Hoshi T. (2004) Reactive oxygen species impair Slo1 BK channel function by altering cysteine-mediated calcium sensing. *Nat Struct Mol Biol* 11:171–178.

Tao HW, Poo M. (2001) Retrograde signaling at central synapses. *Proc Natl Acad Sci USA* 98:11009–11015.

Tapper AR, McKinney SL, Nashmi R, Schwarz J, Deshpande P, Labarca C, Whiteaker P, Marks MJ, Collins AC, Lester HA. (2004) Nicotine activation of  $\alpha 4^*$  receptors: sufficient for reward, tolerance, and sensitization. *Science* 306:1029–1032.

Temburni MK, Blitzblau RC, Jacob MH. (2000) Receptor targeting and heterogeneity at interneuronal nicotinic cholinergic synapses in vivo. *J Physiol* 525(1):21-9.

Tomlinson DR, Gardiner NJ. (2008) Glucose neurotoxicity. *Nat. Rev. Neurosci.* 9:36-45.

Toonen RF, de Vries KJ, Zalm R, Südhof TC, Verhage M. (2005). Munc18-1 stabilizes syntaxin 1, but is not essential for syntaxin 1 targeting and SNARE complex formation. *J Neurochem.* 93(6):1393-400.

Triana-Baltzer GB, Liu Z, Berg DK. (2006) Pre- and postsynaptic actions of L1-CAM in nicotinic pathways. *Mol Cell Neurosci.* 33(2):214-26.

Triana-Baltzer GB, Liu Z, Gounko NV, Berg DK. (2008) Multiple cell adhesion molecules shaping a complex nicotinic synapse on neurons. *Mol Cell Neurosci.* 39(1):74-82.

Tuček S. (1978) *Acetylcholine Synthesis in Neurons*. Halstead Press, New York.

Turrigiano GG, Nelson SB. (2004) Homeostatic plasticity in the developing nervous system. *Nat Rev Neurosci* 5:97–107.

Ullian EM, McIntosh JM, Sargent PB. (1997) Rapid synaptic transmission in the avian ciliary ganglion is mediated by two distinct classes of nicotinic receptors. *J Neurosci* 17: 7210–7219.

Unwin N. (2005) Refined structure of the nicotinic acetylcholine receptor at 4 Å resolution. *J Mol Biol* 346:967–989.

Usdin TB, Eiden LE, Bonner TI, Erickson JD. (1995) Molecular biology of the vesicular ACh transporter. *Trends Neurosci.* 18(5):218-24.

van Marken Lichtenbelt WD, et al. (2009) Cold-activated brown adipose tissue in healthy men. *N Engl J Med.* 360:1500-8.

Varoqueaux F, Sigler A, Rhee J, Brose N, Enk C, Reim K, Rosenmund C. (2002) Total arrest of spontaneous and evoked synaptic transmission but normal

synaptogenesis in the absence of munc13-mediated vesicle priming. *Proc. Natl. Acad. Sci. USA* 99:9037–9042.

Varoquaux F, Sons MS, Plomp JJ, Brose N. (2005) Aberrant morphology and residual transmitter release at the Munc13-deficient mouse neuromuscular synapse. *Mol. Cell. Biol.* 25:5973–5984.

Varoqui H, Diebler MF, Meunier FM, Rand JB, Usdin TB, Bonner TI, Eiden LE, Erickson JD. (1994) Cloning and expression of the vesamicol binding protein from the marine ray *Torpedo*. Homology with the putative vesicular acetylcholine transporter UNC-17 from *Caenorhabditis elegans*. *FEBS Lett.* 342(1):97-102.

Verhage M, Maia AS, Plomp JJ, Brussaard AB, Heeroma JH, Vermeer H, Toonen RF, Hammer RE, van den Berg TK, Missler M, Geuze HJ, Thomas C, Sudhof TC. (2000) Synaptic assembly of the brain in the absence of neurotransmitter secretion. *Science* 287:864–869.

Vernino S, Sandroni P, Singer W, Low PA. (2008) Autonomic ganglia: target and novel therapeutic tool. *Neurology*. 70(20):1926-32.

Vernino S, Ermilov LG, Sha L, Szurszewski JH, Low PA, Lennon VA, (2004) Passive transfer of autoimmune autonomic neuropathy to mice. *J. Neurosci.* 24:7037–7042.

Vernino S, Hopkins S, Wang Z. (2009) Autonomic ganglia, acetylcholine receptor antibodies, and autoimmune ganglionopathy. *Auton Neurosci.* 146(1-2):3-7.

Vernino S, Low PA, Lennon VA. (2003) Experimental autoimmune autonomic neuropathy. *J. Neurophysiol.* 90:2053–2059.

Vincent AM, McLean LL, Backus C, Feldman EL. (2005) Short-term hyperglycemia produces oxidative damage and apoptosis in neurons. *FASEB J* 19:638–640.

Vinik AI, Ziegler D. (2007) Diabetic cardiovascular autonomic neuropathy. *Circulation.* 115(3):387-97.

Vinik AL, Freeman R, Erbas T. (2003) Diabetic autonomic neuropathy. *Semin Neurol* 23:365–372.

Virtanen KA, Lidell ME, Orava J, Heglind M, Westergren R, Niemi T, Taittonen M, Laine J, Savisto NJ, Enerbäck S, Nuutila P. (2009) Functional brown adipose tissue in healthy adults. *N Engl J Med.* Apr 9;360(15):1518-25.

Volpicelli-Daley LA, Hrabovska A, Duysen EG, Ferguson SM, Blakely RD, Lockridge O, Levey AI. (2003) Altered striatal function and muscarinic cholinergic receptors in acetylcholinesterase knockout mice. *Mol Pharmacol* 64:1309–1316

Voyvodic JT. (1987) Development and regulation of dendrites in the rat superior cervical ganglion. *J Neurosci.* 7(3):904-12.

- Voyvodic JT. (1989) Peripheral target regulation of dendritic geometry in the rat superior cervical ganglion. *J Neurosci.* 9(6): 1997-2010.
- Wada E, Wada K, Boulter J, Deneris E, Heinemann S, Patrick J, Swanson LW. (1989) Distribution of alpha 2, alpha 3, alpha 4, and beta 2 neuronal nicotinic receptor subunit mRNAs in the central nervous system: a hybridization histochemical study in the rat. *J Comp Neurol* 284:314–335.
- Waites CL, Craig AM, Garner CC. (2005) Mechanisms of vertebrate synaptogenesis. *Annu Rev Neurosci.* 28:251-74.
- Wang B, Yang L, Wang Z, Zheng H. (2007) Amyloid precursor protein mediates presynaptic localization and activity of the high-affinity choline transporter. *Proc. Natl. Acad. Sci. USA* 104:14140–14145.
- Wang N, Orr-Urtreger A, Korczyn AD. (2002) The role of neuronal nicotinic acetylcholine receptor subunits in autonomic ganglia: lessons from knockout mice. *Prog Neurobiol* 68:341–360.
- Wang H-S, Pan Z, Shi W, Brown BS, Wymore R, Cohen IS, Dixon JE, McKinnon D (1998) KCNQ2 and KCNQ3 potassium channel subunits: molecular correlates of the M-channel. *Science* 282:1890-1893.
- Wang Z, Low PA, Jordan J, Freeman R, Gibbons CH, Schroeder C, Sandroni P, Vernino S. (2007) Autoimmune autonomic ganglionopathy: IgG effects on ganglionic acetylcholine receptor current. *Neurology.* 68(22):1917-21.
- Washbourne P, Thompson PM, Carta M, Costa ET, Mathews JR, López-Bendito G, Molnár Z, Becher MW, Valenzuela CF, Partridge LD, Wilson MC. (2002) Genetic ablation of the t-SNARE SNAP-25 distinguishes mechanisms of neuroexocytosis. *Nat Neurosci* 5:19–26.
- Weihe E, Schäfer MK, Schütz B, Anlauf M, Depboylu C, Brett C, Chen L, Eiden LE. (1998) From the cholinergic gene locus to the cholinergic neuron. *J Physiol Paris.* 92(5-6):385-8.
- Westerfield M, Liu DW, Kimmel CB, Walker C. (1990) Pathfinding and synapse formation in a zebrafish mutant lacking functional acetylcholine receptors. *Neuron* 4:867–874.
- Wheeler DG, Cooper E. (2004) Weak synaptic activity induces ongoing signaling to the nucleus that is enhanced by BDNF and suppressed by low-levels of nicotine. *Mol. Cell. Neurosci.* 26:50–62.
- Wheeler DG, Cooper E. (2001) Depolarization strongly induces human cytomegalovirus major immediate-early promoter/enhancer activity in neurons. *J Biol Chem* 276:31978–31985.
- Winston N, Vernino S. (2009) Autoimmune autonomic ganglionopathy. *Front Neurol Neurosci.* 26:85-93.

- Williams BM, Temburni MK, Levey MS, Bertrand S, Bertrand D, Jacob MH. (1998) The long internal loop of the  $\alpha 3$  subunit targets nAChRs to subdomains within individual synapses on neurons in vivo. *Nat, Neurosci* 1:557–562.
- Wu D, Hersh LB. (1994) Choline acetyltransferase: celebrating its fiftieth year. *J Neurochem.* 62(5):1653-63.
- Wu D, Hersh LB. (1995) Identification of an active site arginine in rat choline acetyltransferase by alanine scanning mutagenesis. *J Biol Chem* 270(49):111-6.
- Xu W, Gelber S, Orr-Urtreger A, Armstrong D, Lewis RA, Ou CN, Patrick J, Role L, De Biasi M, Beaudet AL. (1999a) Megacystis, mydriasis, and ion channel defect in mice lacking the alpha3 neuronal nicotinic acetylcholine receptor. *PNAS* 96(10):5746-51.
- Xu W, Orr-Urtreger A, Nigro F, Gelber S, Sutcliffe CB, Armstrong D, Patrick JW, Role LW, Beaudet AL, De Biasi M. (1999b) Multiorgan autonomic dysfunction in mice lacking the beta2 and the beta4 subunits of neuronal nicotinic acetylcholine receptors. *J Neurosci.* 19(21):9298-305.
- Xu X, Scott MM, Deneris ES. (2006) Shared long-range regulatory elements coordinate expression of a gene cluster encoding nicotinic receptor heteromeric subtypes. *Mol Cell Biol.* 26(15):5636-49.
- Yip JW. (1987) Target cues are not required for the guidance of sympathetic preganglionic axons. *Brain Res.* 429(1):155-9.
- Yip JW. (1990) Identification of location and timing of guidance cues in sympathetic preganglionic axons of the chick. *J Neurosci.* 10(7):2476-84.
- Zhang Y, Proenca R, Maffei M, Barone M, Leopold L, Friedman JM. (1994) Positional cloning of the mouse obese gene. *Nature* 372:425–431.
- Zhang Z, Coggan J, Berg DK. (1996) Synaptic currents generated by neuronal acetylcholine receptors sensitive to alpha-bungarotoxin. *Neuron* 17:1231–1240.
- Ziegler D. (2008) Painful diabetic neuropathy: treatment and future aspects. *Diabetes. Metab. Res. Rev.* 24 52-7.
- Ziv NE, Garner CC. (2004) Cellular and molecular mechanisms of presynaptic assembly. *Nat Rev Neurosci.* 5(5):385-99.
- Zoli M, Moretti M, Zanardi A, McIntosh MJ, Clementi F, Gotti C. (2002) Identification of the nicotinic receptor subtypes expressed on dopaminergic terminals in the rat striatum. *J Neurosci* 22:8785–8789.

**APPENDIX:**

**ENGINEERING NEURONAL NICOTINIC ACETYLCHOLINE RECEPTORS  
WITH FUNCTIONAL SENSITIVITY TO  $\alpha$ -BUNGAROTOXIN: A NOVEL  
 $\alpha$ 3-KNOCK-IN MOUSE**



**Engineering neuronal nicotinic acetylcholine receptors with functional sensitivity to  $\alpha$ -bungarotoxin: A novel  $\alpha$ 3-knock-in mouse**



Journal:	<i>European Journal of Neuroscience</i>
Manuscript ID:	EJN-2009-05-15497
Manuscript Type:	Research Report
Date Submitted by the Author:	17-May-2009
Complete List of Authors:	Caffery, Philip; Brown University, Molecular Pharmacology, Physiology, and Biotechnology Krishnaswamy, Arjun; McGill University, Physiology Sanders, Tanya; Brown University, Molecular Pharmacology, Physiology, and Biotechnology Hartlaub, Hilary; Brown University, Molecular Pharmacology, Physiology, and Biotechnology Liu, Jing; Brown University, Molecular Pharmacology, Physiology, and Biotechnology Klysik, Jan; Brown University, Molecular Biology, Cell Biology & Biochemistry Cooper, Ellis; McGill University, Physiology Hawrot, Edward; Brown University, Molecular Pharmacology, Physiology, and Biotechnology
Key Words:	acetylcholine, superior cervical ganglion, trafficking, clustering, autonomic



Proposed Journal Section: Synaptic Mechanisms  
Nomination for Associate Editor: Christophe Mulle

## **Engineering neuronal nicotinic acetylcholine receptors with functional sensitivity to $\alpha$ -bungarotoxin: A novel $\alpha$ 3-knock-in mouse**

Philip M. Caffery<sup>1\*</sup>, Arjun Krishnaswamy<sup>2\*</sup>, Tanya Sanders<sup>1</sup>, Hilary Hartlaub<sup>1</sup>,  
Jing Liu<sup>1</sup>, Jan Klysik<sup>3</sup>, Ellis Cooper<sup>2</sup>, and Edward Hawrot<sup>1</sup>

<sup>1</sup>Department of Molecular Pharmacology, Physiology & Biotechnology  
Brown University, Providence, RI

<sup>2</sup>Department of Physiology, McGill University, Montreal, Quebec, Canada

<sup>3</sup>Department of Molecular Biology, Cell Biology & Biochemistry  
Brown University, Providence, RI

\*These authors contributed equally to this work

Correspondence should be addressed to Dr. Edward Hawrot, Department of Molecular Pharmacology, Physiology & Biotechnology, Brown University, Box G-E336, Providence, RI 02912-G. Email: Edward\_Hawrot@Brown.edu

Total number of pages: 39

Total number of figures: 5

Total number of tables: 2

Total number of equations: 0

Total number of words: (i) manuscript, 9379; (ii) abstract, 243; (iii) introduction, 483

Running title: A knock-in mouse with  $\alpha$ -BTX-sensitive  $\alpha$ 3 nAChRs

Keywords: acetylcholine; superior cervical ganglion; trafficking; autonomic

## Abstract

As new approaches are needed for investigating the physiological roles of heteromeric neuronal nicotinic acetylcholine receptors, we report here the construction of a novel knock-in mouse expressing chimeric  $\alpha 3$  nAChR subunits with pharmacological sensitivity to  $\alpha$ -bungarotoxin ( $\alpha$ BTX) block. Sensitivity to  $\alpha$ BTX was generated by substituting five amino acids in the loop C ( $\beta 9$ - $\beta 10$ ) region of the mouse  $\alpha 3$  subunit with the corresponding residues from the  $\alpha 1$  subunit of the muscle type receptor from *Torpedo californica*. The expression of  $\alpha 3[5]$  subunits was characterized in the superior cervical ganglia (SCG) of homozygous knock-in mice, where postsynaptic  $\alpha 3$ -containing nAChR clusters could now, for the first time, be directly visualized by live-staining with rhodamine-conjugated  $\alpha$ BTX. The  $\alpha$ BTX-labeled puncta colocalized with a marker for synaptic varicosities and persisted following *in vivo* deafferentation, consistent with the predicted postsynaptic localization of ganglionic nAChRs. Compound action potentials and excitatory postsynaptic potentials recorded from SCG of mice homozygous for  $\alpha 3[5]$  were abolished by 100 nM  $\alpha$ BTX, even in an  $\alpha 7$  null background, demonstrating that synaptic throughput in the SCG is completely dependent on a functional  $\alpha 3$ -subunit. In addition, we observed that the genetic background of various inbred and outbred mouse lines greatly affects the surface expression of  $\alpha 3[5]$ -nAChRs, suggesting a powerful new approach for exploring the molecular mechanisms underlying receptor assembly and trafficking. As similar approaches can be used for introducing  $\alpha$ BTX-sensitivity into other nicotinic receptor subunits normally insensitive to  $\alpha$ BTX, the findings described here should be applicable to many other receptors.

## Introduction

Multiple nicotinic acetylcholine receptor (nAChR) subtypes populate the peripheral and central nervous systems of vertebrates. At present, 5 neuromuscular nicotinic subunits ( $\alpha 1$ ,  $\beta 1$ ,  $\gamma$ ,  $\delta$ , and  $\epsilon$ ) and 12 neuronal nicotinic subunits ( $\alpha 2$ - $\alpha 10$  and  $\beta 2$ - $\beta 4$ ) have been identified and cloned (Karlin, 2002; Colquhoun et al., 2003). Unlike muscle-type nAChRs, which are constrained to a single pentameric arrangement in adult tissue, neuronal nAChRs can assemble with varied subunit compositions and stoichiometries, resulting in an undetermined number of receptor isoforms (McGehee and Role, 1995; Role and Berg, 1996; Hogg et al., 2003). Alterations in nicotinic receptor function are thought to contribute to the pathological mechanisms underlying a wide range of neurological and psychiatric disorders, including Alzheimer's disease, Parkinson's disease, schizophrenia, epilepsy, and drug addiction. Yet the relationship between the subunit composition of most neuronal nAChR isoforms and their physiological roles *in vivo* remains unclear (Gotti et al., 2006; Hogg and Bertrand, 2007).

Neuronal nAChRs containing the  $\alpha 3$  subunit mediate fast excitatory neurotransmission in both sympathetic and parasympathetic autonomic ganglia in mammals (Mandelzys et al., 1995; Perry et al., 2002; Rassadi et al., 2005). Of all the neuronal nAChR genes,  $\alpha 3$  is the only single subunit that produces a lethal phenotype when deleted in inbred mice (Xu et al., 1999; Krishnaswamy and Cooper, 2009). There is also evidence which suggests that  $\alpha 3$ -containing receptors are expressed in select regions of the central nervous system, including the medial habenula, pineal gland, interpeduncular nucleus, dorsal horn of the spinal cord, hypothalamus, cerebellum, locus coeruleus, inferior colliculus, and

hippocampus (Sudweeks and Yakel, 2000; Yeh et al., 2001; Perry et al., 2002; Whiteaker et al., 2002; Liu et al., 2003; Hernandez et al., 2004; Turner and Kellar, 2005).

Previous heterologous expression studies in our lab using *Xenopus* oocytes demonstrated that the  $\alpha 3$  neuronal nAChR subunit can be mutated into a  $\alpha$ BTX-sensitive form by substituting from one to five amino acids in the loop C region of the  $\alpha 3$  subunit with the corresponding residues from the  $\alpha 1$  subunit of *Torpedo californica* (Levandoski et al., 1999). In the oocyte expression system, these chimeric  $\alpha 3$ -containing nAChRs exhibited  $EC_{50}$  values for ACh ranging from 50-500  $\mu$ M and  $IC_{50}$  values for block by  $\alpha$ BTX ranging from 20-200 nM, depending on (1) the specific amino acid substituted, (2) the total number of residues mutated, and (3) whether  $\beta 2$  or  $\beta 4$  was co-expressed. These studies led us to hypothesize that minimally mutated  $\alpha$ BTX-sensitive  $\alpha 3$  nAChR subunits could be utilized as part of a knock-in strategy for the study of  $\alpha 3$ -containing neuronal nAChRs *in vivo*. Toward this goal, a gene-targeting vector was designed to introduce five mutations in the mouse  $\alpha 3$  nAChR subunit: Y184W, E187W, I188V, K189Y, and N191T (*Torpedo* numbering) (Levandoski et al., 1999). Here we report that these mutations have been introduced into the genome of mouse ES cells using gene replacement technology and that functional,  $\alpha$ BTX-sensitive  $\alpha 3[5]$ -containing nAChRs can be studied and characterized in SCG neurons.

## Materials and Methods

*Preparation of the  $\alpha 3[5]$  targeting construct.* A gene-targeting vector containing genomic, mouse  $\alpha 3$  nAChR DNA and a neomycin-resistance cassette in pBluescript SK (-) (Stratagene, La Jolla, CA) was the generous gift of Dr. Changhai Cui, Salk Institute.

The genomic DNA sequence in this construct included exonV of the CHRNA3 gene along with ~2,000 to 3,000 of flanking, homologous nucleotides. PCR-based mutagenesis (QuikChange XL, Stratagene) was used to generate two alterations in the targeting vector. First, seven nucleotides were altered to produce the  $\alpha 3[5]$  substitutions in the  $\alpha 3$  gene product (YKHEIKYN toWKHWVYYT), along with a *Bst*Z17I restriction enzyme cleavage site. Mutagenic PCR primers were designed according to the guidelines in the QuikChange technical manual: forward (5'-GCCATCATTAAAGCCCCGGGCTGGAAACATTGGGTAT ACTACACCTGCTGT GAGGAGATCTACC-3') and reverse (5'-GGTAGATCTCCTCACAGCAGGTGTAGT ATACCCAATGTTTCCAGCC CGGGGCTTTAATGATGGC-3'). Positive clones were identified by a restriction analysis using *Bst*Z17I.

Second, a 57 nucleotide region containing a Cre-recombinase recognition sequence (*loxP*) positioned just 5' to exonV in the original targeting vector was removed. The sequences of the mutagenic primers used for the *loxP* removal were as follows: forward (5'-GGTGATAAGTGTGGCAAATTATGTGCC AGCAGAGGCGGG GGTGGTGG TGGTGAATAACCAATGTGGG-3') and reverse (5'-CCCACATTGGTTATTC ACCACCACCACCCCGCCTCTGCTGGCACAT AATTGCCCACTTATCACC-

3'). Positive clones were identified by standard PCR methods. Plasmid DNA was isolated using Mini or Maxi Plasmid Kits (Qiagen).

*Gene targeting in embryonic stem (ES) cells.* AB2.2 ES cells derived from a 129S7 male embryo were grown on mitotically inactive SNL76/7 cells and used for targeting. Ten million ES cells were electroporated with 25  $\mu$ g of  $\alpha$ 3[5] targeting vector linearized with *SalI*, and G418 selection was initiated after 24 h. One-hundred and ninety-two neomycin resistant clones were selected for further analysis. Correctly targeted ES cell clones were identified as described (Ramirez-Solis et al., 1995).

*Generation of mice.* All breeding and procedures were carried out according to approved institutional procedures at Brown University Animal Facility and in agreement with the NIH Guide for the Use and Care of Laboratory Animals. The targeted ES cells were grown to 90% confluence and trypsinized before injection. E3.5 blastocysts were derived from C57BL/6-*Tyr<sup>c-Brd</sup>* female mice and injected with 12-20 ES cells. The injected blastocysts were implanted into the uteri of day 2.5 pseudo-pregnant females for generation of chimeras. About 8-10 injected embryos were implanted per uterine horn. The resulting male chimeras were mated with C57BL/6-*Tyr<sup>c-Brd</sup>* females to obtain F1 progeny. Thus, the strain carrying the germ line transmitted  $\alpha$ 3[5] allele (designated *Chrna3<sup>tm1.0Hwrt</sup>*) (Fig. 1A) was obtained and initially maintained on a mixed C57BL/6-129S7 background. To obtain mutant mice carrying  $\alpha$ 3[5] with Neo cassette deleted (allele designated *Chrna3<sup>tm1.1Hwrt</sup>*), heterozygous *Chrna3<sup>tm1.0Hwrt/+</sup>* mutants were mated with 129S1-*Hprt1<sup>tm1(cre)Mnn</sup>/J* mice (The Jackson Laboratory, Bar Harbor, ME) and the

offspring were screened for the presence of the  $\alpha 3[5]$  mutations and for the deletion of Neo ( $Chrna3^{tm1.1Hwrt/+}$  mice). Congenic mice were generated by 10 consecutive backcrosses of  $Chrna3^{tm1.1Hwrt/+}$  to wild-type C57BL/6 mice. To obtain  $Chrna3^{tm1.1Hwrt/tm1.1Hwrt} Chrna7^{tm1Bay/tm1Bay}$  double homozygous animals ( $\alpha 3[5]$ -homozygous  $\alpha 7(-/-)$ ),  $Chrna3^{tm1.1Hwrt/+}$  animals were mated with  $Chrna7^{tm1Bay/tm1Bay}$  mice (B6.129S7- $Chrna7^{tm1Bay}/J$ ; the Jackson Laboratory, Bar Harbor, ME) and double heterozygous mice were selected. In the next step  $Chrna3^{tm1.1Hwrt/+} Chrna7^{tm1Bay/+}$  animals were intercrossed and screened for  $Chrna3^{tm1.1Hwrt/+} Chrna7^{tm1Bay/tm1Bay}$ . In the final step,  $Chrna3^{tm1.1Hwrt/+} Chrna7^{tm1Bay/tm1Bay}$  and  $Chrna3^{tm1.1Hwrt/+} Chrna7^{tm1Bay/+}$  animals were intercrossed and offspring selected for  $Chrna3^{tm1.1Hwrt/tm1.1Hwrt} Chrna7^{tm1Bay/tm1Bay}$ .

*Southern blot analysis.* ES cell clones and transgenic animals were screened for the knock-in allele using Southern blot analysis. The Southern strategy utilized a *KpnI* restriction cleavage site in the targeting construct. Digestion with *KpnI* was expected to produce 17.4 kb fragment from the wild-type allele, and 8.9 kb and 10.5 kb fragment in the case of the mutated allele. Two 0.6 kb nucleotide probes were designed to anneal outside of the targeted region of *Chrna3*. The Southern probes were generated by PCR, purified using QIAquick PCR Purification Kit (Qiagen). The probes were labeled with  $^{32}\text{P}$ -dCTP by the random primer labeling method according to the manufacturer's protocol in the Megaprime DNA Labeling Systems (Amersham, GE Healthcare Biosciences). *KpnI* digested genomic DNA (10-15  $\mu\text{g}$  /sample) from ES cell clones or transgenic animals was separated by agarose gel electrophoresis (1% gel; run at 50V for 16 h) and transferred to a nylon membrane, Hybond-XL (Amersham, GE Healthcare

Biosciences), by the capillary blotting method. Southern hybridizations were performed using standard protocols.

*Animals.* Mice were housed in Brown University Animal Care Facility and McGill University Animal Resource Center mouse rooms. Routine cage maintenance, including feeding and watering, was performed by the animal facility staff. Mice were maintained on a 12 hour light/dark cycle. Mating cages were typically set up with one male and one female. Pups were weaned at 21 days. Tail biopsies were used as tissue sources for DNA extraction and genotyping. All survival surgeries were performed using sterile procedures within the animal care facility mouse rooms. In cases in which euthanasia was necessary, mice were asphyxiated with CO<sub>2</sub> according to Brown University's policy on the "Use of CO<sub>2</sub> as a Euthanasia Agent for Small Laboratory Animals" and guidelines established by the Canadian Council on Animal Care.

*Genotyping.* Pups were screened using two PCR-based strategies. The first method screened directly for the wild-type or recombinant allele using the following forward primers: GCTGGAAACATTGGGTATACTACACC specific for the knock-in allele and GGCTACAAACATGAAATCAAGTACAACCTGC specific for the wild-type allele. The same reverse primer positioned 400 bp downstream of the targeted region CCGTAGAAGTTCCTCGTCTTTGGG was used in both reactions. "Triple-Master PCR System" (Eppendorf, Hamburg, DE) was used for all PCR-based screens.

The second PCR-based method for genotyping the  $\alpha 3[5]$ -containing allele utilized a *Bst*Z17I restriction site in the mutated region. The digestion-based PCR screen amplified a ~650 bp product with an internal restriction site. A forward primer GTGACCTACTTCCCGTTTGACTACC was designed to anneal ~250 bp upstream of the mutated region. The reverse primer CCGTAGAAGTTCCTCGTCTTTGGG was placed ~400 bp downstream of the targeted region. The PCR products were subjected to restriction digestion using *Bst*Z17I (NE Biolabs, Ipswich, MA) and agarose gel electrophoresis (2% gels). Reaction products from wild-type alleles were resistant to digestion, whereas PCR products from heterozygous or homozygous mutants were partially or completely digested with *Bst*Z17I, respectively.

Primers GGATCTCCTGTCATCTCACCTTGCT and ATCCTGATCGACAAGACCGGCTTC were used to identify mice positive for the Neo cassette. Primers CTTGTCCATCGTCATCACAGTCT TTGTG and GAGTCTAATTTTCTAACCTCTGCCCTATGC were used to identify mice negative for Neo.

Primers TGCTGTTTCACTGGTT GTGCGGCG and TGCCTTCTCTACACCTGCGGTGCT were used to identify mice positive for the Cre-recombinase expression cassette. Primers CCTGATTTTATTTCTATAGGACTGAAAGAC and TAAGTAATTATACTTACACAGTAGCTC TTC were used to identify mice negative for Cre.

The *Chrna7*<sup>tm1Bay</sup> allele in  $\alpha 7$  knockout mice (B6.129S7-*Chrna7*<sup>tm1Bay</sup>/J) was detected by PCR as recommended by the Jackson Laboratory (Bar Harbor, ME) using primers IMR1002, IMR1003 and IMR1004.

*Reverse-transcriptase PCR.* SCG tissue from wild-type and knock-in mice was dissected and placed immediately into ice-cold RNA-later solution (Ambion, Austin, TX) and stored at 4° overnight. RNA isolation was performed using RNAqueous-4PCR (Ambion) according to the manufacturer's protocol. In brief, SCG tissue was disrupted in 500  $\mu$ l of lysis/binding buffer using a 1 ml Potter-Elvehjem tissue grinder (Kontes, Vineland, NJ). DNase I treatment was performed by adding 7  $\mu$ l of 10X DNase buffer to 1  $\mu$ l of DNase. To precipitate the RNA, 2.5 volumes of 100% EtOH were added, and the mixture was stored overnight at -20°C. The pellet was resuspended in 12  $\mu$ l of RNase-free H<sub>2</sub>O. Total RNA concentration was measured by UV absorbance using a NanoDrop spectrophotometer (NanoDrop Technologies, Wilmington, DE). Reverse transcriptase (RT) reactions were performed using the RETROscript Kit (Ambion, Austin, TX) according to manufacturer's protocol for 2-step RT-PCR without heat denaturation of RNA. 0.4-1  $\mu$ g of total RNA was used per RT reaction. Random primers were used for all RT reactions. PCR primer pairs were designed to generate ~480 bp products from wild-type and mutant cDNA templates. If genomic DNA was present and amplified, ~8500 bp PCR products would be expected. A wild-type forward primer (CATCCAGTTTGAGGTGTCTATGTCTCAG) was designed to anneal within exon II of mouse *Chrna3*. Mutant and wild-type allele-specific reverse primers were designed to

anneal within the targeted region of exon V (wild-type, GCAGTTGTA CTTGATTTTCATGTTTGTAGC and  $\alpha 3[5]$ , CAGGTGTAGTATA CCAATGTTTCCAGC). TripleMaster PCR System (Eppendorf, Hamburg, DE) was used for all amplification reactions, which were assembled using 600 ng of total cDNA per reaction. Positive control primers designed to amplify the *rig/S15* “housekeeping” gene sequence were supplied by Ambion and negative controls included reagent-only and RNA-only reactions.

*Live-staining of SCG.* To label recombinant  $\alpha 3[5]$ -containing receptors, freshly dissected ganglia from  $\alpha 3[5]$ -homozygous mice (>2 months of age) were placed in L15 Air solution containing rhodamine conjugated  $\alpha$ BTX (rhoBTX) for 1 h. Next, ganglia were placed in 0.5% paraformaldehyde (PFA) in 0.1 M phosphate buffer (PB) for 1 h, transferred into a solution of 3% Triton-X in phosphate buffered saline (PBS) for 3 h, and then incubated overnight with primary antibodies (polyclonal goat anti-VACHT (1:750, Chemicon, Temecula, CA) and monoclonal mouse anti-neurofilament (NFM; 1/10000, Sternberger) or polyclonal goat anti-post synaptic density 93 (PSD93; 1/100, Synaptic Systems) dissolved in PBS containing 10% normal donkey serum at 4°C. The next day ganglia were rinsed twice for 15 min in PBS and placed in secondary antibodies Alexa 488 donkey anti-goat antibodies (1/1000, Molecular Probes) or Alexa 402 donkey anti-mouse antibodies (1/1000, Molecular Probes) in PBS containing 10% normal donkey serum for 2.5 h at room temperature. The ganglia were then rinsed twice for 15 min with PBS and mounted with Vectashield (Vector Laboratories, Burlingame, CA). Nonspecific staining was assessed by processing the sections without primary antibody.

*Imaging.* A series of z stacks (0.3  $\mu\text{m}/\text{plane}$ ) was obtained with a confocal microscope (LSM 510; Zeiss) and a 63 $\times$ , 1.4 numerical aperture Plan Neofluor oil-immersion objective. In experiments with denervated ganglia, we set values for detector gain, detector offset, and amplifier offset by imaging control ganglia from the same mouse stained with rhoBTX and anti-VACHT and found values that captured the distribution of intensities within an image depth of 8 bits. We then used these acquisition parameters to image denervated ganglia. For colocalization experiments where the intensities of the signals were less important, we adjusted the acquisition settings to optimize the staining for synaptic proteins.

Images were quantified off-line with MetaMorph (Universal Imaging Corporation). The representative images in figures of rhoBTX stained and VACHT-stained SCG were created by averaging three consecutive image planes from a z stack, cropping the averaged image, splitting the color components of the cropped image, thresholding each color channel individually to 2x the value of background intensity, and adding the two component images back together. Representative images of NFM/VACHT/rhoBTX triple stained ganglia were processed in a similar way. Occasionally, we used the low pass filter tool with a 2x2 convolution kernel to remove single pixel noise from our images.

*Extracellular and intracellular recordings.* Ganglia from mice greater than 2 months of age were pinned down in a small recording chamber (1.5 ml volume) with minutia pins, perfused continuously at 3-4 ml/min with oxygenated modified Tyrode's solution supplemented with glucose (5.6 mM) and choline (0.01 mM) (pH = 7.3-7.4) at 36-37°C,

and viewed through a dissecting microscope (SMZ-10; Nikon, Tokyo, Japan). The preganglionic nerve in the cervical sympathetic trunk was connected to a stimulator (Warner instruments) with a suction electrode, and the postganglionic trunk was connected to an alternating current differential amplifier (DP-301; Warner Instruments, Hamden, CT) with a suction electrode. The postganglionic compound action potentials were amplified (1000×), filtered at 10 Hz (low-pass cutoff) and 3 kHz (high-pass cutoff), digitized, displayed, and stored on a Pentium II-based personal computer with Patchkit (Alembic Software, Montreal, Quebec, Canada). The data were analyzed off-line with Igor (WaveMetrics, Lake Oswego, OR). All drugs were added directly to the oxygenated Ringer's solution.

Glass microelectrodes with a resistance of 40-80 M $\Omega$  (G150F-4; Warner Instruments) made with a DMZ universal puller (Zeitz Instruments, Munich, Germany) and filled with 1 M potassium acetate (KAc) were used for intracellular recordings from ganglion cells. Stable intracellular recordings were achieved with a high inertial precision microdrive (Inchworm 8200; EXFO, Vanier, Quebec, Canada) attached to a micromanipulator (SM11; Narishige, Tokyo, Japan) to drive the electrode through the ganglion. The recording electrode was connected by a thin silver chlorided wire to the head stage of an Axoclamp 2A amplifier (Axon Instruments, Union City, CA) used in current-clamp mode. Depolarizing or hyperpolarizing constant current pulses were applied through the recording electrode, and membrane potentials were filtered at 10 kHz, sampled, displayed, and stored on a Pentium II-based personal computer. Stimulation and acquisition was done with Patchkit software (Alembic Software), and the data were analyzed with IGOR. The preganglionic nerve was stimulated with brief (0.1-0.2 ms)

voltage pulses applied to the cervical sympathetic trunk through the suction electrode.  $\alpha$ BTX (100 nM) and methyllycaconitine (MLA; 50 nM) were dissolved in oxygenated Tyrode's solution modified as above. Only neurons with membrane potentials more negative than -40 mV were included in this study.

*Acute dissociation and culturing of SCG neurons.* SCG ganglia were removed under sterile conditions from neonatal mice (P12-P14). The ganglia were incubated at 37° C in a trypsin solution (1 mg/ml of trypsin from Worthington Biochemical Corp., 3X crystallized TRL3) in Hank's Balanced Salt Solution (HBSS) without  $\text{Ca}^{+2}$  or  $\text{Mg}^{+2}$ . After 1 hour the ganglia were triturated gently with a fire polished glass pipet. The resultant solution was centrifuged for 5 minutes and rinsed with growth media (L-15 media supplemented with vitamins, cofactors, penicillin-streptomycin, 5% rat serum and NGF (25-50 ng/ml). The cells were then plated on laminin-coated coverslips and incubated at 37° (5%  $\text{CO}_2$ ) until needed. The neurons were transferred to 30°C for 24 h prior to recording.

*Whole-cell electrophysiology.* Whole-cell patch-clamp recordings were made with an Axopatch 200B integrated patch clamp. Patch electrodes had a resistance of between 2-5 M $\Omega$ . Data were recorded with Axon Clampex 9.0 and visualized on Axon Clampfit 9.0. Axon Patch electrodes were filled with 65 mM KF, 55 mM KAc, 5 mM NaCl, 0.2 mM  $\text{CaCl}_2$ , 1 mM  $\text{MgCl}_2$ , 10 mM EGTA, and 10 mM HEPES, pH 7.4. The cells were continuously perfused with extracellular recording media (140 mM NaCl, 5.4 mM KCl, 0.33 mM  $\text{NaH}_2\text{PO}_4$  0.44 mM  $\text{KH}_2\text{PO}_4$ , 2.8 mM  $\text{CaCl}_2$ , 0.18 mM  $\text{MgCl}_2$ , 10 mM HEPES, 5.6 mM glucose, 2 mM glutamine, 5  $\mu\text{g/ml}$  phenol red and 1-2  $\mu\text{M}$  atropine, pH 7.4). The

agonist ACh was dissolved in extracellular recording media and delivered through an Eppendorf Femtojet pressure perfusion system at 500 P<sub>i</sub> for 1 sec through a glass capillary drawn to a diameter of 5-10 μm.

*Denervation.* For denervation experiments, we modified procedures described by McFarlane and Cooper (1992) for neonatal rats. Briefly, mice older than 2 months of age were anesthetized with Ketamine-Xylazine by intraperitoneal injection. The preganglionic cervical sympathetic trunk on one side was exposed and transected approximately halfway between the SCG and the first rib. After the surgery, the mice were returned to their cages for different times up to 2 wk. We observed that all denervated animals exhibited pronounced ptosis of the eye on the operated side. In most animals, we confirmed that the denervation was complete by electrophysiologically recording from the postganglionic nerve with extracellular electrodes while stimulating the preganglionic stump. All procedures were carried out at McGill University in accordance with the guidelines established by the Canadian Council on Animal Care.

## Results

### Generation and characterization of $\alpha 3[5]$ mice

Mice with  $\alpha$ BTX-sensitive  $\alpha 3$ -containing nAChRs (*Chrna3*<sup>tm1.0Hwrt</sup>) were generated by introducing mutations to the  $\alpha 3$  gene (*Chrna3*) located on chromosome 9. Following electroporation of the targeting DNA into mouse ES cells, a total of 192 G418-resistant candidates were collected and screened. Six recombinant ES cell clones were successfully identified using Southern blot analysis (Fig. 1B). The 3' probe detected a single band of ~17.4 kb in the wild-type sample, and a ~17.4 kb band along with a band of ~10.5 kb in the correctly targeted clones. With the 5' probe, a ~17.5 kb band was detected from the wild-type allele and an ~8.9 kb band from the targeted allele.

Genomic DNAs from the correctly targeted ES cell clones were further analyzed by the *KpnI* restriction site-based PCR detection assay and allele-specific PCR to confirm the presence of the  $\alpha 3[5]$  mutation (data not shown). Although the neomycin resistance cassette was detected by Southern blot and PCR in all six of the homologous recombinants, the  $\alpha 3[5]$  mutations could only be identified in three of six ES cell clones (A6, D4, and D12). These clones were used to generate chimeras and F1 and F2 *Chrna3*<sup>tm1.0Hwrt/+</sup> animals.

Next, we removed the neomycin cassette by mating *Chrna3*<sup>tm1.0Hwrt/+</sup> males and 129S1-*Hprt1*<sup>tm1(cre)Mnn</sup>/J females. The 129S1-*Hprt1*<sup>tm1(cre)Mnn</sup>/J strain carries an X-linked Cre-recombinase expression cassette that mediates the excision of DNA segments flanked by

*loxP* sites (Tang et al., 2002). The Neo-deleted offspring (*Chrna3<sup>tm1.1Hwrt/+</sup>*) were intercrossed to generate homozygous *Chrna3<sup>tm1.1Hwrt/tm1.1Hwrt</sup>* pups, which were identified by Southern blot analysis (Fig. 1C). Initial breeding attempts indicated that ~87% of *Chrna3<sup>tm1.1Hwrt/tm1.1Hwrt</sup>* animals died within two weeks of birth (data not shown) and exhibited a phenotype resembling that previously reported for  $\alpha3$ -null (-/-) mutants (Xu et al., 1999), with the exception that the eyelids of  $\alpha3[5]$  homozygotes appeared to be more fully open.

To ensure that  $\alpha3[5]$  mRNA was being produced in knock-in animals, we performed RT-PCR using RNA isolated from the SCG of *Chrna3<sup>tm1.1Hwrt/+</sup>*, *Chrna3<sup>tm1.1Hwrt/tm1.1Hwrt</sup>*, and wild-type mice. With the wild-type allele-specific primers, an expected ~480 bp product was detected from *Chrna3<sup>tm1.1Hwrt/+</sup>* ( $\alpha3[5]/+$ ) and wild-type cDNAs, but not from *Chrna3<sup>tm1.1Hwrt/tm1.1Hwrt</sup>* ( $\alpha3[5]/\alpha3[5]$ ) cDNA. The  $\alpha3[5]$  allele-specific primers amplified a 480 bp product from both mutant samples, but not from the wild-type template (Fig. 1D). These results indicated that the mutated allele was actively transcribed and mRNA produced in the SCG of *Chrna3<sup>tm1.1Hwrt/+</sup>* and *Chrna3<sup>tm1.1Hwrt/tm1.1Hwrt</sup>* mice.

### **Crosses with inbred and outbred strains demonstrate the influence of genetic background on the phenotype of $\alpha3[5]$ homozygotes**

Our  $\alpha3[5]$  knock-in mice were maintained initially on a mixed S129S7/C57BL/6 background. After removing the neomycin cassette, we backcrossed them 10 times into C57BL/6 strain to generate congenic *Chrna3<sup>tm1.1Hwrt/+</sup>* animals. The transmissibility of the mutant allele was then characterized in these congenic mice (Table I). Matings of

*Chrna3*<sup>tm1.1Hwrt/+</sup> animals with wild-type mice produced the expected Mendelian distribution of genotypes (1:1). Since *Chrna3*<sup>tm1.1Hwrt/+</sup> animals were fertile and normal for at least the first 12 months of life, no obvious dominant effects resulted from the presence of the mutant allele. Intercrosses of *Chrna3*<sup>tm1.1Hwrt/+</sup> males and females, however, failed to produce the expected proportion of *Chrna3*<sup>tm1.1Hwrt/tm1.1Hwrt</sup> pups, indicating that about 50% of homozygous mutants died before genotyping was conducted (1-2 weeks of age). The surviving *Chrna3*<sup>tm1.1Hwrt/tm1.1Hwrt</sup> animals in the C57BL/6 background typically die within three months of birth. Pathologic examination performed on a deceased *Chrna3*<sup>tm1.1Hwrt/tm1.1Hwrt</sup> animal at the age of three months identified mild hydronephrosis of the kidney. However, other major organs were determined to be within normal limits, and the cause of premature death remains unknown. All together, our mating analyses indicate that the five amino acid substitution in the  $\alpha 3$  subunit of nAChR constitutes a recessive, hypomorphic mutation that reduces lifespan of these animals in the C57BL/6 inbred background.

To increase viability and lifespan of mutant mice, it is sometimes advantageous to transfer the generated mutation on an outbred background. Outbred mice maintain maximum heterozygosity and can offer numerous advantages over inbred strains, such as longer life spans, disease resistance, and more robust breeding (Silver, 1995).

To test whether outbred genetic backgrounds would influence the observed phenotypes, we outcrossed *Chrna3*<sup>tm1.1Hwrt/+</sup> mice with two outbred strains: ICR (Taconic, Hudson, NY) and CD-1 (Charles River Canada, St. Constante, Qc). Intercrosses between ICR outbred *Chrna3*<sup>tm1.1Hwrt/+</sup> animals are summarized in Table II. Although in the sample

tested the proportion of homozygous *Chrna3*<sup>tm1.1Hwrt/tm1.1Hwrt</sup> mice was somewhat lower than expected, the differences were not statistically significant ( $P>0.05$ ). Moreover, lifespan was increased to an average of five months following outcrosses with the ICR strain. Similar results were obtained with mice outcrossed to the CD-1 strain. For these reasons, outbred-derived  $\alpha 3[5]$  homozygotes were chosen for our characterizations of intact SCG.

### **$\alpha 3[5]$ -homozygous mice contain $\alpha$ BTX-binding sites that colocalize with synaptic markers in sympathetic ganglia**

In murine sympathetic ganglia,  $\alpha 3$ -containing nAChRs are essential for fast synaptic transmission (Krisnaswamy and Cooper, 2009). Therefore, to determine whether  $\alpha 3[5]$  subunits were surface-expressed at synapses, we stained living SCG with rhodamine-conjugated  $\alpha$ BTX (rhoBTX, 100 nM for 1 h). The ganglia were then post-fixed and stained with anti-neurofilament (NFM-H) to locate the preganglionic axons, and with anti-vesicle ACh transporter (VACHT) to locate the presynaptic terminals. Sympathetic neurons in SCG of 2-3 month *Chrna3*<sup>tm1.1Hwrt/tm1.1Hwrt</sup> mice had bright  $\alpha$ BTX-labeled clusters that colocalized with presynaptic varicosities on the soma and dendrites of sympathetic neurons (Fig. 2A). Moreover, these  $\alpha$ BTX-labeled clusters colocalized with PSD93 (Fig. 2B), indicating that  $\alpha 3[5]$ -containing receptors are targeted to synapses, although the signal from the clusters of  $\alpha 3[5]$ -containing receptors was too low to be resolved from the background at the majority of PSD-93 sites. In all cases, fluorescent labeling by  $\alpha$ BTX was completely abolished by preincubation with 100 nM unlabeled  $\alpha$ BTX (Fig. 2C).

Rodent sympathetic neurons express  $\alpha 7$  mRNA (Mandelzys et al., 1995; De Koninck and Cooper, 1995) and have  $^{125}\text{I}$ - $\alpha\text{BTX}$ -binding sites (Smolen 1983; De Koninck and Cooper, 1995). This raised the possibility that the  $\alpha\text{BTX}$  labeling in  $\alpha 3[5]$ -containing ganglia from *Chrna3<sup>tm1.1Hwrt/tm1.1Hwrt</sup>* mice was due to  $\alpha 7$  nAChRs rather than  $\alpha 3[5]$ -containing receptors. To rule out this possibility, we crossed  $\alpha 3[5]$  mice with  $\alpha 7$  null mutants and generated *Chrna3<sup>tm1.1Hwrt/tm1.1Hwrt</sup> Chrna7<sup>tm1Bay/tm1Bay</sup>* homozygous double mutants ( $\alpha 3[5]$ -homozygous and  $\alpha 7(-/-)$ ). Punctate  $\alpha\text{BTX}$  labeling on sympathetic neurons from these  $\alpha 3[5]$ -homozygous  $\alpha 7(-/-)$  ganglia was similar to that on neurons from  $\alpha 3[5]$ -homozygous  $\alpha 7(+/+)$  ganglia, indicating that  $\alpha 7$  nAChRs are not contributing to the fluorescent signal (Fig. 2C). Moreover, preincubation with 50 nM MLA, a specific  $\alpha 7$  antagonist, had no effect on rhoBTX labeling in  $\alpha 3[5]$ -homozygous  $\alpha 7(+/+)$  ganglia (Fig. 2C).

### **Synaptic transmission in SCG of $\alpha 3[5]$ -homozygous mice is blocked by $\alpha\text{BTX}$**

The results above indicate that  $\alpha 3[5]$ -containing postsynaptic receptors are located at synapses in the SCG of *Chrna3<sup>tm1.1Hwrt/tm1.1Hwrt</sup>* mice. Next, we asked whether  $\alpha\text{BTX}$  blocked synaptic activity in the SCG of these mice. To measure synaptic transmission, we stimulated the preganglionic nerve and recorded the nerve-evoked compound action potentials (CAP) extracellularly from the postganglionic trunk. In wild-type ganglia, stimulating the preganglionic nerve produced a 1.5-3 mV CAP (n=12). In line with previous studies, the CAP was unaffected by  $\alpha\text{BTX}$  (100 nM for 20-30 min; n=6) (Fig.

3A). The nerve-evoked CAPs recorded from *Chrna3<sup>tm1.1Hwrt/tm1.1Hwrt</sup>* mice were smaller (0.2-0.3 mV; n=15) than those from wild-type ganglia. However, unlike CAPs from wild-type ganglia, the CAPs from  $\alpha 3[5]$ -homozygous ganglia were completely blocked by  $\alpha$ BTX (Fig. 3A). Similar levels of block were observed in all CAPs tested (n=12).

To further investigate synaptic transmission of intact SCG, we recorded excitatory postsynaptic potentials (EPSPs) intracellularly from these sympathetic neurons. With SCG from wild-type mice, the nerve-evoked EPSPs on sympathetic neurons were large (20-30 mV; n=20) and suprathreshold (Fig. 3B). As with the CAPs, none of the EPSPs recorded from wild-type ganglia were blocked by  $\alpha$ BTX (100 nM for 20-30 min; n=6). In contrast, the majority (>80%) of nerve-evoked EPSPs on sympathetic neurons in *Chrna3<sup>tm1.1Hwrt/tm1.1Hwrt</sup>* SCG were subthreshold (n=25) with peak amplitudes of only  $3.6 \pm 0.8$  mV (n=25). Most relevantly, however, all EPSPs (10/10) on  $\alpha 3[5]$ -homozygous neurons were blocked by  $\alpha$ BTX (Fig. 3B).

To ensure that the nerve-evoked EPSPs on  $\alpha 3[5]$ -homozygous neurons did not inadvertently result from  $\alpha 7$ -containing nAChRs (Cuevas et al., 2000; Severance et al., 2004), we examined nerve-evoked EPSPs in ganglia from *Chrna3<sup>tm1.1Hwrt/tm1.1Hwrt</sup>Chrna7<sup>tm1Bay/tm1Bay</sup>* ( $\alpha 3[5]$ -homozygous  $\alpha 7(-/-)$ ) mice. All nerve-evoked EPSPs on sympathetic neurons in the SCG of these homozygous double mutants were similarly blocked by  $\alpha$ BTX (n=12), indicating that the  $\alpha$ BTX-sensitive EPSPs were mediated by  $\alpha 3[5]$ -containing receptors (Fig. 3B).

Although we observed reproducible labeling of  $\alpha 3[5]$  subunits at synapses, we wondered why the nerve-evoked EPSPs on  $\alpha 3[5]$ -homozygous sympathetic neurons were smaller than those on wild-type neurons. Conceivably, replacing 5 amino acids in the  $\alpha 3$  subunit with corresponding residues from  $\alpha 1$  of *Torpedo californica* may have interfered with the function or appearance of receptors on the surface. To examine the latter possibility, we investigated ACh-evoked currents from cultured SCG neurons isolated from neonatal *Chrna3<sup>tm1.1Hwrt/tm1.1Hwrt</sup>* mice that were fully congenic (N10) on the C57BL/6 inbred background. When cultured at 37°C, no ACh-evoked currents were detected from  $\alpha 3[5]$ -homozygous neurons. However, ACh-evoked currents became detectable following a shift in temperature from 37°C to 30°C for 24 h, consistent with studies showing that reduced temperature increases the surface expression of some nAChR subtypes (Ross et al., 1991; Cooper et al., 1999; Wanamaker & Green, 2007). The ACh-evoked current densities recorded from cultured *Chrna3<sup>tm1.1Hwrt/tm1.1Hwrt</sup>* neurons at 30°C were approximately 6% of those from control neurons and were blocked by  $\alpha$ BTX (100 nM) (Fig. 4B). Our analysis of SCG neurons from double homozygous mutant mice ( $\alpha 3[5]$ -homozygous  $\alpha 7(-/-)$ ) yielded similar results (Fig. 4B), further indicating that the observed ACh-evoked currents were not mediated by  $\alpha 7$ -containing nAChRs. These results suggest that the amino acid substitutions in  $\alpha 3[5]$  may have negatively impacted subunit assembly and/or surface expression.

Next, to address the influence of genetic background on the surface expression of functional  $\alpha 3[5]$ -containing nAChRs in primary cultures of SCG neurons, we mated fully congenic C57BL/6 *Chrna3<sup>tm1.1Hwrt/+</sup>* mice with wild-type mice from the following strains:

C3H, DBA, BALB/c, and ICR. Heterozygous F1 offspring from each of the above-mentioned strains were obtained, from which F2 *Chrna3<sup>tm1.1Hwrt/tm1.1Hwrt</sup>* mice were generated through intercrosses. We then prepared primary cultures of SCG neurons from these neonatal *Chrna3<sup>tm1.1Hwrt/tm1.1Hwrt</sup>* mice and measured ACh responses following incubation at 30°C. The ACh-evoked current densities of SCG neurons from *Chrna3<sup>tm1.1Hwrt/tm1.1Hwrt</sup>* mice derived from the outbred ICR background were dramatically increased compared to neurons from congenic C57BL/6 mice (Fig. 4C). Of several inbred strains tested in this fashion, the BALB/c background appears to support an increase in ACh responses in addition to extending the lifespan of *Chrna3<sup>tm1.1Hwrt/tm1.1Hwrt</sup>* mice. In preliminary studies on SCGs dissected from older mice (>P20), cultured SCG neurons from  $\alpha 3[5]$  homozygotes on a mixed C57BL/6-BALB/c background and incubated from 24 to 48 hours at 30°C have produced ACh responses approaching wild-type levels (data not shown). Moreover, in contrast to C57BL/6, we have observed ACh-evoked whole-cell currents in SCG neurons from older BALB/c- and ICR-derived  $\alpha 3[5]$ -homozygous mice without a 30°C incubation period.

**The number of rhoBTX-labeled clusters on sympathetic neurons increases following denervation, indicating a postsynaptic localization**

The colocalization of  $\alpha 3[5]$ -containing receptor clusters with presynaptic terminals at ganglionic synapses, as demonstrated in Fig. 2, prompted us to ask whether the presynaptic nerve has a direct role in clustering receptors, similar to the role of presynaptic terminals at the neuromuscular junction (Sanes and Lichtman, 1999; Gingras et al., 2002). Therefore, we cut the preganglionic nerve to the SCG in

*Chrna3<sup>tm1.1Hwrt/tm1.1Hwrt</sup>* mice and examined denervated neurons at different times up to 2 weeks. Within 2 days of denervation, we observed an increase in the size of the  $\alpha$ BTX-labeled clusters as well as an increase in the number of clusters compared to control (Fig. 5A,B). This increase in  $\alpha$ BTX clusters likely reflects denervation supersensitivity, a process observed in many other synaptic systems (Sharpless, 1975; Cangiano, 1985). Interestingly, these changes in clustering were transient, and, by 1 wk after denervation, the receptor clusters were not significantly different from those on neurons in the contralateral control ganglia (Fig. 5C). Over the following week, the clusters continued to decrease in size and number (Fig. 5D). We did not determine whether this decrease in cluster-labeling, as summarized in Fig. 5E, reflects a dispersal of receptors similar to what is observed on autonomic neurons in PSD93-null mice after denervation (Parker et al., 2004), or whether it reflects a decrease in the total number of receptors at the surface.

## Discussion

Efforts to understand fully the physiological roles of specific heteromeric nAChR subtypes in the central nervous system are limited by lack of reliable subtype-selective ligands. Antibodies against neuronal nAChR subunits are often problematic for isolating receptors from intact tissue or neurons, as most endogenous antigenic determinants are localized to the cytoplasmic portion of the subunits. Moreover, studies with knock-out mice have raised serious questions concerning the specificity of several types of neuronal nAChR antibodies (Herber et al., 2004; Moser et al., 2007). Although some  $\alpha$ -conotoxins have demonstrated remarkable selectivity among particular nAChR subunit interfaces, additional strategies are still needed to address the critical questions concerning subunit identification in the physiological setting (Millard et al., 2009).

The  $\alpha 1$  subunit from the muscle-type nAChR contains the major determinants for binding the classic nicotinic antagonist,  $\alpha$ BTX, while most neuronal nAChRs, apart from the  $\alpha 7$  subgroup, are completely insensitive to  $\alpha$ BTX. Given the considerable homologies shared by the genes encoding the muscle and neuronal nAChR subunits, we hypothesized that functional sensitivity to  $\alpha$ BTX could be conferred with minimally mutated neuronal nAChR subunits. This approach has been validated in principle with the neuronal rat  $\alpha 3$  subunit as studied in *Xenopus* oocytes (Levandoski et al., 1999).

For decades,  $\alpha$ BTX has been used extensively for the study of nicotinic receptors. Fluorescent-labeling with  $\alpha$ BTX has many practical advantages over staining with antibodies:  $\alpha$ BTX is a relatively small, cell-impermeant protein with numerous

commercially available conjugates. Antibodies, on the other hand, are relatively large divalent molecules which may cap or cluster surface antigens and compromise surface trafficking (Sekine-Aizawa, 2004). Efforts in our lab have been focused on extending these experimental capabilities to the study of  $\alpha$ BTX-insensitive neuronal nAChRs. Recently, we introduced an 11 amino acid  $\alpha$ 1-derived,  $\alpha$ BTX-binding sequence into the loop C region of the  $\beta$ 4 neuronal nAChR subunit. Co-injection of cRNAs from wild-type  $\alpha$ 3 together with the chimeric  $\beta$ 4/ $\alpha$ 1[11] resulted in functional channels that were allosterically inhibited by  $\alpha$ BTX (Sanders & Hawrot, 2004). Similar results have been achieved using an analogous chimeric  $\beta$ 2 subunit (Sanders, unpublished data). In this context, we refer to these ectopic  $\alpha$ BTX-binding sequences as “pharmatopes,” as  $\alpha$ BTX-binding to these sites results in a pharmacological action.

High-affinity  $\alpha$ BTX-binding sequences have been used in a variety of trafficking studies involving non-nicotinic receptor proteins. Sekine-Aizawa and Haganir (2004) inserted a 13-mer peptide sequence known as HAP-1 (Kasher et al., 2001, Fuchs et al., 2003) at the N-terminus of the GluR2, AMPA receptor subunit. This strategy facilitated the monitoring of surface expression and trafficking dynamics of the  $\alpha$ BTX-tagged AMPA receptor subunits expressed in HEK cells using radioactive, fluorescent, and biotinylated  $\alpha$ BTX-conjugates. Bogdanov et al. (2006) utilized a comparable approach for investigating the membrane-trafficking of GABA<sub>A</sub> receptors in hippocampal neurons. Guo et al. (2006) engineered a 13 amino acid  $\alpha$ BTX-binding sequence into the N-terminus of a metabotropic glutamate receptor, mGluR8a, and visualized surface-expressed receptors in rat sympathetic neurons using fluorescein-conjugated  $\alpha$ BTX.

More recently, Wilkins et al. (2008) monitored the cell-surface mobility of  $\alpha$ BTX-tagged GABA<sub>B</sub> subunits (R1a) in real time in transfected hippocampal neurons.

Our present study expands on the simple tagging approach by introducing pharmacological sensitivity to  $\alpha$ BTX. We provide the first example in which the primary determinants for  $\alpha$ BTX-binding are incorporated into the homologous region of a native nAChR subunit that is normally insensitive to  $\alpha$ BTX. Our experiments show that  $\alpha$ BTX-sensitive  $\alpha$ 3[5] subunits are incorporated into functional nicotinic receptors in the SCG neurons of homozygous knock-in mice. Live surface-staining with rhodamine-conjugated  $\alpha$ BTX revealed high-density receptor clusters in ganglia from  $\alpha$ 3[5]-homozygous animals (Fig. 2). Moreover, these  $\alpha$ 3[5]-containing nAChR receptor clusters are targeted to synapses; all  $\alpha$ BTX clusters colocalized with VAcHT, a marker for presynaptic varicosities, and PSD-93, a marker for the postsynaptic membrane.

The results of our denervation experiments indicate that the presynaptic terminals play a role in clustering the  $\alpha$ 3[5]-containing receptors to synapses in SCG neurons, similar to their role at the neuromuscular junction (Sanes and Lichtman, 1999; Gingras et al., 2002). We found that cutting the presynaptic nerve leads to an initial increase in  $\alpha$ BTX-labeled clusters within 2 days, followed by cluster dispersal over the next 1-2 weeks. A similar time course for receptor dispersal on murine sympathetic neurons has been reported by Parker et al. (2004). Denervation of autonomic neurons in amphibians and chick leads to a similar dispersal of receptor clusters (Jacob and Berg, 1987; Sargent, 1988; McEachern et al., 1989; Levey and Jacob, 1996).

Although all  $\alpha$ BTX clusters on sympathetic neurons in  $\alpha$ 3[5]-homozygous ganglia colocalized with PSD-93 and VAcHT, approximately 20-30% of PSD-93-labeled puncta on these neurons coincided with detectable  $\alpha$ BTX clusters, presumably because the receptor density at these remaining synapses was too low to resolve. These results suggest that the replacement of the 5 residues somehow compromised assembly and/or membrane-targeting of  $\alpha$ 3[5]-containing receptors. Consistent with our labeling studies, we found that the amplitudes of both the CAPs and fast EPSPs in SCG neurons containing exclusively  $\alpha$ 3[5] subunit are reduced to approximately 10-20% of wild-type controls. The decrease in amplitude of the nerve-evoked EPSPs may be due to a decrease in the number of functional, surface-expressed  $\alpha$ 3[5]-containing nAChRs, as compared to wild-type ganglia. Studies suggest that the N-terminal extracellular region regulates the association of nAChR subunits (Sumikawa, 1992). Thus, the  $\alpha$ 3[5] mutations may have affected the integrity of pentamer assembly and trafficking, possibly leading to retention in the endoplasmic reticulum (Millar & Harkness, 2008). In principle, the loop C mutations could also affect the surface stability of fully assembled receptors.

The replacement of  $\alpha$ 3 with  $\alpha$ 3[5] within the C57BL/6 genetic background resulted in SCG neurons that did not respond to ACh application when cultured at 37°C. Following a shift to 30°C, however, we observed a significant increase in the number of functional receptors, with ACh-responses reaching a level of about 6% of that seen with wild-type neurons cultured under similar conditions. These results are in line with previous studies demonstrating that reduced temperature increases the surface-expression of neuronal

nAChRs (Cooper et al., 1999; Nelson et al., 2003). Interestingly, these temperature effects appear to vary among different strains of mice. For example, whole-cell recordings of 30°C-treated SCG neurons prepared from outbred ICR-derived mice show considerable increases in their ACh-evoked current densities compared to neurons from mice with a congenic C57BL/6 background (Fig. 4C). The results of our most recent studies with the Balb/c strain show ACh responses approaching near wild-type levels in older mice (<P20) and sometimes in the absence of a 30°C incubation period (data not shown). The prospect that the expression of functional  $\alpha 3[5]$ -containing nAChRs varies among different inbred genetic backgrounds, as observed between the C57BL/6 and BALB/c strains, is exciting, as this would provide a powerful tool for transcriptome analysis and future studies aimed at dissecting the molecular mechanisms underlying the assembly and trafficking of neuronal nAChRs.

The present study has demonstrated that it is possible to transform an  $\alpha$ BTX-insensitive neuronal nAChR subunit into an  $\alpha$ BTX-sensitive variant through a knock-in strategy. This was accomplished by replacing five amino acids in the Loop C region of the murine  $\alpha 3$  subunit with the corresponding residues from the  $\alpha 1$  subunit of *Torpedo californica*. The work described here establishes a mammalian model for the study of  $\alpha 3$  nAChRs and demonstrates the experimental value of the “pharmatope” approach as a general strategy for the study of neuronal nAChRs *in vivo*.

## Acknowledgements

We would like to acknowledge Jim Boulter, UCLA, for his assistance with our targeting strategies. We thank Brigitte Pie for excellent technical assistance. We would also like to thank Geoffrey Chew and Suzanne Whitman for their contributions. P.C. and E.H. have been supported by National Institutes of Health grants #GM32629 and PHS P20 RR15578. A.K and E.C. receive support from the CIHR and HSFC. J.K. is supported by 5P20RR015578.

## Abbreviations

$\alpha$ BTX,  $\alpha$ -bungarotoxin; nAChR, nicotinic acetylcholine receptor; *Chrna3*,  $\alpha 3$  nAChR gene; ES cell, embryonic stem cell; SCG, superior cervical ganglia; VAcHT, vesicular acetylcholine transporter; NFM, neurofilament; CAP, compound action potential; EPSP, excitatory postsynaptic potential; rhoBTX, rhodamine-conjugated  $\alpha$ BTX;.

## References

- Bogdanov, Y., Michels, G., Armstrong-Gold, C., Haydon, P.G., Lindstrom, J., Pangalos, M. & Moss, S.J. (2006) Synaptic GABAA receptors are directly recruited from their extrasynaptic counterparts. *EMBO J*, **25**, 4381-4389.
- Cangiano, A. (1985) Denervation supersensitivity as a model for the neural control of muscle. *Neuroscience*, **14**, 963-971.
- Cheng, X., Wang, H., Grant, B., Sine, S.M. & McCammon, J.A. (2006) Targeted molecular dynamics study of C-loop closure and channel gating in nicotinic receptors. *PLoS Comput Biol*, **2**, e134.
- Colquhoun, D., Unwin, N., Shelley, C., Hatton, C. & Sivilotti, L. (2003) Nicotinic acetylcholine receptors. In Abraham, D. (ed) *Burger's Medicinal Chemistry Vol II Drug Discovery and Drug Development*. Wiley, New York.
- Cooper, S.T., Harkness, P.C., Baker, E.R. & Millar, N.S. (1999) Up-regulation of cell-surface alpha4beta2 neuronal nicotinic receptors by lower temperature and expression of chimeric subunits. *J Biol Chem*, **274**, 27145-27152.
- Cuevas, J., Roth, A.L. & Berg, D.K. (2000) Two distinct classes of functional 7-containing nicotinic receptor on rat superior cervical ganglion neurons. *J Physiol*, **525 Pt 3**, 735-746.
- De Koninck, P. & Cooper, E. (1995) Differential regulation of neuronal nicotinic ACh receptor subunit genes in cultured neonatal rat sympathetic neurons: specific induction of alpha 7 by membrane depolarization through a Ca<sup>2+</sup>/calmodulin-dependent kinase pathway. *J Neurosci*, **15**, 7966-7978.
- Fuchs, S., Kasher, R., Balass, M., Scherf, T., Harel, M., Fridkin, M., Sussman, J.L. & Katchalski-Katzir, E. (2003) The binding site of acetylcholine receptor: from synthetic peptides to solution and crystal structure. *Ann N Y Acad Sci*, **998**, 93-100.
- Gingras, J., Rassadi, S., Cooper, E. & Ferns, M. (2002) Agrin plays an organizing role in the formation of sympathetic synapses. *J Cell Biol*, **158**, 1109-1118.
- Gotti, C., Zoli, M. & Clementi, F. (2006) Brain nicotinic acetylcholine receptors: native subtypes and their relevance. *Trends Pharmacol Sci*, **27**, 482-491.
- Guo, J., Chen, H., Puhl, H.L., 3rd & Ikeda, S.R. (2006) Fluorophore-assisted light inactivation produces both targeted and collateral effects on N-type calcium channel modulation in rat sympathetic neurons. *J Physiol*, **576**, 477-492.

- Herber, D.L., Severance, E.G., Cuevas, J., Morgan, D. & Gordon, M.N. (2004) Biochemical and histochemical evidence of nonspecific binding of alpha7nAChR antibodies to mouse brain tissue. *J Histochem Cytochem*, **52**, 1367-1376.
- Hernandez, S.C., Vicini, S., Xiao, Y., Davila-Garcia, M.I., Yasuda, R.P., Wolfe, B.B. & Kellar, K.J. (2004) The nicotinic receptor in the rat pineal gland is an alpha3beta4 subtype. *Mol Pharmacol*, **66**, 978-987.
- Hogg, R.C. & Bertrand, D. (2007) Partial agonists as therapeutic agents at neuronal nicotinic acetylcholine receptors. *Biochem Pharmacol*, **73**, 459-468.
- Hogg, R.C., Raggenbass, M. & Bertrand, D. (2003) Nicotinic acetylcholine receptors: from structure to brain function. *Rev Physiol Biochem Pharmacol*, **147**, 1-46.
- Jacob, M.H. & Berg, D.K. (1987) Effects of preganglionic denervation and postganglionic axotomy on acetylcholine receptors in the chick ciliary ganglion. *J Cell Biol*, **105**, 1847-1854.
- Karlin, A. (2002) Emerging structure of the nicotinic acetylcholine receptors. *Nat Rev Neurosci*, **3**, 102-114.
- Kasher, R., Balass, M., Scherf, T., Fridkin, M., Fuchs, S. & Katchalski-Katzir, E. (2001) Design and synthesis of peptides that bind alpha-bungarotoxin with high affinity. *Chem Biol*, **8**, 147-155.
- Krishnaswamy, A. & Cooper, E. (2009) An activity-dependent retrograde signal induces the expression of the high-affinity choline transporter in cholinergic neurons. *Neuron*, **61**, 272-286.
- Levandoski, M.M., Lin, Y., Moise, L., McLaughlin, J.T., Cooper, E. & Hawrot, E. (1999) Chimeric analysis of a neuronal nicotinic acetylcholine receptor reveals amino acids conferring sensitivity to alpha-bungarotoxin. *J Biol Chem*, **274**, 26113-26119.
- Levey, M.S. & Jacob, M.H. (1996) Changes in the regulatory effects of cell-cell interactions on neuronal AChR subunit transcript levels after synapse formation. *J Neurosci*, **16**, 6878-6885.
- Liu, Z.W., Yang, S., Zhang, Y.X. & Liu, C.H. (2003) Presynaptic alpha-7 nicotinic acetylcholine receptors modulate excitatory synaptic transmission in hippocampal neurons. *Sheng Li Xue Bao*, **55**, 731-735.
- Mandelzys, A., De Koninck, P. & Cooper, E. (1995) Agonist and toxin sensitivities of ACh-evoked currents on neurons expressing multiple nicotinic ACh receptor subunits. *J Neurophysiol*, **74**, 1212-1221.

- McEachern, A.E., Jacob, M.H. & Berg, D.K. (1989) Differential effects of nerve transection on the ACh and GABA receptors of chick ciliary ganglion neurons. *J Neurosci*, **9**, 3899-3907.
- McGehee, D.S. & Role, L.W. (1995) Physiological diversity of nicotinic acetylcholine receptors expressed by vertebrate neurons. *Annu Rev Physiol*, **57**, 521-546.
- Millar, N.S. & Harkness, P.C. (2008) Assembly and trafficking of nicotinic acetylcholine receptors (Review). *Mol Membr Biol*, **25**, 279-292.
- Millard, E.L., Nevin, S.T., Loughnan, M.L., Nicke, A., Clark, R.J., Alewood, P.F., Lewis, R.J., Adams, D.J., Craik, D.J. & Daly, N.L. (2009) Inhibition of neuronal nicotinic acetylcholine receptor subtypes by alpha-Conotoxin GID and analogues. *J Biol Chem*, **284**, 4944-4951.
- Moser, N., Mechawar, N., Jones, I., Gochberg-Sarver, A., Orr-Urtreger, A., Plomann, M., Salas, R., Molles, B., Marubio, L., Roth, U., Maskos, U., Winzer-Serhan, U., Bourgeois, J.P., Le Sourd, A.M., De Biasi, M., Schroder, H., Lindstrom, J., Maelicke, A., Changeux, J.P. & Wevers, A. (2007) Evaluating the suitability of nicotinic acetylcholine receptor antibodies for standard immunodetection procedures. *J Neurochem*, **102**, 479-492.
- Nelson, M.E., Kuryatov, A., Choi, C.H., Zhou, Y. & Lindstrom, J. (2003) Alternate stoichiometries of alpha4beta2 nicotinic acetylcholine receptors. *Mol Pharmacol*, **63**, 332-341.
- Parker, M.J., Zhao, S., Bredt, D.S., Sanes, J.R. & Feng, G. (2004) PSD93 regulates synaptic stability at neuronal cholinergic synapses. *J Neurosci*, **24**, 378-388.
- Perry, D.C., Xiao, Y., Nguyen, H.N., Musachio, J.L., Davila-Garcia, M.I. & Kellar, K.J. (2002) Measuring nicotinic receptors with characteristics of alpha4beta2, alpha3beta2 and alpha3beta4 subtypes in rat tissues by autoradiography. *J Neurochem*, **82**, 468-481.
- Ramirez-Solis, R., Liu, P. & Bradley, A. (1995) Chromosome engineering in mice. *Nature*, **378**, 720-724.
- Rassadi, S., Krishnaswamy, A., Pie, B., McConnell, R., Jacob, M.H. & Cooper, E. (2005) A null mutation for the alpha3 nicotinic acetylcholine (ACh) receptor gene abolishes fast synaptic activity in sympathetic ganglia and reveals that ACh output from developing preganglionic terminals is regulated in an activity-dependent retrograde manner. *J Neurosci*, **25**, 8555-8566.
- Role, L.W. & Berg, D.K. (1996) Nicotinic receptors in the development and modulation of CNS synapses. *Neuron*, **16**, 1077-1085.

- Ross, A.F., Green, W.N., Hartman, D.S. & Claudio, T. (1991) Efficiency of acetylcholine receptor subunit assembly and its regulation by cAMP. *J Cell Biol*, **113**, 623-636.
- Sanders, T. & Hawrot, E. (2004) A novel pharmacophore tag inserted into the beta4 subunit confers allosteric modulation to neuronal nicotinic receptors. *J Biol Chem*, **279**, 51460-51465.
- Sanes, J.R. & Lichtman, J.W. (1999) Development of the vertebrate neuromuscular junction. *Annu Rev Neurosci*, **22**, 389-442.
- Sargent, P.B. & Pang, D.Z. (1988) Denervation alters the size, number, and distribution of clusters of acetylcholine receptor-like molecules on frog cardiac ganglion neurons. *Neuron*, **1**, 877-886.
- Sekine-Aizawa, Y. & Huganir, R.L. (2004) Imaging of receptor trafficking by using alpha-bungarotoxin-binding-site-tagged receptors. *Proc Natl Acad Sci U S A*, **101**, 17114-17119.
- Severance, E.G., Zhang, H., Cruz, Y., Pakhlevanians, S., Hadley, S.H., Amin, J., Wecker, L., Reed, C. & Cuevas, J. (2004) The alpha7 nicotinic acetylcholine receptor subunit exists in two isoforms that contribute to functional ligand-gated ion channels. *Mol Pharmacol*, **66**, 420-429.
- Sharpless, S.K. (1975) Supersensitivity-like phenomena in the central nervous system. *Fed Proc*, **34**, 1990-1997.
- Silver, L.M. (1995) *Mouse Genetics: Concepts and Applications*. Oxford University Press.
- Skok, V.I. (2002) Nicotinic acetylcholine receptors in autonomic ganglia. *Auton Neurosci*, **97**, 1-11.
- Smolen, A.J. (1983) Specific binding of alpha-bungarotoxin to synaptic membranes in rat sympathetic ganglion: computer best-fit analysis of electron microscope radioautographs. *Brain Res*, **289**, 177-188.
- Sudweeks, S.N. & Yakel, J.L. (2000) Functional and molecular characterization of neuronal nicotinic ACh receptors in rat CA1 hippocampal neurons. *J Physiol*, **527 Pt 3**, 515-528.
- Sumikawa, K. (1992) Sequences on the N-terminus of ACh receptor subunits regulate their assembly. *Brain Res Mol Brain Res*, **13**, 349-353.
- Tang, S.H., Silva, F.J., Tsark, W.M. & Mann, J.R. (2002) A Cre/loxP-deleter transgenic line in mouse strain 129S1/SvImJ. *Genesis*, **32**, 199-202.

- Taxi, J. & Eugene, D. (1995) Effects of axotomy, deafferentation, and reinnervation on sympathetic ganglionic synapses: a comparative study. *Int Rev Cytol*, **159**, 195-263.
- Turner, J.R. & Kellar, K.J. (2005) Nicotinic cholinergic receptors in the rat cerebellum: multiple heteromeric subtypes. *J Neurosci*, **25**, 9258-9265.
- Wanamaker, C.P. & Green, W.N. (2007) Endoplasmic reticulum chaperones stabilize nicotinic receptor subunits and regulate receptor assembly. *J Biol Chem*, **282**, 31113-31123.
- Whiteaker, P., Peterson, C.G., Xu, W., McIntosh, J.M., Paylor, R., Beaudet, A.L., Collins, A.C. & Marks, M.J. (2002) Involvement of the alpha3 subunit in central nicotinic binding populations. *J Neurosci*, **22**, 2522-2529.
- Wilkins, M.E., Li, X. & Smart, T.G. (2008) Tracking cell surface GABAB receptors using an alpha-bungarotoxin tag. *J Biol Chem*, **283**, 34745-34752.
- Xu, W., Gelber, S., Orr-Urtreger, A., Armstrong, D., Lewis, R.A., Ou, C.N., Patrick, J., Role, L., De Biasi, M. & Beaudet, A.L. (1999) Megacystis, mydriasis, and ion channel defect in mice lacking the alpha3 neuronal nicotinic acetylcholine receptor. *Proc Natl Acad Sci U S A*, **96**, 5746-5751.
- Yeh, J.J., Yasuda, R.P., Davila-Garcia, M.I., Xiao, Y., Ebert, S., Gupta, T., Kellar, K.J. & Wolfe, B.B. (2001) Neuronal nicotinic acetylcholine receptor alpha3 subunit protein in rat brain and sympathetic ganglion measured using a subunit-specific antibody: regional and ontogenic expression. *J Neurochem*, **77**, 336-346.

## TABLES

Table I. Distribution of genotypes in offspring from backcrosses and intercrosses of congenic  $\alpha 3[5]$  carriers ( $n \geq 9$ ).

male x female	heterozygous	wild-type	homozygous	<i>P</i>
<i>Chrna<sup>tm1.1Hwrt/+</sup></i> x <i>Chrna<sup>tm1.1Hwrt/+</sup></i>	177 (58%)	86 (28%)	41 (14%)	<i>P</i> <0.005
<i>Chrna<sup>tm1.1Hwrt/+</sup></i> x wild-type (C57BL/6)	117 (50%)	118 (50%)	-	<i>P</i> >0.95

Table II. Distribution of genotypes in offspring obtained from ICR-outcrossed parents.

male x female	heterozygous	wild-type	homozygous	<i>P</i>
<i>Chrna<sup>tm1.1Hwrt/+</sup></i> x <i>Chrna<sup>tm1.1Hwrt/+</sup></i>	99 (58%)	42 (25%)	30 (18%)	0.06> <i>P</i> >0.05

\* *P* values were calculated using the Chi-squared method

## Figure Legends

### Figure 1.

(A) Overview of the  $\alpha 3[5]$  knock-in targeting strategy. Illustration depicting WT *Chrna3* allele,  $\alpha 3[5]$  targeting DNA, and recombinant allele before (*Chrna3<sup>tm1.0Hwrt</sup>*) and after (*Chrna3<sup>tm1.1Hwrt</sup>*) deletion of the neomycin cassette, along with anticipated regions of homologous recombination and restriction cleavage sites. WT exons are represented as solid rectangles. The mutated ExonV is shown as a hatched rectangle. (B) Southern analysis of targeted ES cell clone. A single band at ~17.5 kb is detected by the 3' probe in the WT control (left, lane 1). In targeted ES cell clone A6, the ~17.5 kb WT band is detected along with a second band at ~10.5 kb, the anticipated size of the 3' KpnI fragment in the recombinant allele (left, lane 2). A single band is detected at ~17.5 kb in the WT sample with the 5' probe (right, lane 1). In targeted ES cell clone A6, the ~17.5 kb band appeared along with a second band at ~8.9 kb, the anticipated size of the 5' KpnI fragment in the mutant allele (right, lane 2). (C) Southern analysis of  $\alpha 3[5]$  knock-in mice. Following deletion of the neomycin cassette, the mutant allele is reduced by ~2 kb from 8.9 kb in an  $\alpha 3[5]$  heterozygote (+neo, lane 1) to 6.9 kb in an  $\alpha 3[5]$  homozygote (-neo, lane 2). (D) RT-PCR analysis of SCG tissue extract. cDNAs were prepared from WT (+/+),  $\alpha 3[5]$ -heterozygous mice (+/tm), and  $\alpha 3[5]$ -homozygous mice (tm/tm). The WT-specific primer amplified 480 bp PCR products from the  $\alpha 3[5]$  (+/tm) and WT samples, but not with cDNAs from the  $\alpha 3[5]$  (tm/tm). The  $\alpha 3[5]$ -specific primer amplified 480 bp PCR-products with cDNAs prepared from heterozygote and homozygote mice, and nothing is produced using WT cDNA. *Chrna3<sup>tm1.1Hwrt</sup>* mice (i.e., neo-deleted) on a mixed C57BL/6-129S background at age <P20 were used in the RT-PCR experiments.

### Figure 2. Synaptic receptors can be labeled using rhodamine-conjugated $\alpha$ BTX in $\alpha 3[5]$ -homozygous mice.

(A) Rhodamine-labeled  $\alpha$ BTX (rhoBTX, red) clusters colocalize with vesicular acetylcholine transporter (VACHT, green) in SCG from  $\alpha 3[5]$ -homozygous mice (left,  $\alpha 3^{tm/tm}$ ) but not in SCG from WT mice (right). Immunostaining for neurofilament (NFM, blue) shows the preganglionic axons. These results were seen in 5/5 mice and indicate that  $\alpha 3[5]$ -containing receptors are targeted to synapses. Inset shows regions of NFM-labeled axons that have VACHT-positive varicosities that colocalize with receptor clusters. (B) RhoBTX-labeled clusters (red) colocalize with postsynaptic density 93 (PSD93, green). All rhoBTX-clusters colocalize with PSD93 but many PSD93 puncta do not have detectable with rhoBTX clusters, suggesting a problem with trafficking or insertion of  $\alpha 3[5]$ -containing receptors to synapses. (C) RhoBTX-labeling is abolished by pre-incubating SCG from  $\alpha 3[5]$ -homozygous mice with unlabeled  $\alpha$ BTX (100 nM, left), but is normal when SCG are pre-incubated with MLA (50 nM, middle). RhoBTX-labeled clusters present on SCG neurons from homozygous double ( $\alpha 3[5]$ -homozygous  $\alpha 7$  (-/-)) mice (right). *Chrna3<sup>tm1.1Hwrt</sup>* mice on a mixed C57BL/6-CD-1 background aged

2-3 months were used in these experiments. Scale bar is 2  $\mu\text{m}$  for A and B and 0.5  $\mu\text{m}$  for the insets in A.

**Figure 3. Fast synaptic transmission in SCG from  $\alpha 3[5]$ -homozygous mice is blocked by  $\alpha\text{BTX}$ .**

(A) Extracellular compound action potentials (CAP) recorded from the sympathetic trunk in 2-month old WT (top row) and a 2-month old  $\alpha 3[5]$ -homozygous mouse (bottom row); the traces on the right show CAPs recorded from the same ganglia in the presence of 100 nM  $\alpha\text{BTX}$ . CAPs recorded from  $\alpha 3[5]$ -homozygous SCG are approximately 10-20% the amplitude of control and are completely blocked by  $\alpha\text{BTX}$ . Similar results were seen in 12 WT mice and in 15 C57BL/6/CD-1 *Chrna3<sup>tm1.1Hwrt</sup>* homozygous mice greater than 2 months of age. (B) Nerve-evoked EPSPs recorded intracellularly from sympathetic neurons in 2-month old WT (top row), 2-month old C57BL/6/CD-1 *Chrna3<sup>tm1.1Hwrt</sup>* homozygous (middle row) and 5-month old homozygous double mutant ( $\alpha 3[5]$ -homozygous  $\alpha 7(-/-)$ ) SCG (bottom row). Suprathreshold stimulation of the preganglionic nerve evokes small  $\sim 3\text{mV}$  EPSPs on sympathetic neurons from 5-month old  $\alpha 3[5]$ -homozygous SCG that are completely blocked by  $\alpha\text{BTX}$ . Similar results were seen for 20 EPSPs from WT neurons and 30 EPSPs from  $\alpha 3[5]$ -homozygous SCG neurons dissected from mice greater than 2 months of age.

**Figure 4. Cultured SCG neurons from neonatal  $\alpha 3[5]$ -homozygous mice congenic on C57BL/6 generate ACh-evoked whole-cell currents that are sensitive to  $\alpha\text{BTX}$ .**

(A) Bar graph showing whole-cell current density measurements recorded from cultured SCG neurons from WT C57BL/6 mice (<P20). Reducing the culturing temperature to 30°C for 1 day has no significant effect on the mean current density in WT SCG neurons (middle,  $P=0.10$ ). The mean current density at 30°C is unaffected following a 1 h incubation with 100 nM  $\alpha\text{BTX}$  (right,  $P=0.74$ ). Values represent the mean (n=15) and SEM from 3 mice (5 cells/mouse). (B) SCG neurons from  $\alpha 3[5]$ -homozygous mice congenic on C57BL/6 (<P20) are unresponsive to ACh application when cultured at 37°C (left). Following 1 day at 30°C, SCG neurons from  $\alpha 3[5]$ -homozygous mice generate small ACh-evoked currents which are unaffected by the deletion of the  $\alpha 7$  subunit (middle,  $P$  values >0.70). The ACh responses at 30°C are reduced following 1 h incubation with 100 nM  $\alpha\text{BTX}$  (right). No significant differences in the levels of  $\alpha\text{BTX}$  block were observed among  $\alpha 7$  genotypes ( $P$  values >0.1). Values represent the mean and SEM (n=5) from 1 mouse. (C) Data points representing ACh-evoked current densities in cultured SCG neurons from  $\alpha 3[5]$ -homozygous mice (<P20) congenic on C57BL/6, F2 mixed-background inbred (C3H, DBA, and BALB/c), and outbred (ICR) strains.  $P$  values were calculated using an unpaired  $t$  test.

**Figure 5.  $\alpha$ BTX-labeled clusters depend on presynaptic innervation**

(A) Shows the size distribution of rhoBTX labeled receptor clusters in innervated  $\alpha$ 3[5]-homozygous SCG (n=5 ganglia). The red line is a gaussian fit of the data. (B) Size distribution of rhoBTX labeled receptor clusters in  $\alpha$ 3[5]-homozygous SCG 2 days after denervation (n=5 ganglia). There is an increase in the number and the size of puncta 2 days following denervation. (C) Size distribution of rhoBTX labeled receptor puncta in  $\alpha$ 3[5]-homozygous SCG 1 week after denervation (n=5 ganglia). The number and the size of cluster 1 week following denervation are reduced slightly compared with control. (D) Size distribution of rhoBTX labeled receptor cluster in  $\alpha$ 3[5]-homozygous SCG 2 weeks after denervation (n=5 ganglia). Cluster number and size are markedly reduced 2 weeks following denervation. For A-D, The red lines are gaussian fits of the data and the insets show representative images of SCG live stained with rhoBTX and immunostained for VACHT. Scale bars are 1  $\mu$ m. (E) Average number and mean intensity of receptor clusters at different times after denervation. (number of clusters counted in each condition at for each time point is >1000). *Chrna3<sup>tm1.1Hwrt</sup>* mice on a mixed C57BL/6-CD-1 background were used in these experiments

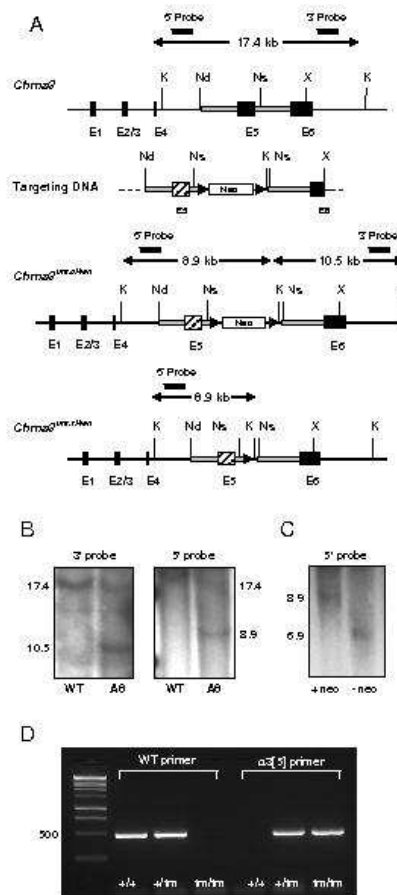


Figure 1  
215x279mm (72 x 72 DPI)

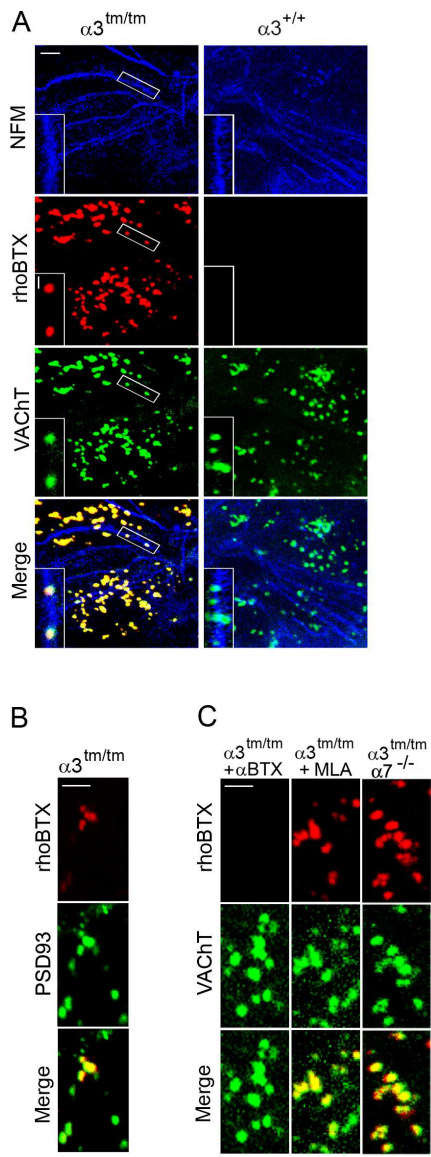


Figure 2  
74x207mm (300 x 300 DPI)

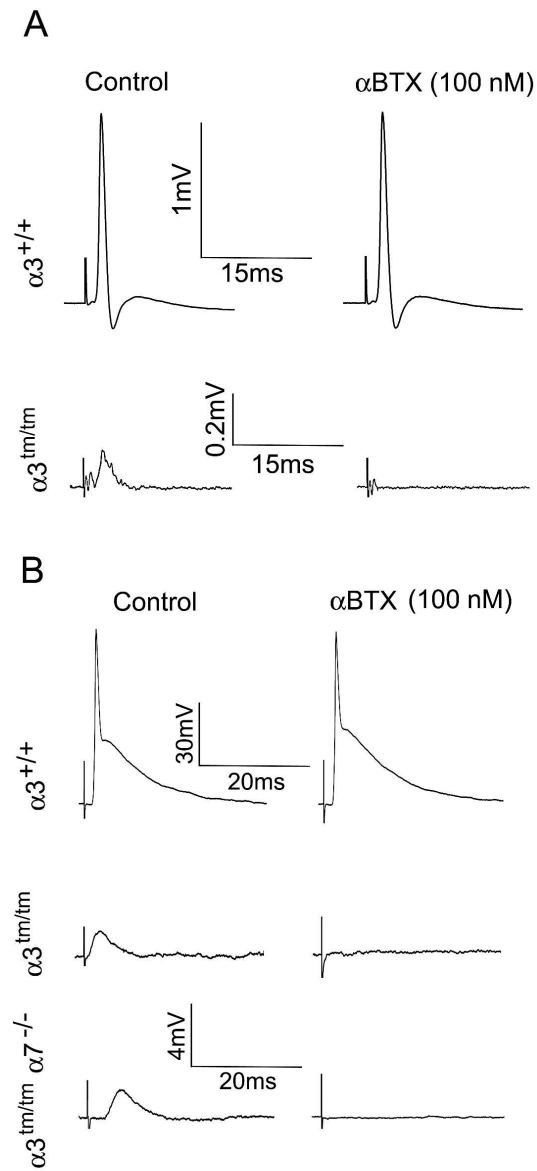
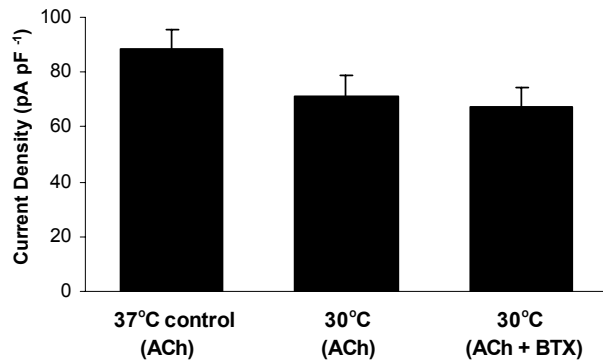


Figure 3

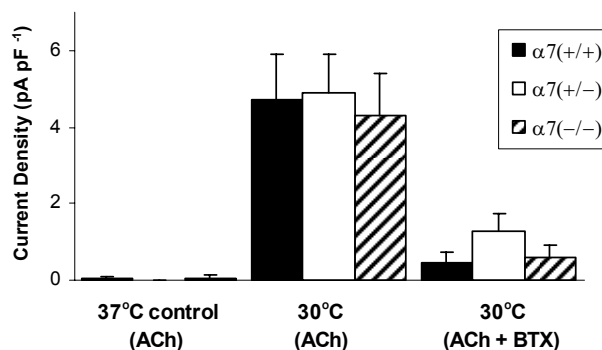
**A**

Effect of 24 h incubation at 30°C on ACh responses in SCG neurons from wild-type C57BL/6



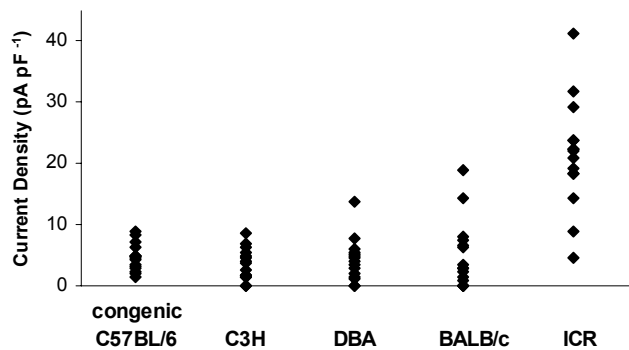
**B**

Effect of 24 h incubation at 30°C on ACh responses in homozygous  $\alpha 3[5]$  SCG neurons from congenic C57BL/6



**C**

Effect of genetic background on ACh responses in homozygous  $\alpha 3[5]$  SCG neurons incubated for 24 h at 30°C



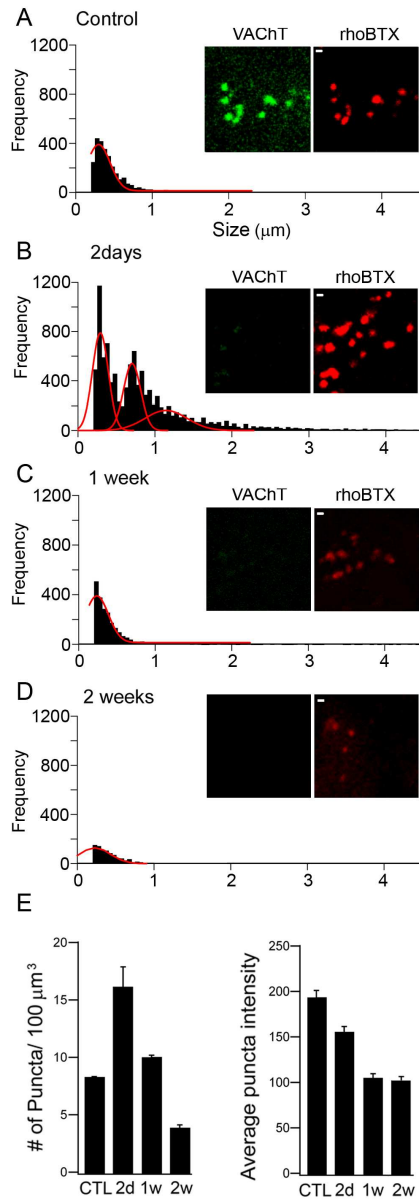


Figure 5  
88x240mm (300 x 300 DPI)

**APPENDIX:2**  
**ANIMAL USE PROTOCOLS**



## McGill University Animal Use Protocol – Research

For Office Use Only:

Protocol #: 5572  
Approval End Date: NOV. 30, 2008

*Effects of elevations in cytosolic reactive oxygen*  
**Title:** Effects of reactive oxygen species on synaptic transmission in sympathetic ganglia  
*(must match the title of the funding source application)*

Facility Committee: Doc  
*Species postsynaptically on synaptic transmission in sympathetic ganglia*  
Category (see section 11): C

New Application       Renewal of Protocol # \_\_\_\_\_       Pilot

### 1. Investigator Data:

Principal Investigator: Ellis Cooper      Phone #: 398 4334  
Unit/Department: Physiology      Fax#: 398 7452  
Address: McIntyre Med Sci Rm 1127      Email: Ellis.Cooper@McGill.ca

### 2. Emergency Contacts: Two people must be designated to handle emergencies.

Name: Ellis Cooper      Work #: 4334      Emergency #: (514) 932 6667  
Name: Brigitte Pie      Work #: 4337      Emergency #: (450) 444 0428

### 3. Funding Source:

External       Internal   
Source (s): HSFC      Source (s): \_\_\_\_\_  
Peer Reviewed for the project proposed in this Animal Use Protocol:  YES       NO\*\*  
Peer Reviewed:  YES       NO\*\*  
Status:  Awarded       Pending  
Funding period: 01/07/2007 to 30/06/10

For Office Use Only:

ACTION	✓	DATE
CCs		
DB	✓	NOV 30 07
APPROVED		

\*\* All projects that have not been peer reviewed for scientific merit by the funding source require 2 Peer Review Forms to be completed e.g. Projects funded from industrial sources. Peer Review Form available at [www.mcgill.ca/research/compliance/animal/forms](http://www.mcgill.ca/research/compliance/animal/forms)

Proposed Start Date of Animal Use (d/m/y): 01/07/2007      or ongoing

Expected Date of Completion of Animal Use (d/m/y): 30/06/10      or ongoing

**Investigator's Statement:** The information in this application is exact and complete. I assure that all care and use of animals in this proposal will be in accordance with the guidelines and policies of the Canadian Council on Animal Care and those of McGill University. I shall request the Animal Care Committee's approval prior to any deviations from this protocol as approved. I understand that this approval is valid for one year and must be approved on an annual basis.

Principal Investigator's signature:

*[Handwritten Signature]*

Date: Sept 20 2007

Approved by:

Chair, Facility Animal Care Committee:	<i>[Handwritten Signature]</i>	Date: <u>16 Nov 2007</u>
RESEARCH ETHICS OFF.	<i>[Handwritten Signature]</i>	Date: <u>Dec 10 07</u>
Chair, Ethics Subcommittee (as per UACC policy):	_____	Date: _____
Approved Animal Use	Beginning: <u>Dec 1, 2007</u>	Ending: <u>NOV. 30, 2008</u>

This protocol has been approved with the modifications noted in Section 13.

**Renewal next year requires submission of full Animal Use Protocol form**

ACTION	✓	DATE
CCs		
DB	✓	Nov 9 '06
APPROVED		

www.mcgill.ca/rgo/animal/forms/



# McGill University Animal Care Committee RENEWAL of Animal Use Protocol

For Office Use Only:

Protocol #: 1159  
 Approval end date: June 30, 2007  
 Facility Committee: DCU  
 Renewal#: 1<sup>st</sup> (2<sup>nd</sup>)

For: Research  Teaching  project

Principal Investigator: Ellis Cooper Protocol # 1159  
 Protocol Title: The role of activity on neuronal differentiation and synapse formation on sympathetic neurons Phone: 398 4334  
 Unit, Dept. & Address: Physiology, McIntyre Rm 1127 Fax: 398 7452  
 Email: Ellis.Cooper@Mcgill.ca Level: C Funding source: CIHR 17463  
 Start of Funding: 01/04/2004 End of Funding: 31/03/09 4632  
 Emergency contact #1 + work AND home phone #s: Ellis Cooper, 398 4334 AND 514 932 6667  
 Emergency contact #2 + work AND home phone #s: Brigitte Pie, 398 4337 AND 450 444 0428

## 1. Personnel and Qualifications

List the names of the Principal Investigator and of all individuals who will be in contact with animals in this study and their employment classification (investigator, technician, research assistant, undergraduate/ graduate student, fellow). If an undergraduate student is involved, the role of the student and the supervision received must be described. Training is mandatory for all personnel listed here. Refer to [www.animalcare.mcgill.ca](http://www.animalcare.mcgill.ca) for details. Each person listed in this section must sign. (Space will expand as needed)

Name	Classification	Animal Related Training Information	Occupational Health Program *	Signature "Has read the original full protocol"
Ellis Cooper	Professor	over 30 years experience	No	<i>Ellis Cooper</i>
Brigitte Pie	Research Associate	over 20 years experience	No	<i>Brigitte Pie</i>
Nancy Grenier	Technician	3 years experience	No	<i>Nancy Grenier</i>
Veronica Campanucci	PostDoc	10 years experience	No	<i>Veronica Campanucci</i>
Arjun Krishnaswamy	Graduate Student	4 years	No	<i>Arjun Krishnaswamy</i>

\* Indicate for each person, if participating in the local OHP Program, see <http://www.mcgill.ca/rgo/animal/occupational/> for details.

Approved by:

## 2. Approval Signatures

Principal Investigator/ Course Director	<i>Ellis Cooper</i>	Date: <u>Sept 7 / 06</u>
Chair, Facility Animal Care Committee	<i>Arjun Kr</i>	Date: <u>Sept 21, 06</u>
UACC Veterinarian	<i>[Signature]</i>	Date: <u>Nov 8 06</u>
Chairperson, Ethics Subcommittee (D level or Teaching Protocols Only)	<i>[Signature]</i>	Date: <u>—</u>
Approved Animal Use Period	Start: <u>July 1, 2006</u>	End: <u>June 30, 2007</u>

## 3. Summary (in language that will be understood by members of the general public)

AIMS AND BENEFITS: Describe, in a short paragraph, the overall aim of the study and its potential benefit to human/animal health or to the advancement of scientific knowledge (was section 5a in main protocol).

We are investigating the cellular mechanisms that are involved in synapse formation among neurons during early postnatal development. For our experiments, we study the growth and differentiation of neonatal rat

07 NOV, 2006

ACTION	✓	DATE
CCs		
DB	✓	Oct 11 '06
APPROVED		

www.mcgill.ca/rgo/animal/forms/



# McGill University Animal Care Committee RENEWAL of Animal Use Protocol

For: Research  Teaching  project

For Office Use Only:  
 Protocol #: 1159  
 Approval end date: June 30, 2006  
 Facility Committee: DOW  
 Renewal#: 1<sup>st</sup> 2<sup>nd</sup>

Principal Investigator: Ellis Cooper Protocol # 1159  
 Protocol Title: The role of activity on neuronal differentiation and synapse formation on sympathetic neurons Phone: 398 4334  
 Unit, Dept. & Address: Physiology, McIntyre Rm 1127 Fax: 398 7452  
 Email: Ellis.Cooper@McGill.ca Level: [REDACTED] Funding source: CIHR  
 Start of Funding: 01/04/2004 End of Funding: 31/03/09  
 Emergency contact #1 + work AND home phone #: Ellis Cooper, 398 4334 AND 514 932 6667  
 Emergency contact #2 + work AND home phone #: Brigitte Pie, 398 4337 AND 450 444 0428

## 1. Personnel and Qualifications

List the names of the Principal Investigator and of all individuals who will be in contact with animals in this study and their employment classification (investigator, technician, research assistant, undergraduate/ graduate student, fellow). If an undergraduate student is involved, the role of the student and the supervision received must be described. Training is mandatory for all personnel listed here. Refer to [www.animalcare.mcgill.ca](http://www.animalcare.mcgill.ca) for details. Each person listed in this section must sign. (Space will expand as needed)

Name	Classification	Animal Related Training Information	Occupational Health Program *	Signature "Has read the original full protocol"
Ellis Cooper	Professor	over 30 years experience	No	[Signature]
Brigitte Pie	Research Associate	over 20 years experience	No	[Signature]
Nancy Grenier	Technician	3 years experience	No	[Signature]
Veronica Campanucci	PostDoc	10 years experience	No	[Signature]
Arjun Krishnaswamy	Graduate Student	4 years	No	[Signature]

\* Indicate for each person, if participating in the local OHP Program, see <http://www.mcgill.ca/rgo/animal/occupational/> for details.

Approved by:

## 2. Approval Signatures

Principal Investigator/ Course Director	[Signature]	Date: <u>Sept 7 / 06</u>
Chair, Facility Animal Care Committee	[Signature]	Date: <u>Sept 27 / 06</u>
UACC Veterinarian	[Signature]	Date: <u>Oct 20 06</u>
Chairperson, Ethics Subcommittee (D level or Teaching Protocols Only)	[Signature]	Date: <u>                    </u>
Approved Animal Use Period	Start: <u>July 1, 2005</u>	End: <u>June 30, 2006</u>

## 3. Summary (in language that will be understood by members of the general public)

AIMS AND BENEFITS: Describe, in a short paragraph, the overall aim of the study and its potential benefit to human/animal health or to the advancement of scientific knowledge (was section 5a in main protocol).

We are investigating the cellular mechanisms that are involved in synapse formation among neurons during early postnatal development. For our experiments, we study the growth and differentiation of neonatal rat

29 SEP 2006



## McGill University Animal Use Protocol – Research

Protocol #: 1111  
 Investigator #: 341  
 Approval End Date: June 30, 2005  
 Facility Committee: MED

**Title:** Structure-Function Relationships and Regulation of Neuronal Nicotinic Acetylcholine Receptors  
*(must match the title of the funding source application)*

New Application       Renewal of Protocol # 1111       Pilot      Category (see section 11): B

### 1. Investigator Data:

Principal Investigator: Ellis Cooper      Phone #: 4334  
 Department: Physiology      Fax #: 7452  
 Address: McIntyre Med Sci Building, Rm 1127      Email: Ellis.Cooper@mcgill.ca

### 2. Emergency Contacts: Two people must be designated to handle emergencies.

Name: Ellis Cooper      Work #: 4334      Emergency #: 514 932 6667  
 Name: Brigite Pie      Work #: 4337      Emergency #: 450 444 0428

### 3. Funding Source:

External       Internal   
 Source (s): CIHR      Source (s): \_\_\_\_\_  
 Peer Reviewed:  YES     NO\*\*      Peer Reviewed:  YES     NO\*\*  
 Status:  Awarded     Pending      Status:  Awarded     Pending  
 Funding period: July 2001- June 2006      Funding period: \_\_\_\_\_

For Office Use Only:

ACTION	✓	DATE
CCs		
DB	✓	Aug 5/04
APPROVED		

\*\* All projects that have not been peer reviewed for scientific merit by the funding source require 2 Peer Review Forms to be completed e.g. Projects funded from industrial sources. Peer Review Forms are available at [www.mcgill.ca/rgo/animal](http://www.mcgill.ca/rgo/animal)

Proposed Start Date of Animal Use (d/m/y): \_\_\_\_\_ or ongoing

Expected Date of Completion of Animal Use (d/m/y): \_\_\_\_\_ or ongoing

**Investigator's Statement:** The information in this application is exact and complete. I assure that all care and use of animals in this proposal will be in accordance with the guidelines and policies of the Canadian Council on Animal Care and those of McGill University. I shall request the Animal Care Committee's approval prior to any deviations from this protocol as approved. I understand that this approval is valid for one year and must be approved on an annual basis.

Principal Investigator's signature: [Signature]      Date: Aug 5/2004

Approved by:

Chair, Facility Animal Care Committee:	<u>[Signature]</u>	Date: <u>8/9/04</u>
University Veterinarian:	<u>[Signature]</u>	Date: <u>August 10, 2004</u>
Chair, Ethics Subcommittee (as per UACC policy):	_____	Date: _____
Approved Animal Use	Beginning: <u>July 1, 2004</u>	Ending: <u>June 30, 2005</u>

This protocol has been approved with the modifications noted in Section 13.



## McGill University Animal Use Protocol – Research

Protocol #: 1111  
 Investigator #: 341  
 Approval End Date: June 30, 2004  
 Facility Committee: MED

**Title:** Structure-Function Relationships and Regulation of Neuronal Nicotinic Acetylcholine Receptors  
 (must match the title of the funding source application)

New Application       Renewal of Protocol # 1111       Pilot      Category (see section 11): B

### 1. Investigator Data:

Principal Investigator: Ellis Cooper      Phone #: 4334  
 Department: Physiology      Fax#: 7452  
 Address: McIntyre Med Sci Building, Rm 1127      Email: Ellis.Cooper@mcgill.ca

### 2. Emergency Contacts: Two people must be designated to handle emergencies.

Name: Ellis Cooper      Work #: 4334      Emergency #: 514 932 6667  
 Name: Brigite Pie      Work #: 4337      Emergency #: 450 444 0428

### 3. Funding Source:

External       Internal   
 Source (s): CIHR      Source (s): \_\_\_\_\_  
 Peer Reviewed:  YES     NO\*\*      Peer Reviewed:  YES     NO\*\*  
 Status:  Awarded     Pending      Status:  Awarded     Pending  
 Funding period: July 2001- June 2006      Funding period: \_\_\_\_\_

### For Office Use Only:

ACTION	✓	DATE
CCs	✓	Jun 4 '03
DE		
APPROVED		

\*\* All projects that have not been peer reviewed for scientific merit by the funding source require 2 Peer Review Forms to be completed e.g. Projects funded from industrial sources. Peer Review Forms are available at [www.mcgill.ca/rgo/animal](http://www.mcgill.ca/rgo/animal)

Proposed Start Date of Animal Use (d/m/y): \_\_\_\_\_ or ongoing   
 Expected Date of Completion of Animal Use (d/m/y): \_\_\_\_\_ or ongoing

**Investigator's Statement:** The information in this application is exact and complete. I assure that all care and use of animals in this proposal will be in accordance with the guidelines and policies of the Canadian Council on Animal Care and those of McGill University. I shall request the Animal Care Committee's approval prior to any deviations from this protocol as approved. I understand that this approval is valid for one year and must be approved on an annual basis.

Principal Investigator's signature: [Signature]      Date: Jun 3/03  
 Approved by: \_\_\_\_\_

Chair, Facility Animal Care Committee:	<u>Pam Sciana</u>	Date: <u>3/6/03</u>
University Veterinarian:	<u>R. L. Leith</u>	Date: <u>6/3/03</u>
Chair, Ethics Subcommittee (as per UACC policy):		Date: _____
Approved Animal Use	Beginning: <u>July 1, 2003</u>	Ending: <u>June 30, 2004</u>
<input type="checkbox"/> This protocol has been approved with the modifications noted in Section 13.		



# McGill University



## APPLICATION TO USE BIOHAZARDOUS MATERIALS

Projects involving potentially biohazardous materials should not be commenced without approval from Environmental Health & Safety. Submit applications before 1) starting new projects, 2) renewing existing projects, or 3) changing the nature of the biohazardous materials within existing projects.

1. PRINCIPAL INVESTIGATOR: Dr. Ellis Cooper PHONE: 398 4334

DEPARTMENT: Physiology FAX: 398 7452

ADDRESS: McIntyre medical Building Rm 1127 E-MAIL: ellis.cooper@mcgill.ca

PROJECT TITLE(S): 1. Hyperglycemia-induced ROS depresses ganglionic synaptic transmission (JDRF).

2. Structure-function relationship and regulation of neuronal nicotinic acetylcholine receptors. (CIHR MT-10910)

3. Effects of elevation in cytosolic reactive oxygen species postsynaptically on synaptic transmission in sympathetic ganglia. (HSFC)

### 2. EMERGENCY: Person(s) designated to handle emergencies

Name: Ellis Cooper Phone No: work: 398 4334 home: 932 6667

Name: Brigitte Pie Phone No: work: 398 4337 home: 450 444 0428

### 3. FUNDING SOURCE OR AGENCY: list all sources when information in Sections 5-12 is identical:

Source JDRF Grant No. 5-2007-1007 Start date 09/01/07 End date 08/31/08

Source CIHR Grant No. MT-10910 Start date 07/01/01 End date 03/31/08

Source HSFC Grant No. Start date 07/01/07 End date 06/30/10

### 4. Indicate if this is

Renewal: procedures previously approved without alterations.

Approval End Date: Mar 2006

New funding source: project previously reviewed and approved under an application to another agency.

Agency: \_\_\_\_\_ Approval End Date: \_\_\_\_\_

New project: project not previously reviewed.

Approved project: change in biohazardous materials or procedures.

Work/project involving biohazardous materials in teaching/diagnostics.

CERTIFICATION STATEMENT: Environmental Health & Safety approves the experimental procedures proposed and certifies with the applicant that the experiment will be in accordance with the principles outlined in the Public Health Agency of Canada's "Laboratory Biosafety Guidelines" and in the "McGill Laboratory Biosafety Manual".

Containment Level (select one):  1  2  2 with additional precautions  3

Principal Investigator or course director: [Signature] date: 10 07 07  
day month year

Approved by Environmental Health & Safety: [Signature] date: 12 07 07  
day month year

Expiry: 30 06 10  
day month year